Batista, José Miguel Sebastiao Fernandes (2016) *FAM49 - A novel regulator of the protrusive behaviour and motility of cells.* PhD thesis.

http://theses.gla.ac.uk/7690/

FAM49 – A novel regulator of the protrusive behaviour and motility of cells

José Miguel Sebastião Fernandes Batista

BSc (Hons), MSc

Submitted in fulfilment of the requirements for the degree of
Doctor of Philosophy

The Beatson Institute for Cancer Research
Institute of Cancer Sciences
College of Medical, Veterinary and Life Sciences

University of Glasgow

April 2016

Abstract

Most eukaryotic cell motility relies on plasma membrane protrusions, which depend on the actin cytoskeleton and its tight regulation. The SCAR/WAVE complex, a pentameric assembly comprising SCAR/WAVE, Nap1, CYFIP/Pir121, Abi and HSPC300, is a key driver of actin-based protrusions such as pseudopods. SCAR/WAVE is thought to activate the Arp2/3 complex, a crucial actin nucleator, after being itself activated by upstream signals such as active Rac1. Despite recent progress on the study of the SCAR/WAVE complex, its regulation is still incompletely understood, with Nap1's role being particularly enigmatic. Upon screening for potential Nap1 binding partners in the social amoeba *Dictyostelium discoideum* – a well established model organism in the study of the actin cytoskeleton and cell motility – we found FAM49, a ~36 kDa protein of unknown function which is highly conserved in Metazoa (animals) and evolutionarily closer species such as *D. discoideum*. Interestingly, *D. discoideum*'s FAM49 and its homologs contain a DUF1394 domain, which is also predicted in CYFIP/Pir121 proteins and most likely involved in their direct binding to active Rac1, which in turn contributes to SCAR/WAVE's activation. FAM49's unknown role, apparent high degree of conservation and potential connections to SCAR/WAVE and Rac1 persuaded us to start investigating its function and biological relevance in *D. discoideum*, leading to the work presented in this thesis. Several pieces of our data collectively support a function for FAM49 in modulating the protrusive behaviour, and ultimately motility, of *D. discoideum* cells, as well as a regulatory link between FAM49 and Rac1. FAM49's involvement in protrusion regulation was first hinted at by our observation that GFP-tagged FAM49 is enriched in pseudopods. The possibility of a link with Rac1 was then strengthened by two additional observations: first, pseudopodial GFP-FAM49 is substantially co-enriched with active Rac, both showing fairly comparable spatio-temporal accumulation dynamics; second, when dominant-active (G12V) Rac1 is expressed in cells, it triggers the recruitment and persistent accumulation of GFP-FAM49 at the plasma membrane, where both become highly co-enriched. We subsequently determined that *fam49* KO cells differ from wild-type cells in the way they protrude and move, as assessed in under-agarose chemotaxis assays. In particular, our data indicate that *fam49* KO cells tend to display a lower degree of global protrusive activity, their protrusions extend

more slowly and are less discrete, and the cells end up moving at lower speeds and with higher directional persistence. This phenotype was substantially rescued by FAM49 re-expression. While re-expressing FAM49 in *fam49* KO cells we generated putative FAM49 overexpressor cells; compared to wild-type cells, they displayed atypically thin pseudopods and what seemed to be an excessively dynamic, and perhaps less coordinated, protrusive behaviour. Additional data in our study suggest that pseudopods made by *fam49* KO cells are still driven by SCAR/WAVE, which is clearly not being replaced by WASP (as is now known to be the case in *D. discoideum* cells lacking a functional SCAR/WAVE complex). Nonetheless, the peculiar dynamics of those pseudopods imply that SCAR/WAVE's activity is regulated differently when FAM49 is lost, though it remains to be determined how. This thesis is the first report of a dedicated study on FAM49 and lays the foundation for future research on it.

Table of Contents

List of Tables

List of Figures

List of Accompanying Material

DVD containing movies 1 to 22 (described in Appendix C).

Acknowledgements

Huge thanks to my supervisor, Prof. Robert Insall, for bearing with me all along, helping and supporting with not only the science but also more personal matters.

I'm also thankful to the following:

Fundação para a Ciência e Tecnologia (FCT) and Cancer Research UK, for financial support.

Past and present R6 members, especially Peter Thomason, Andrew Davidson, Douwe Veltman, Seiji Ura, Jason King and Clelia Amato, for helping out with all sorts of Dicty-related things. And for the camaraderie.

Prof. Laura Machesky, Heather Spence and Loïc Fort, for thinking that FAM49 could be cool.

Past and present members of the microscopy, mass spectrometry (especially Sergio Lilla) and molecular biology units at the Beatson Institute for Cancer Research, for all services provided and helpful support. Also everyone else at the Beatson whose work directly or indirectly provided for my research.

Jackie Beesley, for helping to sort out things with the Graduate School on a number of occasions.

My family, for being hopeful.

And Catarina, my beloved soul mate, for always standing by my side with her childlike smile.

Author's Declaration

I hereby declare that this thesis and the results herein presented are the product of my own work, except where stated otherwise. Furthermore, none of the results herein presented have been previously used to obtain a degree in any University.

José Miguel S. F. Batista

1 Introduction

1.1 The actin cytoskeleton

Actin (Straub, 1942) is one of the most abundant and highly conserved proteins in eukaryotic cells (Campellone and Welch, 2010). It is also the basic unit of the actin cytoskeleton, a very dynamic and highly regulated system of actin filaments and associated high order networks.

Cycles of actin filament polymerization and disassembly allow cells to constantly remodel their actin cytoskeleton and use it as a key structural scaffold and force-generating system in diverse, fundamental processes (Michelot and Drubin, 2011; Campellone and Welch, 2010). These include providing internal mechanical support and driving cell motility, cytokinesis, endocytosis and intracellular vesicle trafficking (Pollard and Cooper, 2009). Participating in these tasks requires high order actin assemblies to be generated at precise subcellular regions, and this is thought to be triggered by distinct local stimuli (Michelot and Drubin, 2011).

The geometrical, mechanical and dynamic properties of actin filament networks are specifically adjusted to each cellular function and highly regulated by specific, and often extensive, sets of actin-binding and actin regulatory proteins (Michelot and Drubin, 2011). Though often overlooked, it is now well established that the actin cytoskeleton is also modulated and somewhat complemented by two other cytoskeletal subsystems, microtubules and intermediate filaments (Huber *et al.*, 2015).

1.1.1 G-actin and F-actin

Actin is a ~42 kDa, ATP-/ADP-binding protein generally thought of as existing in two possible states: monomeric (also known as globular or G-actin) or polymeric (also known as filamentous or F-actin). Actin's ability to polymerize into, and be recycled from, filaments is what allows it to perform most of its recognized roles in cells (Pollard and Cooper, 2009; Campellone and Welch, 2010).

Many organisms express a number of actin isoforms, which differ in few amino acid residues and are thought to share basic structural and biochemical properties, namely the capacity to assemble into filaments, ATPase activity and nucleotide-dependent dynamics (Hild *et al.*, 2010). Nonetheless, important functional and regulatory differences are believed to exist between actin isoforms, such as between muscle and non-muscle actins in vertebrates (Rubenstein, 1990; Herman, 1993; Tondeleir *et al.*, 2012).

The atomic-resolution 3D structure of rabbit muscle G-actin reveals that it has a cubic-like shape with two main domains (Kabsch *et al.*, 1990). These two domains are separated by a central cleft where ATP or ADP bind in association with a divalent cation (Kabsch *et al.*, 1990), thought to be Mg^{2+} *in vivo* (Estes *et al.*, 1992). G-actin shows much higher affinity for ATP (K_D = 7.5 nM) than for ADP (K_D = 450 nM) (Neidl and Engel, 1979).

An actin filament (F-actin) consists of two long-pitch helical strands of stacked actin monomers/subunits (G-actin). The strands are stabilized by both intra-strand and inter-strand actin subunit interactions (von der Ecken *et al.*, 2015). Actin filaments display kinetic polarity, with a fast growing barbed end (also known as the plus [+] end) and a slow growing pointed end (also known as the minus [-] end); filament growth, or elongation, proceeds through the addition of ATP-G-actin subunits, mostly to the barbed end (Pollard, 1986). The bulk of cytosolic G-actin is likely complexed with proteins such as profilin and thymosin β4 (Pollard *et al.*, 2000), which block G-actin addition to the pointed end (Pollard and Cooper, 1984; Pring *et al.*, 1992; Safer *et al.*, 1991; Cassimeris *et al.*, 1992); filament growth at this end may therefore not be physiologically relevant.

ATP-G-actin assembly at the barbed end is coupled with conformational changes which ultimately trigger ATP hydrolysis (Oda *et al.*, 2009; Murakami *et al.*, 2010). *In vitro*, phosphate (P_i) release can be slow (Carlier and Pantaloni, 1986). Its release has been suggested to occur through a cylindrical cavity seen in actin subunits within F-actin (Murakami *et al.*, 2010). It is not known how delayed P_i's release is *in vivo*. ADP-P_i-F-actin is more stable than ADP-F-actin *in vitro* (Belmont *et al.*, 1999), suggesting P_i release may be a biologically relevant factor controlling F-actin depolymerisation.

Actin filaments also display structural polarity, determined not only by the arrangement of actin subunits within the filament but also by the fact that different filament conformations are adopted depending on which nucleotide is bound – ATP, ADP-P$_i$ or ADP (Belmont *et al.*, 1999; Kudryashov *et al.*, 2010; Murakami *et al.*, 2010).

1.1.2 Actin nucleation

The first step towards generating actin filaments *de novo* is called nucleation. It consists of assembling two- or three-monomer actin "nuclei" (also known as actin "seeds"), which can then serve as templates for subsequent filament growth (Hild *et al.*, 2010).

Spontaneous nucleation of actin alone is unfavourable due to the instability of actin dimers and trimers (Pollard *et al.*, 2000). Furthermore, as stated above, most cytosolic G-actin is bound to proteins such as profilin and thymosin β4, which prevent nucleation events (Pollard and Cooper, 1984; Goldschmidt-Clermont *et al.*, 1991; Safer *et al.*, 1991). Nucleation is thus a rate-limiting step in *de novo* filament assembly.

To overcome such barrier, cells employ specialized actin nucleation factors (also known as actin nucleators) that stabilize or structurally mimic actin nuclei. Several actin nucleators have been described so far, the most well-studied being the Arp2/3 complex and formins.

1.1.2.1 Arp2/3 complex

The first key actin nucleator to be identified was the Arp2/3 complex (Machesky *et al.*, 1994; Mullins *et al.*, 1998). This stable, ~220 kDa complex is composed of seven subunits, namely Arp2, Arp3 and ArpC1-ArpC5, all highly conserved in eukaryotes (Campellone and Welch, 2010).

In vitro, the Arp2/3 complex binds to the side of an existing actin filament
("mother" filament) and catalyses the assembly of a new filament ("daughter"
filament) at a ~70° Y-branch angle, firmly linking the two (Mullins *et al.*, 1998;
Rouiller *et al.*, 2008). Amongst all known actin nucleators, the Arp2/3 complex is
unique in its ability to produce branched filaments. Its peculiar nucleation
scheme is believed to drive the creation of high order branched, or "dendritic",
actin networks in cells, typically associated with lamellipods (wide, sheet-like
plasma membrane protrusions made by many cell types when moving on flat
surfaces or 3D environments *in vivo* – Insall and Machesky, 2009; Ridley, 2011;
Krause and Gautreau, 2014), clathrin-mediated endocytosis and some forms of
cell-cell adhesion (Chesarone and Goode, 2009; Svitkina, 2013).

The Arp2/3 complex is thought to nucleate actin through structural mimicry,
whereby its two actin-related proteins, Arp2 and Arp3, mimic an actin dimer
from which a new filament can be assembled (Rouiller *et al.*, 2008). Efficient
activation of, and nucleation by, the Arp2/3 complex seems to require
engagement of a nucleation-promoting factor (NPF) (Machesky *et al.*, 1999), as
well as binding to the side of an existing actin filament (Bailly *et al.*, 2001) and
phosphorylation of Arp2 (LeClaire *et al.*, 2008). ATP binding by both Arp2 and
Arp3 appears to be important for nucleation *in vitro*, though this is less clear *in
vivo* (Goley *et al.*, 2004; Martin *et al.*, 2005).

The main NPFs of the Arp2/3 complex are WASP family proteins, which include
WASP, N-WASP, SCAR/WAVE, WASH and others (Machesky and Insall, 1998;
Machesky *et al.*, 1999; Higgs *et al.*, 1999; Linardopoulou *et al.*, 2007;
Campellone and Welch, 2010). All WASP family members contain a C-terminal
WCA domain, comprised of one or more WASP homology 2 (WH2) subdomains, an
amphipathic connector region (C) and an acidic motif (A) (Campellone and
Welch, 2010). While the connector and acidic portions jointly bind to and help
activating the Arp2/3 complex, which involves conformational changes in the
latter, WH2 binds G-actin and delivers it to the Arp2/Arp3 mimic barbed end
(Goley *et al.*, 2004; Rodal *et al.*, 2005; Boczkowska *et al.*, 2008), effectively
priming the new filament. Recent evidence suggests the Arp2/3 complex is
bound and activated by two WCA domains, each delivering one actin monomer
(Padrick *et al.*, 2011; Boczkowska *et al.*, 2014). One WCA binding site is located

on ArpC1 and Arp2, while the other is on Arp3. The two bindings are thought to be sequential and have distinct roles in activating the Arp2/3 complex (Padrick *et al.*, 2011; Boczkowska *et al.*, 2014).

Cortactin, another Arp2/3 complex NPF, appears to be a weak activator on its own, supposedly because it lacks a G-actin binding motif (Helgeson *et al.*, 2014). Nevertheless, biochemical assays suggest cortactin might synergise with different WASP family proteins to strongly activate the Arp2/3 complex (Helgeson and Nolen, 2013; Helgeson *et al.*, 2014). *In vitro*, this requires dimerization of the WASP family protein in all cases. Cortactin is also thought to stabilize newly formed filament branch junctions (Weaver *et al.*, 2001).

1.1.2.2 Formins

Apart from the Arp2/3 complex, the most studied actin nucleators are the formins, present in virtually all eukaryotes (Campellone and Welch, 2010). All formins contain a formin homology 1 (FH1) domain and a FH2 domain. *In vitro*, FH2 domains are active as dimers and sufficient to trigger actin nucleation (Campellone and Welch, 2010). The crystal structure of budding yeast's formin Bni1p FH2 domain in complex with tetramethylrhodamine-actin, together with complementary biochemical analyses, suggests an FH2 pair may bind and stabilise three actin monomers in a conformation approximating an actin filament's helix, and from which a new filament may grow (Otomo *et al.*, 2005). It is still unclear, nonetheless, how nucleation is mechanistically achieved by full-length formins (Mullins and Hansen, 2013).

At least 15 mammalian formins have been described so far, which can be categorized into 7 classes based of FH2 sequence divergence (Campellone and Welch, 2010). Mammalian Diaphanous-related formins (DRFs), namely mDia1-mDia3, are the most studied. DRFs are thought to be controlled by auto-inhibition, whereby regulatory domains at the C and N termini bind each other (Campellone and Welch, 2010). *In vitro*, auto-inhibition is relieved by binding of active Rho family GTPases to a GTPase-binding domain (GBD) at the N terminus; mDia1 requires RhoA, -B or -C, whereas mDia2 and mDia3 are more promiscuous and also accept

Rac1 and Cdc42 (Lammers *et al.*, 2008). At least in the case of mDia1, GTPase binding is not sufficient for full activation, suggesting additional regulatory factors may be relevant *in vivo* (Li and Higgs, 2005; Li and Higgs, 2003). Numerous other formins are structurally related to DRFs and probably regulated in a similar manner (Campellone and Welch, 2010). Importantly, auto-inhibition of DRFs and other formins might be a general regulatory process controlling not only their activity towards actin assembly but also their subcellular localization (Seth *et al.*, 2006).

Formin-mediated actin assembly is involved in the formation of a notable variety of cellular structures. Key examples include filopods (needle-like plasma membrane protrusions containing bundled, parallel actin filaments; thought to have important roles in cell-cell signalling, guidance toward chemoattractants and adhesion to substrates – Gupton and Gertler, 2007), lamellipods, certain cell-cell adhesions, stress fibres (bundles of parallel, contractile actin-myosin II filaments with major functions in cell adhesion and mechano-transduction – Tojkander *et al.*, 2012) and the contractile cytokinetic actin-myosin II ring (Yang *et al.*, 2007; Chesarone and Goode, 2009; Campellone and Welch, 2010).

Besides nucleating new filaments, formins are known to associate with barbed ends and enhance their growth. Importantly, not all formins show nucleating activity *in vitro,* and it is not known whether their major role in cells is to nucleate new filaments, promote their elongation or both (Mullins and Hansen, 2013). Despite this, it seems likely that different formins may drive nucleation and/or filament elongation to different extents (Campellone and Welch, 2010).

1.1.2.3 WH2 domain-containing nucleators

Actin nucleators have been recently identified which contain a tandem cluster of three or more G-actin-binding regions, mostly WH2 domains, as their signature. Such nucleators include Spire, Cordon-bleu, Leiomodin and JMY (Zuchero *et al.*, 2009; Campellone and Welch, 2010). Their WH2 domains are thought to drive actin nucleation by joining three or more actin monomers in either a single-

stranded long-pitch multimer or a short-pitch trimer, but the precise molecular details are unknown (Campellone and Welch, 2010).

Whereas Spire orthologs have been identified in several species of Metazoa (animals), Cordon-bleu, Leiomodin and JMY seem to be vertebrate-specific, with Leiomodin further restricted to muscle cells (Zuchero *et al.*, 2009; Campellone and Welch, 2010).

1.1.3 Filament elongation and capping

Barbed ends, which can be generated by nucleation or filament severing (described later), may have their growth either boosted by elongation factors or terminated by capping proteins. These two functional groups, briefly described below, are crucial in modelling the dynamics of actin networks.

1.1.3.1 Elongation factors: Formins

As mentioned earlier, formins can act both as actin nucleators and filament elongation factors. After nucleation, formins' dimerised FH2 domain remains associated with the barbed end and moves processively with it as it elongates. By means of multiple proline-rich tracts in their FH1 domain, formins are thought to rapidly recruit profilin-G-actin and "deliver" it to the FH2-coupled barbed end for assembly (Kovar *et al.*, 2006; Chesarone and Goode, 2009). Different formins accelerate filament elongation to different extents, 1.25 to 5.0-fold *in vitro* (Kovar *et al.*, 2006; Chesarone and Goode, 2009).

Both profilin-bound G-actin and formins' FH1-FH2 module are required for the barbed end elongation rate to be increased beyond free barbed end levels (Kovar *et al.*, 2006). In the presence of free G-actin only, formins generally slow barbed end growth *in vitro* (Kovar and Pollard, 2004; Kovar *et al.*, 2006).

1.1.3.2 Elongation factors: Ena/VASP

Ena/VASP proteins, found in Metazoa and more ancient single-celled eukaryotes such as *Dictyostelium discoideum*, comprise another important family of filament elongation factors. Their relevance is well documented for actin-based processes such as filopods and lamellipods (Breitsprecher *et al.*, 2008; Hansen and Mullins, 2010). Three Ena/VASP proteins are present in vertebrates, namely VASP, Mena and EVL (Breitsprecher *et al.*, 2008).

Ena/VASP family members share a conserved domain architecture. An N-terminal Ena/VASP homology 1 (EVH1) domain binds target sequences in upstream regulators, controlling Ena/VASP localisation. A C-terminal coiled-coil motif mediates self-assembly of Ena/VASP into stable tetramers. The central region of Ena/VASP contains not only a G-actin binding (GAB) site and an F-actin binding (FAB) site, shown to bind actin monomers and filaments, respectively, but also a proline-rich region, able to bind profilin and recruit profilin–G-actin (Edwards *et al.*, 2014; Hansen and Mullins, 2010).

Like formins, Ena/VASP proteins can associate processively with barbed ends and enhance the inclusion of actin subunits (Hansen and Mullins, 2010; Breitsprecher *et al.*, 2008). Different Ena/VASP proteins accelerate filament elongation to different extents, 1.2 to 7.0-fold *in vitro* (Chesarone and Goode, 2009; Breitsprecher *et al.*, 2008). Importantly, the fold change for single Ena/VASP proteins may vary substantially with the assay conditions (Hansen and Mullins, 2010).

Contrary to formins, Ena/VASP proteins are able to accelerate filament elongation in the presence of either profilin-G-actin or free G-actin (Hansen and Mullins, 2010; Breitsprecher *et al.*, 2008). Profilin–G-actin can bind simultaneously to the proline-rich and GAB regions of human VASP (hVASP) (Ferron *et al.*, 2007). In addition, the GAB site of hVASP has higher affinity for profilin-G-actin than for free G-actin (Ferron *et al.*, 2007), suggesting profilin-bound G-actin may be the unit most commonly employed by Ena/VASP proteins in driving filament elongation *in vivo*.

1.1.3.3 Capping factors: CP and others

A number of different proteins possess capping activity, whereby they bind a free, growing barbed end and block further addition or loss of actin subunits. Among capping factors, the heterodimeric "capping protein" (CP) is the most ubiquitous and abundant, with orthologs present in nearly all eukaryotic organisms (Edwards *et al.*, 2014). In most studied scenarios, CP plays a key role in shaping actin dynamics and determining interactions of filament barbed ends. CP's activity is crucial, for instance, in regulating the Arp2/3 complex-mediated assembly of dendritic actin filament networks (Edwards *et al.*, 2014). It has been suggested that barbed end capping ensures Arp2/3 complex-derived actin networks consist of short, highly branched filaments, and this is thought to provide those networks with the necessary mechanical strength to generate force efficiently, e.g. towards the plasma membrane in a lamellipod. Capping is also proposed to prevent the growth of non-productive barbed ends, allowing the available pool of G-actin to be used in filament elongation at more valuable locations, e.g. near and towards the plasma membrane in a lamellipod (Edwards *et al.*, 2014).

CP's activity is regulated in different ways. Filament elongation factors, such as formins and Ena/VASP, compete with CP for binding to barbed ends and shield from CP the ones they associate with (Chesarone and Goode, 2009; Edwards *et al.*, 2014). Protein V-1 and acidic membrane phospholipids such as PI(4,5)P2 bind directly to CP and can sterically block its interaction with barbed ends (Edwards *et al.*, 2014). Additionally, a diverse group of proteins interact with CP through a conserved "capping protein interaction" (CPI) motif and modulate its activity via allosteric effects; this group includes CARMIL, whose binding to CP promotes its dissociation from barbed ends (Edwards *et al.*, 2014).

Other capping factors, including gelsolin-family members, adducins and EPS8, have more specialized roles, with restricted cell and tissue expression patterns and distinct modes of regulation (Edwards *et al.*, 2014).

1.1.4 Filament cross-linking

Numerous and functionally diverse classes of proteins can bind the sides of actin filaments. Among them are the so-called filament cross-linkers and bundlers, all of which make use of at least two F-actin-binding sites to cross-link neighbouring filaments (Eichinger *et al.*, 1999). This large class of proteins, many of which members of the α-actinin/spectrin family (e.g. α-actinin, fimbrin and filamin), is believed to have fundamental roles in defining the architecture and mechanical properties of actin filament structures and networks, notably their resilience and elasticity (Tseng *et al.*, 2002).

Several studies with single gene knockout (KO) cell lines of *D. discoideum*, a haploid eukaryote, suggest some level of functional redundancy within the cross-linker repertoire (Eichinger *et al.*, 1999). Still, there is now evidence that some cross-linkers can act synergistically to strengthen and maintain actin network integrity at levels not achievable by each cross-linker alone, at least *in vitro*. This is the case with α-actinin and fascin (Tseng *et al.*, 2002; Tseng *et al.*, 2005), as well as with α-actinin and filamin (Esue *et al.*, 2009).

1.1.5 Filament motors: Myosins

Myosins, the molecular motors of the actin cytoskeleton, are another large and diverse group of filament side-binding proteins. All myosins have a conserved, catalytic head domain with F-actin and ATP binding sites, as well as ATPase activity. This activity controls the head's association with F-actin and allows myosins to move along actin filaments (Hartman and Spudich, 2012). All myosins so far characterised move towards the barbed end of actin filaments, except class VI myosins, which move towards the pointed end (Wells *et al.*, 1999). The head domain, typically located at the N-terminus, is followed by the so-called neck region, which in most myosins contains one or more IQ motifs where light chains – calmodulin or calmodulin-related proteins – bind (Heissler and Sellers, 2014; Sebe-Pedros *et al.*, 2014). Light chains are thought to provide structural support to myosins and, at least in some cases, such as with class II myosins, regulate their mechano-enzymatic activity (Heissler and Sellers, 2014; Vicente-

Manzanares *et al.*, 2009). Myosins' C-terminal tail, located after the neck, is the most divergent region among the various myosin classes. Depending on its sequence and specific domains, which vary considerably across myosin classes (Sebe-Pedros *et al.*, 2014), the tail region may serve roles such as mediating homodimerisation or even multimerisation, and binding to specific proteins and/or cellular membranes (Hartman *et al.*, 2011; Hartman and Spudich, 2012).

According to the most recent survey of eukaryotic genomes and phylogenetic analysis of the myosin gene family (Sebe-Pedros *et al.*, 2014), there are 31 myosin classes. Myosin abundance and domain architectural diversity are highest in the Holozoa clade, which includes animals and their evolutionarily closest single-celled relatives (Sebe-Pedros *et al.*, 2014).

Class II myosins, also known as "conventional" myosins (for historical reasons), are the most extensively studied. Unlike most other myosins (Peckham, 2011), those of class II have long coiled-coil forming sequences in their C-terminal tail, which lead to homodimerisation; as a result, class II myosins exist as two-headed motors (Vicente-Manzanares *et al.*, 2009). Interactions between the coiled-coil domains of these dimeric myosins also allow them to assemble into bipolar filaments (antiparallel arrays of myosin molecules), which can cross-link actin filaments and exert contractile forces on them (Vicente-Manzanares *et al.*, 2009). Bipolar filament formation is unique to class II myosins (Hartman and Spudich, 2012). Class II myosins play key roles in various aspects of animal cell biology; for instance, they help driving cytokinesis by acting at the contractile ring/cleavage furrow of dividing cells (Glotzer, 2001), and govern cell motility by controlling the dynamics of integrin-based substrate adhesion (Parsons *et al.*, 2010) and aiding the retraction of the cell rear/trailing edge (Cramer, 2013).

Myosins belonging to classes other than class II are frequently referred to as "unconventional". It is currently believed that, as a whole, unconventional myosins perform a wide variety of functions in cells (Hartman *et al.*, 2011). For example, class V myosins have been implicated in the intracellular transport of various organelles in budding yeast (Hill *et al.*, 1996; Schott *et al.*, 2002; Fagarasanu *et al.*, 2006) and vertebrate cells (Rogers and Gelfand, 1998; Wang *et al.*, 2008; Wagner *et al.*, 2011), whereas vertebrate class I myosins appear to be involved in regulating endocytosis (Krendel *et al.*, 2007; Sokac *et al.*, 2006),

exocytosis (Bose *et al.*, 2004; Kim *et al.*, 2006), phagocytosis (Maxeiner *et al.*, 2015), and lamellipod and integrin adhesion dynamics (Gupta *et al.*, 2013).

D. discoideum's genome encodes 13 different myosins (Kollmar, 2006), including one class II myosin (MhcA), seven class I myosins (MyoA-MyoF and MyoK), two class V-like myosins (MyoH and MyoJ; recently placed in class XXXIII - Sebe-Pedros *et al.*, 2014) and one class VII-like myosin (MyoI; recently placed in class XXV - Sebe-Pedros *et al.*, 2014), most of which have received dedicated studies. Class II MhcA, the most well-characterised *D. discoideum* myosin, is enriched at the cleavage furrow of dividing cells, at the posterior cortex of moving cells, and briefly at the tips of retracting pseudopods (Fukui *et al.*, 1989; Moores *et al.*, 1996). *mhcA* KO cells show only minor cytokinesis defects when grown on Petri dishes; however, they are seemingly unable to divide when cultured in suspension. Their multicellular development also proceeds more slowly, only to become blocked at an early stage (Manstein *et al.*, 1989). Under permissive conditions, *mhcA* KO cells can still move and chemotax, albeit less well than wild-type cells (Wessels *et al.*, 1988). Regardless, *mhcA* KO cells are unable to move under agarose overlays, a physically restrictive environment (Laevsky and Knecht, 2003). Interestingly, *D. discoideum*'s movement under agarose seems to require MhcA's actin filament cross-linking abillity but not its motor activity (Laevsky and Knecht, 2003). According to various reports, all seven *D. discoideum*'s class I myosins likely contribute to the regulation of cell motility and/or chemotaxis (Jung *et al.*, 1996; Schwarz *et al.*, 2000; Falk *et al.*, 2003; Chen *et al.*, 2012). Their involvement may range from controlling pseudopod frequency (as suggested for e.g. MyoA – Wessels *et al.*, 1996) to promoting the cell's response to chemoattractants (as proposed for e.g. MyoB - Falk *et al.*, 2003). Some class I myosins have also been implicated in phagocytosis (MyoB, MyoC, MyoE and MyoK) and/or endocytosis (MyoB, MyoC and MyoD) (Jung *et al.*, 1996; Durrwang *et al.*, 2006; Dieckmann *et al.*, 2010), in line with observations for their vertebrate counterparts (already mentioned). Other *D. discoideum* myosins have been associated with other roles; for instance, class V-like MyoJ has been suggested to tether contractile vacuole membranes to the actin cortex and contribute to their movement along the cortex (Jung *et al.*, 2009), whereas class VII-like MyoI seems to promote cell-substrate and cell-cell adhesion (Tuxworth *et al.*, 2001).

1.1.6 Filament turnover

In order to grow and generate force continuously, actin networks must not only polymerize but also turnover, both processes often happening simultaneously (Bugyi and Carlier, 2010; Ydenberg *et al.*, 2013). Dynamic filament turnover also allows cells to swiftly remodel or disassemble their actin networks as required. This turnover can be driven by three complementary processes, namely filament severing, debranching and depolymerisation (Carlsson, 2010).

1.1.6.1 Filament severing: ADF/cofilin

Among the best studied filament severing factors are ADF/cofilin proteins, found in virtually all eukaryotes (Michelot and Drubin, 2011). *In vitro*, ADF/cofilin binds to the sides of filaments, showing higher affinity for ADP-F-actin than ATP- or ADP-P_i-F-actin (Chan *et al.*, 2009). Furthermore, ADF/cofilin is often seen "decorating" continuous regions of filaments (Suarez *et al.*, 2011; Ngo *et al.*, 2015). This ADF/cofilin "clustering" induces a conformational change in the bound filament segments, namely a shortening of the helical pitch, which also propagates to the immediate neighbouring ADF/cofilin-free regions of the filament, and uniquely towards the pointed-end (Ngo *et al.*, 2015). This conformational change is thought to favour the observed cooperative binding of ADF/cofilin on filaments (Mullins and Hansen, 2013). Filament severing is most commonly observed at or near boundaries between bare and ADF/cofilin-decorated filament segments, possibly as a result of filament structural stress (Suarez *et al.*, 2011; Ngo *et al.*, 2015). *In vivo*, proteins like coronin might help restricting the severing activity of ADF/cofilin to older, ADP-F-actin (Gandhi *et al.*, 2009). Importantly, filament severing generates new free barbed ends, which may be either elongated or capped (Edwards *et al.*, 2014).

1.1.6.2 Filament debranching

ADF/cofilin also stimulates filament debranching - i.e., the detachment of Arp2/3 complex-derived branched filaments – *in vitro*. It has been suggested

that the propagated conformational change ADF/cofilin induces in actin filaments reduces the binding affinity between the Arp2/3 complex and those filaments, as well as the stability of existing branch junctions, effectively contributing to debranching (Chan *et al.*, 2009). Glia maturation factor (GMF), an homolog of ADF/cofilin, has recently been shown to bind the Arp2/3 complex with high affinity, which in turn potently stimulates debranching and inhibits further nucleation (Gandhi *et al.*, 2010). GMF's debran-ching activity and associated molecular mechanism appear to be conserved in yeasts and mammals (Ydenberg *et al.*, 2013). Experiments *in vitro* and *in vivo* suggest that ATP hydrolysis on Arp2 and Arp3 is also important for efficient debranching (Martin *et al.*, 2006; Ingerman *et al.*, 2013). P_i release from Arp2/3 complex-derived filaments may be yet another factor favouring debranching (Blanchoin *et al.*, 2000).

1.1.6.3 Filament depolymerisation

Filament depolymerisation is required for G-actin recycling and replenishment of its cytosolic pool, allowing further assembly elsewhere. Binding of profilin to recycled G-actin accelerates the exchange of ADP for ATP (Vinson *et al.*, 1998).

In vitro, P_i release from ADP-P_i-F-actin weakens the actin subunit interactions and is linked to a 5- to 10-fold increase in the rate of depolymerisation (Bugyi and Carlier, 2010). Thus, in a setting where the barbed end is actively suppor-ting filament growth, depolymerisation can be expected to occur mainly at the pointed end (Bugyi and Carlier, 2010). This scenario is clearly observed, for example, in actin networks driving steady-state lamellipods (Lai *et al.*, 2008). These networks sustain a filament treadmilling regime, whereby actin subunits are continuously added to barbed ends near the plasma membrane, move in-wards as part of the filament lattice and get released at the rear, with barbed end growth and pointed end disassembly happening simultaneously (Lai *et al.*, 2008; Carlsson, 2010).

Pointed end actin depolymerisation is substantially enhanced by *Arabidopsis thaliana* ADF/cofilin *in vitro* (Carlier *et al.*, 1997); however, this observation is yet to be extended to homologous proteins from other organisms.

1.1.7 Control of actin dynamics at the membrane level

Actin structures and networks are typically associated with cellular membranes to some degree. Furthermore, actin polymerisation often occurs near membrane surfaces. It therefore comes to no surprise that much of the regulation of actin dynamics takes place at the membrane level, in many cases involving the plasma membrane (Saarikangas *et al.*, 2010; Bezanilla *et al.*, 2015). Major players in this regulation include membrane-binding Rho family GTPases, scaffold proteins such as those belonging to the Bin-Amphiphysin-Rvs161/167 (BAR) domain superfamily, and the membranes themselves by means of their lipid composition.

1.1.7.1 Rho family GTPases

Rho GTPases constitute one of the five families of GTPases within the Ras superfamily (Rojas *et al.*, 2012). Twenty Rho family members have been described in mammals, with Rac1, Cdc42 and RhoA being the best characterised (Murali and Rajalingam, 2014). These three and most other Rho GTPases cycle between inactive GDP-bound and active GTP-bound conformational states, working as dynamic molecular switches in the control of diverse signal transduction pathways (Hall, 2012; Murali and Rajalingam, 2014). Invariably, active Rho GTPases signal downstream through interactions with specific effectors.

Activation of Rho GTPases is promoted by Rho GEFs (guanine nucleotide exchange factors), which catalyse the exchange of GDP for GTP. Inactivation is a result of GTP hydrolysis, which is intrinsically slow but can be stimulated by Rho GAPs (GTPase-activating proteins) (Murali and Rajalingam, 2014). So far, 67 Rho GAPs and 82 Rho GEFs have been described in mammals, supporting the idea that numerous complex signalling pathways or networks work through Rho GTPases; the biological relevance of so many GEFs and GAPs, however, is still unclear

(Hall, 2012). Adding to the intrigue is the fact that many GEFs, as well as some GAPs, can act on different Rho GTPases (Heasman and Ridley, 2008).

Rho GTPases are also regulated by post-translational modifications, including isoprenylation at a typically present C-terminal CAAX sequence, which in some cases is complemented by upstream palmitoylation. These lipid modifications, combined with an often existent polybasic region, help targeting and anchoring Rho GTPases to specific membrane compartments and modulate their signalling activity (Garcia-Mata *et al.*, 2011; Murali and Rajalingam, 2014). GTP-bound Rho GTPases signal from membranes. When GDP-bound, Rho GTPases are extracted from membranes by Rho GDIs (guanine nucleotide dissociation inhibitors). Rho GDIs keep inactivated Rho GTPases in the cytosol, prevent their uncontrolled re-activation and protect them from misfolding and degradation (Garcia-Mata *et al.*, 2011). Three mammalian Rho GDIs are known to exist (Hall, 2012).

Rho GTPases are perhaps best known for their key, well-conserved role in controlling actin dynamics (Heasman and Ridley, 2008; Hall, 2012; Murali and Rajalingam, 2014). As mentioned above, mammalian Rac1, Cdc42 and RhoA are the most extensively studied. All three are known to act at the plasma membrane and have major regulatory roles in actin-based processes.

Rac1 is widely recognized as being responsible for the formation of lamellipods in many cell types, likely through activation of SCAR/WAVE, an Arp2/3 complex NPF (Heasman and Ridley, 2008; Steffen *et al.*, 2013; Steffen *et al.*, 2004; Eden *et al.*, 2002; Machesky *et al.*, 1999; Miki *et al.*, 1998). Rac1 also activates members of the p21-activated kinase (PAK) family of serine/threonine kinases, which modulate actin dynamics by phosphorylating various proteins; among them is LIM kinase (LIMK), which phosphorylates and thereby inhibits ADF/cofilin, providing control over actin filament turnover (Murali and Rajalingam, 2014; Heasman and Ridley, 2008).

Cdc42 is often implicated in the regulation of filopod formation (Heasman and Ridley, 2008). Unsurprisingly, some of its effectors have been shown to help making filopods, especially the formin mDia2 and the I-BAR protein IRSp53 (Kast *et al.*, 2014; Heasman and Ridley, 2008). Cdc42 can also activate N-WASP (an

Arp2/3 complex NPF), additional formins and PAK (a target shared with Rac1) (Lammers *et al.*, 2008; Hall, 2012; Murali and Rajalingam, 2014).

RhoA is commonly linked to the assembly of stress fibres and the cytokinetic contractile ring (Glotzer, 2001; Tojkander *et al.*, 2012; Murali and Rajalingam, 2014). Multiple formins may be activated by RhoA (Lammers *et al.*, 2008; Campellone and Welch, 2010). RhoA also activates Rho-associated protein kinase (ROCK), prompting signalling events that stimulate the contractile activity of myosin II (Glotzer, 2001; Murali and Rajalingam, 2014).

It is not well understood how Rho GTPase target/effector specificity is demarcated. It may be that Rho GEFs help defining the signal output. This could be achieved if a GEF is bound to an effector at the time it activates a GTPase, as suggested for Cdc42 during bud formation in budding yeast (Hall, 2012). If widespread, this mechanism could perhaps explain the diversity of GEFs.

It should be highlighted that extensive crosstalk, mediated through different mechanisms, takes place between Rho GTPases, likely contributing to the coordination of their activities in cells (Guilluy *et al.*, 2011). Perhaps the best characterised case is that of Rac1 and RhoA, which in most circumstances display an antagonistic relationship that operates at multiple levels (Guilluy *et al.*, 2011).

1.1.7.2 BAR proteins

BAR domain-containing proteins have emerged as important regulators of membrane remodelling during organelle biogenesis, vesicle trafficking, cell division and cell migration (Frost *et al.*, 2009; Suetsugu and Gautreau, 2012). BAR domains are coiled-coils that dimerise in an antiparallel fashion, forming folds with a positively charged surface that promotes recruitment to cellular membranes. Moreover, BAR domains are typically curved and may sense, induce and/or stabilise a certain degree of membrane curvature. Three main families of BAR domains are described: BAR, F-BAR and I-BAR. While BAR and F-BAR domains usually display concave membrane binding surfaces and induce invaginations, I-BAR domains are typically convex and induce protrusions (Frost *et al.*, 2009; Suetsugu

and Gautreau, 2012). Several BAR proteins can also bind actin assembly-controlling factors; this is hypothesised to help recruit those factors to membrane surfaces of a particular curvature and regulate their activity, thus coordinating membrane remodelling and actin dynamics (Frost *et al.*, 2009; Suetsugu and Gautreau, 2012). Cellular processes where such interactions and regulation are thought to happen include clathrin-mediated endocytosis (CME) and plasma membrane protrusions such as filopods.

Numerous BAR proteins are involved in CME, many of which contain an SH3 domain that binds the proline-rich region on N-WASP, the major Arp2/3 complex NPF in CME (Suetsugu and Gautreau, 2012). *In vitro*, mammalian CME-associated BAR proteins such as Toca-1, FBP17 and Snx9 help recruit N-WASP to the surface of liposomes and stimulate its NPF activity in a membrane curvature-dependent way (Takano *et al.*, 2008; Gallop *et al.*, 2013; Suetsugu and Gautreau, 2012), suggesting a similar control might be in place *in vivo*.

Several lines of evidence indicate that the mammalian I-BAR protein IRSp53 is a major organizer of filopods, likely coordinating different actin-related activities (Suetsugu and Gautreau, 2012; Kast *et al.*, 2014). IRSp53 can bind and seemingly modulate the activities of many proteins, including Arp2/3 complex NPFs N-WASP and SCAR/WAVE, the formin mDia1, filament elongation factors Mena and VASP, and EPS8. All these interactions involve IRSp53's SH3 domain (Suetsugu and Gautreau, 2012; Kast *et al.*, 2014). IRSp53 is probably regulated by auto-inhibition, adopting a closed, inactive conformation. Its activation *in vitro* requires binding to both GTP-Cdc42 and an SH3 target (Kast *et al.*, 2014). Observations *in vivo* suggest IRSp53 is indeed an effector of Cdc42 in filopod generation (Krugmann *et al.*, 2001). IRSp53 has also been reported to bind active Rac1 and act downstream of it, stimulating the formation of Rac1-dependent membrane protrusions (Miki *et al.*, 2000; Abou-Kheir *et al.*, 2008). This is thought to depend on IRSp53 bridging active Rac1 and SCAR/WAVE (Miki *et al.*, 2000; Abou-Kheir *et al.*, 2008).

1.1.7.3 Membrane phosphoinositides

Membrane phosphoinositides (phosphorylated derivatives of phosphatidylinositol, PI), are a range of acidic phospholipids which play a key role in the control of actin dynamics by acting as platforms for the recruitment of many actin-binding, scaffold and/or regulatory proteins, thereby controlling their localisation and often modulating their activity (Saarikangas *et al.*, 2010). Recruitment is commonly mediated by polybasic regions and/or specific phosphoinositide-binding domains – such as PH, PX or FYVE domains –, which generally recognize only one or two species of phosphoinositide (Saarikangas *et al.*, 2010). Eukaryotic cells produce seven phosphoinositide species – PI(3)P, PI(4)P, PI(5)P, PI(3,4)P2, PI(3,5)P2, PI(4,5)P2 and PI(3,4,5)P3 –, each of which has a distinctive subcellular localisation in membrane compartments. This helps defining compartment/organelle identities, as well as specifying protein-membrane interactions (Saarikangas *et al.*, 2010).

Among phosphoinositides, PI(4,5)P2 is the best characterised regulator of actin dynamics. Artificially changing PI(4,5)P2 levels or protein accessibility in cultured mammalian cells invariably leads to substantial changes in actin cytoskeleton behaviour (Rozelle *et al.*, 2000; Yamamoto *et al.*, 2001; Raucher *et al.*, 2000). PI(4,5)P2 is primarily enriched in the plasma membrane, where it is thought to interact with several proteins and shape their activities as a result (Ling *et al.*, 2006; Saarikangas *et al.*, 2010). PI(4,5)P2 can directly inhibit the actin binding activities of a number of proteins, such as ADF/cofilin, CP and profilin. Other proteins, however, have their respective activities directly enhanced by PI(4,5)P2 binding, like WASP/N-WASP and some regulators of cell adhesion dynamics (Rohatgi *et al.*, 2000; Higgs and Pollard, 2000; Ling *et al.*, 2006; Edwards *et al.*, 2014; Saarikangas *et al.*, 2010).

Plasma membrane PI(4,5)P2 levels depend on the activity of various signal-responsive metabolic enzymes. Most PI(4,5)P2 is generated by type I PIP kinases from PI(4)P. Enzymes that consume PI(4,5)P2 include phospholipase C (PLC) and PI(3)-kinase (PI3K) (Saarikangas *et al.*, 2010; Ling *et al.*, 2006). Importantly, restricted membrane regions can become enriched in PI(4,5)P2 in a very dynamic way, and this seems to be crucial for driving actin cytoskeleton remodelling in

processes such as phagocytosis and cell motility (Botelho *et al.*, 2000; Coppolino *et al.*, 2002; Ling *et al.*, 2006).

1.2 Protrusion-based cell motility

Active, and often directed, motility allows many eukaryotic cells to aptly interact with their environment. Free living, single-celled organisms such as *D. discoideum* rely on movement to actively search for food. In animals, directed cell migration is intimately associated with key physiological processes like embryogenesis, organogenesis, wound healing and immune cell surveillance. Cell migration also constitutes a major pathological element in disease conditions such as cancer metastases and atherosclerosis (Parent and Weiner, 2013; Schwab *et al.*, 2012).

In the above-mentioned cases, cell motility frequently involves a complex coordination between plasma membrane protrusions at the front (also known as "leading edge"), adhesions to a surface (e.g. extracellular matrix), and retractions of the cell rear (or "trailing edge") (Ridley, 2011; Parsons *et al.*, 2010; Insall and Machesky, 2009). Importantly, this protrusion-based cell movement [note: for the remainder of this thesis, all references to cell motility concern protrusion-based cell motility only] is often directed, thus also depending on the cell's ability to sense, integrate and adequately respond to guidance cues, which may range from soluble chemoattractants and chemorepellants to various mechanical forces and electric fields (Roca-Cusachs *et al.*, 2013; Insall, 2013).

With few known exceptions (Panopoulos *et al.*, 2011), cell motility relies on the actin cytoskeleton (Insall and Machesky, 2009; Parsons *et al.*, 2010). In recent years, numerous proteins and signalling/regulatory pathways were described as crucial modulators of actin dynamics and/or other key aspects of cell motility. Despite our rapidly increasing knowledge on the individual molecular mechanisms, we are still far from fully understanding how the many different parts (proteins, pathways, etc.) are globally coordinated and ultimately translate into a dynamic motile cell (Insall and Machesky, 2009; Abu Shah and Keren, 2013).

1.2.1 Actin polymerisation-driven protrusions and Blebs

One major class of plasma membrane protrusions (simply "protrusions" from here onwards) includes lamellipods, filopods and pseudopods (the latter are relatively bulky and rounded, and often present in cells such as *D. discoideum* and leukocytes – Lammermann and Sixt, 2009), all of which appear to be driven by actin polymerisation beneath and towards the membrane and are supported by high order actin filament assemblies (Ridley, 2011; Insall and Machesky, 2009). These assemblies do, nevertheless, vary in architecture, protein composition, regulation and dynamics, perhaps more strikingly so between protrusion subtypes, e.g. lamellipods and filopods (Svitkina, 2013; Ridley, 2011). Different subtypes of actin polymerisation-based protrusions (simply "actin protrusions" from here onwards) can co-exist at the leading edge of some cell types (Ridley, 2011).

Lamellipods (and likely also pseudopods) contain extensive, branched actin filament networks, the making of which invariably requires the Arp2/3 complex (Svitkina, 2013; Wu *et al.*, 2012; Suraneni *et al.*, 2012; Rogers *et al.*, 2003; Krause and Gautreau, 2014). Lamellipod formation can occur in response to numerous extracellular stimuli, such as growth factors, cytokines and extracellular matrix (ECM) adhesion through integrins, all of which trigger downstream signalling pathways (Serrels *et al.*, 2007; Ridley, 2011). Reports suggest that different mammalian Rho GTPases, such as Rac1, RhoA, Cdc42 and RhoG, can become activated at the leading edge and play a role in lamellipod dynamics; this may involve, at least in part, coordinating each other's activities through crosstalk (Ridley, 2011; Machacek *et al.*, 2009; Meller *et al.*, 2008; Kurokawa and Matsuda, 2005; Guilluy *et al.*, 2011). Among participating Rho GTPases, Rac1 is perhaps the most relevant, as it is commonly required for lamellipod formation (Heasman and Ridley, 2008; Steffen *et al.*, 2013). This is likely a consequence of active Rac1 stimulating SCAR/WAVE, which in turn activates the Arp2/3 complex and thus promotes actin assembly at the leading edge (Steffen *et al.*, 2004; Miki *et al.*, 1998; Eden *et al.*, 2002; Machesky *et al.*, 1999). While many regulatory and structural proteins have been reported to be involved in lamellipod extension or dynamics, the exact molecular players can be expected to vary to some extent with cell type and extracellular stimuli (Ridley, 2011; Insall and Machesky, 2009; Krause and Gautreau, 2014).

Unlike lamellipods, filopods are uniquely composed of bundles of parallel actin filaments. These filaments are mainly cross-linked/bundled by fascin, which stabilizes and stiffens the high order actin structure (Svitkina, 2013). Filopod formation is perhaps most often associated with Cdc42 activity (Heasman and Ridley, 2008); there are, nonetheless, other Rho GTPases seemingly capable of inducing this particular kind of protrusion, such as Rif and RhoA (Mellor, 2010; Pellegrin and Mellor, 2005). Regardless of which Rho GTPase is implicated in any particular case, mDia formins appear to act as major effectors in filopod gene-ration (Pellegrin and Mellor, 2005; Mellor, 2010; Peng *et al.*, 2003). Proteins like N-WASP and IRSp53, both of which can be activated by Cdc42, may also contri-bute towards making filopods (Mellor, 2010; Ridley, 2011; Kast *et al.*, 2014).

Studies on B16F1 melanoma cells and vertebrate neuronal cells suggest filopods can, at least in certain cases, be initiated from within lamellipods. This seems to occur through gradual convergence, association and privileged elongation of actin filaments in the lamellipodial dendritic network (Svitkina *et al.*, 2003; Korobova and Svitkina, 2008). Interestingly, more recent observations on mouse fibroblasts indicate that filopods may themselves serve as templates for lamel-lipod generation and orientation, and this seems to involve integrin adhesion-based signalling (Johnson *et al.*, 2015). It thus appears that different actin protrusion subtypes can share nodes of regulatory networks and affect each other's dynamics, though this is likely to vary with cell type.

Blebs constitute a second class of protrusions. They are typically rounded and smooth and, contrary to actin protrusions, seem to be propelled by intracellular hydrostatic pressure and cytoplasmic flow (Paluch and Raz, 2013). New blebs are initially devoid (or nearly so) of F-actin and leave behind an F-actin "scar", which represents the former actin cortex from which the plasma membrane detached and protruded. Over time, the "scar" is removed and a new cortex is assembled beneath the expanded membrane, possibly preventing further bleb growth (Paluch and Raz, 2013; Zatulovskiy *et al.*, 2014). Three main factors, which may act in combination, are thought to promote bleb formation: a local decrease in cortex-to-membrane attachment (by means, for example, of a loca-lised reduction of cortex-to-membrane protein linkers); a local rupture of the

cortex; and high intracellular hydrostatic pressure, which can result from increased actin-myosin II contractility levels (Paluch and Raz, 2013).

A recent study in *D. discoideum* suggests that moving cells are induced to bleb more when exposed to increased external mechanical resistance (Zatulovskiy *et al.*, 2014). This could partially explain why bleb-based cell migration is more often observed in 3D environments (Insall and Machesky, 2009; Paluch and Raz, 2013), within which cells might regularly experience higher resistance levels than on 2D flat surfaces. It is not known whether mechanical resistance may favour bleb formation by triggering specific signalling pathways and/or by having a more physical impact on cells, affecting, for instance, plasma membrane curvature and tension (Zatulovskiy *et al.*, 2014; Tyson *et al.*, 2014). Also in *D. discoideum*, blebs orientate with gradients of the chemoattractant cAMP, and such directed blebbing seems to rely on PI3K signalling (Zatulovskiy *et al.*, 2014). Similar bleb-promoting signalling mechanisms have not been reported in other cell types.

It may be that some cell types rely exclusively on actin protrusions (e.g. fish keratocytes) or blebs (e.g. zebrafish primordial germ cells) for their movement (Paluch and Raz, 2013). Well-documented cases of cell motility using a combination of actin protrusions and blebs include those of *D. discoideum* cells under various experimental conditions (Yoshida and Soldati, 2006; Tyson *et al.*, 2014) and zebrafish mesendoderm germ layer progenitor cells *in vivo*, during gastrulation (Diz-Munoz *et al.*, 2010). At least in the case of *D. discoideum*, blebs sometimes evolve into actin protrusions (pseudopods), this being a result of continued actin polymerisation at the bleb's cortex (Zatulovskiy *et al.*, 2014).

Certain types of tumor cells, such as melanoma, are thought not to normally combine actin protrusions and blebs; nevertheless, those cells are able to interconvert between two distinct motility modes, one supported by actin protrusions (often referred to as "mesenchymal" mode) and another by blebs (generally but confusingly known as "amoeboid" mode) (Sanz-Moreno *et al.*, 2008; Insall and Machesky, 2009). Switching between the two modes can occur through changes in Rac1- and Rho-associated signalling pathways, the interplay and balance between which ultimately determines actin polymerisation and actin-myosin II contractility levels (Sanz-Moreno *et al.*, 2008). Recent obser-

vations in Walker carcinosarcoma cells suggest tumour cells may quickly and reversibly switch between actin protrusions and blebs without undergoing the extensive morphological changes typically associated with amoeboid-to-mesenchymal mode transitions and vice versa (Bergert *et al.*, 2012). The authors also demonstrate that substrate adhesiveness can strongly impact the protrusive behaviour of cells – in their study, high adhesiveness rapidly promotes lamellipods, while low adhesiveness favours blebbing in the long term (Bergert *et al.*, 2012). Importantly, the ability of tumour cells to change their protrusive behaviour might assist their migration in complex *in vivo* environments and ultimately enhance cancer dissemination.

1.2.2 Integrin-mediated adhesions

Cells may express various types of adhesion receptors on their surface. Among them, integrins are perhaps the best studied and understood, commonly playing a prominent role in cell migration (Parsons *et al.*, 2010). Integrins are heterodimeric transmembrane receptors consisting of non-covalently coupled α and β subunits. In mammals, 18 α and 8 β subunits can combine as 24 different heterodimers with distinctive extracellular ligand specificities. Ligands include various ECM proteins, such as fibronectins, collagens and laminins (Margadant *et al.*, 2011; Parsons *et al.*, 2010). Once bound to their ECM ligands, most integrin heterodimers become intracellularly linked, through their cytosolic tails, to the actin cytoskeleton. This linkage is not direct but instead mediated by scaffold multi-protein assemblies, which constitute an integral part of the integrin-based adhesion structure (simply "integrin adhesion" from here onwards) (Margadant *et al.*, 2011; Parsons *et al.*, 2010). The integrin-actin linkage allows integrin adhesions to not only anchor new protrusions and the cell body, but also support traction forces on the substrate, generated through actin-myosin II contractions. These traction forces, coupled with adhesion turnover at the cell rear, are fundamental in helping many cells move forward (Parsons *et al.*, 2010). Much evidence indicates that newly formed, as well as more mature integrin adhesions, also act as major signalling hubs, recruiting various cytosolic proteins that trigger and regulate diverse signalling pathways. These pathways, some of which specific of certain integrin heterodimers, are involved in the regulation of cell

shape, motility and other important aspects of cell behaviour, in part through modulation of actin cytoskeleton dynamics (Scales and Parsons, 2011; Margadant *et al.*, 2011; Parsons *et al.*, 2010).

Many, if not all, integrins can adopt low-, intermediate- and high-affinity conformations for ligand binding. A shift from a low- to a high-affinity state is denominated "integrin activation" (Moser *et al.*, 2009; Margadant *et al.*, 2011). Integrin activation is thought to require the binding of both talin and kindlin proteins to the cytosolic tail of the integrin β subunit ("inside-out" activation), perhaps in combination with extracellular integrin-ligand binding ("outside-in" activation), which promotes integrin clustering. Inside-out activation can, at least in some cases, be triggered by specific extracellular cues; for example, binding of thrombin to its receptor on platelets leads to inside-out activation of integrin αIIbβ3 (Moser *et al.*, 2009; Scales and Parsons, 2011; Margadant *et al.*, 2011). Proteins like filamin A and Dok1, which have been suggested to compete with talin for β subunit cytosolic tail binding, may help keeping integrins in an inactive, low-affinity state when required (Anthis *et al.*, 2009; Liu *et al.*, 2015; Scales and Parsons, 2011). It is still unclear, however, how integrin activators and inhibitors are coordinated in dynamic contexts, such as during cell migration (Scales and Parsons, 2011).

Integrin adhesions are typically classified based on size, stability and location in the cell. Commonly defined classes include nascent adhesions (NAs), focal complexes (FCs) and focal adhesions (FAs) (Parsons *et al.*, 2010; Scales and Parsons, 2011). NAs are small adhesion structures that form just behind the advancing leading edge. They are also rather short-lived (up to ~1 min), rapidly turning over or maturing into FCs, which are slightly larger and more stable. FCs may mature even further, becoming FAs; these are big, quite elongated, and typically associate with the ends of stress fibres (Parsons *et al.*, 2010; Scales and Parsons, 2011). The proportion and spatial distribution of integrin adhesions of each class depends not only on the cell type, but also on the composition and mechanical properties (e.g. rigidity) of the ECM (Parsons *et al.*, 2010). Moreover, not all cells display the full range of integrin adhesion classes. Neutrophils and macrophages, for instance, only have small and highly dynamic adhesions (NAs and FCs), which assist these cells in their rapid movement (Parsons *et al.*, 2010).

Integrin adhesion maturation is thought to require α-actinin- and myosin II-mediated cross-linking/bundling of adhesion-associated actin filaments, as well as the contractile activity of myosin II on those same filaments (Choi *et al.*, 2008; Parsons *et al.*, 2010). Myosin II-driven contractions are believed to generate tension on adhesions and induce conformational changes in some adhesion-associated proteins (e.g. talin and paxillin), which then expose new protein-binding and/or regulatory sites (Parsons *et al.*, 2010). Interestingly, integrin adhesion turnover also seems to be highly dependent on the contractile activity of actin-myosin II, which in this context might be regulated by FAK-Src signalling and/or other FAK-mediated molecular events (Webb *et al.*, 2004; Iwanicki *et al.*, 2008; Parsons *et al.*, 2010). Other processes/events driving adhesion turnover include calpain-mediated proteolysis of talin and integrin endocytosis (Franco *et al.*, 2004; Margadant *et al.*, 2011).

It is now clear that integrin adhesions comprise diverse scaffold and signalling proteins, which collectively form the so-called "adhesome" (Parsons *et al.*, 2010; Geiger and Zaidel-Bar, 2012). Key adhesome members include talin, paxillin, vinculin and FAK, all of which have been extensively studied and are involved in multiple regulatory protein-protein interactions (Parsons *et al.*, 2010; Scales and Parsons, 2011). Importantly, integrin adhesions at different stages of maturation may have substantially different adhesomes, as suggested by comparative proteomic analysis of isolated NAs/FCs and FAs (Geiger and Zaidel-Bar, 2012; Schiller *et al.*, 2011; Kuo *et al.*, 2011). These studies also indicate that adhesomes may be very complex, potentially comprising a network of well above 100 different proteins, particularly in more matured adhesions like FAs (Geiger and Zaidel-Bar, 2012; Schiller *et al.*, 2011; Kuo *et al.*, 2011). The highly stratified organisation of proteins within integrin adhesions has been recently revealed by super resolution microscopy (Kanchanawong *et al.*, 2010).

A substantial body of work indicates that integrin adhesions regulate the activity of various Rho GTPases, namely Rac1, RhoA and Cdc42 (Clark *et al.*, 1998; Parsons *et al.*, 2010; Scales and Parsons, 2011). This seems to be largely achieved through the recruitment of specific Rho GEFs and GAPs to adhesion sites, a process mediated by FAK, Src and likely other scaffold/signalling proteins (Chang *et al.*, 2007; Iwanicki *et al.*, 2008; Tomar and Schlaepfer, 2009; Arthur *et al.*,

2000; Elias *et al.*, 2010; Scales and Parsons, 2011; Parsons *et al.*, 2010). Other Rho GTPase regulating factors might also be engaged (Kuo *et al.*, 2011). The maturation stage of integrin adhesions is probably an important factor determining which GEFs and GAPs may be recruited, and thus which Rho GTPases may be directly regulated and how (Kuo *et al.*, 2011; Arthur *et al.*, 2000; Tomar and Schlaepfer, 2009). Early adhesions are thought to primarily enhance Rac1 activity and restrain that of RhoA, while more matured ones may lean towards RhoA stimulation instead (Kuo *et al.*, 2011; Arthur *et al.*, 2000; Tomar and Schlaepfer, 2009; Parsons *et al.*, 2010). By dynamically regulating different Rho GTPases, which in turn control actin polymerisation and actin-myosin II contractility, integrin adhesions may influence their own fate (maturation or turnover), as well as the dynamics of protrusions and cell rear retractions, possibly contributing towards a global coordination of all these cell motility steps (Parsons *et al.*, 2010).

It should be noted that integrin adhesions have been predominantly studied and characterised in cells on 2D surfaces (Parsons *et al.*, 2010; Scales and Parsons, 2011). Though we now know that dynamic integrin adhesions also form in cells in 3D environments, it remains to be clarified if their molecular composition and roles are comparable to those of their 2D-based counterparts, especially in the context of cell motility (Kubow and Horwitz, 2011; Fraley *et al.*, 2010; Scales and Parsons, 2011; Lammermann *et al.*, 2008). Murine leukocyte migration in 3D environments *in vitro* and *in vivo* has been shown not to require integrins, which are nevertheless necessary for 2D-based motility (Lammermann *et al.*, 2008). It thus appears that some cell types may rely solely on protrusive and contractile forces, without surface attachment, for moving in 3D spaces, though this is likely to depend on several factors, such as the mechanical properties of the substrate.

Recent data suggest that integrin α and β subunits originated before the divergence of the Opisthokonta, the clade that includes animals and fungi (Sebe-Pedros *et al.*, 2010). A few major components of the canonical integrin adhesome in mammals, such as talin, paxillin and vinculin (Horton *et al.*, 2015), seem to have evolved even earlier than integrins (Sebe-Pedros *et al.*, 2010). *D. discoideum* is an interesting case: firstly, *D. discoideum* cells express homologs

of various proteins typically associated with integrin adhesions, such as the just mentioned talin (Kreitmeier *et al.*, 1995; Tsujioka *et al.*, 1999), paxillin (Bukharova *et al.*, 2005) and vinculin (Huber and O'Day, 2012; Sebe-Pedros *et al.*, 2010); secondly, although no integrin α or α-like protein has so far been identified in *D. discoideum* (Froquet *et al.*, 2012), cells do express proteins that share a number of features with integrin β subunits (detailed below), and have accordingly been named Sib (<u>s</u>imilar to <u>i</u>ntegrin <u>b</u>eta) proteins (Cornillon *et al.*, 2006; Cornillon *et al.*, 2008).

Five distinct Sib proteins, SibA-SibE, are encoded in *D. discoideum*'s genome; they are clear homologs of each other and share a nearly identical overall structure (Cornillon *et al.*, 2006). The few studies to date on Sib proteins focused on SibA, and to a lesser extent SibC (Cornillon *et al.*, 2006; Cornillon *et al.*, 2008; Froquet *et al.*, 2012). All Sib proteins are predicted to be single-pass transmembrane proteins, like integrin β subunits. Accordingly, SibA has been shown to be present at the cell surface (Cornillon *et al.*, 2006). The putative extracellular region of Sib proteins, located at their N-terminus, contains a von Willebrand factor type A (VWA) domain similar to that present in the extracellular (and also N-terminal) region of integrin β subunits (Cornillon *et al.*, 2006) and which is thought to be involved in the binding of integrins to their ligands (Whittaker and Hynes, 2002). Apart from the VWA domain, however, the extracellular regions of Sib proteins and integrin β subunits are essentially different, with distinct domains and/or motifs present in each. With regard to their transmembrane region, Sib proteins contain a GxxxG motif (Cornillon *et al.*, 2006) that is also typical of integrin β subunits, where it is believed to stabilise an association with α subunits (Gottschalk *et al.*, 2002; Schneider and Engelman, 2004). The short cytosolic tail of Sib proteins constitutes their C-terminus and includes two highly conserved motifs: a membrane-proximal NPxY motif and a membrane-distal NxxY motif (Cornillon *et al.*, 2006). Both these motifs are also present, and are similarly highly conserved, in the short cytosolic tails (C-terminal) of integrin β subunits (Legate and Fassler, 2009). Integrin β's membrane-proximal NPxY motif is essential for talin binding, which in turn is required for integrin inside-out activation (Calderwood *et al.*, 1999; Calderwood, 2004). Interestingly, one of the two *D. discoideum*'s talins, talin A (the other being talin B), has been shown to bind the cytosolic tail of all Sib proteins *in*

vitro, and binding also requires the membrane-proximal NPxY motif (binding of talin B was not tested) (Cornillon *et al.*, 2006).

Since *D. discoideum* cells KO for either SibA or talin A show substantial defects in substrate adhesion (Cornillon *et al.*, 2006; Niewohner *et al.*, 1997; Simson *et al.*, 1998), it may very well be that Sib proteins are: 1) true adhesion receptors, and thus functionally equivalent to integrins; 2) regulated by a talin-dependent inside-out activation mechanism, perhaps resembling, on a molecular level, that of integrins (despite the fact that no integrin α or α-like protein, or an alternative dimer partner, has been identified so far; Froquet *et al.*, 2012). Confirming the previous points, as well as determining other relevant aspects of Sib protein biology (e.g. whether Sib proteins homodimerise, or if they bind specific extracellular ligands), will require further studies. It is conceivable, in view of the similarities described above, that Sib proteins and integrin β subunits evolved from the same ancestor integrin β-like protein (Cornillon *et al.*, 2006).

D. discoideum cells lacking both talins (by means of double gene KO) show a particularly striking phenotype. Depending on the experimental conditions, those cells are either completely unable to attach to the substrate or, if they do attach, their adhesion is weak (compared to wild-type) and they are incapable of moving, despite actively making protrusions (Tsujioka *et al.*, 2008). The latter observation strongly suggests that talin proteins are essential for *D. discoideum* cells to generate productive traction forces on substrates, and thus move. It might, therefore, be that *D. discoideum*'s talins have a role in linking the cytosolic tail of Sib proteins to the actin cytoskeleton (in addition to promoting Sib activation); such scenario would, in fact, parallel that of mammalian talins, which link integrin β's cytosolic tail to the actin cytoskeleton (Critchley, 2009). As mentioned above, *D. discoideum*'s genome also encodes homologs of paxillin and vinculin, as well as of at least a few other proteins characteristically associated with integrin adhesions, e.g. α-actinin (Condeelis *et al.*, 1984; Sebe-Pedros *et al.*, 2010). Among those, paxillin has received the most attention in the context of cell adhesion. Like SibA and talin KOs, *D. discoideum* cells KO for paxillin also exhibit substantially weaker substrate adhesion (Bukharova *et al.*, 2005). Interestingly, *D. discoideum*'s paxillin becomes enriched in small stationary spots at sites where cells are in close contact with the substrate,

suggesting that those spots represent adhesion structures (Bukharova *et al.*, 2005). It is also clear that paxillin is temporarily co-enriched with talin A at those sites, and that talin A accumulates shortly before paxillin (Patel *et al.*, 2008). A role for vinculin in *D. discoideum*'s substrate adhesion has not yet been addressed. Cells KO for α-actinin seem to be only slightly impaired in substrate adhesion (Weber, 1999), thus α-actinin might not be particularly important in the process; however, functional compensation by other actin filament cross-linkers might be at play (Eichinger *et al.*, 1999).

1.2.3 Retracting the cell rear

Cell rear retraction can seemingly be driven by forces from different sources. Overall, the strongest and most relevant of those forces is provided by actin-myosin II contractions (Cramer, 2013). Additional, yet weaker, forces contributing to cell rear retraction might be generated as a result of the following processes: myosin II-mediated cross-linking of actin filaments (Lombardi *et al.*, 2007); actin filament depolymerisation on the flanks of the cell rear (Mseka and Cramer, 2011); and actin polymerisation at the leading edge (Fournier *et al.*, 2010; Cramer, 2013). Plasma membrane tension might play an important role, possibly in conjunction with one or more of the above processes (Cramer, 2013; Abu Shah and Keren, 2013).

While the relative contribution of each source of force towards cell rear retraction may vary with cell type and extracellular environment, actin-myosin II contractile activity is expected to be crucial in many occasions, such as when cells need to overcome high substrate adhesiveness and/or move through confined 3D spaces (Cramer, 2013; Lammermann *et al.*, 2008). Myosin II-mediated contractions may, nevertheless, not be essential in some situations, as reported for *D. discoideum* cells and fish epidermal keratocytes lacking myosin II motor activity (Lombardi *et al.*, 2007; Fournier *et al.*, 2010). Importantly, and as previously mentioned, localised adhesion turnover is also a key factor determining the ability of cells to retract their rear (Parsons *et al.*, 2010).

1.3 The SCAR/WAVE complex

SCAR/WAVE (Bear *et al.*, 1998; Miki *et al.*, 1998) is a key player in the production and dynamics of actin protrusions, especially lamellipods and pseudopods, as exemplified by studies with murine (Suetsugu *et al.*, 2003; Yan *et al.*, 2003; Yamazaki *et al.*, 2005), *Drosophila melanogaster* (Kunda *et al.*, 2003) and *D. discoideum* cells (Pollitt and Insall, 2009). As far as its currently understood, SCAR/WAVE links upstream signals to actin nucleation at the leading edge, activating the Arp2/3 complex at such location (Machesky *et al.*, 1999; Insall and Machesky, 2009; Krause and Gautreau, 2014). As previously mentioned, SCAR/WAVE belongs to the WASP family of proteins, whose other members – which include WASP (after which the family was named), WASH and the more recently identified WHAMM and JMY – are also NPFs of the Arp2/3 complex (Campellone and Welch, 2010). Despite their rather similar C-terminal WCA domains, different WASP family members show more distinctive N-terminal and central sequences (Veltman and Insall, 2010; Campellone and Welch, 2010); these allow for unique ways of regulation, which are ultimately reflected in the specific cellular functions of each particular WASP family member (Campellone and Welch, 2010). Processes as relevant and diverse as cell migration and membrane trafficking are thought to be largely orchestrated by WASP family proteins.

Current evidence indicates that SCAR/WAVE is part of a fairly large (~400 kDa) pentameric complex (the "SCAR/WAVE complex") *in vivo*, together with Nap1, CYFIP/Pir121, Abi and HSPC300 (Eden *et al.*, 2002; Lebensohn and Kirschner, 2009; Derivery *et al.*, 2009). Studies in different model systems show that when any complex subunit other than SCAR/WAVE is not expressed (as a result of targeted RNAi or gene KO), SCAR/WAVE protein levels are greatly reduced – in certain cases down to undetectable amounts, depending on which other subunit is absent (Kunda *et al.*, 2003; Steffen *et al.*, 2004; Ibarra *et al.*, 2006; Pollitt and Insall, 2009; Davidson *et al.*, 2013b). While organisms such as *D. discoideum* possess only one isoform of each subunit (Pollitt and Insall, 2009), others, among them vertebrates, are known or predicted to contain two or more of each in most cases; for example, three SCAR/WAVE isoforms are present in humans (WAVE1–3), together with two isoforms of Nap1 (Nap1 and Hem1), two of CYFIP/Pir121 (CYFIP1-2) and three of Abi (Abi1-3) (Stovold *et al.*, 2005; Insall and Machesky, 2009).

The SCAR/WAVE complex is thought to be evolutionary ancient and exist in many species across diverse eukaryotic lineages (Veltman and Insall, 2010). Moreover, all its subunits are well conserved, particularly Nap1, CYFIP/Pir121 and HSPC300, whose orthologous proteins from different evolutionary branches show high sequence similarity over their entire length (Veltman and Insall, 2010).

The recently published crystal structure of a recombinant human SCAR/WAVE1 complex (Chen *et al.*, 2010) suggests that Nap1 and CYFIP/Pir121, the two biggest subunits, are structurally homologous and contact each other extensively, creating an elongated, pseudo-symmetric dimer platform on which SCAR/WAVE, Abi and HSPC300 dock (see Figure 1.1 A). Considering the extent of sequence conservation among the various complex subunits (Veltman and Insall, 2010), it may well be the case that such structure is reasonably well conserved in evolution.

1.3.1 Regulation of the SCAR/WAVE complex's activity

There is strong evidence that the SCAR/WAVE complex is basally inactive towards the Arp2/3 complex (Lebensohn and Kirschner, 2009; Derivery *et al.*, 2009; Ismail *et al.*, 2009) and that multiple coincident signals/inputs are required for its efficient activation (Lebensohn and Kirschner, 2009; Chen *et al.*, 2010; Koronakis *et al.*, 2011; Padrick *et al.*, 2008), which might occur without dissociation of any subunits (Lebensohn and Kirschner, 2009; Ismail *et al.*, 2009).

According to Chen *et al.*, 2010, SCAR/WAVE's WCA domain is likely to be normally sequestered within the complex by a combination of intramolecular and intermolecular contacts, which may explain its basal inactivity. The same report also suggests that Rac1-GTP, a widely recognized – and possibly essential – SCAR/WAVE complex activator (Eden *et al.*, 2002; Steffen *et al.*, 2004; Lebensohn and Kirschner, 2009; Chen *et al.*, 2010), binds a surface on CYFIP/Pir121 and perhaps also a nearby non-WCA region on SCAR/WAVE, and that such interaction might cause conformational changes in one or both of those subunits which contribute to the release of SCAR/WAVE's WCA domain (and thus its activity). Although Rac1-GTP can bind and activate recombinant human SCAR/WAVE complex *in*

vitro, such activation is only detectable when fairly high concentrations of the former are employed (above 2.5 μM; Ismail *et al.*, 2009), indicating a low affinity interaction (K_D measured at 7–10 μM; Chen *et al.*, 2010); this suggests that factors other than Rac1-GTP may be important for SCAR/WAVE activation *in vivo*. Indeed, several published works support such hypothesis. For instance, Lebensohn and Kirschner, 2009, have shown that purified native/endogenous SCAR/WAVE complexes (mammalian) can be efficiently activated in the presence of both nanomolar amounts of prenylated Rac1-GTP (its unprenylated form also works in the same context, albeit less well) and liposomes with acidic phospholipids; however, no detectable activation takes place when either Rac1 (prenylated or not) or liposomes alone are used, which indicates a cooperative, perhaps synergistic effect in the former conditions. Acidic phospholipids might bind a large positively charged surface on both CYFIP/Pir121 and Nap1 and a polybasic region on SCAR/WAVE (Chen *et al.*, 2010); *in vivo*, such kind of interaction may conceivably help recruiting and/or stabilising the SCAR/WAVE complex at the plasma membrane in a way which facilitates binding to Rac1-GTP (Chen *et al.*, 2010). Lebensohn and Kirschner also determined that purified native SCAR/WAVE complexes could only be activated when displaying their endogenous phosphorylations, mapped to a number of sites on SCAR/WAVE and Abi (none were detected on Nap1, CYFIP/Pir121 or HSPC300); phosphatase treatment would abolish activation in a dose-dependent fashion. The impact of SCAR/WAVE's phosphorylation state on its *in vivo* activity is well documented in other studies (reviewed in Mendoza, 2013), yet still not fully understood. It appears that phosphorylation on certain amino acid residues, such as the highly conserved Y125 and Y151 (positions in human WAVE1), promotes SCAR/WAVE's activation (Leng *et al.*, 2005; Stuart *et al.*, 2006; Sossey-Alaoui *et al.*, 2007a; Ardern *et al.*, 2006; Chen *et al.*, 2010), possibly by helping to release its WCA domain (Chen *et al.*, 2010), located downstream. Other residues, however, might need to be dephosphorylated instead if SCAR/WAVE is to be efficiently activated, as has been suggested for some conserved serines on the acidic region of the WCA domain (Ura *et al.*, 2012).

Besides active Rac, acidic membrane phospholipids and a particular state of phosphorylation, a number of other factors are thought to also promote, or otherwise modulate, the activity of the SCAR/WAVE complex. Among them is

IRSp53, an I-BAR protein, which has long been proposed to bridge active Rac1 and SCAR/WAVE and help activating the latter as a result (Miki *et al.*, 2000; Suetsugu *et al.*, 2006; Abou-Kheir *et al.*, 2008). According to Miki *et al.*, 2000, active Rac1 can bind an N-terminal region in IRSp53, and a C-terminal SH3 domain in IRSp53 may simultaneously interact with SCAR/WAVE via its polyproline region (Suetsugu *et al.*, 2006). It is not known, however, whether IRSp53 may scaffold/promote a direct interaction between active Rac1 and the SCAR/WAVE complex (Chen *et al.*, 2010) or instead favour SCAR/WAVE's activation through an alternative molecular mechanism, which nevertheless still requires Rac1.

There is evidence that lamellipodin, a regulator of lamellipodial dynamics (Krause *et al.*, 2004), can also interact directly with both active Rac and the SCAR/WAVE complex (Law *et al.*, 2013). It is unclear whether both interactions might, as for IRSp53, occur simultaneously; regardless, the study by Law *et al.*, 2013, strongly suggests that active Rac stimulates lamellipodin's binding to the SCAR/WAVE complex – which occurs via Abi's SH3 domain, present in Metazoa but absent from more ancient organisms such as *D. discoideum* (Veltman and Insall, 2010) – and it is the latter that mediates lamellipodin's control over lamellipodial behaviour and cell migration. How lamellipodin regulates SCAR/WAVE's activity at the molecular level is still a mystery.

Some reports have put forward the possibility that GTPases other than Rac1, namely Arf family members, might also be directly involved in SCAR/WAVE activation *in vivo*. One such report suggests that human Arf GTPases of different classes (Arf1, Arf5 and Arl1) can synergise with Rac1 in directly recruiting and activating SCAR/WAVE complexes from cell extracts on the surface of membrane-coated beads (Koronakis *et al.*, 2011). In another work, *Drosophila*'s Arf1 homolog is suggested to co-localise with the SCAR/WAVE complex at lamellipodial tips and to be necessary for cultured cells to generate SCAR/WAVE-driven lamellipods (Humphreys *et al.*, 2012). The mechanism(s) which might allow Arf GTPases to bind the SCAR/WAVE complex and support its activation are currently unknown.

More recently, Chen *et al.*, 2014, identified a large group of potential SCAR/WAVE complex ligands consisting of ~120 diverse transmembrane and other membrane-associated proteins, including protocadherins, ROBO proteins, netrin

receptors, neuroligins, G-protein coupled receptors and ion channels. The authors assert that all such hypothetical ligands contain a conserved six residue WIRS motif (in the case of transmembrane proteins, present in their cytoplasmic tail), which *in vitro* can bind a composite surface on the SCAR/WAVE complex formed by CYFIP/Pir121 and Abi. The binding surface is likely to be well conserved in animals and their closest relatives (choanoflaggelates), but absent from other protists, fungi or plants. Chen *et al.*, 2014, also provide evidence that a previously reported interaction between protocadherin-10 and the SCAR/WAVE complex, proposed to cause the recruitment of the latter to cell-cell contacts and modulate its activity towards increasing cell motility (Nakao *et al.*, 2008), is indeed mediated by protocadherin-10's WIRS motif. Moreover, they show that mutating the WIRS-binding surface on the SCAR/WAVE complex disrupts oogenesis in *Drosophila*. An additional paper (Chia *et al.*, 2014) further explores the WIRS-SCAR/WAVE complex connection and its relevance, demonstrating that a novel interaction between the SCAR/WAVE complex and the synaptic cell adhesion protein SYG-1 requires SYG-1's WIRS motif, and that such interaction is critical for actin polymerisation in synapse formation and axon branching. Clearly, WIRS-containing proteins might link numerous signals to the SCAR/WAVE complex *in vivo*, with diverse regulatory and physiological roles and often essential outcomes. This matter is likely to receive much attention in future research.

Another layer of control over the SCAR/WAVE complex might be provided by its dimerisation or oligomerisation, though proper evidence that either can occur is still needed. Its dimerisation/oligomerisation has been suggested to possibly happen through interactors with a bridging/dimerising capability (Padrick *et al.*, 2008) and/or binding associations between different SCAR/WAVE complex molecules (Chen *et al.*, 2010). *In vitro*, dimerised SCAR/WAVE WCA domains have much higher affinity for the Arp2/3 complex, and consequently activate it much more, than free WCA monomers (Padrick *et al.*, 2008); a similar effect *in vivo*, with dimers/oligomers of SCAR/WAVE complex, would not surprise.

As a final note, it should be mentioned that positive and negative feedback loops are also expected to play a fundamental part in how the SCAR/WAVE complex's activity is spatially and temporally delimited (Krause and Gautreau, 2014). Such

loops, at least some of which are suggested to work between the F-actin network and Rac1, are yet to be fully elucidated (Krause and Gautreau, 2014).

Figure 1.1 B summarises the various molecular interactions and additional factors believed to regulate SCAR/WAVE complex's activity, as explained above.

Figure 1.1 – Structure and regulatory factors of the SCAR/WAVE complex
A) Ribbon diagram of the human SCAR/WAVE1 complex crystal structure (PDB entry: 3p8c), as published by Chen *et al.*, 2010. Each subunit is shown in a different color (specified in the accompanying legend). The dashed red form indicates WAVE1's WCA domain. **B)** Various proteins, as well as acidic membrane phospholipids, are thought to bind the SCAR/WAVE complex (arrows pointing to the latter) and regulate its activity as a result. Boxes along arrows indicate which SCAR/WAVE complex subunits are bound by the specified interacting partners. In addition to the depicted interactions, other factors (listed) are believed to modulate the behaviour of the SCAR/WAVE complex. See main text for details.

2 Results – *FAM49, a novel regulator of the protrusive behaviour and motility of cells*

2.1 Why FAM49?

2.1.1 Where it all began: looking for potential Nap1 interactors

Much progress has been made in the study of the SCAR/WAVE complex in recent years. Highlights include the publication of the 2.3-Å crystal structure of a recombinant human SCAR/WAVE1 complex (with Nap1, CYFIP1, Abi2 and HSPC300) and complementary mechanistic analyses (Chen *et al.*, 2010), which provided much needed insight into how SCAR/WAVE's WCA domain may be inhibited within the complex and suggested plausible mechanisms not only for SCAR/WAVE's activation by Rac1-GTP and phosphorylations upstream of the WCA, but also for the recruitment of the complex to the plasma membrane by both Rac1-GTP and acidic phospholipids. Despite these and other substantial findings (already mentioned in the *Introduction* chapter), important questions still remain.

Nap1 is a particularly enigmatic piece of the puzzle (Davidson and Insall, 2011), with no assigned function within the SCAR/WAVE complex beyond that of being a structural scaffold and perhaps aiding the complex to bind plasma membrane acidic phospholipids (Chen *et al.*, 2010). Nap1 is both relatively large (typically 128-130 kDa in Metazoa (animals); 133.5 kDa in *D. discoideum*) and evolutionarily well conserved over its entire length (Veltman and Insall, 2010), which suggests it has additional, key conserved roles in the complex. Intriguingly, no recognizable subdomains or motifs are present in Nap1 (Veltman and Insall, 2010), making functional predictions difficult.

We hypothesised that Nap1 might act as a platform for signalling inputs to the SCAR/WAVE complex, interacting directly with one or more yet-to-be-identified regulatory proteins. These protein-protein interactions (PPIs) could involve Nap1 alone or perhaps in combination with other SCAR/WAVE complex subunits; the second scenario would, in fact, be hardly surprising – it has already been proposed that composite surfaces formed by CYFIP and WAVE (Chen *et al.*, 2010), and by CYFIP and Abi (Chen *et al.*, 2014), may be required for the binding of the complex to active Rac1 and to WIRS motif-containing membrane proteins, respectively. We also speculated that regulatory PPIs involving Nap1 – if they indeed take place – might be of low affinity and/or transient, which would largely explain why no Nap1 interactors had been discovered (including in past

attempts by members of our lab): the likelihood of finding such interactors using traditional screening methods, such as co-immunoprecipitation (co-IP) from "plain" cell lysates followed by mass spectrometry (MS), is, at best, very low.

With the above in mind we decided to look for potential Nap1 interactors using a non-conventional, yet potentially much more effective, "cell lysis/co-IP/MS"-based approach. Unlike one would do for standard co-IP/MS screens, we chose to include a chemical cross-linker, formaldehyde, in the cell lysis buffer; such cross-linker would, we expected, quickly stabilize numerous PPIs, including weak and/or transient ones (Sutherland *et al.*, 2008), hence allowing us to circumvent the limitations of "plain" lysates. We opted for formaldehyde over other cross-linking agents for various reasons: it is a tiny, water-soluble molecule; due to its short spacer arm (2.3-2.7 Å) it presumably only cross-links proteins in close proximity, which helps avoiding false positive hits; its cross-links are reversible and compatible with MS (Sutherland *et al.*, 2008). Though still an uncommon strategy nowadays, the use of formaldehyde for stabilising and analysing PPIs has been proven very effective over the years (Vasilescu *et al.*, 2004; Schmitt-Ulms *et al.*, 2004; Bai *et al.*, 2008; Guerrero *et al.*, 2008; Muller *et al.*, 2011; Sobczyk *et al.*, 2014).

We successfully implemented and optimised our "cell lysis plus cross-linking/co-IP/MS" method using *D. discoideum* Ax3-derived *napA* (gene coding Nap1) KO cells expressing GFP-tagged Nap1 from a genomically inserted construct (*napA⁻*/GFP-Nap1 cells). These cells show no *napA* KO phenotype (Ibarra *et al.*, 2006), which is fully rescued by GFP-Nap1, itself expressed at close to wild-type levels (Seiji Ura and Robert Insall, unpublished data). Working with GFP-Nap1 allowed us to make use of the extremely efficient GFP-trap IP/co-IP beads (Rothbauer *et al.*, 2008). We used *napA⁻*/GFP-Nap1 cells also in our final screens, for which we chose to lyse/cross-link starving cells clumping slightly in suspension, as such conditions are likely associated with high SCAR/WAVE activity levels in both pseudopods and cell-cell contacts (Veltman *et al.*, 2012). A schematic outline of the procedure we followed in our screens is presented in Figure 2.1 A.

Repeated screens yielded several potential Nap1 interactors – see Table 2.1 (for a clear understanding of the table's data and description, the reader should first see Figure 2.1 A and B and its respective description). Among them were

subunits of heterotrimeric G proteins, particularly G-alpha 1 and G-alpha 2, the second of which is a fundamental player in chemoattractant signal transduction at the plasma membrane (Kumagai *et al.*, 1989; Kumagai *et al.*, 1991; Kortholt *et al.*, 2011). G-alpha 2 was deemed interesting enough to merit a few follow-up experiments, the results of which, however, were inconclusive (not shown), at which point we decided to halt that particular line of research.

FAM49, a ~36 kDa protein of unknown function (UniProt entry: Q8T2H0), also stood out from our screens (see Figure 2.1 B and Table 2.1). FAM49 was detected by MS in *napA⁻*/GFP-Nap1 samples of three distinct experiments and consistently not found in the negative control samples (corresponding to wild-type cells expressing free GFP) (not shown). A number of reasons (below) persuaded us to focus entirely, from this point onwards, on FAM49, the study of which is the subject of this thesis. Despite the fact that a direct interaction between FAM49 and Nap1 – or, more generally, the SCAR/WAVE complex – was not tested further (and therefore not validated), the work presented herein allowed important insights onto FAM49 itself, the way it might affect SCAR/WAVE activity, and its likely influence on the protrusive behaviour and motility of *D. discoideum* cells.

A

napA⁻ cells
expressing
GFP-Nap1

WT cells
expressing
free GFP
(negative control)

······· *In parallel* ·······

"Mild" lysis (0.2% Triton X-100)
with
cross-linking (3% formaldehyde)
5 min, 4°C

Quenching of excess
formaldehyde

Collection and washing of
non-solubilized fraction

Extraction with RIPA buffer
(0.1% SDS, 1% sodium deoxycholate, 1% Triton X-100)
1 h, 4°C

GFP-Trap IP
2 h, 4°C

Elution in 1% SDS
10 min, 70°C

Vacuum centrifugation of elute,
to evaporate most liquid phase

Solubilization in small volume of
loading buffer for SDS-PAGE
10 min, 70°C

Division in half:

Cross-linked sample   Uncross-linked sample
no further heating   *20 min, 100°C*

SDS-PAGE

Gel staining with
Coomassie blue

Excision of
lane segments

Trypsinisation and
further processing

LC-MS/MS

Protein identification
and data analysis

Figure 2.1 – Screening for potential Nap1 interactors using a "cell lysis plus cross-linking/co-IP/MS" method
(*continues next page*)

A) Schematic outline of our "cell lysis plus cross-linking/co-IP/MS" method, as performed in our screens looking for potential Nap1 interactors. Only key steps are shown. As mentioned in the main text, we used starved cells in suspension. Immediately before SDS-PAGE, each GFP-trap IP elute – corresponding to either *napA⁻*/GFP-Nap1 cells or negative control cells (wild-type cells expressing free GFP) – was divided in two halves. One half was heated at 100°C for 20 min, so as to reverse most formaldehyde cross-links; this produced what we call the "uncross-linked sample". The other half was not subjected to further heating, thus preserving its cross-links; this was (…)
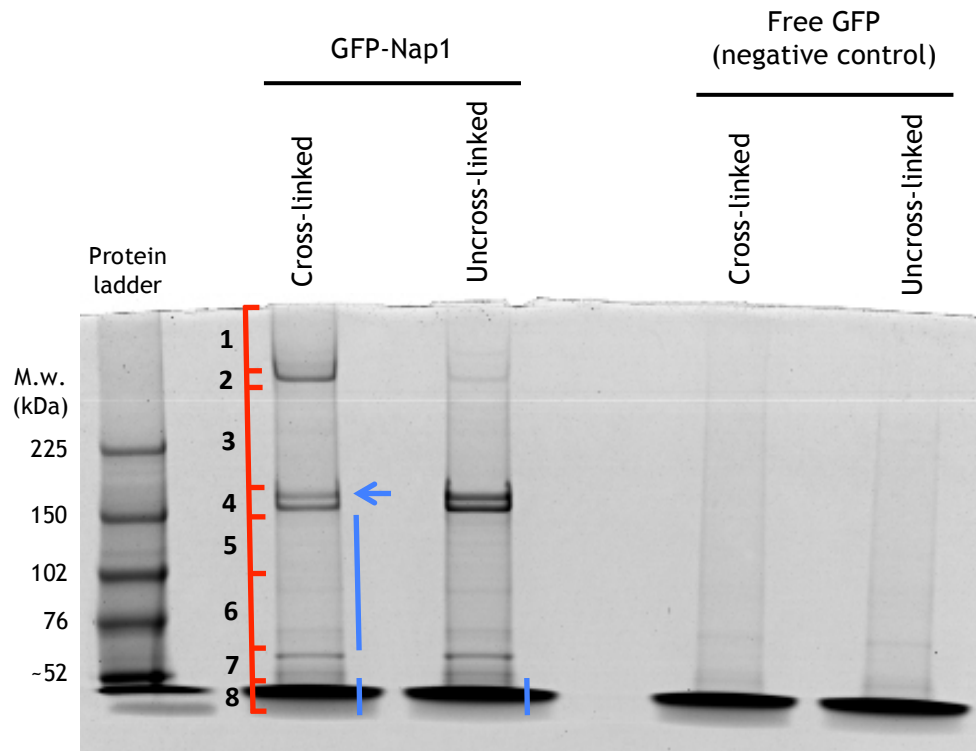
Figure 2.1 – Screening for potential Nap1 interactors using a "cell lysis plus cross-linking/co-IP/MS" method *(continued)*

(…) our "cross-linked sample". Comparing cross-linked and uncross-linked samples from *napA⁻*/ GFP-Nap1 cells – first by eye, following the Coomassie blue-staining of SDS-PAGE gels, and then by MS – allowed us to confirm the presence of cross-linked forms of GFP-Nap1 in the former. **B)** Coomassie blue-stained gel (following SDS-PAGE) with cross-linked and uncross-linked samples from *napA⁻*/GFP-Nap1 cells ("GFP-Nap1" samples) and negative control cells ("Free GFP" samples). This particular gel represents our first – and most thoroughly examined – screen. For MS analysis purposes, each sample's lane was identically sectioned in 8 segments, exactly as illustrated for the cross-linked GFP-Nap1 sample (red line with numbered segments). It should be noted that not all GFP-Nap1 molecules in our cross-linked GFP-Nap1 sample were actually cross-linked with other protein molecules. This is evident from the gel band that represents "plain" (i.e. *non*-cross-linked) GFP-Nap1, pinpointed by the blue arrow. The staining intensity of that band is clearly increased in the uncross-linked GFP-Nap1 sample, indicating an efficient reversal of previously existent cross-links. An example of a cross-linked form of GFP-Nap1 is given by the intense band in lane segment 2 of the cross-linked GFP-Nap1 sample. This band, which corresponds – perhaps uniquely – to GFP-Nap1 cross-linked with Pir121 (as determined by MS), is mostly absent from the uncross-linked GFP-Nap1 sample. The band just below that of "plain" GFP-Nap1 represents "plain" PIR121 (lane segment 4 in both GFP-Nap1 samples). Blue lines indicate the lane segments where FAM49 peptides were identified by MS (segments 5, 6 and 8 in the cross-linked GFP-Nap1 sample; segment 8 in the uncross-linked GFP-Nap1 sample). FAM49's potential binding and/or cross-linking to the SCAR/WAVE complex is discussed in the description of Table 2.1. Negative control samples have most of their GFP molecules in lane segment 8 (confirmed by MS).

Table 2.1 – SCAR/WAVE complex subunits and candidate Nap1 interactors identified in our screens
(continues next page)

Listed proteins were identified in GFP-Nap1 samples (i.e. samples from *napA⁻*/GFP-Nap1 cells) of at least two of our screens – one being the very first we performed, and which we examined more thoroughly – and consistently not detected in free GFP negative control samples (with few exceptions, as explained below). Numbers shown for each protein (e.g. total spectra) were derived from the cross-linked samples of our first screen, whose Coomassie blue-stained gel is depicted in Figure 2.1 B – please refer to it for the position of gel lane segments 1 to 8. Only peptides with ≥95% identification probability were considered in our analyses.

SCAR/WAVE complex subunits (all of which were always detected in GFP-Nap1 samples) are listed at the top, ordered by molecular mass. Candidate Nap1 interactors are listed next, ordered by percent sequence coverage (% cov.). Residual amounts of Nap1 and Pir121 were typically detected in the negative control samples – see total spectra values in the table. For this reason, and on grounds of potential scientific relevance, we decided to also consider G-protein alpha 2 subunit – the only other listed protein for which very small amounts (as estimated by total spectra) were usually found in negative control samples – as a candidate Nap1 interactor (see main text for additional details).

For each listed protein, a particular gel lane segment's entry (in the context of GFP-Nap1 sample's spectrum counts) is highlighted in grey (e.g. lane segment 4 for Pir121). This is meant to indicate each protein's "basal segment", where all (or most) of their "plain"/*non*-crosslinked form is expected to be found ("basal segments" were identified by comparing MS data from cross-linked and uncross-linked GFP-Nap1 samples). For some of the proteins we list, peptides were detected in gel lane segments far above the "basal segment", where typically only proteins with much higher molecular mass are expected to occur. Importantly, those peptides were exclusively – or mostly, in the case of GFP-Nap1, Pir121 and SCAR/WAVE – identified in cross-linked GFP-Nap1 samples (as shown in the table), and not in uncross-linked ones. This strongly suggests that the proteins being considered were, to some extent, truly cross-linked in our cross-linked GFP-Nap1 samples. (…)

Table and description continue next page				GFP-Nap1 (*cross-linked sample*)											Free GFP (*idem*)	
Identified protein	Mol. mass (kDa)	Gene	Accession number (UniProt)	Total spectra	Total unique peptides	% cov.	Spectrum count in each gel lane segment								Total spectra	Gel lane segments with peptides
							1	2	3	4	5	6	7	8		
GFP-Nap1	162	(*napA*)	(Q869Q3)	1682	120	72%	374	403	263	474	158	10	-	-	2	2
Pir121	153	*pirA*	Q6UK63	1497	111	72%	372	410	307	361	40	7	-	-	5	2-4
SCAR/WAVE	48	*scrA*	Q54NF8	239	18	40%	30	2	30	5	33	42	97	-	0	-
Abi	35	*abiA*	Q55FT9	46	7	22%	-	-	-	-	-	-	44	2	0	-
HSPC300	8	*hspc300*	Q54X65	15	6	71%	2	1	1	-	-	1	2	8	0	-
G-protein alpha 2 subunit	41	*gpaB*	P16051	58	12	39%	1	-	1	-	6	19	12	19	1	6
FAM49	36	*fam49*	Q8T2H0	17	10	36%	-	-	-	-	1	1	-	15	0	-

Table 2.1 – SCAR/WAVE complex subunits and candidate Nap1 interactors identified in our screens *(continued)*

(…)

In the case of small to medium size proteins (roughly up to GFP-Nap1's molecular mass), the detection of peptides in GFP-Nap1 samples' gel lane segments 1 to 3 is particularly suggestive of cross-linked forms containing GFP-Nap1. Except for Abi, all SCAR/WAVE complex subunits had peptides identified in those lane segments. The same is true for a few candidate Nap1 interactors, namely G-protein alpha 1 and G-protein alpha 2 subunits. Most – including FAM49 –, however, did not have any peptides detected that high up in the gel lane. This raises the possibility that most candidate Nap1 interactors we list, such as FAM49, did not form cross-links with GFP-Nap1. Different scenarios might explain our data. It might be, for instance, that an interaction between one or more of those proteins (e.g. FAM49) and GFP-Nap1 was stabilized by cross-links between the latter and other SCAR/WAVE complex subunits – this could be the case if those cross-links help keeping GFP-Nap1 and perhaps also other SCAR/WAVE complex subunits in a 3D conformation that favours stable binding to the participating interaction partners. In the case of FAM49, it is also conceivable (and not mutually exclusive) that some of its molecules formed cross-links not with GFP-Nap1 but with other SCAR/WAVE complex subunits, namely SCAR/WAVE and/or HSPC300; this could, in particular, explain why we detected a few FAM49 peptides in lane segments 5 and 6. A similar situation might also apply to G-protein alpha 1 and G-protein alpha 2 subunits, which had peptides detected in several lane segments above their "basal segment".

Continued from previous page				GFP-Nap1 *(cross-linked sample)*											Free GFP *(idem)*	
Identified protein	Mol. mass (kDa)	Gene	Accession number (UniProt)	Total spectra	Total unique peptides	% cov.	Spectrum count in each gel lane segment								Total spectra	Gel lane segments with peptides
							1	2	3	4	5	6	7	8		
G-protein alpha 1 subunit	40	*gpaA*	P16894	34	8	25%	-	-	1	-	4	6	7	16	0	-
Copine D	59	*cpnD*	Q55GG1	22	11	24%	-	-	-	-	-	-	22	-	0	-
Calpain-like cysteine protease	73	*cplA*	Q8MUF9	11	8	16%	-	-	-	-	-	11	-	-	0	-
C2 domain-/LR repeat-containing protein	69	*DDB_G0284461*	Q54PM1	10	7	13%	-	-	-	-	-	10	-	-	0	-
Ubiquitin-like domain-containing protein	90	*DDB_G0277329*	Q86K66	12	8	11%	-	-	-	-	12	-	-	-	0	-
Putative fatty acid-CoA ligase	107	*DDB_G0270106*	Q55CD5	13	7	9%	-	-	3	10	-	-	-	-	0	-
DG1112 (putative RasGAP)	121	*DG1112*	Q869U6	10	5	6%	-	-	-	-	10	-	-	-	0	-
RCC1 domain-/RhoGEF domain-/RasGAP domain-containing protein	223	*DDB_G0269934*	Q55CR5	19	13	5%	-	-	18	-	-	1	-	-	0	-

2.1.2 Reasons for selecting FAM49 for further study

Three main reasons prompted us to investigate FAM49:

1) FAM49 seems to be highly conserved in Metazoa and evolutionarily close species like *D. discoideum*.

2) FAM49 homologs (and putative homologs) contain a single Pfam domain (Finn *et al.*, 2014) termed DUF1394; the same domain is predicted to also be present in CYFIP/Pir121 proteins, where it is expected to be involved in binding active Rac1 (Chen *et al.*, 2010).

3) No studies on FAM49 had been published. It had been reported that FAM49B in mice is the source of the peptide antigen presented by the major histocompatibility complex (MHC) class Ib molecule Qa-1[b] in the absence of ERAAP function, with implications in T cell immunosurveillance (Nagarajan *et al.*, 2012); however, the authors did not investigate any aspects of the full-length FAM49 protein, thereby leaving its biological role(s) and relevance a mystery.

The following section (2.2) illustrates points 1) and 2) and includes some additional bioinformatic analyses of relevant FAM49 features. Subsequent sections (2.3 and 2.4) detail cell biology studies of FAM49 in *D. discoideum*.

2.2 Bioinformatic analyses of FAM49

2.2.1 FAM49 is present in diverse eukaryotic lineages and seems highly conserved in Metazoa and related organisms

To determine if FAM49 homologs are present in other eukaryotes we decided to use *D. discoideum* FAM49 as a BLASTP query (Camacho *et al.*, 2009) against the whole UniProtKB database (The-UniProt-Consortium, 2015). The result was quite striking: an extensive list of highly significant hits, many of which aligning with the query at an E-value far below 1.00E-20, including proteins from numerous and vastly diverse eukaryotic species; see Table 2.2 for selected examples. Remarkably, most alignments comprised the entire sequences (or nearly so) of both query and hit, which very often have comparable lengths. Regarding sequence identity and similarity percentages (definitions provided in the description of

Table 2.2), they were invariably well in excess of 20% and 40%, respectively. It is thus clear that FAM49 homologs most likely exist (Pearson, 2013), and are perhaps even widespread, in several branches of eukaryotic evolution. Table 2.2 lists putative homologs in species from Excavata, Sar, Amoebozoa and Opisthokonta lineages, including Metazoa.

The above BLASTP search, together with additional searches using various FAM49 homologs, also suggested that while many organisms possess a single FAM49 form, others, such as vertebrate species, have at least a couple of FAM49 paralogs and/or express different isoforms. A brief investigation of this matter indicated that the exact number of vertebrate paralogs and/or isoforms likely differs between lineages – possibly 4 or more in fish (e.g. *Danio rerio*) and amphibians (e.g. *Xenopus tropicalis*), and perhaps 3 in reptiles (e.g. *Anolis carolinensis*), birds (e.g. *Gallus gallus*) and mammals (e.g. *Mus musculus* and *Homo sapiens*) (not shown). FAM49A and FAM49B (designations adopted from the corresponding UniProtKB/Swiss-Prot entries for mouse and human proteins – The-UniProt-Consortium, 2015) seem to be paralogs that originated early in the history of vertebrates and started diverging around that point – see the phylogenetic tree in Figure 5.1 (Appendix A). The presence of FAM49 paralogs throughout vertebrates is not surprising, as two distinct genome duplication events are thought to have occurred early in vertebrate evolution (Dehal and Boore, 2005).

In order to assess how conserved FAM49 might be between a broad range of evolutionary branches we decided to generate a sequence multi-alignment using *D. discoideum* FAM49 and its putative homologs in Table 2.2 – see Figure 5.2 (Appendix A). Despite many positions with low conservation and a number of cases of potential insertion or deletion mutations, the obtained multi-alignment shows various regions that are reasonably conserved among all or most sequences. This suggests FAM49 might, to this day, have preserved some of its structural and functional features even between certain very evolutionarily distant eukaryotes.

We went on to generate an additional sequence multi-alignment, this time with *D. discoideum* FAM49 and homologs from diverse Metazoa species and a close Metazoa relative, the choanoflaggelate *Monosiga brevicollis*, in order to restrict

the conservation analysis to this range of organisms (Figure 2.2). Unlike between more distantly related eukaryotes (Figure 5.2 – Appendix A), it appears that FAM49 is quite highly conserved in Metazoa and at least some living relatives, not only the closest (e.g. *M. brevicollis*) but also more distant ones. It is therefore possible that FAM49 homologs in those organisms still share many key structural and functional properties, and as a result still hold common or closely related molecular role(s). This leads us to believe that studying FAM49 in *D. discoideum* may provide good insights into the function(s) and regulation of its homologs in higher eukaryotes, including *H. sapiens*. Global pairwise alignments between *D. discoideum* FAM49 and either human FAM49A or FAM49B (Figures 5.3 and 5.4, respectively, in Appendix A) show very clearly the high levels of sequence identity (45.5% and 47.7%, respectively) and similarity (63.4% and 63.6%, respectively); this was, in fact, already patent in the results of our initial BLASTP search (Table 2.2).

As mentioned above and illustrated in Figure 5.1 (Appendix A), FAM49A and FAM49B seem to have originated at an early stage of vertebrate evolution and then started to diverge. It is thus conceivable that one or both of those paralogs – perhaps among others, possibly present in certain vertebrate lineages – have acquired and/or lost some specific functional and/or regulatory properties. Global pairwise alignments between human and mouse FAM49A sequences, as well as between human and mouse FAM49B sequences, reveal virtually no changes (a single amino acid substitution in each case; not shown), suggesting FAM49A and FAM49B are extremely highly conserved in mammals. This, we think, is certainly a result of their relevant (but still largely unknown) physiological role(s).

Table 2.2 – Selected hits from BLASTP search using *D. discoideum* FAM49 as query

"High taxonomic classification" is in accordance with Adl *et al.*, 2012. "Hit coverage" details the BLASTP-computed, locally aligned region of each hit, namely its boundaries (positions of the first and last amino acid residues within the complete sequence) and relative size (percentage of complete sequence). "Query coverage" parallels "Hit coverage" but concerns the query. "Identity" specifies the percentage of query-hit alignment positions with conserved (i.e. identical) residues. "Similarity" denotes the percentage of alignment positions with a positive score in the BLOSUM62 substitution matrix (Eddy, 2004); these positions show either conserved residues or substitutions that often are conservative (i.e. the different residues have rather similar physicochemical properties). "E-value" (Expectation or Expect value) represents the number of different alignments with a score equal to, or better than, that of a query-hit alignment that would be expected to occur by chance when BLASTP-searching a selected database (chosen database was UniProtKB). The lower the E-value, the more statistically significant the query-hit alignment under consideration.

UniProt entry	Length (aa)	Species	High taxonomic classification	Hit coverage	Query coverage	Identity (%)	Similarity (%)	E-value
D2VER1	292	*Naegleria gruberi*	Excavata – Discoba	79–229 (51.7%)	82–256 (55.6%)	24.0	41.7	3.30E-03
A2E1F1	310	*Trichomonas vaginalis*	Excavata – Metamonada	1–309 (99.7%)	1–312 (99.0%)	28.6	48.1	1.40E-25
H3GY74	276	*Phytophthora ramorum*	Sar – Stramenopiles	41–274 (84.8%)	62–312 (79.7%)	27.2	46.3	6.30E-17
D7G5C5	327	*Ectocarpus siliculosus*	Sar – Stramenopiles	49–325 (84.7%)	32–312 (89.2%)	33.0	52.6	3.30E-37
X6MU15	380	*Reticulomyxa filosa*	Sar – Rhizaria	1–378 (99.5%)	1–312 (99.0%)	24.7	43.8	1.90E-22
L8GXE8	302	*Acanthamoeba castellanii*	Amoebozoa – Discosea	1–299 (99.0%)	1–312 (99.0%)	62.7	74.1	9.60E-130
F4P086	313	*Batrachochytrium dendrobatidis*	Opisthokonta – Fungi	1–311 (99.4%)	1–312 (99.0%)	41.6	60.6	2.90E-73
A0A0D2U1D3	323	*Capsaspora owczarzaki*	Opisthokonta – Filasterea	1–322 (99.7%)	1–312 (99.0%)	50.9	66.8	1.60E-96
A9UXH2	325	*Monosiga brevicollis*	Opisthokonta – Choanomonada	1–323 (99.4%)	1–312 (99.0%)	46.7	63.8	1.70E-84
Q7K1H0	324	*Drosophila melanogaster*	Opisthokonta – Metazoa	1–322 (99.4%)	1–312 (99.0%)	46.0	63.6	9.50E-84
Q9H0Q0 (FAM49A)	323	*Homo sapiens*	Opisthokonta – Metazoa	1–322 (99.7%)	1–312 (99.0%)	45.7	63.7	5.80E-85
Q9NUQ9 (FAM49B)	324	*Homo sapiens*	Opisthokonta – Metazoa	1–323 (99.7%)	1–312 (99.0%)	48.0	64.1	4.70E-90

```
                        10          20          30          40
D.discoideum   MG--------------QLLSFINGND-------HTEQIFIDFEHAQPSD 28
M.brevicollis  MG--------------NIVQVLRRDA-Q----TLDKDIFVDFEKASPSD 30
A.queenslandica MG-------------NLLRVLNDKG-P----VPKVDFYVDFESAEPTD 30
N.vectensis    MG--------------NLLRLLSRDDPG----TGKVDIFLDFENAQPTE 31
C.elegans      MPSNIRESDASCLEMIRSIIRSTADDN-S-----KWVEIFVDFENAQPTD 44
D.melanogaster MG--------------KLLSLLSRDD-SNCCAAKSYDVFLDFENAAPTE 34
B.floridae     MG--------------NLLKVLSKDD-N----TPKVDIFLDFENAQPTE 30
C.intestinalis MG--------------NLLKVLQCKE-E----AFEDFFLDFENARPSE 29
D.rerio_A      MG--------------NLLKVLTREI-E-----NYPHFFLDFENAQPTD 29
G.gallus_A     MG--------------NLLKVLTREI-E-----NYPHFFLDFENAQPTD 29
H.sapiens_A    MG--------------NLLKVLTREI-E-----NYPHFFLDFENAQPTE 29
D.rerio_B      MG--------------NLLKVLTCTDLE-----QEPNFFLDFENAQPTE 30
G.gallus_B     MG--------------NLIKVLTRDI-D----HNAAHFFLDFENAQPTE 30
H.sapiens_B    MG--------------NLLKVLTCTDLE-----QGPNFFLDFENAQPTE 30
Conservation
               *7--------------5+95464353-0-----1204799**4*3*99
Consensus
               MG--------------NLLKVLTRDDLE----TN+PDFFLDFENAQPTE
```

```
                        60          70          80          90
D.discoideum   DERELHKTVNEVLIRGPAIIDKLLAYAGCNEFIRRAITNPGP-ETEDAAW 77
M.brevicollis  AELETYEKVNAVLSKADGILKDLETYEGAGDPIRKAISNGSDEELQKQAW 80
A.queenslandica AEKEVYSKVSEILTDAPRILEELRSYKGAGESIREAISNPQSSEHQEKAW 80
N.vectensis    TEREVYEVVKGVLDSADRMLEELRSYPGASQAIREAISNPMNEDLQEIAW 81
C.elegans      EEREIYNMAEEVLNDCDLVLADVSSYGNGCYAERNQLKNDSDTQALKVLM 94
D.melanogaster TERAVYDEVERVLRESEVVLDEIQIYRGAGKEIREAIADPSP-EVTAKAW 83
B.floridae     SEHEVHQVVERVLSTSHGLLIELQQYKGADNEIREAISNPSRDDLQEKAW 80
C.intestinalis EEKEVYDQVSHVLSFAPGIITELKSYKGAGDEIRVAISNPSSQEKQADTW 79
D.rerio_A      CEREVWNQVNAVLQESESILSGLQAYKGAGQEIRDAIQNPNDMLLQERAW 79
G.gallus_A     GEREVWNQISAVLQDSESMLADLQAYKGAGQEIRDAIQNPNDIQLQEKAW 79
H.sapiens_A    GEREIWNQISAVLQDSESILADLQAYKGAGPEIRDAIQNPNDIQLQEKAW 79
D.rerio_B      AERETWEEVDVVLKDALGILDELQAYKGAGQEIREAIQNPNDEALQDQAW 80
G.gallus_B     SEKEIYNQVNVVLKDAEGILEDLQSYRGAGHEIREAIQHPNDEKLQEKAW 80
H.sapiens_B    SEKEIYNQVNVVLKDAEGILEDLQSYRGAGHEIREAIQHPADEKLQEKAW 80
Conservation
               4*44684374419*227138+23925*27952225*36+44463022432 58
Consensus
               +EREVYNQVNAVL+DAEGILE+LQSYKGAGQEIREAIQNP+DEELQEKAW
```
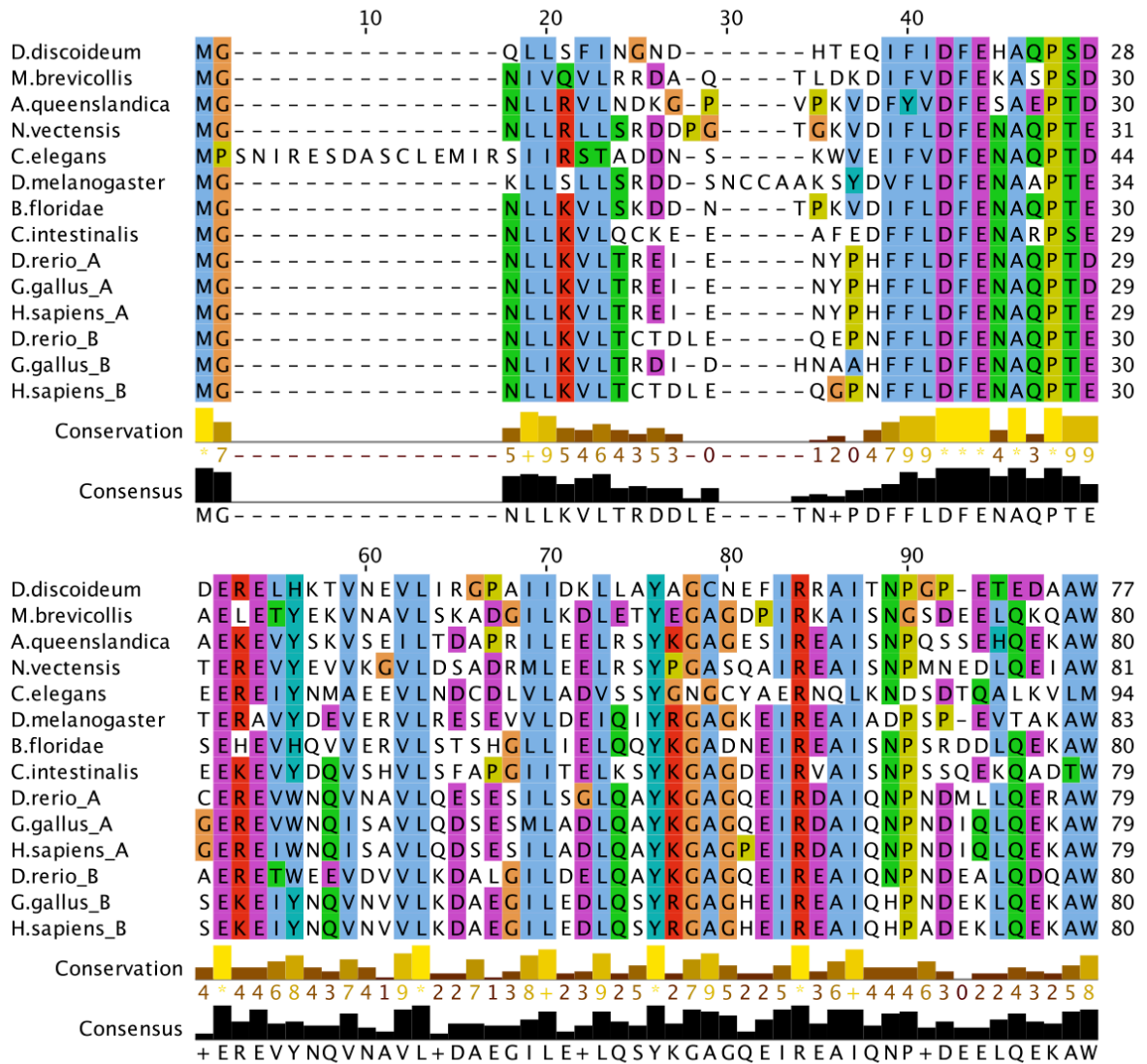
Figure 2.2 – Multi-alignment of *D. discoideum* FAM49 and homologs from a choanoflagellate and various metazoans
(*continues next page*)

The aligned sequences are associated with the following UniProt entries (from top to bottom): Q8T2H0 (*D. discoideum*), A9UXH2 (*M. brevicollis* – choanoflagellate), I1F5T7 (*A. queenslandica* – sponge), A7SA43 (*N. vectensis* – cnidarian), Q09387 (*C. elegans* – nematode), Q7K1H0 (*D. melanogaster* – "fruit fly"), C3Y224 (*B. floridae* – cephalochordate), F6PYR8 (*C. intestinalis* – tunicate), Q7ZW35 (*D. rerio* – zebrafish; FAM49A), Q5ZI04 (*G. gallus* – chicken; FAM49A), Q9H0Q0 (*H. sapiens* – human; FAM49A), Q6NYL6 (*D. rerio*; FAM49B), E1BWS3 (*G. gallus*; FAM49B), Q9NUQ9 (*H. sapiens*; FAM49B). Numbers above the top sequence pinpoint alignment positions. Numbers on the right side of each sequence indicate the cumulative number of amino acid residues used in the alignment. Dashes (–) represent gaps, which suggest insertion or deletion mutations in one or more sequences. Residues in the alignment are background-coloured according to the default ClustalX colour scheme, as emulated by Jalview 2 (Waterhouse *et al.*, 2009; Procter *et al.*, 2010; Chenna *et al.*, 2003). Briefly, residues are assigned a colour on the basis of both their type and their frequency at each alignment position; moreover, colours generally reflect certain physicochemical properties (Procter *et al.*, 2010). Two annotation rows, "Conservation" and "Consensus", are displayed below the alignment. "Conservation" states the overall conservation of physicochemical properties at each alignment position by means of a score (0 to 10) and a proportionally sized coloured bar. Conservation scores were calculated by Jalview 2, in accordance with a method and a property index described by Livingstone and Barton, 1993. Essentially, shown scores indicate the number of physicochemical properties, out of 10 being considered, that are conserved at any given position. Gaps are regarded as holding all properties. Asterisks (*) mark fully identical positions, while plus signs (+) specify positions with one or more substitutions but where all properties are conserved. "Consensus" shows the most frequent residue at each position; (+) is used where two or more residues are the most frequent. Consensus bars are proportional to the frequencies of the top residues.
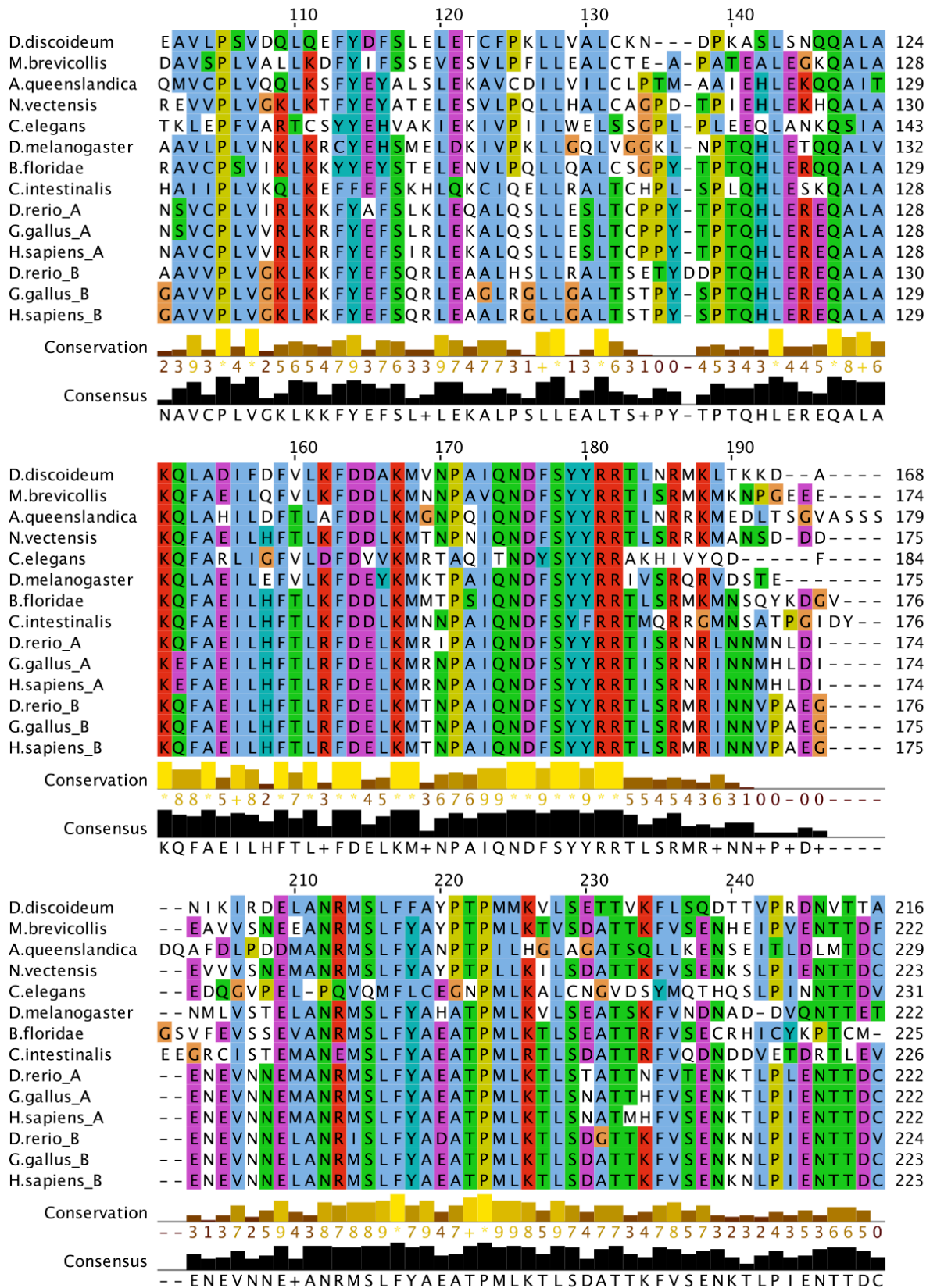
Figure 2.2 – Multi-alignment of *D. discoideum* FAM49 and homologs from a choanoflagellate and various metazoans (*continued*)
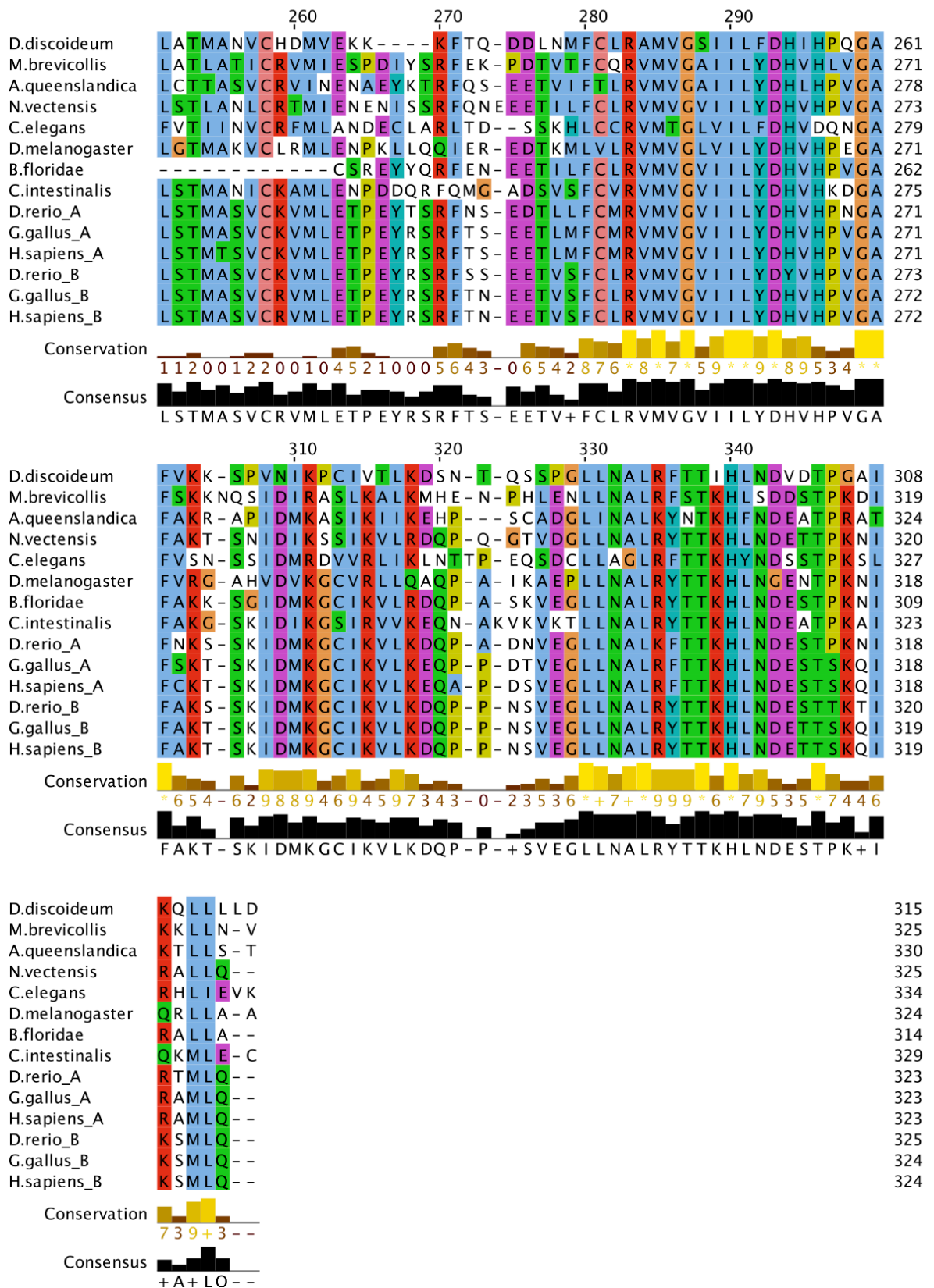(*continues next page*)

Figure 2.2 – Multi-alignment of *D. discoideum* FAM49 and homologs from a choanoflagellate and various metazoans (*continued*)

2.2.2 FAM49 shows prominent sequence similarities with CYFIP in Metazoa and related organisms – the DUF1394 domain

According to the Pfam database of curated protein domains (Finn *et al.*, 2014), putative FAM49 homologs from a wide variety of eukaryotes are predicted to contain a single domain, termed DUF1394 ("Domain of unknown function 1394"; entry PF07159 in Pfam 28.0), which extends through most (usually over 85%) of the sequence of any inspected FAM49 protein - including *D. discoideum* FAM49 and homologs in Metazoa (Table 2.3).

Like all other protein domains in Pfam, DUF1394 is defined by its own profile hidden Markov model (HMM). A profile HMM is a probabilistic model built from, and representative of, a sequence multi-alignment, which it converts into a position-specific scoring system suitable for searching sequence databases for homologies – especially more remote ones –, which may be statistically inferred (Eddy, 1998; Finn *et al.*, 2014). Pfam profile HMMs are generated from so-called "seed" multi-alignments, which incorporate a set of domain-representative sequences defined by curators (Finn *et al.*, 2014). According to Pfam 28.0, the profile HMM of DUF1394 – which is 303 positions in length – was built from a seed alignment of 38 sequences, all from FAM49 homologs in various eukaryotic lineages (Table 5.1 – Appendix B).

Taking into account that FAM49 seems fairly well conserved in eukaryotic evolution (section 2.2.1), it comes as no surprise that DUF1394 is often predicted with very high significance (E-values of profile HMM hits regularly below 1.00E-40) even in FAM49 homologs not included in its profile HMM – such as some of those listed in Table 2.3, e.g. from *Phytophthora infestans*, *Ectocarpus siliculosus* and *H. sapiens*.

Interestingly, the only other major group of proteins predicted to contain DUF1394 comprises known and putative CYFIP/Pir121 homologs. According to Pfam, a single DUF1394 domain is expected to be located near the N-terminus (commonly starting within the first 60 amino acid residues) of CYFIP/Pir121 proteins in numerous eukaryotic species, including *D. discoideum* and all examined metazoans (Table 2.4). CYFIP/Pir121 proteins are regularly between 1200 and 1450 residues in length, meaning DUF1394 may cover only a modest fraction of

their sequence (~16% to ~21% in most analysed cases). It should be noted that E-values for DUF1394 in CYFIP/Pir121 proteins are, on average, much higher than in putative FAM49 proteins: 2.30E-13 in *D. discoideum* CYFIP/Pir121, between 0.05 and 3.40E-08 in the inspected metazoan homologs, and between 3.50E-04 and 1.90E-05 in those from vertebrates (Table 2.4). This indicates that DUF1394-associated sequence similarities between FAM49 and CYFIP/Pir121 proteins are unlikely to be very high. It seems, nevertheless, that some degree of homology might connect FAM49 and CYFIP/Pir121. The fact that no statistically significant DUF1394 profile HMM match occurs in CYFIP/Pir121 homologs from species such as *Trichomonas vaginalis* and *P. infestans* (Table 2.4) could be a consequence of higher CYFIP/Pir121 sequence divergence in those organisms.

To have a more clear idea of the sequence similarities between FAM49 and CYFIP/Pir121 proteins, particularly those from *D. discoideum* and Metazoa up to *H. sapiens*, we generated a multi-alignment with their DUF1394 domains (Figure 2.3). Remarkably, and despite noteworthy global differences, several positions throughout much of the alignment are fully identical (i.e. at a given position, the same amino acid residue is present in all sequences) or highly conservative (i.e. at a given position, different residues are present in one or more sequences but they share many physicochemical properties, as assessed through the conservation score system described in Figure 2.2), some of them concentrating in certain regions (e.g. alignment positions 118-147). We also produced global pairwise alignments between DUF1394 domains of same-species FAM49 and CYFIP/Pir121 homologs, namely those from *D. discoideum* and *H. sapiens*, and obtained identity and similarity percentages of 16.7%-19.0% and 31.5%-35.5%, respectively (Figures 5.5-5.7 - Appendix A).

The sequence similarities we see are intriguing. They do seem substantial and, in our view, suggest an evolutionary link between the FAM49 and CYFIP/Pir121 "families" of proteins. The observation that several residue positions appear to be co-conserved or very conservative in DUF1394 domains from both FAM49 and CYFIP/Pir121 proteins among *D. discoideum* and a number of Metazoa, including *H. sapiens* (Figure 2.3), also hints at the possibility that those proteins might share some structural, functional and/or regulatory features, which could have been under related evolutionary pressures.

According to Chen *et al.*, 2010, the human SCAR/WAVE1 complex likely interacts with active (GTP-bound) Rac1 through a surface in CYFIP1 that partially includes DUF1394 (Figure 2.4). Furthermore, and perhaps more importantly, an earlier study (Kobayashi *et al.*, 1998) shows that truncated human CYFIP1 comprising residues 1-407, and thus containing DUF1394 (Table 2.4), still binds active Rac1 *in vitro* with surprising efficiency (in the absence of any other SCAR/WAVE complex subunits). CYFIP/Pir121 homologs in mice, *Drosophila melanogaster* and *D. discoideum* are also thought to mediate a regulatory interaction between the SCAR/WAVE complex and active Rac1, supposedly in a similar fashion to their human counterparts (Steffen *et al.*, 2004; Kunda *et al.*, 2003; Veltman *et al.*, 2012); this could be expected since both CYFIP/Pir121 and Rac1 appear to be well conserved from *D. discoideum* to *H. sapiens* (Veltman and Insall, 2010; Rivero *et al.*, 2001).

It is therefore conceivable that FAM49 proteins, which might share the required features (e.g. structural motifs) with CYFIP/Pir121 – having perhaps even "improved" them throughout evolution –, are also be able to interact with active Rac1 (and/or related Rho-family GTPases) in certain organisms. Such interaction could, among other possibilities, lead to competition with the SCAR/WAVE complex (by means of steric blockage) and end up having regulatory effects on the activity of both SCAR/WAVE and Rac1. This hypothesis makes it perhaps more difficult to conceptualise a potential interaction between FAM49 and the SCAR/WAVE complex (section 2.1.1), which may nevertheless be indirect and/or occur at slightly different times and/or subcellular locations.

Table 2.3 – Putative FAM49 homologs and corresponding DUF1394 domains in diverse eukaryotes

DUF1394 domains are as defined/predicted by Pfam 28.0 (entry PF07159). "Coverage" specifies the boundaries (positions of the first and last aminoacid residues in the complete protein sequence) and relative size (percentage of complete sequence) of each DUF1394. "E-value" represents the number of different DUF1394 profile HMM matches with a score equal to, or better than, that of a given hit (i.e. listed FAM49 homolog) that would be expected to occur by chance when searching the Pfam sequence database (based on UniProtKB) (Finn *et al.*, 2014). The lower the E-value, the more statistically significant the hit under consideration (i.e. the more likely it is that DUF1394 is indeed present, on the basis of its Pfam-curated profile HMM). Represented non-metazoan species and respective FAM49 homologs are those from Table 2.2, except for *Phytophthora infestans* and *D. discoideum*.

Species	FAM49 homologs			
	UniProt entry	Length (aa)	DUF1394	
			Coverage	E-value
Naegleria gruberi	D2VER1	292	25–267 (83.2%)	2.40E-08
Trichomonas vaginalis	A2E1F1	310	13–306 (94.8%)	3.30E-73
Phytophthora infestans	D0P263	283	3–278 (97.5%)	2.90E-45
Ectocarpus siliculosus	D7G5C5	327	40–322 (86.5%)	1.40E-57
Reticulomyxa filosa	X6MU15	380	30–146 149–375 (91.1%)	0.043 7.3E-28
Acanthamoeba castellanii	L8GXE8	302	36–296 (86.4%)	2.20E-99
Dictyostelium discoideum	Q8T2H0	315	16–309 (93.3%)	4.10E-122
Batrachochytrium dendrobatidis	F4P086	313	19–308 (92.7%)	5.00E-101
Capsaspora owczarzaki	A0A0D2U1D3	323	18–319 (93.5%)	5.90E-130
Monosiga brevicollis	A9UXH2	325	18–320 (93.2%)	3.00E-129
Amphimedon queenslandica (sponge)	I1F5T7	330	18–325 (93.3%)	6.00E-123
Nematostella vectensis (cnidarian)	A7SA43	325	19–321 (93.2%)	7.10E-141
Caenorhabditis elegans (nematode)	Q09387	334	32–328 (88.9%)	1.90E-96
Drosophila melanogaster ("fruit fly")	Q7K1H0	324	22–319 (92.0%)	3.00E-126
Branchiostoma floridae (cephalocordate)	C3Y224	314	18–310 (93.3%)	3.00E-128
Ciona savignyi (tunicate)	H2ZNC1	284 (fragment?)	17–284 (94.4%)	2.20E-107
Danio rerio (zebrafish)	Q7ZW35 (FAM49A)	323	17–319 (93.8%)	5.60E-142
	Q6NYL6 (FAM49B)	325	18–321 (93.5%)	1.20E-142
Gallus gallus (chicken)	Q5ZI04 (FAM49A)	323	17–319 (93.8%)	1.80E-144
	E1BWS3 (FAM49B)	324	18–320 (93.5%)	1.40E-148
Homo sapiens (human)	Q9H0Q0 (FAM49A)	323	17–319 (93.8%)	7.90E-144
	Q9NUQ9 (FAM49B)	324	18–320 (93.5%)	1.30E-148

Table 2.4 – Putative CYFIP/Pir121 homologs and corresponding DUF1394 domains in diverse eukaryotes

DUF1394 domains are as defined/predicted by Pfam 28.0 (entry PF07159). Represented species are the same as in Table 2.3, shown in the same order. For details on "Coverage" and "E-value" see description of Table 2.3. ND – "not detected" (i.e. no DUF1394 profile HMM match scores above the Pfam-defined threshold).

Species	CYFIP/Pir121 homologs			
	UniProt entry	Length (aa)	DUF1394	
			Coverage	E-value
N. gruberi	D2VQD6	1443	50–280 (16.0%)	0.0031
T. vaginalis	several	variable	ND	ND
P. infestans	D0NAC2	1018	20–185 (16.3%)	1.2
E. siliculosus	D7G6Y8	1965	57–275 (11.1%)	0.15
R. filosa	X6MLV7	478 (N-terminal fragment)	30–172 (? %)	0.0044
A. castellanii	L8H6F1	1439	47–299 (17.6%)	5.60E-06
D. discoideum	Q6UK63	1336	57–331 (20.6%)	2.30E-13
B. dendrobatidis	F4NU01	1231	62–315 (20.6%)	5.00E-06
C. owczarzaki	A0A0D2WGK4	1275	62–301 (18.8%)	6.10E-04
M. brevicollis	A9UZ01	1245	54–304 (20.2%)	5.10E-09
A. queenslandica (sponge)	I1FQU7	1200	54–273 (18.3%)	0.05
N. vectensis (cnidarian)	A7S3J0	1332 (fragment?)	354–565 (15.9%)	0.0013
C. elegans (nematode)	O44518	1262	56–288 (18.5%)	3.60E-06
D. melanogaster ("fruit fly")	Q9VF87	1291	58–281 (17.4%)	3.40E-08
B. floridae (cephalocordate)	C3XWM2	1236	57–280 (18.1%)	2.60E-05
C. savignyi (tunicate)	H2YIL6	1256	56–255 (15.9%)	3.50E-06
D. rerio (zebrafish)	Q90YM8 (CYFIP1)	1253	59–281 (17.8%)	3.00E-04
	A5A5E1 (CYFIP2)	1253	59–295 (18.9%)	1.90E-05
G. gallus (chicken)	E1BW56 (CYFIP1)	1254	59–302 (19.5%)	3.20E-04
	F1NE09 (CYFIP2)	1253	59–303 (19.6%)	3.30E-05
H. sapiens (human)	Q7L576 (CYFIP1)	1253	59–301 (19.4%)	3.50E-04
	Q96F07 (CYFIP2)	1278	59–303 (19.2%)	3.50E-05

Figure 2.3 – Multi-alignment of DUF1394 domains from FAM49 and CYFIP/Pir121 homologs in *D. discoideum*, a choanoflagellate and various metazoans (*continues next page*)

DUF1394 domains are as defined/predicted by Pfam 28.0 (entry PF07159). See Table 2.3 (FAM49 homologs) and Table 2.4 (CYFIP/Pir121 homologs) for DUF1394 boundaries in all proteins represented by this alignment. Depicted species are the same as in the alignment in Figure 2.2, except for *C. intestinalis* (not included here). For details on how to interpret this alignment see description of Figure 2.2.
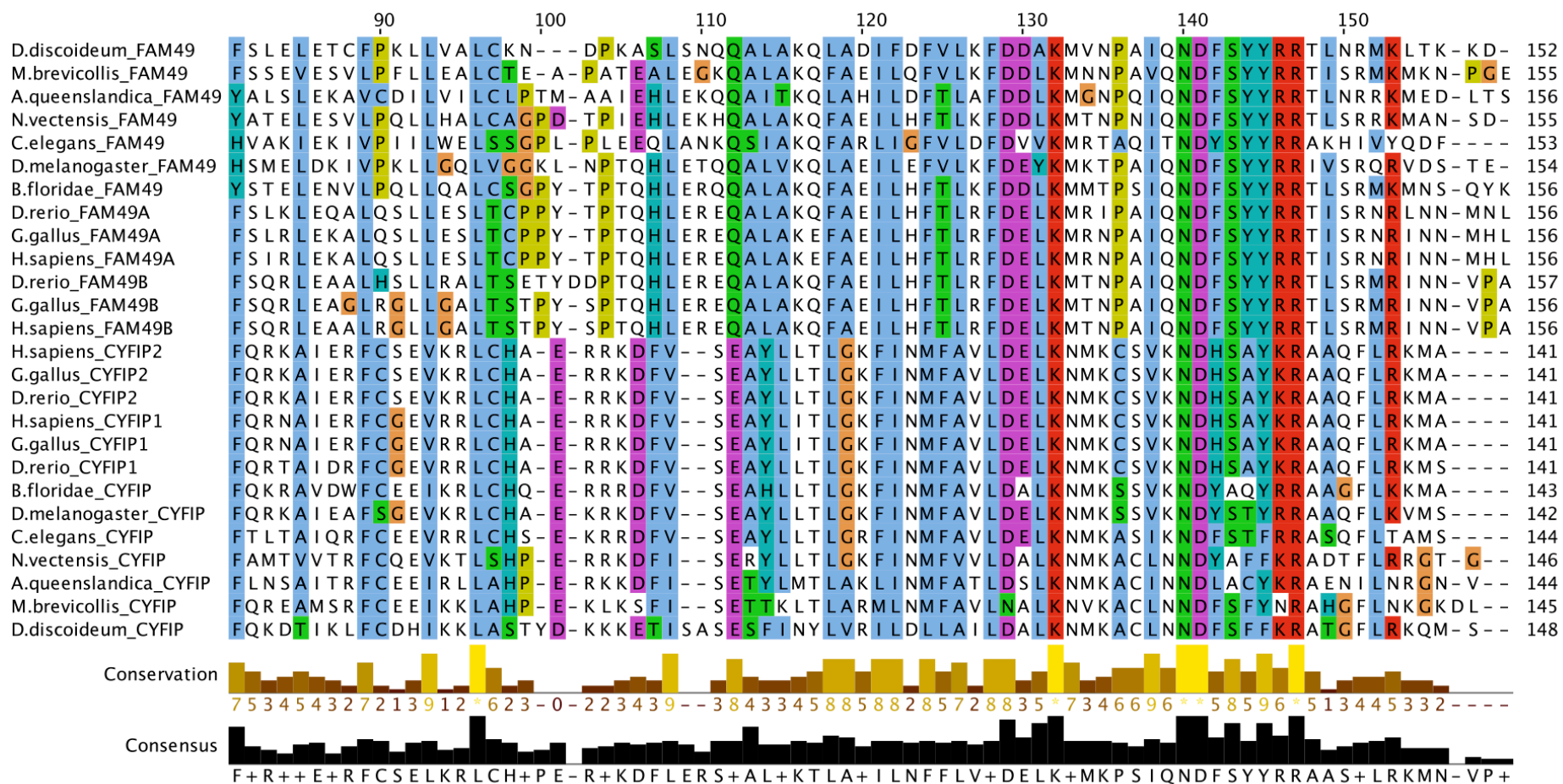
Figure 2.3 – Multi-alignment of DUF1394 domains from FAM49 and CYFIP/Pir121 homologs in _D. discoideum_, a choanoflagellate and various metazoans (continued)
(_continues next page_)

Figure 2.3 – Multi-alignment of DUF1394 domains from FAM49 and CYFIP/Pir121 homologs in *D. discoideum*, a choanoflagellate and various metazoans (continued)
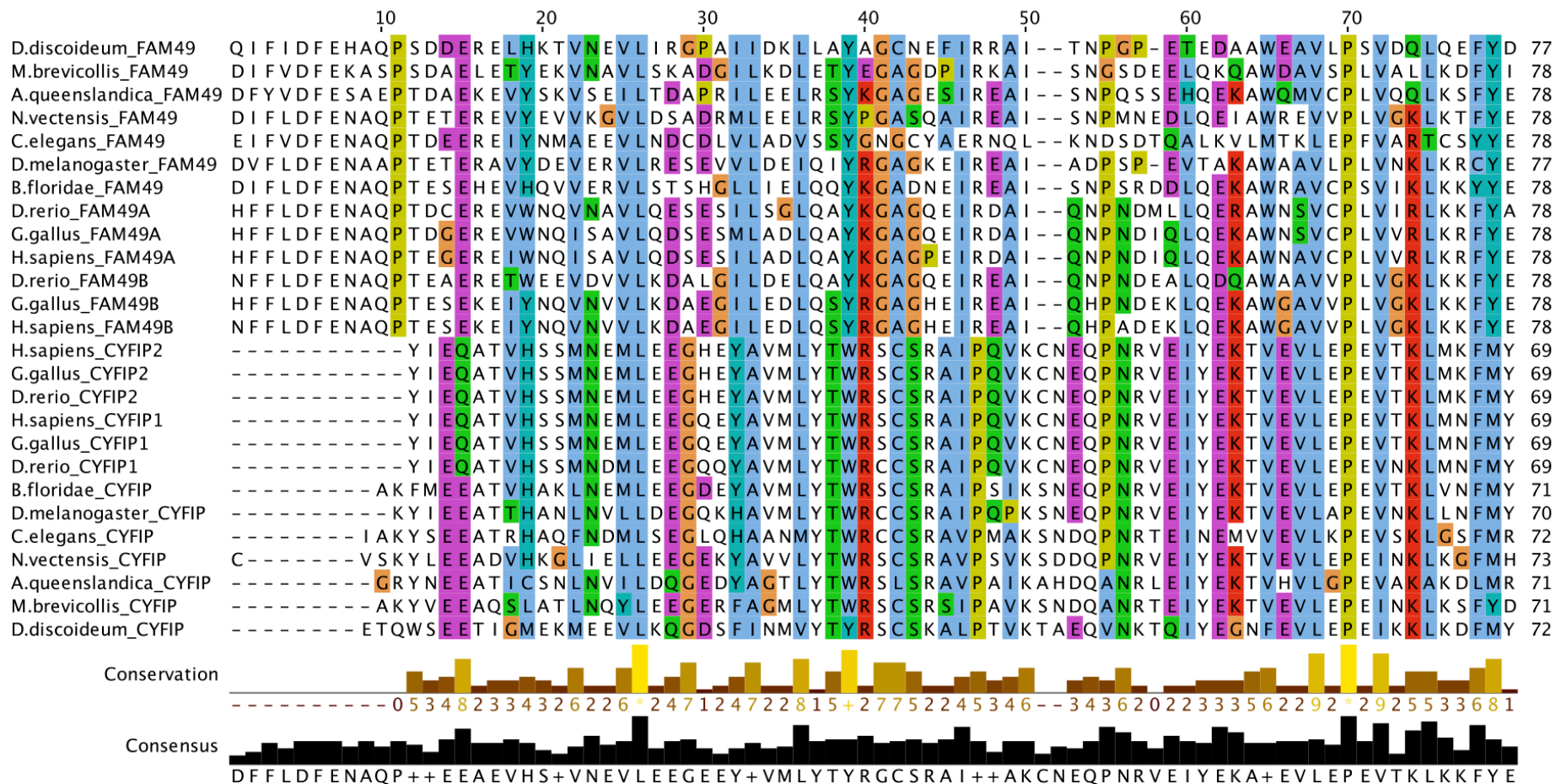(*continues next page*)
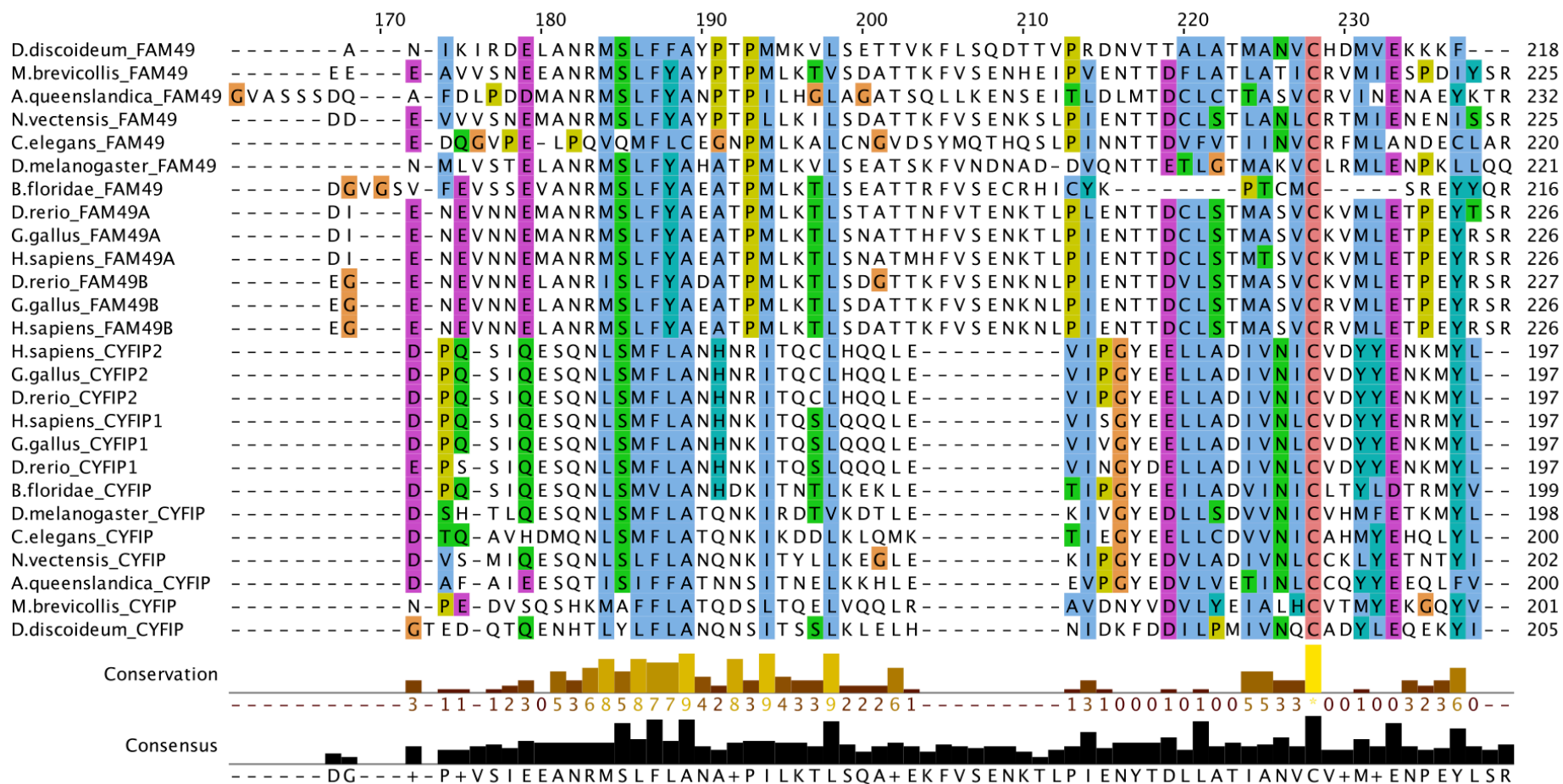
Figure 2.3 – Multi-alignment of DUF1394 domains from FAM49 and CYFIP/Pir121 homologs in *D. discoideum*, a choanoflagellate and various metazoans *(continued)*
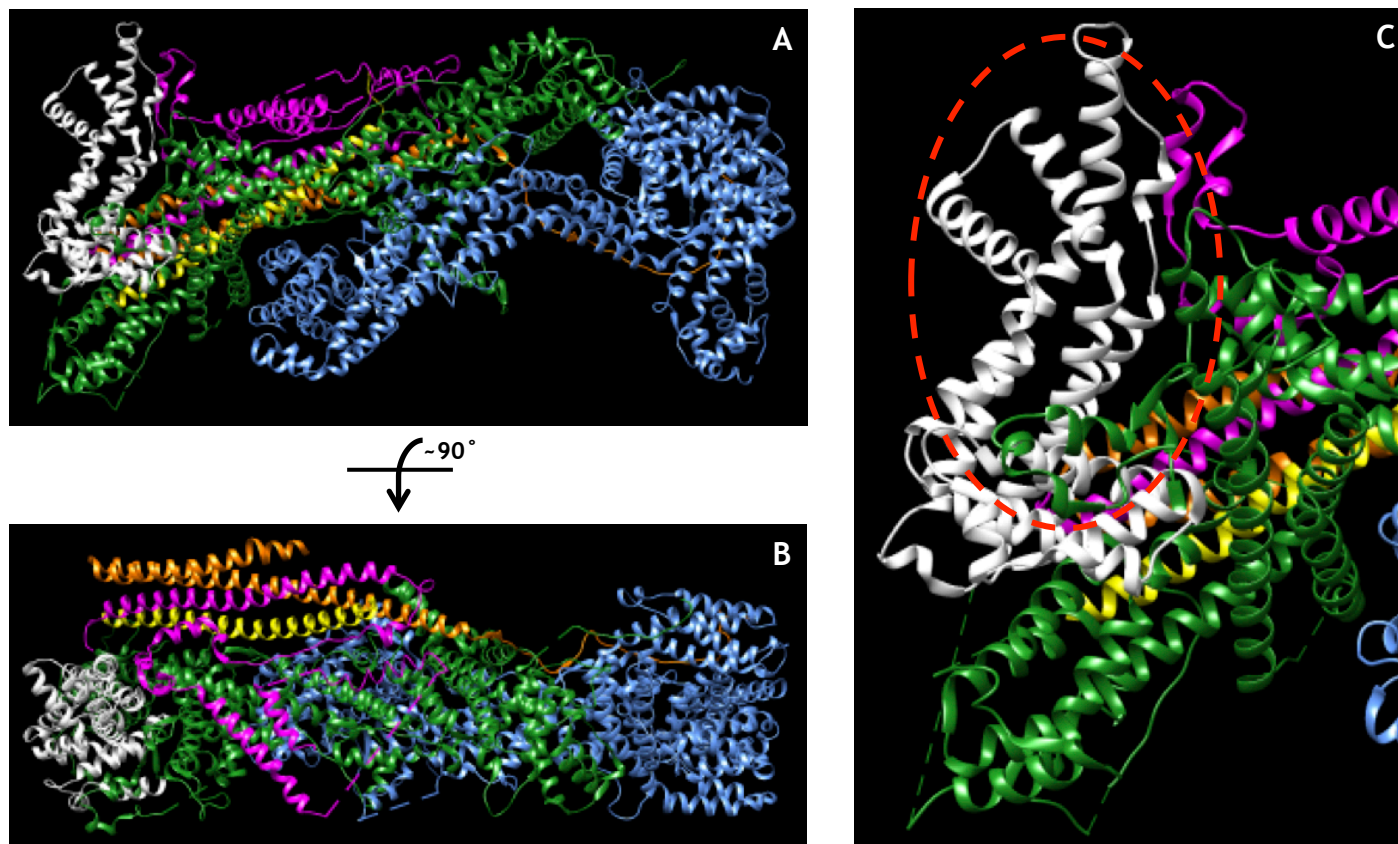
Figure 2.4 – Crystal structure of the human SCAR/WAVE1 complex, highlighting DUF1394 in CIFYP1 and the putative Rac1(GTP)-binding site
A) Ribbon diagram of the human SCAR/WAVE1 complex crystal structure (PDB entry: 3p8c), as published by Chen *et al.*, 2010. This particular view/perspective was obtained through a ~180˚ rotation about a horizontal axis from the perspective shown in Figure 1.1 A (*Introduction* chapter). WAVE1, Abi2, HSPC300, Nap1 and CYFIP1 are shown in magenta, orange, yellow, blue and green/white, respectively. The white region in CYFIP1 corresponds to its predicted DUF1394 (amino acid residues 59−301 – see Table 2.4). **B)** ~90˚ rotation about a horizontal axis from **A**. **C)** Close-up from **A**. The dashed red oval indicates what is thought to be the Rac1(GTP)-binding surface (Chen *et al.*, 2010), which partially comprises DUF1394.

2.2.3 Predicted 3D structure models of FAM49 suggest structural analogies with DUF1394 in human CYFIP1

Computationally predicting a three-dimensional (3D) structure model of a protein for which there is no experimentally determined structure may help gaining insight into that protein's biological function. For instance, predicted models can be structurally matched against annotated structures in the Protein Data Bank (PDB) archive (Rose *et al.*, 2015), which might lead to finding similar fold patterns that hold clues to shared functional features (logically, inferences of this nature require that well-matching PDB structures already have one or more ascribed or predicted functions).

With the above in mind we decided to generate prediction-based 3D structure models of *D. discoideum* FAM49 and human FAM49A and FAM49B. To do so we used the I-TASSER web server (Roy *et al.*, 2010), which has been ranked as one of the best platforms for automated protein structure prediction in recent community-wide critical assessment of structure prediction (CASP) experiments (Cozzetto *et al.*, 2009; Mariani *et al.*, 2011; Huang *et al.*, 2014). Given a query protein sequence, I-TASSER first identifies adequate structural templates in the PDB archive by using an alignment-based, multiple threading approach. It then constructs 3D atomic models from iterative structural assembly simulations based on template segments that align well with the query; for regions of the query lacking suitable templates, *ab initio* modelling is used (Roy *et al.*, 2010). I-TASSER also takes its best predicted 3D model of the query (i.e. the model with the highest confidence score (C-score) among the various models that may be generated; C-score is an estimate of the global accuracy/quality of a structure prediction – see description of Figure 2.5 for more details) and structurally matches it against the proteins in the PDB archive, allowing for structural analogs to be identified.

In all three cases – *D. discoideum* FAM49 and human FAM49A and FAM49B –, I-TASSER considered the crystal structure of human CYFIP1 (Figure 2.4) the best template in the PDB archive – perhaps unsurprisingly. I-TASSER did not disclose, however, if other templates were deemed sufficiently good and consequently used in its prediction-based modelling. The best I-TASSER-generated models of *D. discoideum* FAM49 and human FAM49A and FAM49B are shown in Figure 2.5;

they were estimated to be of fairly good quality overall and probably quite close to the native structures (C-scores between 0.50 and 0.75; estimated "model-against-native structure" TM-scores between 0.78±0.10 and 0.81±0.09; details on each type of score are provided in the description of Figure 2.5). The three models are very alike, suggesting FAM49 might have a well conserved 3D topology. Furthermore, all three models were estimated to be very structurally similar to a region in human CYFIP1 that roughly corresponds to DUF1394 (TM-scores between 0.846 and 0.884; predicted models' coverage between 90.1% and 93%). Interestingly, no other structures in the PDB archive were projected to be nearly as good structural matches/analogs of the models (Figure 2.5).

We also generated a prediction-based 3D model structure of the *D. discoideum* CYFIP/Pir121 homolog (C-score = 0.08; estimated "model-against-native struc-ture" TM-score = 0.72±0.11; model not shown), and as expected it was estima-ted to be very structurally similar to human CYFIP1 over most of its length (TM-score = 0.869; predicted model's coverage = 87.1%, including the DUF1394 domain; structure alignment not shown).

Overall, these results favour the hypothesis of shared structural features (DUF1394-related) between FAM49 and CYFIP/Pir121 proteins in organisms like *D. discoideum* and *H. sapiens*. As stated before, those features could perhaps allow FAM49 to bind active Rac1 in a similar fashion to CYFIP/Pir121.
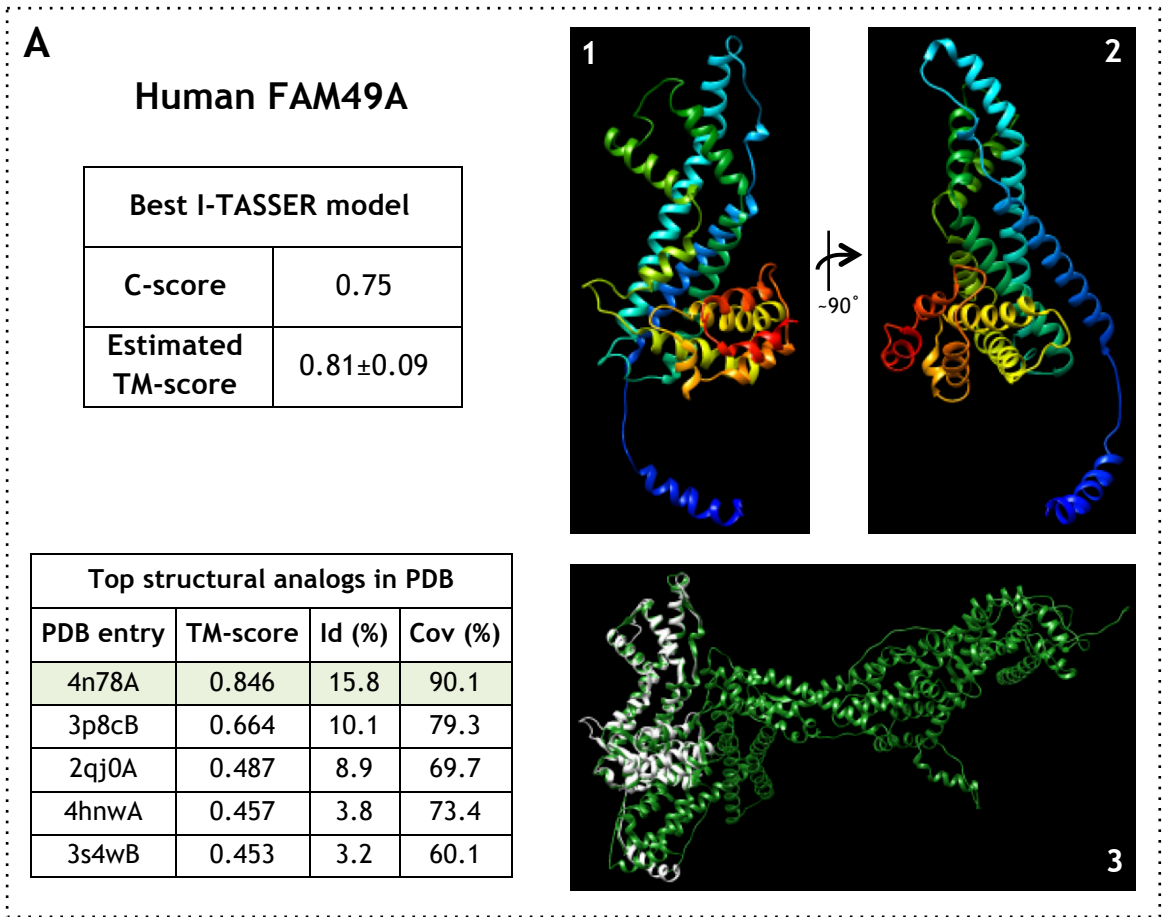
Figure 2.5 – Prediction-based 3D model structures of human FAM49A, human FAM49B and
D. discoideum FAM49 and their structural analogy with human CYFIP1
(continues next page)

A) 1– Ribbon diagram of the best I-TASSER-predicted 3D model structure of human FAM49A
(simply "FAM49A model" for the remaining of this description). Amino acid residues are coloured
according to their position in the sequence; a 5-colour rainbow scheme is used, starting with blue
(N-terminus) and ending with red (C-terminus). **2–** ~90˚ rotation about a vertical axis from **1**. **Top
table–** FAM49A model C-score and estimated 'model-against-native structure' TM-score. "C-score"
(confidence score) is an estimate of the global accuracy/quality of a structure prediction. It is
usually in the range [-5, 2], wherein a higher score reflects an overall better model. Models with
C-score above -1.5 generally have a correct global topology (Roy *et al.*, 2010). "TM-score" (tem-
plate modelling score) is a measure of structural similarity between two protein structures. It takes
values in the range [0, 1], with a higher score denoting a better structural match. A TM-score above
0.5 usually indicates similar topology; the opposite applies if a TM-score is below 0.5 (Xu and
Zhang, 2010; Roy *et al.*, 2010). **Bottom table–** FAM49A model top structural analogs found by
I-TASSER in the PDB archive, on the basis of structure alignments. Shown for each analog are the
TM-score, the percentage of sequence identity in the aligned region (Id %) and the percentage of
FAM49A model sequence covered in the alignment (Cov %). Crystalized human CYFIP1 (PDB
entry: 4n78A; light green row) is by far the best detectable structural analog. Nap1 (PDB entry:
3p8cB), the second best analog and a subunit of the SCAR/WAVE complex like CYFIP1, is known
to be structurally homologous with the latter (Chen *et al.*, 2010) and thus an unsurprising match.
3– Ribbon diagram representing the structure alignment between the FAM49A model (white) and
crystalized human CYFIP1 (green). Note how the model resembles DUF1394 in Figure 2.4.

B and **C** (*next page*) parallel **A** but concern the best I-TASSER-predicted 3D model structures of
human FAM49B and *D. discoideum* FAM49, respectively. The PDB entry 3p8cA, top structural
analog in **B**, also represents crystallised human CYFIP1.

B

Human FAM49B

Best I-TASSER model	
C-score	0.50
Estimated TM-score	0.78±0.10
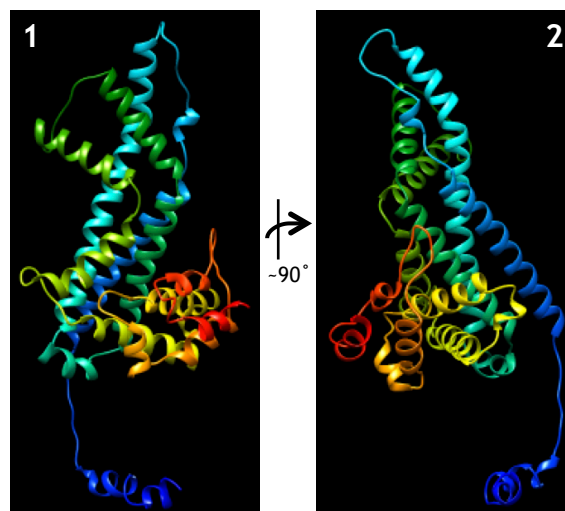
Top structural analogs in PDB			
PDB entry	TM-score	Id (%)	Cov (%)
3p8cA	0.873	17.1	90.4
2qj0A	0.476	9.3	69.1
4hnwA	0.455	5.7	70.7
1yvlB	0.444	6.3	59.6
4d8mA	0.442	4.4	65.1
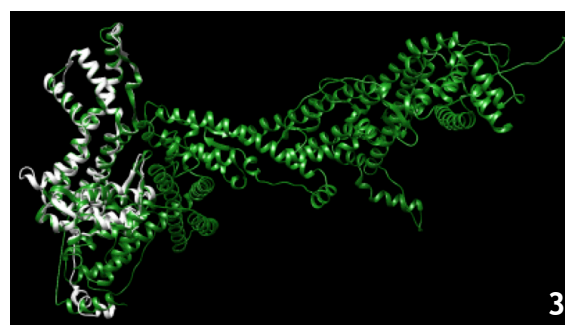
C

D. discoideum FAM49

Best I-TASSER model	
C-score	0.51
Estimated TM-score	0.78±0.10
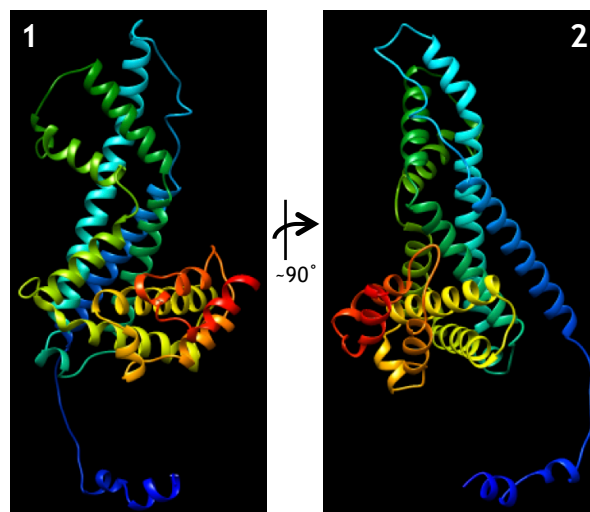
Top structural analogs in PDB			
PDB entry	TM-score	Id (%)	Cov (%)
4n78A	0.884	16.7	93.0
3p8cB	0.676	10.1	81.3
4kf7A	0.492	7.2	69.8
2qj0A	0.483	4.6	67.3
1yvlB	0.469	6.0	63.8
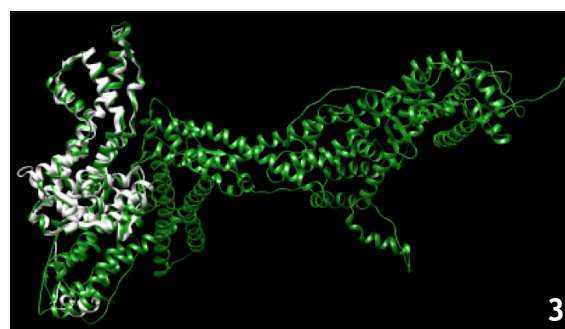
Figure 2.5 – Prediction-based model structures of human FAM49A, human FAM49B and *D. discoideum* FAM49 and their structural analogy with human CYFIP1 *(continued)*

2.3 Assessing the behaviour of GFP-tagged FAM49

2.3.1 GFP-FAM49 is enriched in pseudopods

To obtain some insights into the biological role of FAM49 we first decided to assess its localisation and dynamics in living *D. discoideum* cells. In order to do so we generated expression vectors encoding either an N-terminal or a C-terminal GFP fusion of FAM49 (GFP-FAM49 or FAM49-GFP, respectively), which we transformed individually into Ax3 cells for subsequent fluorescence-based microscopy imaging. Both fusion proteins were confirmed to express with the expected molecular mass in both vegetative and starved cells (Figure 2.6).

We started off by imaging GFP-FAM49 and FAM49-GFP in freely and randomly moving vegetative cells, using laser scanning confocal (LSC; Paddock and Eliceiri, 2014) and total internal reflection fluorescence (TIRF; Mattheyses *et al.*, 2010) microscopies. We could not see an enrichment of either fusion protein in any subcellular structure when using LSC microscopy (not shown); on the other hand, observations with TIRF microscopy hinted at an enrichment of GFP-FAM49, but not FAM49-GFP, in pseudopods (not shown). At this point we opted not to analyse FAM49-GFP any further and centre our attention on GFP-FAM49.

To confirm that GFP-FAM49 is enriched in pseudopods we decided to image it in vegetative cells moving up a chemoattractant gradient under a soft agarose gel (0.4% w/v), using an "under-agarose chemotaxis assay" based on that described by Woznica and Knecht, 2006. Cells moving under agarose are substantially flattened, so a larger proportion of their volume can be visualized – and more cellular processes occur – in the plane of focus; this allows for the localization of fluorescent proteins to be clearer in many instances. Moreover, since chemotaxing *D. discoideum* cells are highly protrusive, imaging of pseudopod-associated proteins is particularly facilitated in an under-agarose context. Much to our satisfaction, we were able to clearly see GFP-FAM49's enrichment in pseudopods of vegetative cells migrating as just described (Figure 2.7 A and B); imaging was performed with spinning-disk confocal (Oreopoulos *et al.*, 2014) and TIRF microscopies (Figure 2.7 A and B, respectively), the second of which provided relatively clearer results due to an often higher contrast between pseudopodial and cytosolic GFP-FAM49 fluorescence. An under-agarose chemotaxis assay and TIRF

microscopy were also employed in order to image GFP-FAM49 in starving cells initiating multicellular development; again, enrichment in pseudopods was observed (Figure 2.7 C).

The imaging experiments described in the previous paragraph also allowed us to notice that GFP-FAM49 is enriched in pseudopods from around the time of their inception (not shown) until they stop extending, at which point GFP-FAM49 is removed (Figure 2.7 B). We did not, however, attempt to determine the exact times of enrichment or removal with respect to pseudopod behaviour.

Assuming GFP-FAM49 localises similarly to its endogenous counterpart[*], our observations suggest that FAM49 has a dynamic role in pseudopods of both vegetative and starved cells.
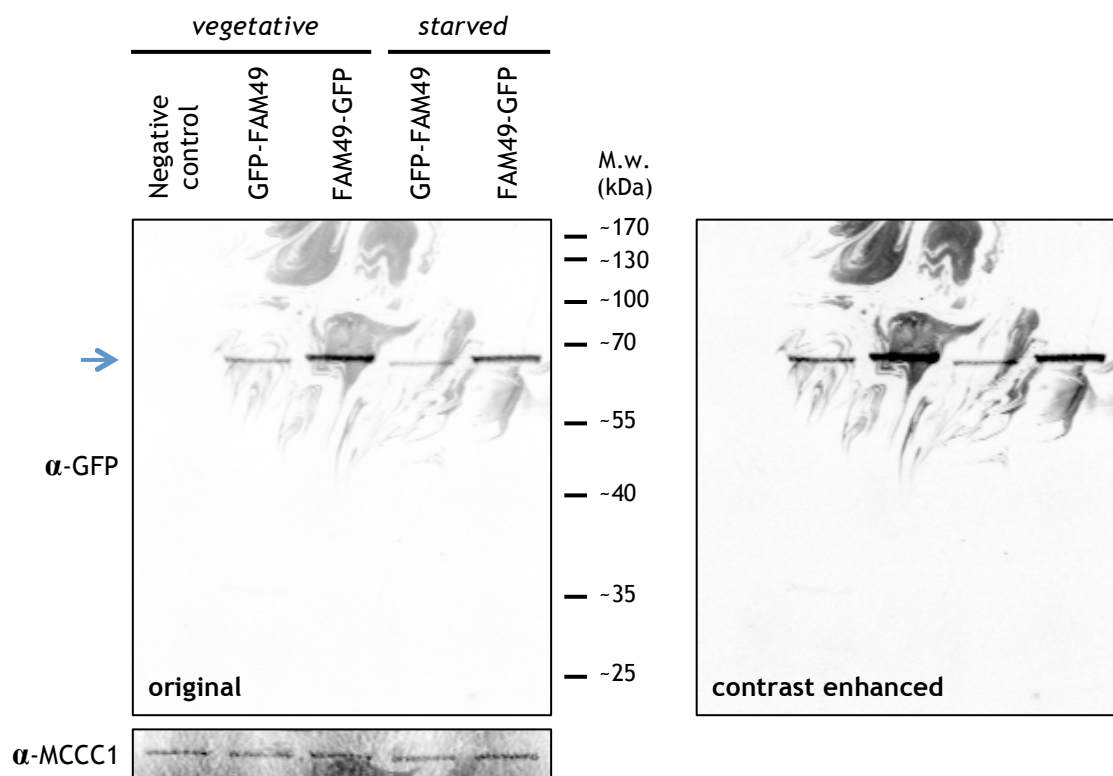
Figure 2.6 – Western blot of GFP-FAM49 and FAM49-GFP expressed in both vegetative and starved Ax3 cells
Whole lysates of cells expressing either GFP-FAM49, FAM49-GFP or no fusion construct (i.e. non-transformed, wild-type Ax3 – negative control) were used. Both fusion proteins were probed for with an anti-GFP antibody. Their single band's position (at the level of the blue arrow) is in agreement with their expected molecular mass – 63,27 and 62,61 kDa, respectively, for GFP-FAM49 and FAM49-GFP. MCCC1 (3-methylcrotonyl-CoA carboxylase α) was used as loading control (Davidson *et al.*, 2013a). A contrast enhanced image of the original blot is shown on the right.

---

[*] Later experiments would show that GFP-FAM49 is at least partially functional, as it rescues some of the phenotype of *fam49* KO cells (section 2.4.3.5). It is therefore plausible that GFP-FAM49 localises in a comparable fashion to endogenous FAM49.
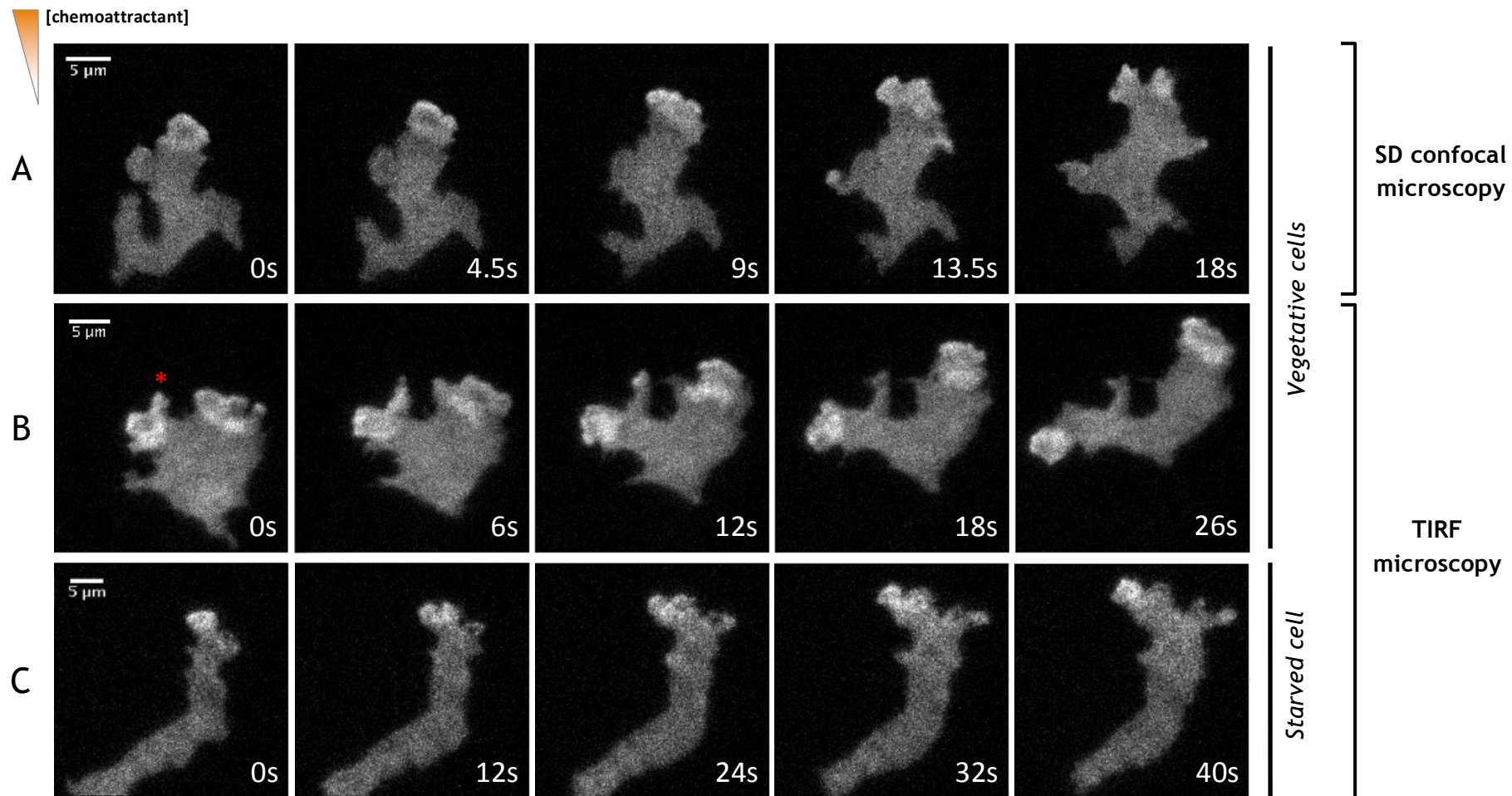
Figure 2.7 – GFP-FAM49 is enriched in pseudopods in both vegetative and starved Ax3 cells
GFP-FAM49 was imaged in cells moving under agarose towards a gradient of chemoattractant – folate in **A** and **B**, used with vegetative cells, and cAMP in **C**, used with starved cells initiating multicellular development. Imaging was performed with a spinning disk confocal microscope in **A** and a TIRF microscope in **B** and **C**. Numbers indicate time in seconds. GFP-FAM49 is clearly enriched in actively extending pseudopods in all cases, being removed when those pseudopods stall; this latter point is well illustrated by the pseudopod below the red asterisk in **B**.

2.3.2 GFP-FAM49 is co-enriched with active Rac and, to a lesser extent, the SCAR/WAVE complex

Seeing that GFP-FAM49 accumulates in pseudopods prompted us to determine if co-enrichment with active Rac and/or the SCAR/WAVE complex takes place, as this would suit the hypothesis – derived from our earlier data (sections 2.1.1, 2.2.2 and 2.2.3) – that FAM49 may interact with one or both. To do so we made vectors for co-expression of either GFP-FAM49 and PakB(CRIB)-RFP or GFP-FAM49 and SCAR-RFP, which we transformed individually into Ax3 cells; TIRF micros-copy was then used for simultaneous imaging of each pair of fluorescent proteins in vegetative cells chemotaxing under agarose. PakB(CRIB), the CRIB domain of *D. discoideum* PakB, interacts strongly with the active forms of Rac1 and closely related Rac GTPases, but not at all with their inactive forms (de la Roche *et al.*, 2005; Rivero *et al.*, 2001); GFP/RFP fusions of such domain can be used as active Rac reporters (Veltman *et al.*, 2012). As for SCAR-RFP, it labels the SCAR/WAVE complex (Veltman *et al.*, 2012).

We were able to observe GFP-FAM49 and active Rac broadly co-enriched throughout pseudopods (Figure 2.8). This co-enrichment seems to take place for as long as pseudopods are actively extending; once they halt, both GFP-FAM49's and active Rac's enrichments cease (Figure 2.8 A and C). We did not attempt to accurately pinpoint and compare GFP-FAM49's and active Rac's times of initial accumulation and later de-enrichment; nonetheless, it appeared to us that GFP-FAM49's removal is finalized slightly earlier (not shown). We appreciate, how-ever, that this may not be the case, as we regularly observed a higher fluores-cence contrast between enriched and non-enriched regions for PakB(CRIB)-RFP, making its images clearer than those of GFP-FAM49.

With respect to GFP-FAM49 and the SCAR/WAVE complex, we saw a much more limited co-enrichment in pseudopods (Figure 2.9). As above, this co-enrichment seems to persist while pseudopods grow (Figure 2.9 A and C); when they stop, both GFP-FAM49 and the SCAR/WAVE complex are removed (not shown). Again, we did not measure the exact times of initial accumulation and removal for either fluorescent protein; we suspect, nevertheless, that GFP-FAM49 and the SCAR/WAVE complex get recruited to, and later removed from, pseudopods at very similar points in time (not shown).
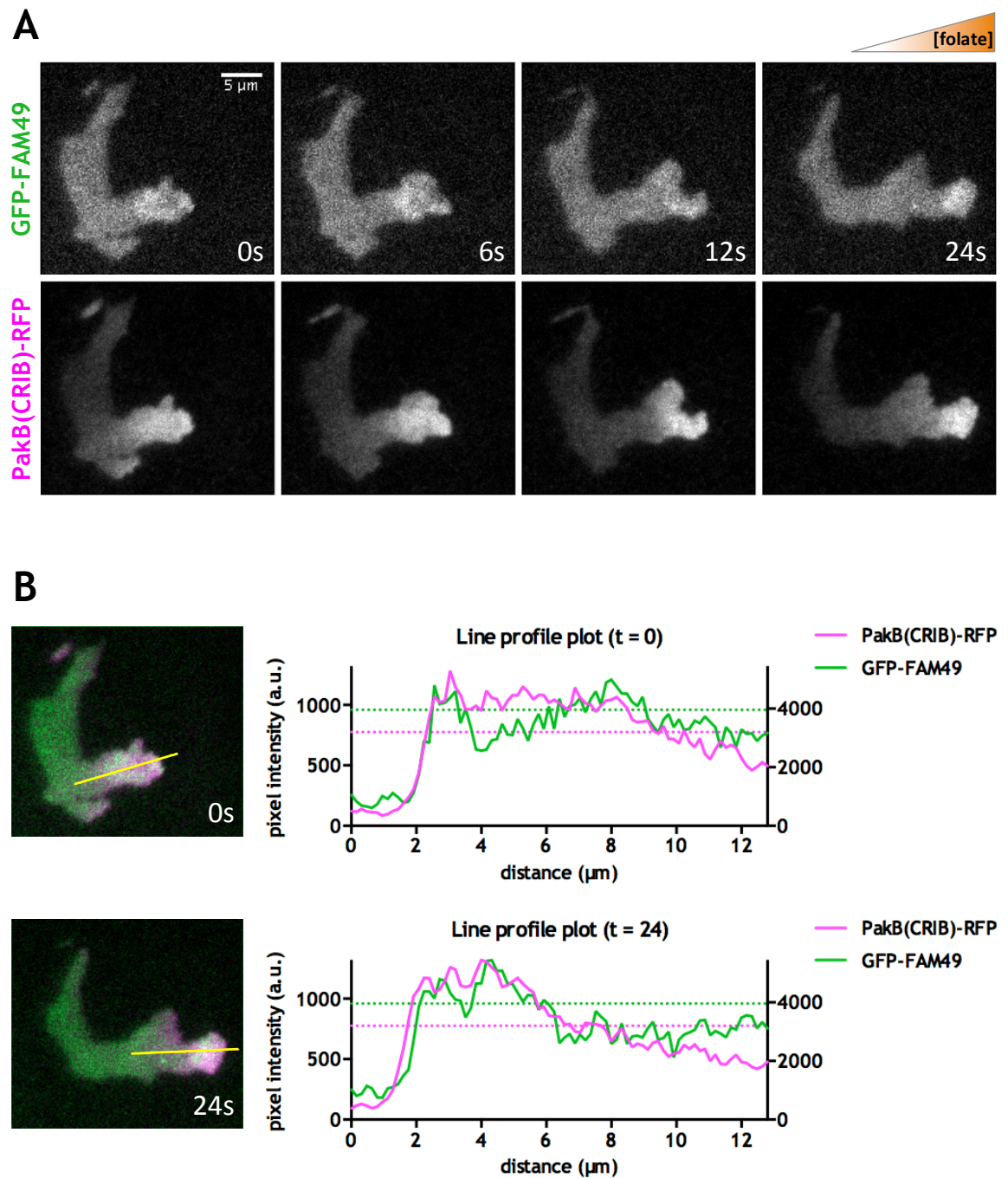
Figure 2.8 – Broad co-enrichment of GFP-FAM49 and active Rac throughout pseudopods *(continues next page)*

A) Simultaneous TIRF microscopy imaging of GFP-FAM49 and PakB(CRIB)-RFP, an active Rac reporter (Veltman *et al.*, 2012), in a vegetative Ax3 cell moving under agarose towards a folate gradient. Numbers indicate time in seconds. **B)** Merged images of GFP-FAM49 (green) and PakB(CRIB)-RFP (magenta) at t = 0s and t = 24s and line profile plots from lines drawn across the cell's leading edge as depicted. In both plots, distance = 0 µm corresponds to the line extremity outside the cell. GFP-FAM49 pixel intensities are plotted on the left *y* axis, while those of PakB(CRIB)-RFP are plotted on the right *y* axis. **C)** Images derived from **A** by thresholding and binary conversion (so as to emphasise enrichment regions), plus merge and co-enrichment (i.e. co-presence of positive binary signal) representations. Applied thresholds are indicated as dotted lines in the plots in **B**.

Figure 2.8 – Broad co-enrichment of GFP-FAM49 and active Rac throughout pseudopods *(continued)*
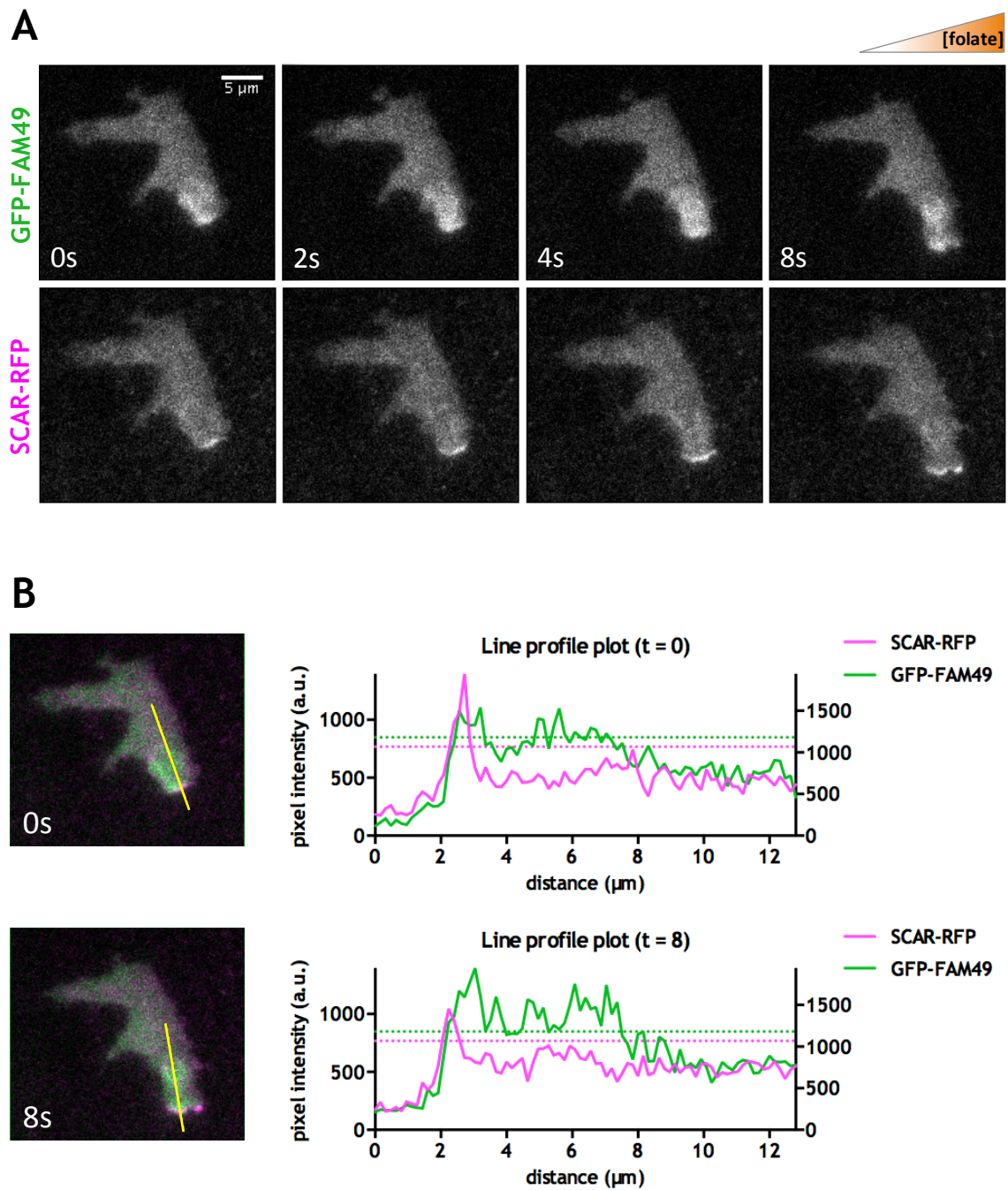
Figure 2.9 – Limited co-enrichment of GFP-FAM49 and SCAR/WAVE complex in pseudopods *(continues next page)*

A) Simultaneous TIRF microscopy imaging of GFP-FAM49 and SCAR-RFP, which labels the SCAR/WAVE complex (Veltman *et al.*, 2012), in a vegetative Ax3 cell moving under agarose towards a folate gradient. Numbers indicate time in seconds. **B)** Merged images of GFP-FAM49 (green) and SCAR-RFP (magenta) at t = 0s and t = 8s and line profile plots from lines drawn across the cell's leading edge as depicted. In both plots, distance = 0 μm corresponds to the line extremity outside the cell. GFP-FAM49 pixel intensities are plotted on the left *y* axis, while those of SCAR-RFP are plotted on the right *y* axis. **C)** Images derived from **A** by thresholding and binary conversion (so as to emphasise enrichment regions), plus merge and co-enrichment (i.e. co-presence of positive binary signal) representations. Applied thresholds are indicated as dotted lines in the plots in **B**.

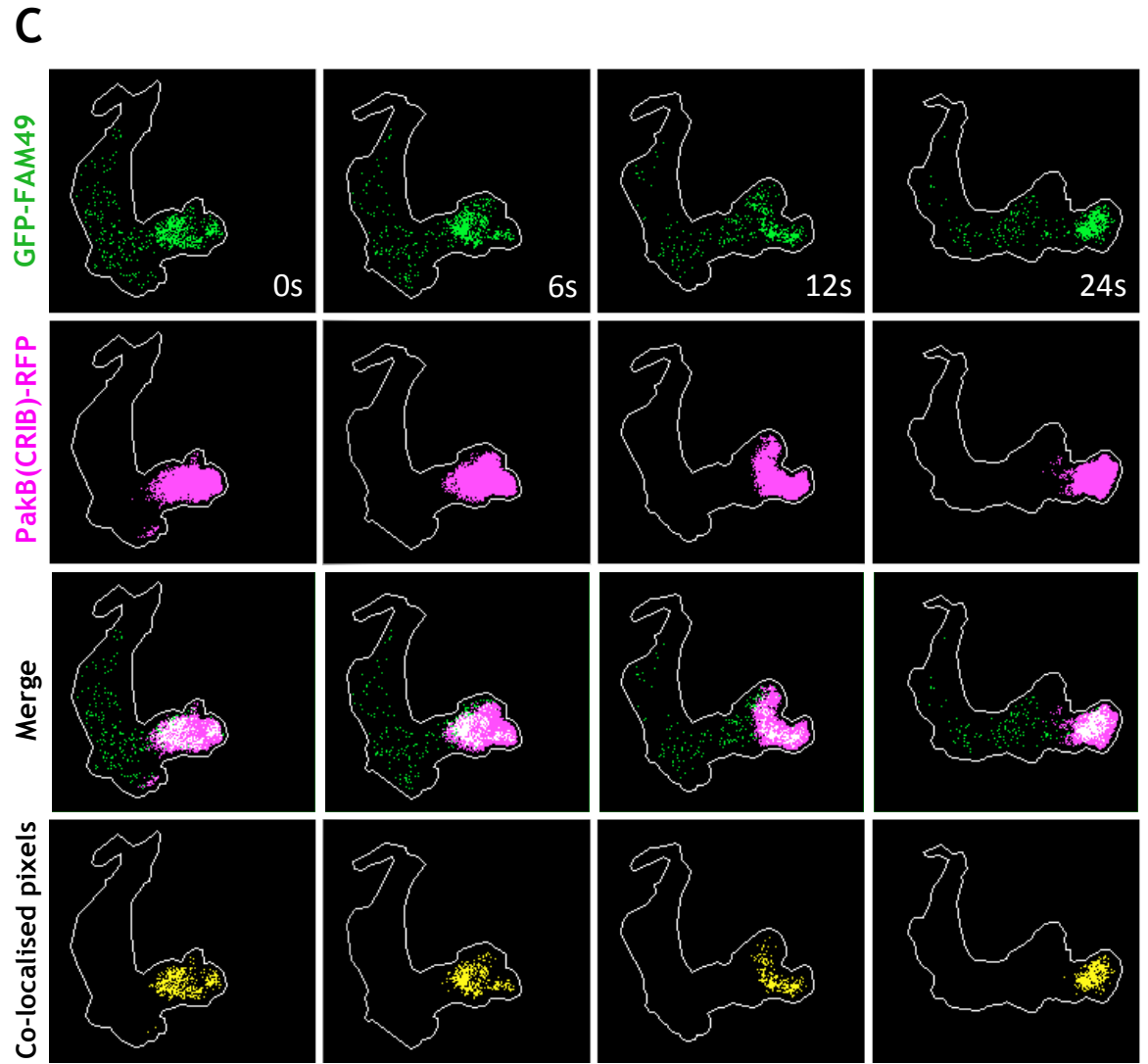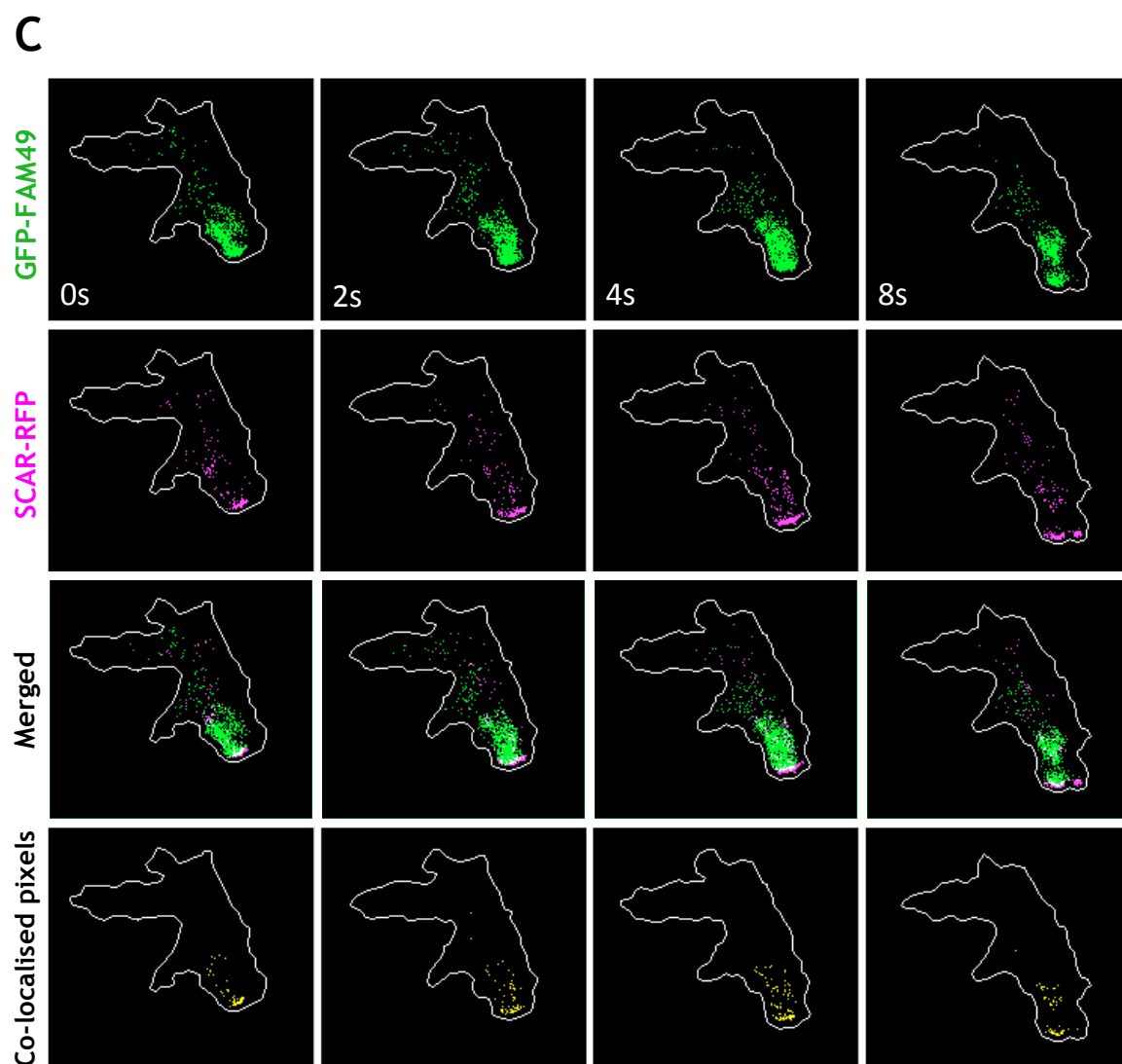**Figure 2.9 – Limited co-enrichment of GFP-FAM49 and SCAR/WAVE complex in pseudopods** *(continued)*

2.3.3 Dominant-active (G12V) Rac1 triggers the recruitment of GFP-FAM49 to the plasma membrane

After observing the broad co-enrichment of GFP-FAM49 and active Rac in pseudopods we decided to perform an additional experiment to further assess the possibility that FAM49 and active Rac may interact in living cells. The experiment in question consisted of inducing the expression of dominant-active (G12V) Rac1 (encoded in a doxycycline-inducible expression vector) in vegetative cells already co-expressing GFP-FAM49 and PakB(CRIB)-RFP (both encoded in another expression vector), then imaging the latter two simultaneously. Upon expression of Rac1 G12V, and unlike in normal circumstances, cells tend to show an accumulation of active Rac all around their periphery – this can be demonstrated by imaging a GFP/RFP fusion of PakB(CRIB), which becomes widely enriched at the plasma membrane (Veltman *et al.*, 2012). We hypothesised that if FAM49 binds active Rac, then it too should get recruited to the plasma membrane in response to Rac1 G12V.

A few hours after inducing the expression of Rac1 G12V in our cells we did indeed observe both active Rac and GFP-FAM49 persistently enriched at the plasma membrane (Figure 2.10). Co-enrichment was clear; however, we most often observed a rather uniform accumulation of active Rac all around the cell along with a more restricted, and apparently polarised, accumulation of GFP-FAM49 (Figure 2.10 A). Global, or nearly so, co-enrichment was seen less frequently (Figure 2.10 B). Addition of doxycycline to cells containing only the vector for co-expression of GFP-FAM49 and PakB(CRIB)-RFP did not affect their behaviour.

These results strongly suggest that active Rac can trigger the recruitment of FAM49 to the plasma membrane, perhaps doing so within pseudopods. It seems, however, that active Rac by itself might not be able to promote such recruitment and/or retain FAM49 at the membrane, and that additional factors might play a role in controlling FAM49's behaviour. Regardless, our observations are in line with the hypothesis that FAM49 and active Rac may interact in living cells.
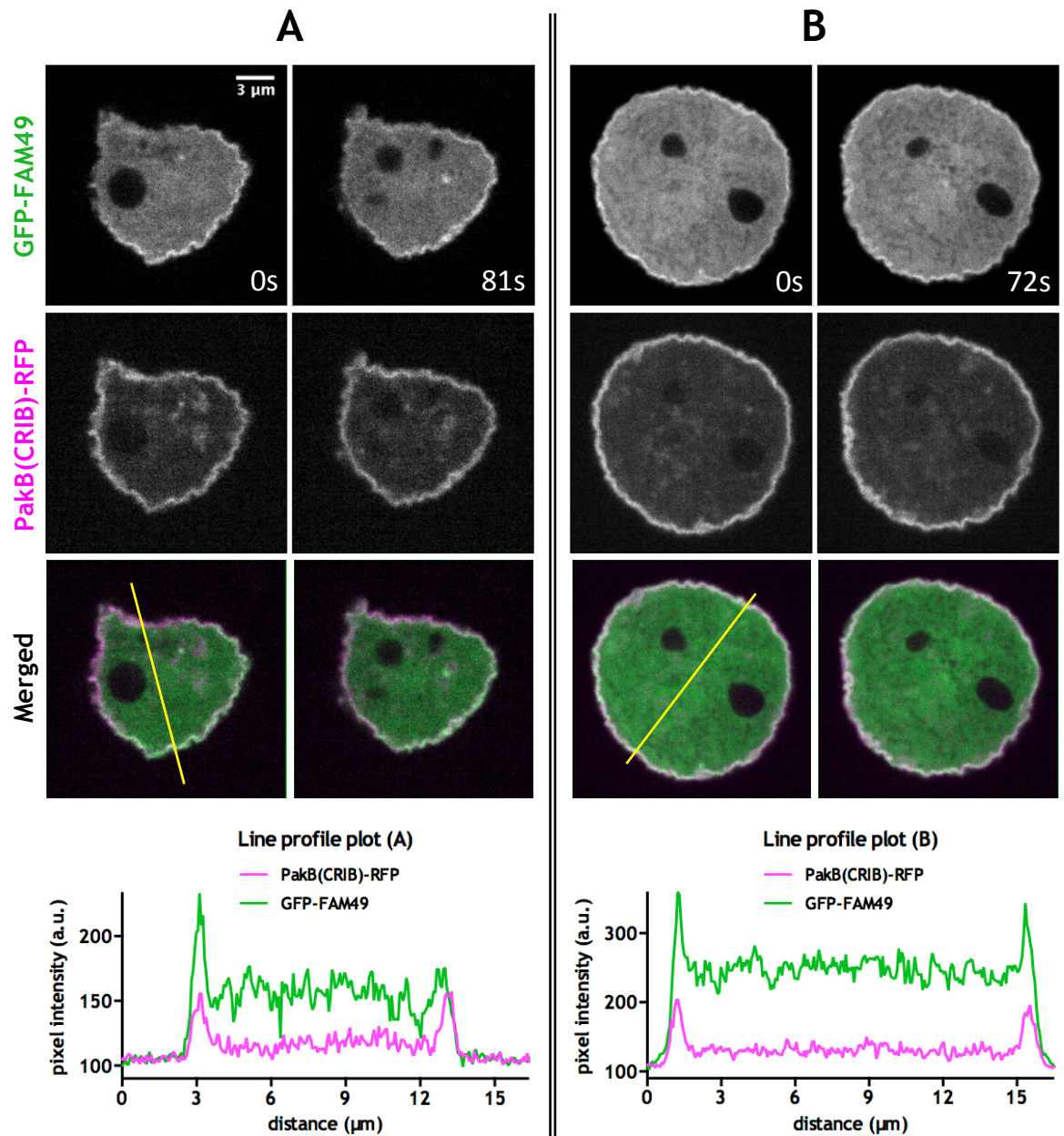
Figure 2.10 – Co-enrichment of GFP-FAM49 and active Rac at the plasma membrane upon expression of dominant-active (G12V) Rac1
GFP-FAM49 and PakB(CRIB)-RFP (an active Rac reporter) were imaged simultaneously in vegetative Ax3 cells after inducing the expression of Rac1 G12V for 2 to 3 hours. Imaging was performed with a spinning-disk confocal microscope. **A)** Cell at two points in time, 81 seconds apart. It is clear that GFP-FAM49 and active Rac become extensively and rather persistently co-enriched at the plasma membrane; however, while active Rac accumulates fairly evenly all around the cell, GFP-FAM49 displays a more restricted and seemingly polarised distribution. **B)** Another cell, also at two points in time (72 seconds apart), exhibiting a more extreme behaviour whereby GFP-FAM49 and active Rac become largely co-enriched. This scenario was observed less often.

2.3.4 GFP-FAM49 is still enriched in pseudopods in the absence of the SCAR/WAVE complex

As shown earlier, GFP-FAM49 and the SCAR/WAVE complex display a rather limited, yet perhaps meaningful, co-enrichment in pseudopods. As with active Rac, and again due to time restrictions, we did not attempt to confirm the potential direct interaction between FAM49 and the SCAR/WAVE complex; we did, nonetheless, start to investigate some potential links, functional and regulatory, connecting FAM49 and SCAR/WAVE – our findings are presented here (section 2.3.4) and in parts of section 2.4.

To determine if FAM49's recruitment to pseudopods requires the SCAR/WAVE complex, we imaged GFP-FAM49 in vegetative *napA* KO cells chemotaxing under agarose. These cells lack Nap1 and for such reason do not possess a functional SCAR/WAVE complex (Ibarra *et al.*, 2006); their pseudopods appear to be driven by WASP A (Veltman *et al.*, 2012). Perhaps unsurprisingly, we could still see GFP-FAM49 enriched in pseudopods in *napA* KO cells (Figure 2.11). This indicates that the SCAR/WAVE complex is not necessary for FAM49 to be recruited to such sites and that other factors are (or can be) involved. We also did not notice any abnormal accumulation of GFP-FAM49 in places other than pseudopods (not shown).

Following the above observation we thought of comparing the spatio-temporal dynamics of GFP-FAM49's recruitment to, and removal from, pseudopods in *napA* KO cells and wild-type cells. We decided, however, to shelve (and ultimately not perform) such analysis because *napA* KO cells and wild-type cells differ in their protrusive behaviour (the former reportedly generate smaller pseudopods; Ibarra *et al.*, 2006) and probably also in their pseudopod-associated active Rac levels (likely to be abnormally increased in the former; Veltman *et al.*, 2012), meaning any potential differences in the above-mentioned aspects of GFP-FAM49's behaviour cannot be interpreted straightforwardly and certainly not deemed a *direct* consequence of the presence/absence of the SCAR/WAVE complex (at least not so without suitable further evidence, which we did not obtain). Using cells KO for other subunits of the SCAR/WAVE complex would pose a similar problem for analogous reasons (Blagg *et al.*, 2003; Pollitt and Insall, 2008; Pollitt and Insall, 2009).

We also did not compare *napA* KO cells and wild-type cells for GFP-FAM49 enrichment levels in pseudopods, arguably a more pertinent analysis. Considering, as stated above, that *napA* KO cells probably have higher-than-wild-type levels of active Rac in pseudopods (Veltman *et al.*, 2012) and assuming active Rac can trigger FAM49's recruitment to such sites (section 2.3.3), we could expect to see a higher enrichment of GFP-FAM49 in pseudopods of *napA* KO cells compared to wild-type. Future experiments using confocal microscopy will be needed for such assessment.
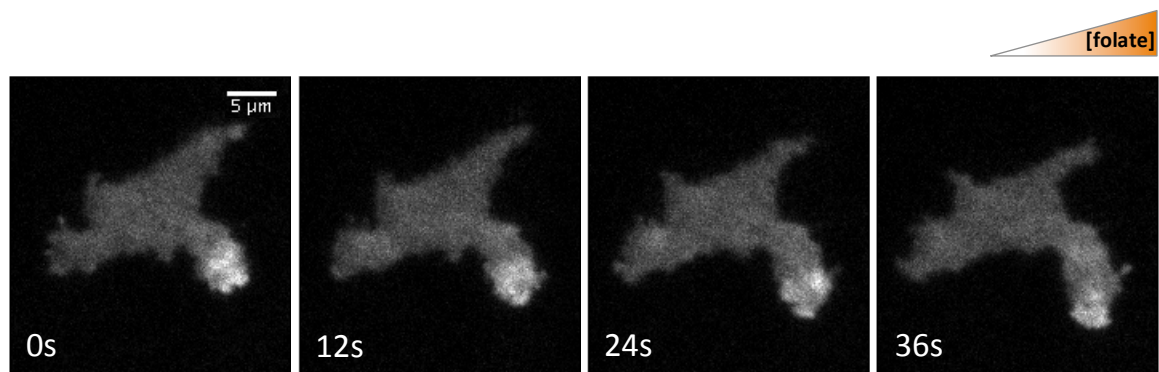
Figure 2.11 – GFP-FAM49 is still enriched in pseudopods in the absence of the SCAR/WAVE complex
TIRF microscopy imaging of GFP-FAM49 in a vegetative Ax3-based *napA* KO cell – which lacks a functional SCAR/WAVE complex (Ibarra *et al.*, 2006) – moving under agarose towards a folate gradient. Numbers indicate time in seconds.

2.4 Generation of *fam49* KO cell lines and analysis of their phenotype

2.4.1 Generation and validation of *fam49* KOs in Ax2 and Ax3 genetic backgrounds

After making use of GFP-FAM49 for obtaining some clues on the function and regulation of FAM49 in living cells (section 2.3) we decided to generate *fam49* KO cell lines and analyse their phenotype, so as to further elucidate FAM49's role and assess its biological relevance. The strategy we followed in order to create and validate *fam49* KOs is illustrated in Figure 2.12 and briefly described in its legend (further details are provided in the *Materials and Methods* chapter). We were able to produce a number of independent KO clones, both in Ax2 and in Ax3 genetic backgrounds, of which some were used for phenotypic studies (as detailed below). It is now known that *D. discoideum*'s axenic strains Ax2 and Ax3 – which were isolated independently and by different methods a few decades back (Watts and Ashworth, 1970; Loomis, 1971) – show some differences at the genomic level (Eichinger *et al.*, 2005; Bloomfield *et al.*, 2008), which may underlie strain-specific traits. Perhaps the most relevant of those differences involves an inverted ~1.5 megabase duplication (containing 608 genes) in chromosome 2, which is present in Ax3 but absent from Ax2 (Eichinger *et al.*, 2005).

2.4.2 Preliminary phenotypic analysis of *fam49* KOs

We started off the phenotypic analysis of *fam49* KOs with preliminary assessments of: population growth in HL5 (in suspension) and on live bacteria (on agar); multicellular development on agar; strength of cell adhesion to plastic (as probe for general defects in cell-substrate adhesion); and cell behaviour in an under-agarose chemotaxis assay (as probe for defects in various aspects of cell motility, including protrusion dynamics). Two independent *fam49* KO clones of each genetic background were examined: Ax2-based KO clones "32" and "111", and Ax3-based KO clones "1" and "3" (Figure 2.12 B and C, respectively) – such designations are used throughout this section (2.4.2). We chose to analyse *fam49* KOs in both genetic backgrounds so as to ascertain which, if any, phenotypic traits/defects could be strain-specific (and therefore not particularly thril-

ling) and which could more safely be assumed to be species-wide (and thus more worthy of further consideration). Moreover, scrutinising at least two KO clones from each background was, we considered, necessary for more solid preliminary results.

As described later in this section (point 2.4.2.5), our preliminary data on cell motility and protrusive behaviour turned out to be of particular interest to us, as it strongly hinted at defects in *fam49* KO cells (of both genetic backgrounds) which were in line with our working hypothesis that FAM49 has a role in pseudo-pods and might be functionally linked to Rac1 and/or the SCAR/WAVE complex. We therefore decided, after the preliminary assays described in this section, to perform follow-up experiments to verify some protrusion-related attributes and other motility parameters of *fam49* KO cells; such experiments comprise the remainder of this thesis (section 2.4.3). Due to time constraints, other phenotypic traits were not investigated further.
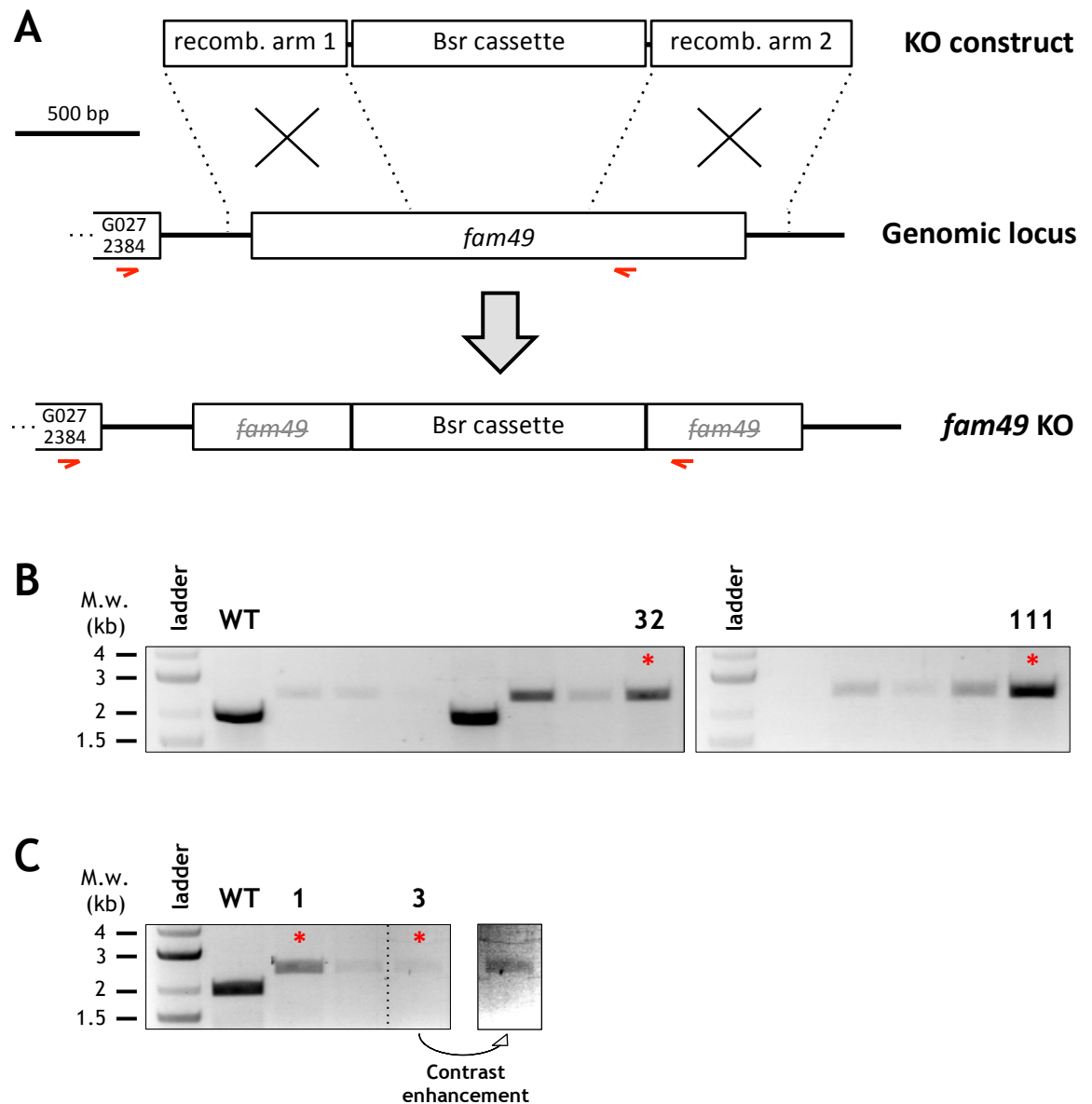
Figure 2.12 – Generation and validation of *fam49* KO cell lines in Ax2 and Ax3 genetic backgrounds
A) Scaled diagram illustrating how *fam49* KO cell lines were generated and validated. Briefly, Ax2 and Ax3 cells (wild-type) were transformed with a linear, blasticidin resistance (Bsr) cassette-containing KO construct which, by means of a double homologous recombination event at the *fam49* gene locus (represented by the two big crosses), would disrupt that gene. Clones obtained after blasticidin selection were screened/validated by PCR, using primers targeted at the sites indicated by the red half-headed arrows. While real *fam49* KOs would yield a 2450 bp PCR product, random integrants (clones with a KO construct integration elsewhere in the genome) and wild-type cells would produce a 1983 bp PCR product instead. **B)** Screening/validation PCR results of some Ax2-derived clones. Clones 32 and 111 (red asterisks) were considered real KOs and selected for phenotypic analysis. "WT" = wild-type. **C)** Screening/validation PCR results of some Ax3-derived clones. Clones 1 and 3 (red asterisks) were considered real KOs and selected for phenotypic analysis.

2.4.2.1 Population growth in HL5 (in suspension)

To determine if *fam49* KO cells have growth defects we first monitored their population growth in HL5 (rich liquid medium, traditionally used for culturing axenic strains of *D. discoideum* – Fey *et al.*, 2007) using shaking suspension cultures, a practical and common alternative to stationary dish cultures (Fey *et al.*, 2007).

As illustrated in Figure 2.13 A and B (graphs on the left), we recorded much slower growth rates for *fam49* KO cells (all clones, both genetic backgrounds) in comparison to wild-type cells. We also noticed, by means of monitoring average cell diameters (Figure 2.13 A and B, graphs on the right) in addition to cell densities, that Ax3-based (but not Ax2-based) *fam49* KO cells would get substantially bigger, over time, than wild-type cells (see also Figure 2.13 C).

Although we did not measure the population growth of *fam49* KO cells in HL5 dish cultures (where cells grow attached to a substrate, as opposed to permanently suspended), we suspect – on the basis of frequent eye inspections of such cultures – it is less affected than in shaking suspension cultures. Moreover, the average size of Ax3-based *fam49* KO cells grown in dish cultures is kept close to that of wild-type cells (Figure 2.13 B, graph on the right – compare data points at t = 0 h, when cells had just been collected from dish cultures to start shaking suspension cultures).

While very preliminary, our observations lead us to speculate that *fam49* KO cells might show substantial defects in myosin II-dependent cytokinesis (so-called cytokinesis A – Zang *et al.*, 1997), which is required for *D. discoideum* cells to divide in suspension. The increased size Ax3-based KO cells develop in suspension is particularly suggestive of problems with such type of cytokinesis (Uyeda *et al.*, 2000; Dumontier *et al.*, 2000; Pollitt and Insall, 2008). It might be that myosin II-independent, adhesion-dependent forms of cytokinesis (cytokinesis B and C – Zang *et al.*, 1997; Uyeda *et al.*, 2000) are also somewhat affected in *fam49* KO cells, which could translate into growth defects on dish.

It is appropriate to stress that the above considerations are merely speculative – again, we did not quantify growth in dish cultures, nor did we perform follow-up

experiments to specifically assess faults in cytokinesis (e.g. comparing *fam49* KO and wild-type cells with respect to nuclei numbers and morphological dynamics during division).

We would like to add, as a final note on the point of cytokinesis, that both Rac1 and SCAR/WAVE seem to be involved in its regulation. Whereas the former is thought to play a role in myosin II-dependent cytokinesis (cells overexpressing constitutively activated or constitutively inactivated Rac1 become highly or moderately multinucleate, respectively, when grown in shaking culture, but such outcome is not observed in dish cultures – Dumontier *et al.*, 2000), the latter has been proposed to be of major importance for myosin II-independent, adhesion-dependent cytokinesis (cells KO for SCAR/WAVE are impaired in cytokinesis B and C – King *et al.*, 2010).
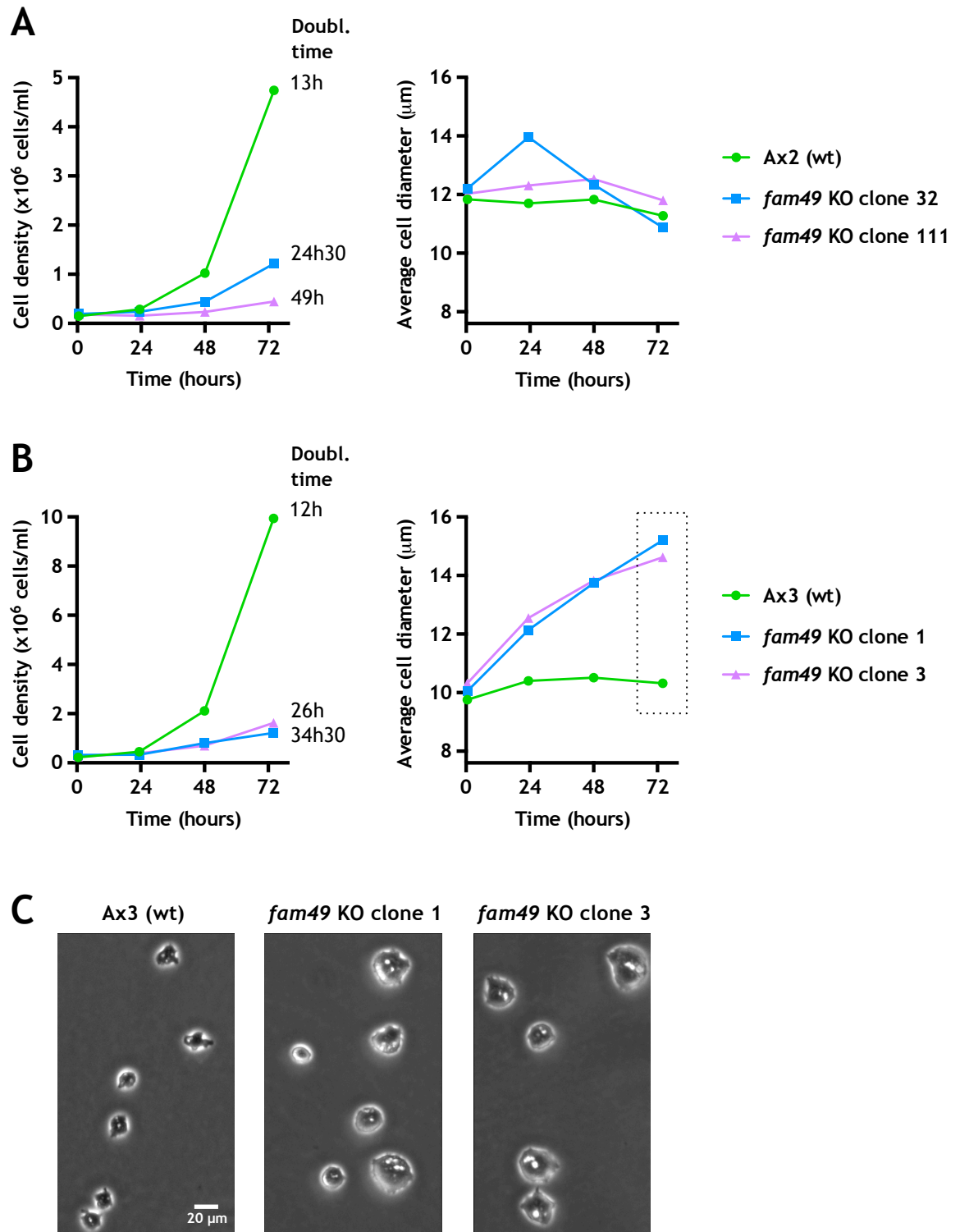
Figure 2.13 – *fam49* KO cells show a growth defect in HL5 in shaking suspension
A) Ax2 and Ax2-derived *fam49* KO clones 32 and 111 were grown in HL5 culture medium in shaking suspension for approximately 3 days, during which time their cell density and average cell diameter were monitored. "Doubl. time" = average population doubling time. **B)** Ax3 and Ax3-derived *fam49* KO clones 1 and 3 were grown and monitored as in **A**. **C)** Phase contrast microscopy images of cells from **B**, recorded at the last timepoint (74h – dotted box in **B**) after cell seeding on dish. Clearly, Ax3-derived *fam49* KO cells become substantially bigger than wild-type cells.

2.4.2.2 Population growth on live bacteria (on agar)

We also assessed the growth of *fam49* KO cells on live bacteria, *D. discoideum*'s natural food source. When in HL5 or other nutrient liquid media, axenic strains of *D. discoideum* feed mostly, if not uniquely, by macropinocytosis (Hacker *et al.*, 1997); growth on bacteria entails a different strategy – *D. discoideum*'s strategy in the wild –, phagocytosis (Hacker *et al.*, 1997; Cardelli, 2001).

To test growth on bacteria we seeded low numbers of vegetative cells in lawns of bacteria (*Klebsiella aerogenes*) on top of agar plates, then monitored the appearance and expansion of colonies. As depicted in Figure 2.14, *fam49* KOs (all clones, both genetic backgrounds) generated smaller colonies than their respective wild-types, a result suggesting that the former have slower population growth rates. Differences in colony size were particularly clear between Ax3-based *fam49* KO clones and their parental cell line.

In theory, the apparent growth defect *fam49* KO cells display on bacteria could be a consequence of deficient cytokinesis, which we already alluded to as a conceivable explanation for their also slower growth in HL5 cultures. Alternatively (or concurrently), *fam49* KO's phenotype on bacteria could be an outcome of less efficient phagocytosis. We feel compelled to speculate such scenario because phagocytosis, like cytokinesis, is thought to be modulated by Rac1 (Dumontier *et al.*, 2000) and the SCAR/WAVE complex (Seastone *et al.*, 2001), and the concept of a regulatory link with FAM49 is, we think, not a far-fetched one.

We did not investigate the phagocytic ability of *fam49* KO cells during the course of our research but suspect, taking into account later results, that it may well be affected; we discuss this point further in the final *Discussion* chapter.
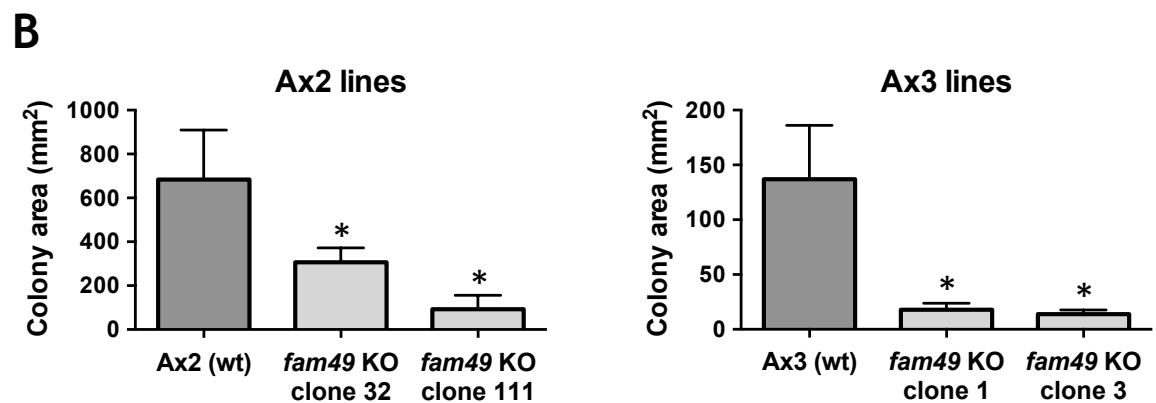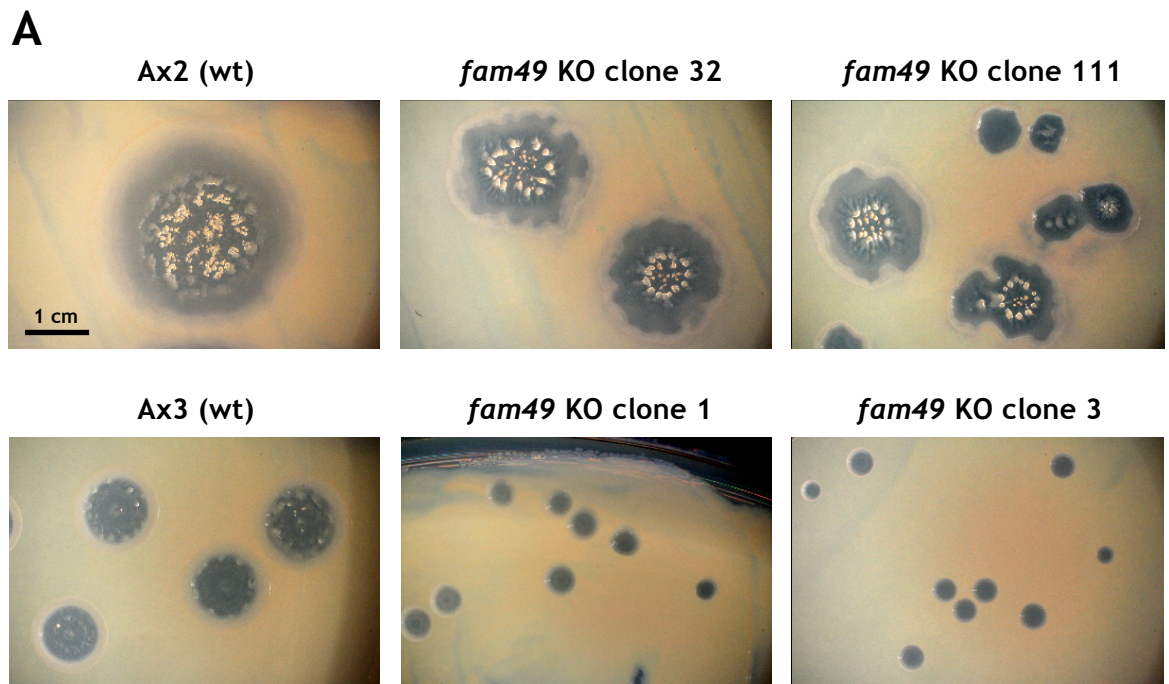
Figure 2.14 – *fam49* KO cells show a growth defect in bacteria lawns
Wild-type and *fam49* KO cell lines were grown in bacteria (*Klebsiella aerogenes*) lawns on SM agar plates for 6 days, at which point the plates were photographed. Colonies expected to originate from single cells were observed in all cases. **A)** Examples of colonies. **B)** Quantification of colony areas. Plotted values are the mean of at least 18 colonies; error bars represent one standard deviation. The mean colony area of each and every KO cell line is significantly different from that of the corresponding wild-type (*$p < 0.0001$ in two-tailed Welch's/unequal variances *t*-tests; Ruxton, 2006).

2.4.2.3 Multicellular development on agar

D. discoideum starvation-induced multicellular morphogenesis (i.e. development) is a complex and tightly regulated process involving gene expression changes, specific signalling pathways, chemotactic cell motility, dynamic cell-substrate and cell-cell adhesion, cell differentiation and sorting of different

subpopulations (Weijer, 2004), and which culminates in the formation of macroscopic fruiting bodies. We decided to assess the ability of *fam49* KOs to develop into fruiting bodies as it would allow us to determine whether FAM49 is essential to any of the multiple molecular events driving such elaborate biological undertaking.

To test for development, vegetative cells were left to starve on buffered agar plates. Under such conditions, all *fam49* KO clones were able to develop into fruiting bodies with seemingly normal morphology (Figure 2.15). Compared to wild-type, Ax3-based KO clones (but not those with an Ax2 background) appeared to make fruiting bodies with slightly less extended stalks, though we did not perform any confirmatory experiments and analysis on this.

Our preliminary results suggest that there are no major defects in the developmental program of *fam49* KO cells. It is important to note, however, that we only assessed the overall ability of *fam49* KOs to generate fruiting bodies and did not analyse any finer aspects of development, such as specific gene expression, degree of cell polarisation, cell streaming dynamics, strength of cell-cell adhesion, timing of different development stages or spore viability. These and other development features are study possibilities for the future, which may reveal if FAM49 contributes to some extent (though likely not essentially) to any of them.

The development assay we used, like other development assays also commonly employed in this research field, is a very permissive one (Ponte *et al.*, 2000): besides the fact that cells are allowed to develop on top of a flat, solid buffered agar surface, meaning that external physical and chemical obstacles are artificially kept to a minimum, the assay is started with a high number of cells in a confluent layer. It is conceivable that if faced with more challenging conditions, namely those *D. discoideum* encounters in its natural habitat (soil), *fam49* KO cells may show more noticeable defects in development; that seems to be the case with cell lines KO for certain actin-binding proteins (Ponte *et al.*, 2000).

Like with FAM49, knocking out SCAR or other subunits of the SCAR/WAVE complex (except Nap1, which is thought to hold functions independent of the complex – Ibarra *et al.*, 2006) does not compromise development in any obvious way (Pollitt and Insall, 2008; Pollitt and Insall, 2009). The same is true when consti-

tutively inactivated Rac1 is overexpressed in wild-type cells; on the other hand, cells overexpressing constitutively activated Rac1 show a significant delay and reduced efficiency in terminal differentiation, despite the fact that they are still able to produce fruiting bodies with viable spores (Dumontier *et al.*, 2000).
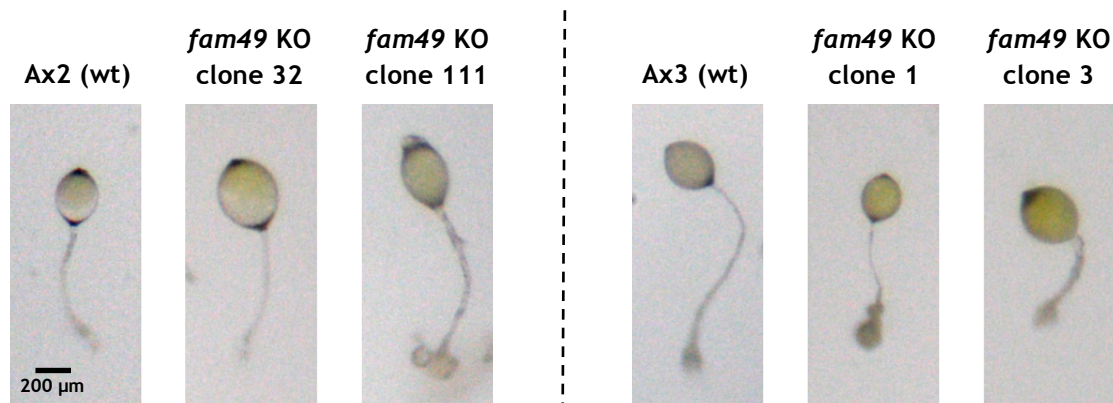
Figure 2.15 – *fam49* KO cells are still able to develop into fruiting bodies
Wild-type and *fam49* KO cell lines were allowed to develop on 1.5% agar plates for approximately 3 days, at which point fruiting bodies of comparable morphology were observed in all cases. No obvious defects were found in fruiting bodies made by *fam49* KOs, except for a generally smaller size (seemingly due to smaller stalks) in those from Ax3-derived KOs.

2.4.2.4 Strength of cell adhesion to plastic

To the best of our knowledge, it is not known whether Rac1 is an important determinant of cell-substrate adhesion in *D. discoideum*. On the other hand, it has been reported that the SCAR/WAVE complex does have a role in such process, since cells KO for SCAR adhere more poorly to plastic than wild-type cells (Ibarra *et al.*, 2006).

To determine if FAM49 might contribute to robust cell-substrate adhesion we performed a simple assay – adapted from Ibarra *et al.*, 2006 – whereby vegetative *fam49* KO and wild-type cells pre-seeded on new plastic dishes with fresh medium were subjected to moderate shear stress for 30 min, then detached cells were counted.

Our preliminary results suggest that *fam49* KO cells are able to adhere to plastic at least as strongly as wild-type cells (Table 2.5). Despite the fact that no cell line with known defects in substrate adhesion was used as control, the shear

stress conditions we employed were certainly stringent enough to expose strong adhesion defects (as in talin A KO cells – Niewohner *et al.*, 1997), and even more moderate ones (as in SCAR KO cells) (Ibarra *et al.*, 2006).

It might be that *fam49* KO cells have only minor adhesion defects, or perhaps adhere more strongly, and/or with different dynamics, than wild-type cells; assessing these possibilities will require future experiments with adequate controls and sensitivity.

Table 2.5 – Results of "cell adhesion to plastic" assay with *fam49* KO cell lines
Vegetative wild-type and *fam49* KO cells in fresh HL5 were seeded in new plastic dishes and allo-wed to attach for 2 h, at which point the dishes were shaken for 30 min at ~100 RPM; detached cells were then counted.

Percentage of detached cells after 30 min shaking at ~100 RPM					
Ax2 (wt)	*fam49* KO clone 32	*fam49* KO clone 111	Ax3 (wt)	*fam49* KO clone 1	*fam49* KO clone 3
11%	11%	8%	4%	2%	3%

2.4.2.5 Cell behaviour in an under-agarose chemotaxis assay

We finalized our preliminary phenotypic analysis of *fam49* KOs by imaging vege-tative cells in under-agarose folate chemotaxis assays (Figure 2.16 A and B; also movies 1 to 6, legends for which are included in Appendix C; these assays were prepared as before, i.e. as in section 2.3.1) and doing a visual assessment of their behaviour, looking for signs of defects in cell motility.

The assays we performed revealed that *fam49* KO cells still chemotax towards folate, apparently fairly normally (chemotactic indexes were not calculated; nonetheless, cells were observed moving steadily in the direction of the chemoattractant gradient – see cell tracks in Figure 2.16 C and D), which indicates that the implicated signal transduction pathways are not faulty in any major way (the same appears to be true for the chemoattractant cAMP, as may be inferred from our results on multicellular development). It also became clear to us that *fam49* KO cells are still able to push their way under a soft agarose gel (0.4% w/v) – an already substantial mechanical barrier –, which suggests they do

not have serious defects in cortical strength or plasma membrane force production.

In spite of the above, we were left with a strong suspicion that *fam49* KO cells of both genetic backgrounds differed from wild-type cells with regard to their protrusive and motility behaviour, as well as overall shape, while chemotaxing under agarose – see and compare movies 1 to 3 (for Ax2 and Ax2-derived *fam49* KO cells), as well as 4 to 6 (for Ax3 and Ax3-derived *fam49* KO cells). In particular, *fam49* KO cells seemed to, on average, protrude more slowly and less dynamically than wild-type cells, exhibiting less prominent changes in shape over time. Furthermore, *fam49* KO cells often looked rounder and more smooth-edged than wild-type cells, apparently a direct consequence of their altered protrusive conduct. We also noticed that *fam49* KO cells were, on occasion, unable to swiftly retract their back/uropod, leaving it firmly attached to the substrate (glass) for quite some time while trying to move forward; this was not observed in wild-type cells. Finally, we calculated lower average speeds and higher directional persistences for *fam49* KO cells in comparison to wild-type cells (Figure 2.16 C and D).

Some of our just described preliminary observations were clearly in line with the hypothesis – set forward from our earlier data – that FAM49 has a function in pseudopods and might be functionally connected with Rac1 and/or the SCAR/WAVE complex. We thus decided (as mentioned earlier) to do follow-up experiments to confirm some protrusion-related attributes and other motility parameters of *fam49* KO cells – such experiments comprise the rest of this thesis (section 2.4.3). Other phenotypic traits were not examined further.
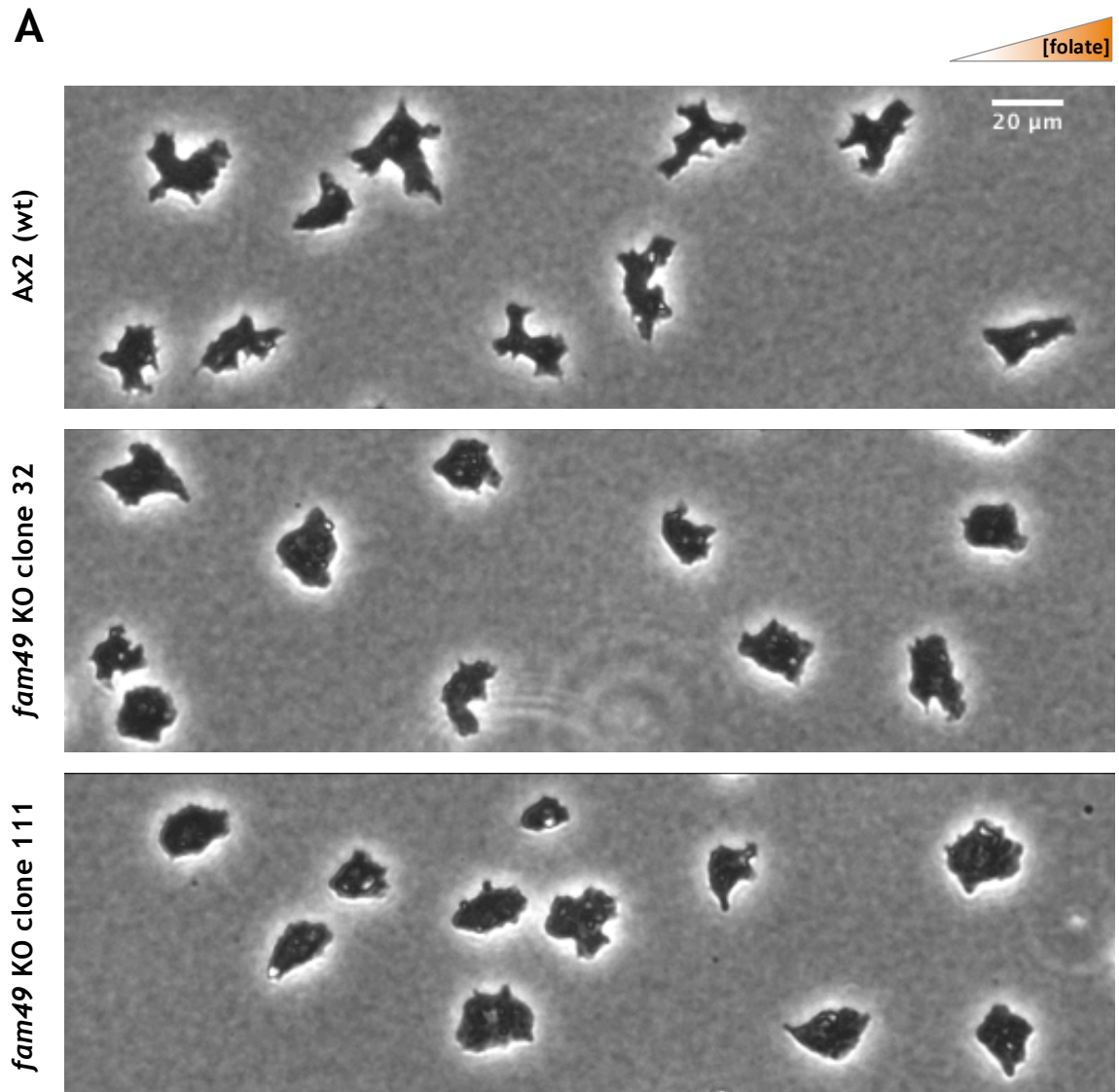
A

Figure 2.16 – Preliminary under-agarose chemotaxis assays suggest motility defects in *fam49* KO cells
(continues next page)

Vegetative wild-type and *fam49* KO cells were imaged with phase contrast microscopy while moving up a folate gradient under a soft agarose gel (0.4% w/v). **A)** Pictures of Ax2 and Ax2-derived *fam49* KO clones 32 and 111, taken from movies 1–3 (Appendix C). The general direction of cell movement is towards the right (towards the chemoattractant gradient, as illustrated). **B)** Pictures of Ax3 and Ax3-derived *fam49* KO clones 1 and 3, taken from movies 4–6 (Appendix C). The general direction of cell movement is as in **A**. **C)** For each represented cell line – Ax2 and corresponding *fam49* KOs –, ten cells were continuously tracked over a period of 10 min, using the MTrackJ plugin for ImageJ (Meijering *et al.,* 2012). The obtained trajectories were then plotted (as shown), being normalised so as to emanate from the origin ($x = 0$, $y = 0$). Axes of trajectory plots represent distance in µm. Different trajectories are shown in different colours. We also calculated the average speed and directional persistence of each tracked cell. For each of those two parameters, plotted values (as shown) represent single cells. Sample mean and 95% confidence interval for the population mean are shown for each data set. Indicated *p*-values were obtained with two-tailed Welch's/unequal variances *t*-tests (Ruxton, 2006). **D)** Same as **C**, but for Ax3 and corresponding *fam49* KOs.

B
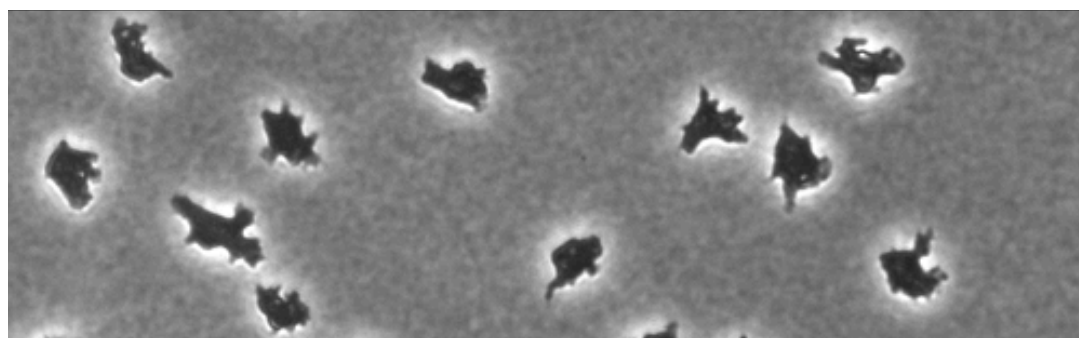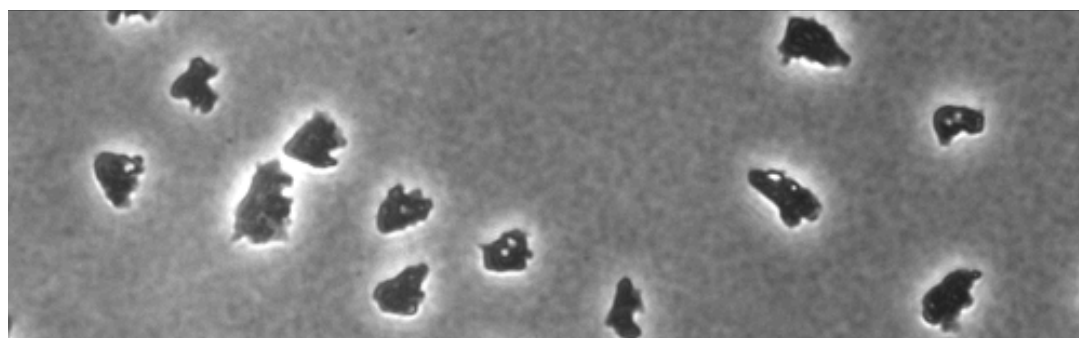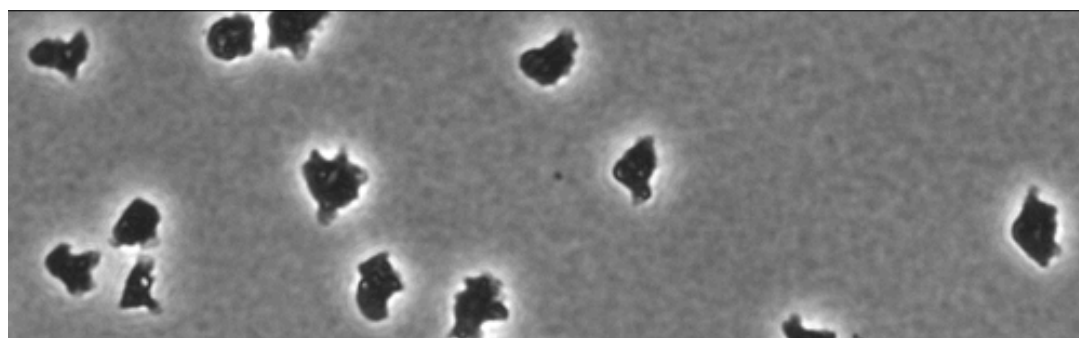
Figure 2.16 – Preliminary under-agarose chemotaxis assays suggest motility defects in *fam49* KO cells *(continued)*
(continues next page)

C
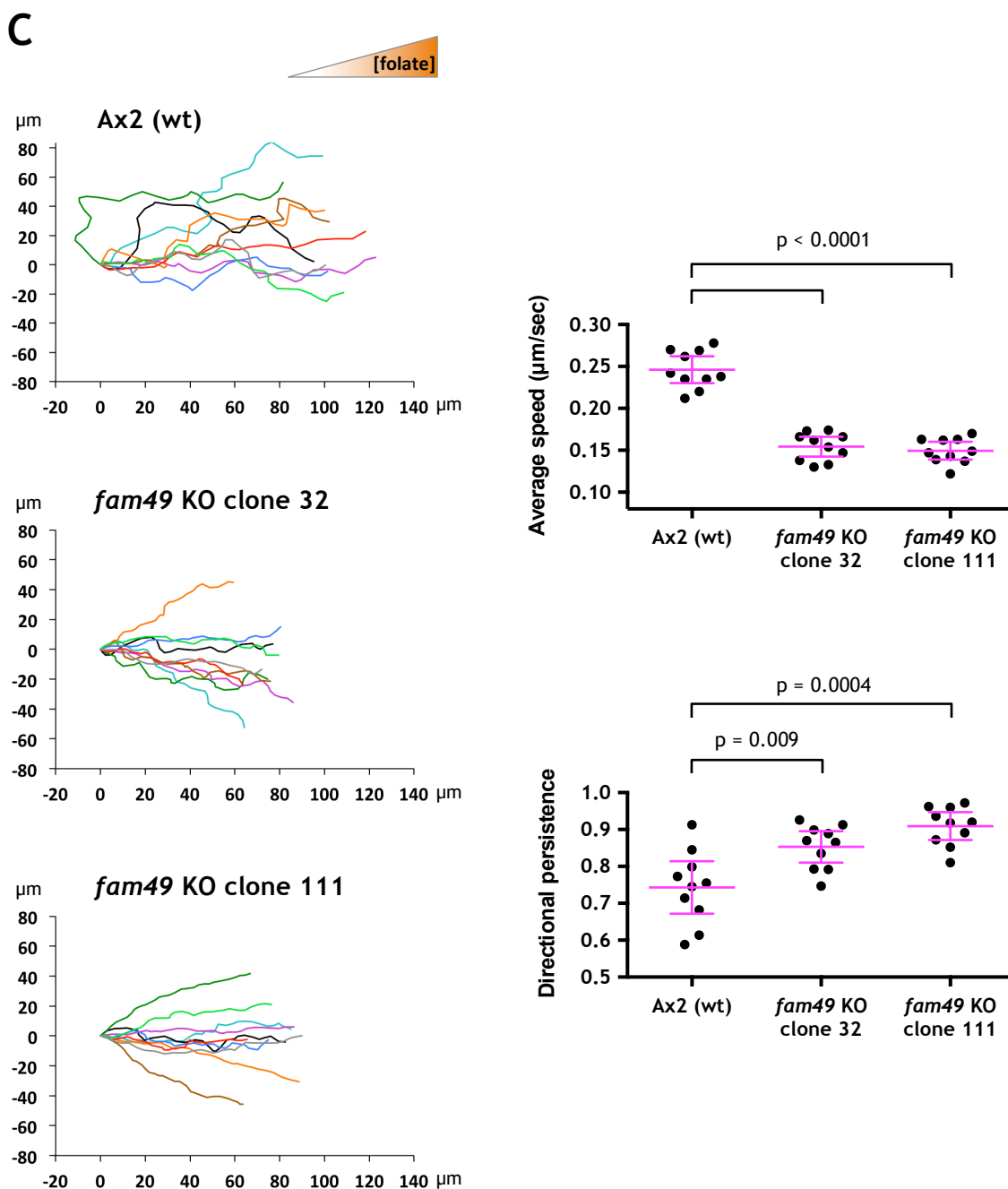
**Figure 2.16 – Preliminary under-agarose chemotaxis assays suggest motility defects in
fam49 KO cells** *(continued)*
(continues next page)
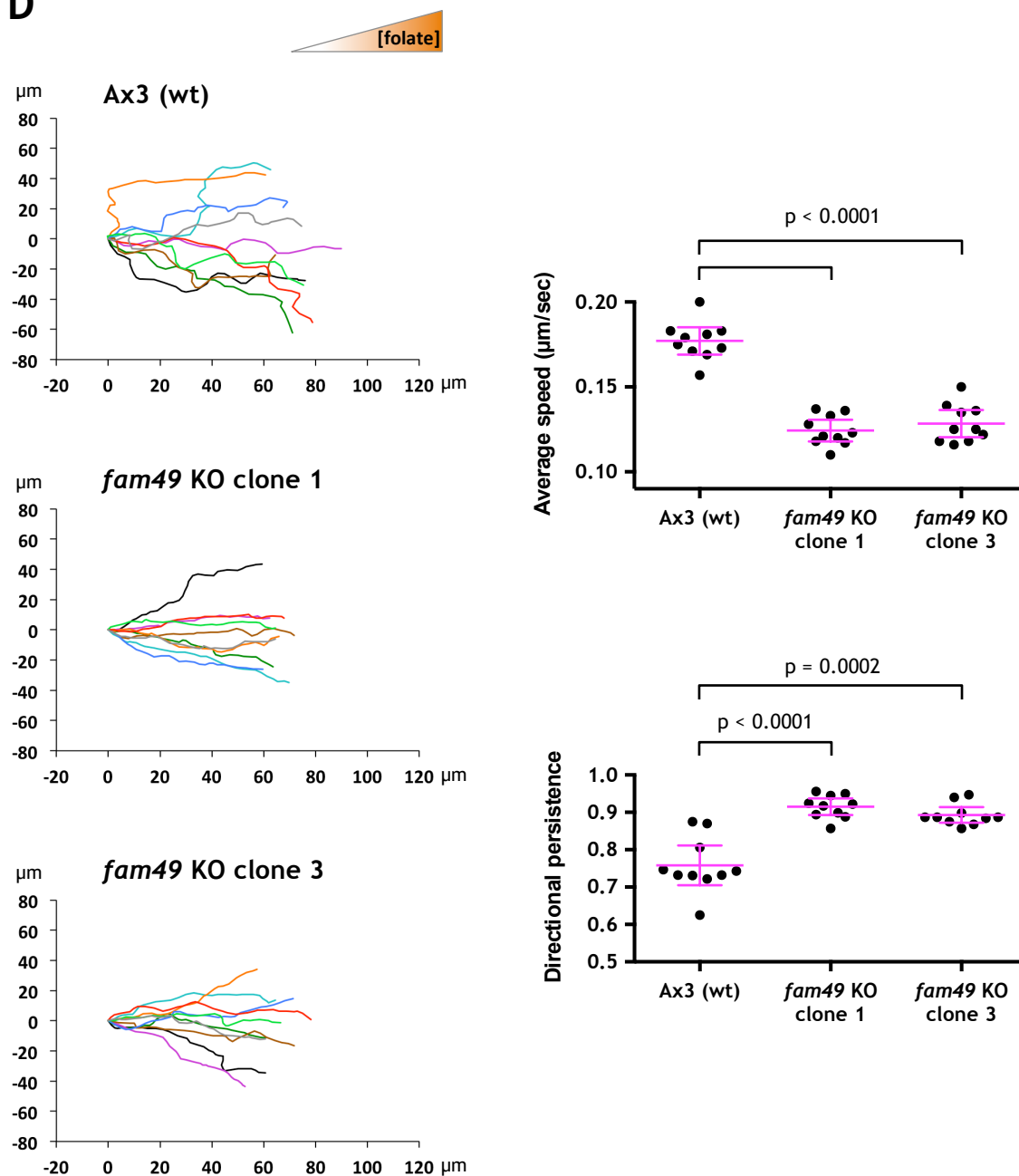
Figure 2.16 – Preliminary under-agarose chemotaxis assays suggest motility defects in *fam49* **KO cells** *(continued)*

2.4.3 Focusing on protrusion- and motility-related traits of *fam49* KO cells

At this point we selected a single *fam49* KO clone from each genomic background to be used in remaining experiments: Ax2-based clone "32" and Ax3-based clone "1". They are simply referred to as "Ax2 *fam49* KO" and "Ax3 *fam49* KO" (or equivalent), respectively, for the remainder of this thesis. Unless specified otherwise, all experiments described below were performed using both KOs.

With regard to Ax2-based clones, "32" was selected over "111" since the latter seemed less healthy (its population growth was the most affected, both in shaking HL5 culture and on bacteria), possibly due to secondary mutations. Ax3-based clones "1" and "3" did not show any obvious phenotypic differences in our early assays and one of them was selected randomly.

2.4.3.1 Pseudopods in *fam49* KO cells are still driven by the SCAR/WAVE complex and not WASP A

To assess if pseudopods made by *fam49* KO cells are, in most likelihood, driven by active Rac–SCAR/WAVE complex–Arp2/3 complex signalling (as in wild-type cells), we imaged PakB(CRIB)-RFP (an active Rac reporter), HSPC300-GFP (a marker for the SCAR/WAVE complex – King *et al.*, 2010), RFP-ArpC4 (a marker for the Arp2/3 complex – Veltman *et al.*, 2012) and GFP-WASP A (Veltman *et al.*, 2012) in vegetative cells chemotaxing under agarose, using TIRF microscopy.

In wild-type cells, the first three of the above-mentioned fluorescent reporter proteins are invariably enriched in pseudopods. Using TIRF microscopy, HSPC300-GFP can typically be seen accumulating in a narrow patch at the protruding edge of pseudopods (other markers for the SCAR/WAVE complex display identical behaviour – Veltman *et al.*, 2012), whereas RFP-ArpC4, and especially PakB(CRIB)-RFP, generally show broader distributions inwards from the edge (Veltman *et al.*, 2012) – see Figure 2.17. GFP-WASP A displays a different behaviour, as observed using the same microscopy technique: it gathers throughout the basal cell body in puncta-like structures (at least some of which are associated with clathrin endocytosis – Veltman *et al.*, 2012), which in moving cells are located

mainly towards the rear (Figure 2.17). In SCAR KO cells, however, GFP-WASP A is redeployed to pseudopods, accumulating in an identical fashion to the SCAR/WAVE complex in wild-type cells; it is therefore believed that WASP A takes over SCAR/WAVE's function in promoting actin polymerisation to drive pseudopod extension, sharing essential upstream regulators and downstream effectors (Veltman *et al.*, 2012). It may be that other circumstances exist, apart from the absence of SCAR, where such taking over (complete or perhaps partial) occurs, which is why we decided to also look at GFP-WASP A.

When we imaged each of the aforesaid fluorescent proteins in *fam49* KO cells we consistently observed enrichment patterns comparable to those in wild-type cells (Figure 2.17). This suggests that active Rac, the SCAR/WAVE complex and the Arp2/3 complex are still responsible for, and thus capable of, promoting pseudopod extension in the absence of FAM49, and also that WASP A does not become involved in such role. While we cannot formally prove that the enrichments of SCAR/WAVE complex and Arp2/3 complex are equivalent to their activity (King *et al.*, 2010), we have no reasons to suspect the contrary.

It is conceivable, despite the above, that differences may exist between *fam49* KO and wild-type cells with regard to the precise spatio-temporal dynamics of enrichment and/or enrichment levels of active Rac, the SCAR/WAVE complex and/or the Arp2/3 complex in pseudopods, something we did not assess. Detecting such differences would favour the possibility that FAM49 has an impact – positive or negative, direct or otherwise – on the activity of those proteins.
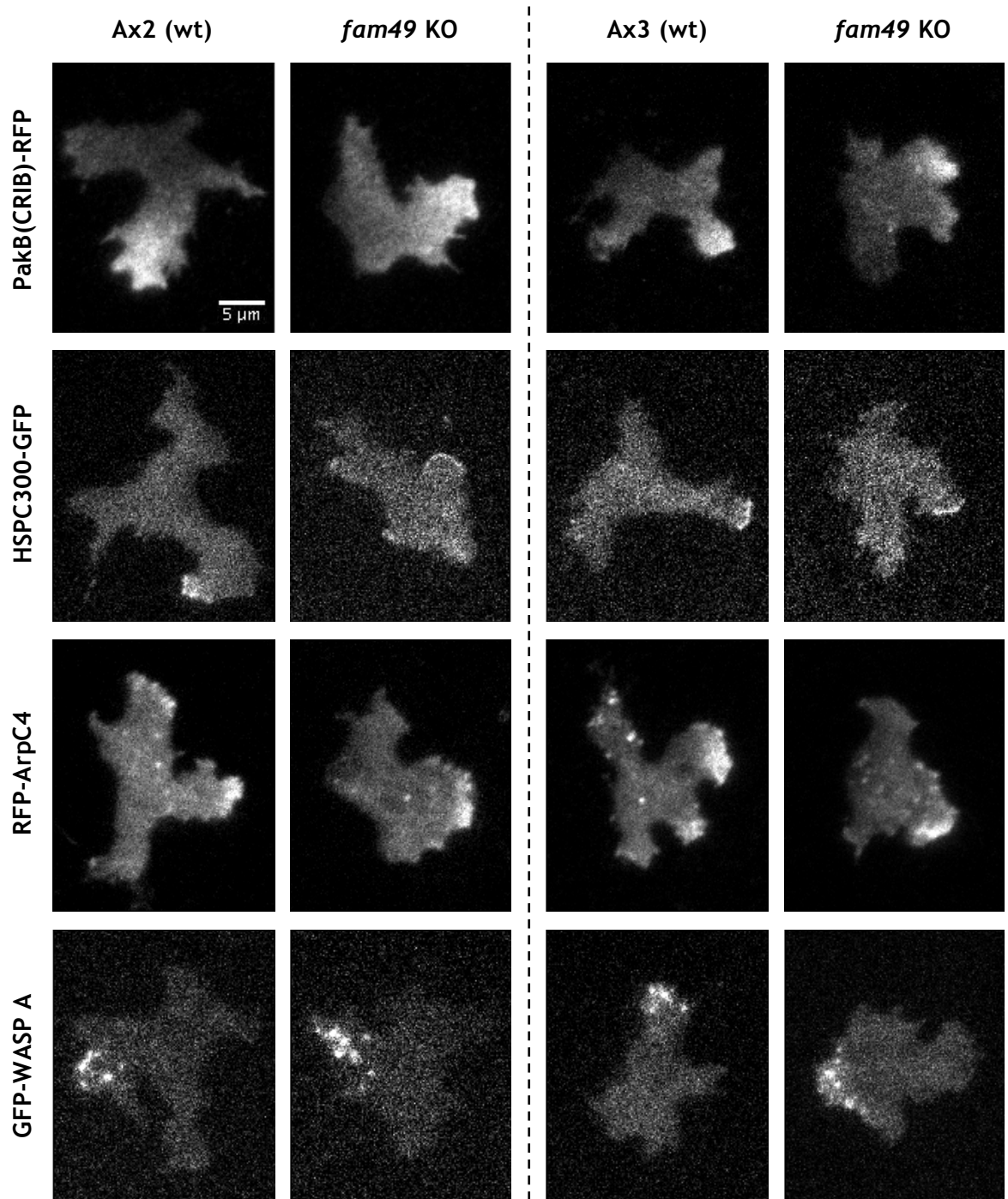
Figure 2.17 – Active Rac, the SCAR/WAVE complex, the Arp2/3 complex and WASP A localise normally in *fam49* KO cells
PakB(CRIB)-RFP (an active Rac reporter), HSPC300-GFP (a marker for the SCAR/WAVE complex – King *et al.*, 2010), RFP-ArpC4 (a marker for the Arp2/3 complex – Veltman *et al.*, 2012) and GFP-WASP A (Veltman *et al.*, 2012) were imaged in vegetative wild-type and *fam49* KO cells moving under agarose towards a folate gradient. Imaging was performed in a TIRF microscope. *fam49* KO cells show seemingly normal localisation/enrichment of all the above fluorescent reporters, i.e. PakB(CRIB)-RFP, HSPC300-GFP and RFP-ArpC4 in pseudopods and GFP-WASP A in punctate structures at the rear.

2.4.3.2 Blebs are still produced in *fam49* KO cells

To determine if *fam49* KO cells are still able to make blebs and may, like wild-type cells, move with some contribution from such type of protrusion, we imaged Lifeact-RFP (an F-actin reporter – Riedl *et al.*, 2008; Zatulovskiy *et al.*, 2014) in vegetative cells chemotaxing under agarose (as in previous experiments).

While pseudopods characteristically display a wide Lifeact accumulation inwards from their protruding edge (examples in Figure 2.18 A, for both wild-type and *fam49* KO cells; Lifeact-RFP was co-imaged with GFP-Nap1, a marker for the SCAR/WAVE complex – Veltman *et al.*, 2012), a consequence of the continuous actin polymerisation that occurs at the membrane and of the broad, pseudopod-associated F-actin mesh, blebs can be recognized from the brief and more limited Lifeact enrichment that takes place at both the original and the newly formed F-actin cortices.

In the course of our observations we managed to identify blebs in *fam49* KO cells, which implies that FAM49 is not required for such protrusions to be generated. Figure 2.18 B shows examples of blebs in chemotaxing Ax2 wild-type and Ax2 *fam49* KO cells; it is evident, in both cases, that the depicted blebs soon "evolved" into pseudopods by continued actin polymerisation. We chose to present such particular examples (i.e. of blebs progressing into pseudopods, as opposed to blebs alone) since they better convey, in our view, the notion that blebs may effectively contribute to cell movement, with or without FAM49. Though not shown, we also observed blebs in Ax3 *fam49* KO cells.

We did not investigate whether the proportion of pseudopods and blebs, as well as their relative contribution to cell movement, is changed in *fam49* KO cells with respect to wild-type cells – such analysis could be informative and should be considered for future experiments.

A
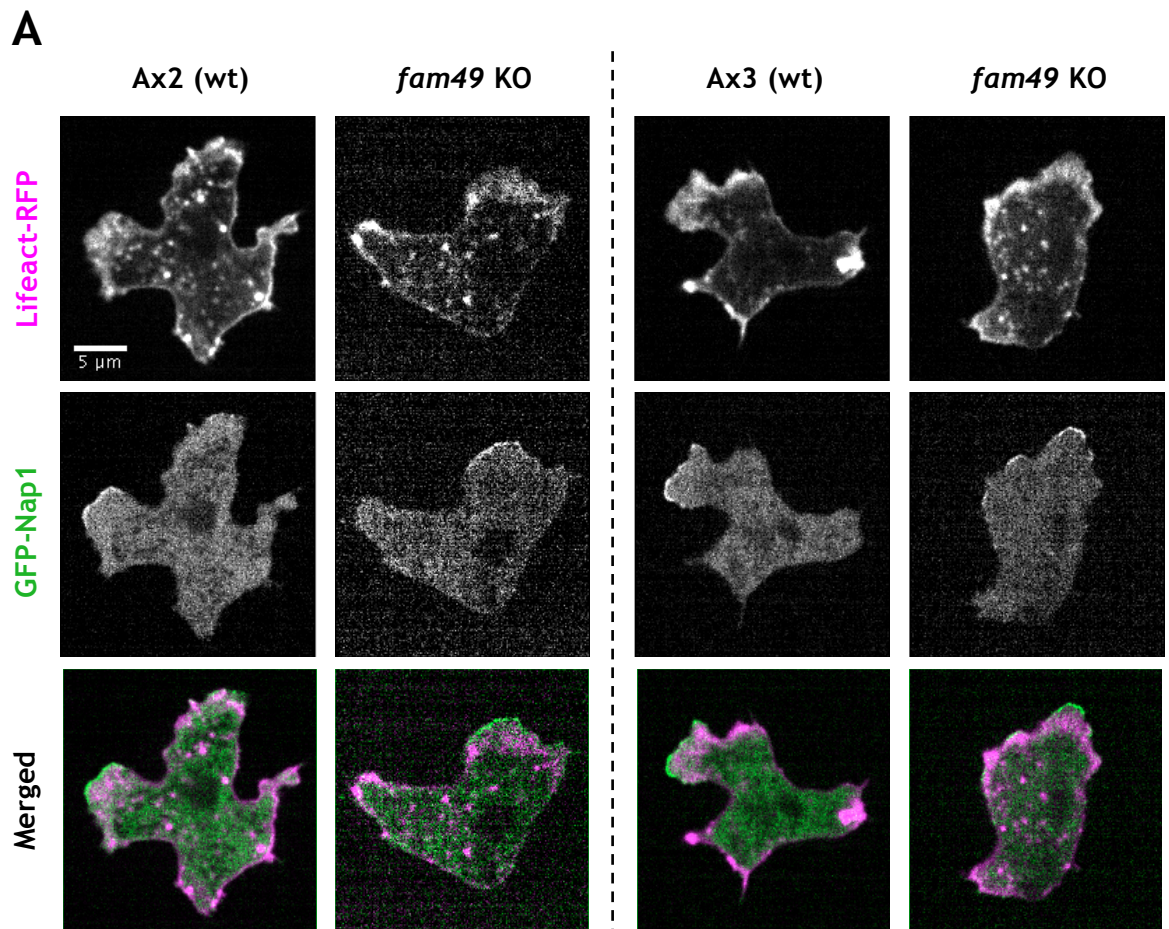
Figure 2.18 – Pseudopods and blebs in *fam49* KO cells
(continues next page)

A) Simultaneous confocal microscopy imaging of Lifeact-RFP (an F-actin reporter – Riedl *et al.*, 2008; Zatulovskiy *et al.*, 2014) and GFP-Nap1 (a marker for the SCAR/WAVE complex – Veltman *et al.*, 2012) in vegetative wild-type and *fam49* KO cells moving under agarose towards a folate gradient. Pseudopods, which display a narrow GFP-Nap1 enrichment patch at the protruding edge closely followed by a broad Lifeact-RFP accumulation, are patent in all represented cell lines.
B) Lifeact-RFP in Ax2 and Ax2-derived *fam49* KO cells, imaged as in **A**. Each sequence of images shows the generation of a bleb (evident at t = 3s) and its subsequent "evolution" into a pseudopod (onwards from t = 3s). For each depicted bleb, arrows in magenta or green indicate the original or the newly formed F-actin cortex, respectively. The original cortices can be seen disappearing over time, while pseudopods start emerging (green asterisks). Numbers are time in seconds.

B

Ax2 (wt)
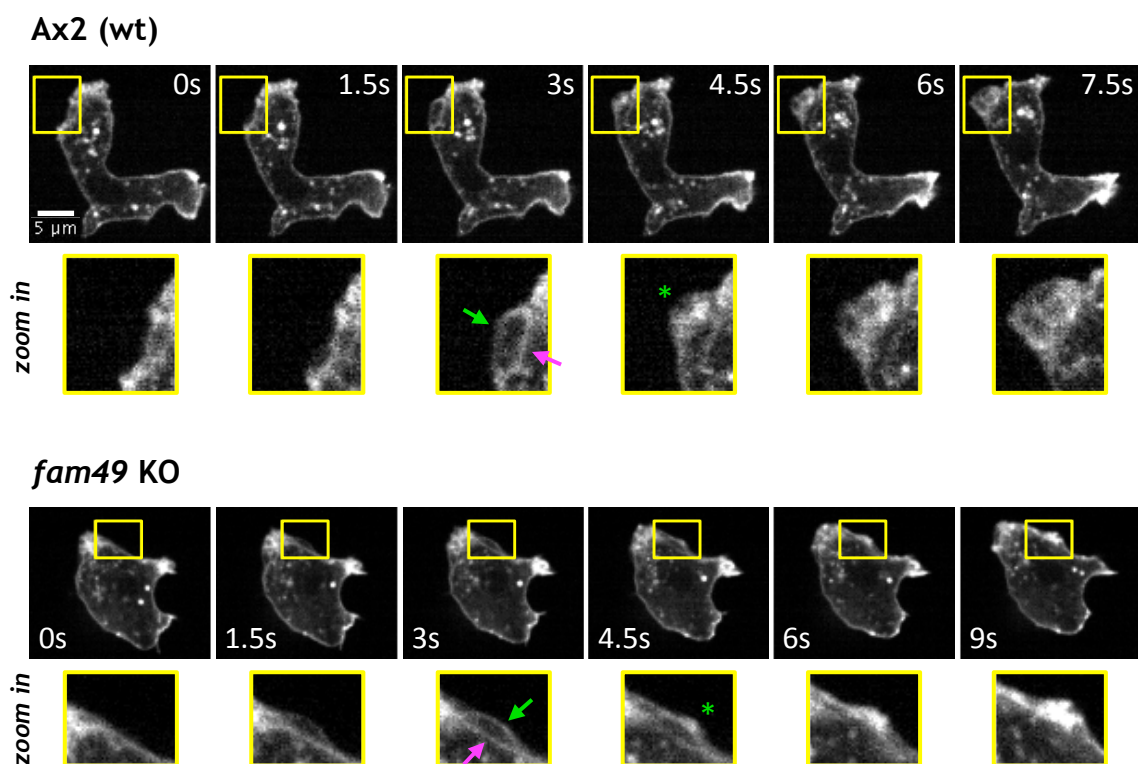
fam49 KO

Figure 2.18 – Pseudopods and blebs in *fam49* KO cells *(continued)*

2.4.3.3 Basal SCAR/WAVE protein levels are not substantially changed in *fam49* KO cells

We were interested to know whether FAM49 might interact genetically with SCAR/WAVE and/or influence its global protein levels in other ways, e.g. by having a large effect on its overall degree of activity (according to Ura *et al.*, 2012, activated SCAR/WAVE is quickly removed from cells by degradation, hence lower or higher SCAR/WAVE levels may, in principle, be an outcome of more or less of it being activated, respectively), so we performed a western blot of SCAR/WAVE from lysates of wild-type and *fam49* KO cells.

We could not see substantial nor consistent (between genetic backgrounds) differences in SCAR/WAVE levels between wild-type and *fam49* KO cells (Figure 2.19), which suggests FAM49 has no major impact on the amount of SCAR/WAVE cells have. It should be noted, however, that we only probed basal SCAR/WAVE levels in vegetative, "non-stimulated" cells; cells under different physiological conditions, such as when actively chemotaxing or starving, might provide a different result.
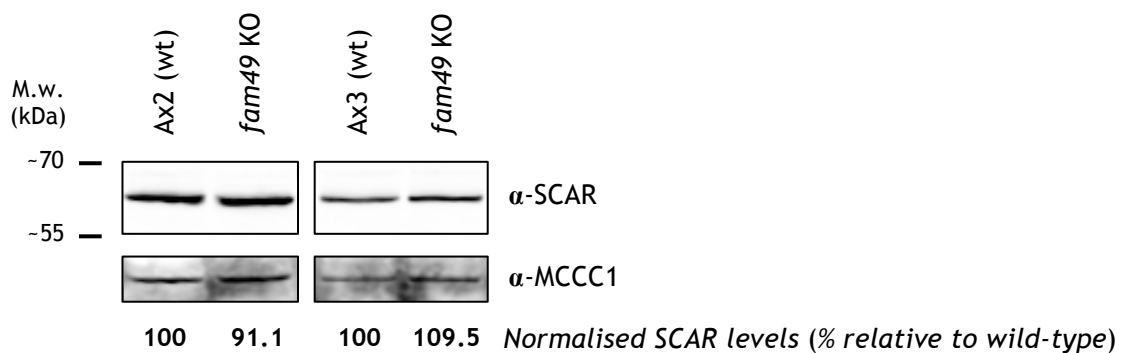
Figure 2.19 – Western blot of SCAR/WAVE from vegetative wild-type and *fam49* KO cells
Whole cell lysates were used. SCAR levels were normalised with those of MCCC1 (3-methylcro-tonyl-CoA carboxylase α), our loading control (Davidson *et al.*, 2013a). Vegetative wild-type and *fam49* KO cells contain roughly the same amount of SCAR.

2.4.3.4 Quantification of parameters of protrusive activity, motility and morphology corroborates abnormal behaviour of *fam49* KO cells

We were very interested in quantifying pseudopod parameters (such as generation rate, average extension speed, average time of extension and average length/width) for comparison between *fam49* KO and wild-type cells – we expected such analysis would allow us to confirm some of our early impressions on the protrusive behaviour of *fam49* KO cells (section 2.4.2.5) and clarify which particular aspect(s) of pseudopod behaviour might be tuned by FAM49. In order to do so we attempted using Lifeact-RFP confocal microscopy and DIC microscopy time-lapse movies of vegetative cells chemotaxing under agarose. We soon realized, however, that protrusions (pseudopods or otherwise) made by *fam49* KO cells were generally less discrete than their wild-type counterparts, and consequently more difficult – too often virtually impossible – to discriminate and thus analyse as individual, separate units.

In light of the above we decided to quantitatively compare the protrusive behaviour of *fam49* KO and wild-type cells through a different approach – one independent of, and thus not able to describe, individual protrusions, but still reasonably informative towards our goals. The method we followed is explained briefly in the legend of Figure 2.20 and at length in the *Materials and Methods* chapter; in essence, it involved using the QuimP v11b package (Tyson *et al.*, 2014; http://www.warwick.ac.uk/QuimP) for generating and analysing highly resolved, node-based cell outlines throughout time-lapse movies. Such method allowed us to quantify not only parameters related to the protrusive behaviour of cells but also other features of cell motility and aspects of cell morphology, which we were also interested in. Figure 2.20 and Table 2.6 list all measured parameters and summarise the results we obtained with vegetative Ax2 *fam49* KO and Ax2 wild-type cells chemotaxing under agarose. Details on the way each parameter was calculated are provided in the *Materials and Methods* chapter.

The data we gathered strongly suggest that the protrusive activity of *fam49* KO cells is lower than that of wild-type cells, in the sense that KO cells are not, by means of protrusions, able to cover as much space over time on a global scale (Figure 2.20 and Table 2.6 – see "Average rate of membrane extension"). Furthermore, it seems highly likely that protrusions made by *fam49* KO cells extend

more slowly, on average, than their wild-type counterparts (see "Average speed of membrane extension – top 25%" and "Average speed of membrane extension – top 10%").

Unsurprisingly (considering the above), our data also point towards *fam49* KO cells moving more slowly than wild-type cells (see "Cell's average speed"), though the former may regularly keep a more steady direction (see "Cell's directional persistence"; this parameter does not reflect chemotactic ability/index, which we did not calculate). These phenotypic differences had already been evident in our earlier, preliminary observations (section 2.4.2.5).

Finally, with regard to cell morphology, our data implies that *fam49* KO cells retain a substantially rounder appearance than wild-type cells (see "Cell's average circularity"), most likely a reflection – as may also be the case with their decreased speed – of their diminished protrusive dynamics. *fam49* KO cells may also show a tendency to elongate less, on average; however, our data on such parameter is less robust (see "Cell's average elongation").

Overall, our results provide a reasonably clear picture of some phenotypic defects *fam49* KO cells seem likely to have with regard to their protrusive and motility behaviour (as assessed in an under-agarose chemotaxis assay), agreeing with our earlier impressions (section 2.4.2.5). Despite the fact that we are unable to tell how much each type of protrusion (pseudopod or bleb) contributed to each of the quantified parameters on protrusive behaviour (i.e. "Average rate of membrane extension", "Average speed of membrane extension – top 25%" and "Average speed of membrane extension – top 10%") in each cell line, our data clearly support the view that FAM49 adds to the regulation of protrusion dynamics in *D. discoideum*. The hypothesis that FAM49 exerts control specifically over pseudopods would be strengthened on the occasion of our final experiments, described next (section 2.4.3.5).

Due to time constraints, we only performed the quantitative analysis detailed in this section (supported on QuimP) for Ax2 and Ax2 *fam49* KO cells. We anticipate, nonetheless, that equivalent data would be derived from Ax3 and Ax3 *fam49* KO cells. We later did, in fact, also perform a quantitative comparison (not based on QuimP) of Ax3 and Ax3 *fam49* KO cells with regard to their circu-

larity, as well as – once again – speed and directional persistence, but not other parameters (namely those of protrusive activity), and the results were comparable to those of Ax2 and Ax2 *fam49* KO cells; such data is presented in the following, final results section.

Average rate of membrane extension (µm^2/sec)

Figure 2.20 – Quantification of parameters of protrusive activity, motility and morphology in Ax2 and Ax2-derived *fam49* KO cells chemotaxing under agarose
(continues next page)

Shown parameters were quantified in vegetative cells moving up a folate gradient under an agarose gel (0.6% w/v, a higher concentration than in earlier experiments). Cells were first imaged with a spinning disk confocal microscope, their outlines being revealed by including a red fluorescent dye (TRITC-dextran) in the agarose as a negative stain. Recorded time-lapse movies (5 to 10 min; 1 frame / 2.5 sec) were then processed in ImageJ/Fiji 1.49i (Schneider *et al.*, 2012) and analysed in QuimP v11b (a set of ImageJ plugins – Tyson *et al.*, 2014; http://www.warwick.ac.uk/QuimP), where most parameters of interest were quantified from high-resolution node-based cell outlines created semi-automatically in every frame. Remaining parameters were calculated from QuimP-generated data (see *Materials and Methods* chapter for further details). The results of each of three independent experiments are displayed in the same order for every parameter. Plotted values represent single cells; except for "Cell's directional persistence", those values are averages (i.e. arithmetic means). In the particular case of "Average speed of membrane extension – top 25%" and "Average speed of membrane extension – top 10%" only the top 25% and top 10% values, respectively, of local membrane extension speed in each cell were used for calculating averages; top 25% values likely originate only from *true* protrusions (and not small membrane fluctuations or noise from cell outlines), whereas top 10% values restrict the analysis to faster protruding regions. Sample mean (i.e. mean of single-cell averages) and 95% confidence interval for the population mean are shown for each data set. Indicated *p*-values were obtained with two-tailed Welch's/unequal variances *t*-tests (Ruxton, 2006); "n.s." = statistically non-significant on the basis of an alpha level of 0.05.

Average speed of membrane extension - top 25% (µm/sec)

Average speed of membrane extension – top 10% (µm/sec)

Cell's average speed (µm/sec)
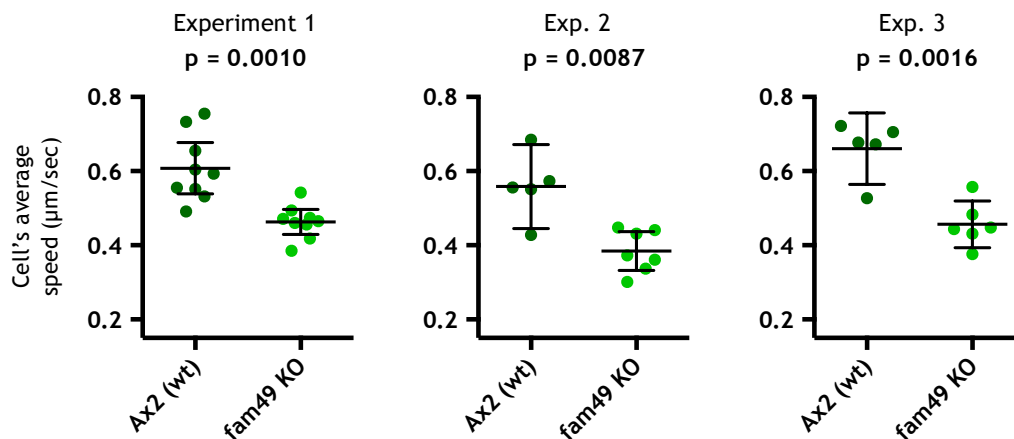
Figure 2.20 – Quantification of parameters of protrusive activity, motility and morphology in Ax2 and Ax2-derived *fam49* KO cells chemotaxing under agarose *(continued)*
(continues next page)

Cell's directional persistence
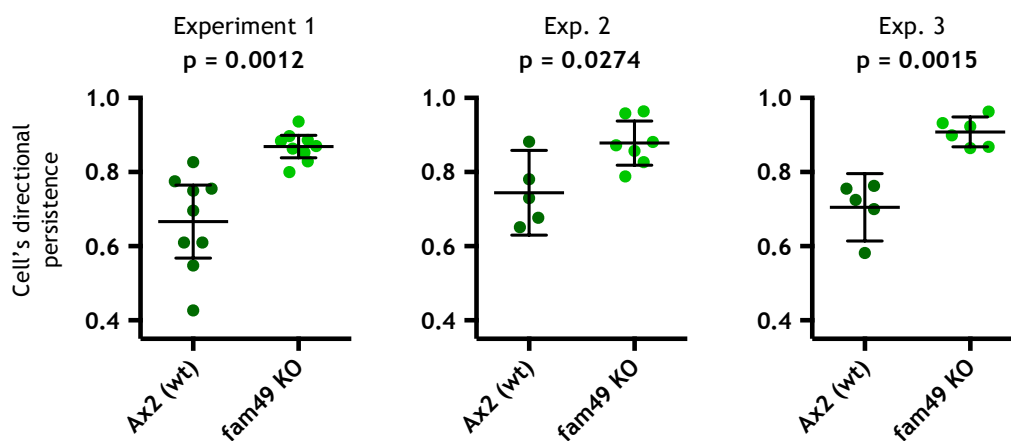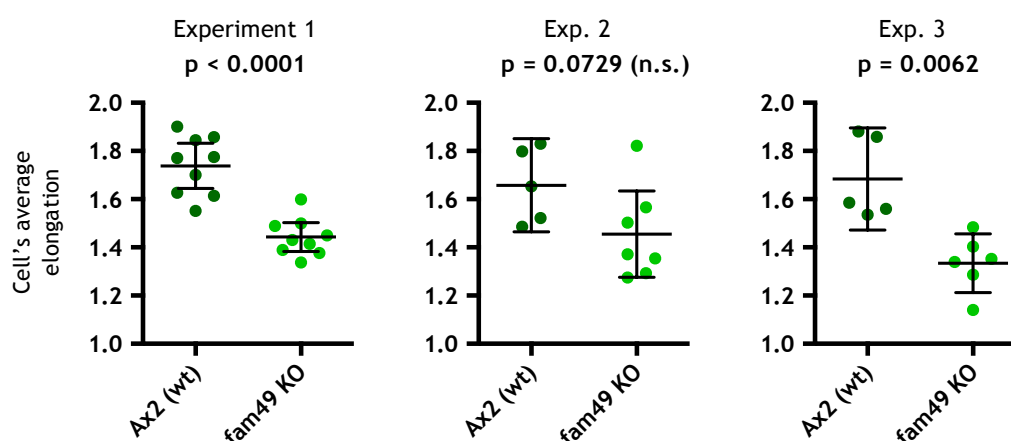
Cell's average circularity
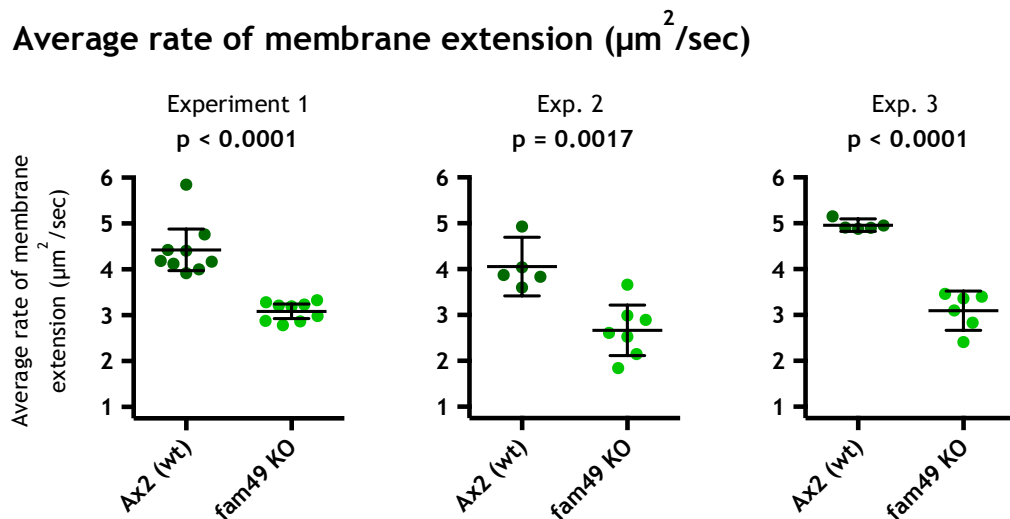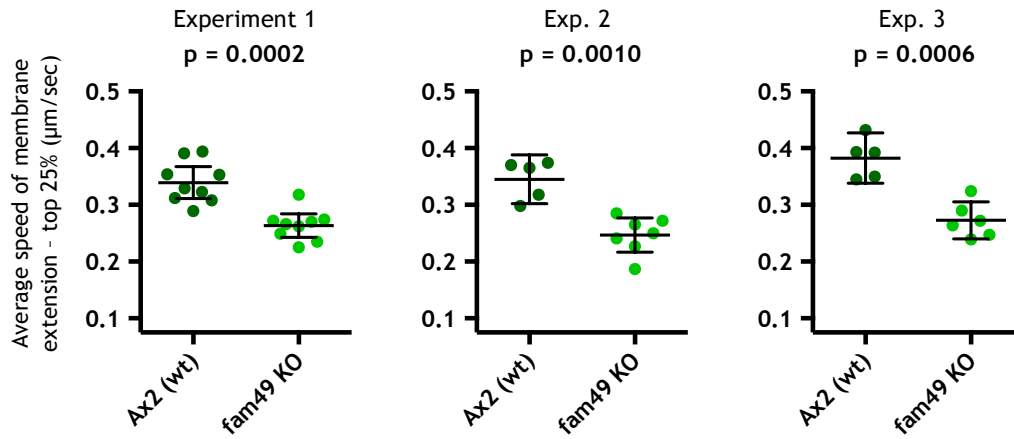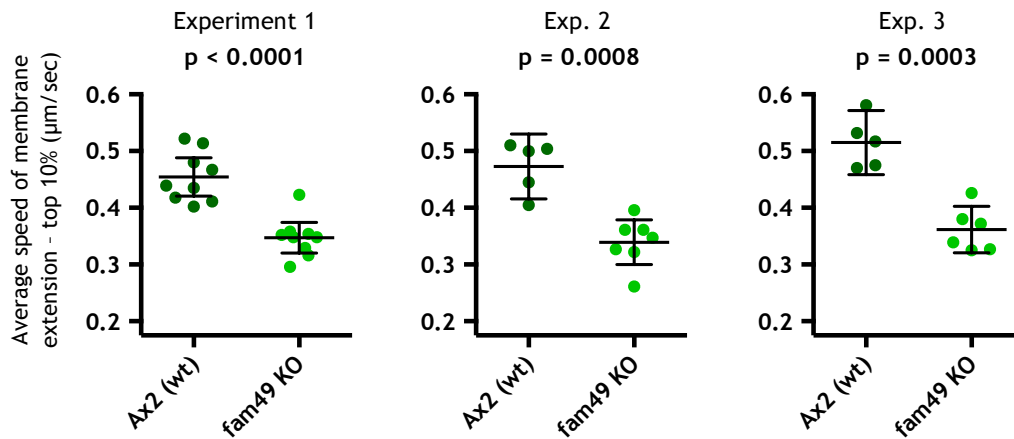

Cell's average elongation

Figure 2.20 – Quantification of parameters of protrusive activity, motility and morphology in Ax2 and Ax2-derived *fam49* KO cells chemotaxing under agarose *(continued)*

Table 2.6 – Percent changes from wild-type to *fam49* KO sample means in each parameter of Figure 2.20
Shown for each parameter are the lowest and highest percent changes from wild-type to *fam49* KO sample means within individual experiments. Arrows indicate the direction of change, pointing up or down to denote an increase or decrease, respectively. Percent changes were calculated using the following formula: **[**(KO sample mean - WT sample mean) / WT sample mean**]** x 100.

Average rate of membrane extension	Average speed of membrane extension (top 25%)	Average speed of membrane extension (top 10%)	Cell's average speed	Cell's directional persistence	Cell's average circularity	Cell's average elongation
⬇	⬇	⬇	⬇	⬆	⬆	⬇
30.3–37.6%	22.3–28.7%	23.5–29.8%	23.8–31.2%	18.0–30.3%	48.9–84.1%	12.2–20.8%

2.4.3.5 Re-expression of FAM49 reverts the phenotype of *fam49* KO cells but its overexpression may lead to an excessively dynamic protrusive behaviour and atypically thin pseudopods

In order to confirm that the altered protrusive behaviour (and ultimately motility) of *fam49* KO cells is caused by the absence of FAM49, and also to estimate the degree of functionality of our GFP-tagged form of FAM49, we individually transformed same-backbone vectors for expression of either non-tagged FAM49 (simply "FAM49" for the remaining of this section, "FAM49(wt)" on figures) or GFP-FAM49 into *fam49* KO cells of both Ax2 and Ax3 backgrounds, then compared transformant, plain KO and wild-type cells in under-agarose chemotaxis assays. Such comparison involved imaging cells with phase contrast microscopy (Figure 2.21 A and B), visually assessing their protrusive conduct (movies 7 to 10 for Ax2 and derived cell lines, 11 to 14 for Ax3 and derived cell lines; corresponding legends are included in Appendix C), and quantifying their circularity at fixed points in time (Figure 2.21 C), as well as their average speed and directional persistence through time (Figure 2.21 D and E).

We chose to measure and place particular focus on cell circularity for two reasons: first, it had been the parameter most prominently and consistently dissimilar between *fam49* KO and wild-type cells in our earlier QuimP-based quantification analysis (section 2.4.3.4); second, we were fairly sure that such contrast in cell circularity was mostly, if not uniquely, a reflection of the distinct protrusive behaviours of *fam49* KO and wild-type cells. Quantifying cell

circularity would therefore allow us to reasonably safely infer the extent of the phenotypic rescue provided by FAM49 and GFP-FAM49 with respect to protrusions, particularly if done in combination with the visual inspection of moving cells. By also calculating average speeds and directional persistences, a clear picture of the degree of rescue of overall cell motility would then emerge. It could be argued that a more comprehensive, QuimP-based quantitative analysis – which would include measurements for parameters of protrusive activity – would have been a better approach; while we do agree with such proposition, time constraints prevented us from considering that option.

With regard to *fam49* KOs re-expressing FAM49 ("*fam49* KO + FAM49" cells), we visually observed a clear phenotypic rescue of protrusive behaviour in most imaged cells with an Ax3 background (compare movies 11, 12 and 14) but only in a modest fraction (probably ≤50%) of those with an Ax2 background (compare movies 7, 8 and 10); in the latter case, remaining cells displayed a phenotype indistinguishable from that of plain *fam49* KO cells (a possible reason for this is described below). Cell circularity measurements were very much in line with our visual assessments of the protrusive activity of moving cells (Figure 2.21 C). Restricting our analysis to *fam49* KO + FAM49 cells that seemed rescued (at least partially) in their protrusive behaviour, we determined that their directional persistence was reverted to wild-type levels and their average speed was also partially rescued (Figure 2.21 D and E).

The visual inspection of moving cells also allowed us to notice that many *fam49* KO + FAM49 cells looking phenotypically rescued in their protrusive behaviour would nevertheless show a rather peculiar conduct, which we strongly suspect to be a consequence of FAM49 overexpression, i.e. re-expression at higher-than-wild-type levels. Our reasons for assuming overexpression – we could not, due to the lack of availability of a *D. discoideum* FAM49 antibody, perform western blots to actually compare FAM49 protein levels between cell lines – are detailed below. Compared to wild-type cells, those putative FAM49 overexpressor cells seemed to display an excessively dynamic – and possibly less coordinated – protrusive behaviour, with atypically high rates of new pseudopods, many of which looking unusually thin (re-compare movies 7 and 10, as well as 11 and 14). The somewhat unorthodox conduct of putative FAM49 overexpressor cells surely explains their often spikier appearance than wild-type cells, and such difference

in cell shape is reflected in our circularity measurements, which were slightly lower, on average, for phenotypically rescued *fam49* KO + FAM49 cells than for wild-type cells (Figure 2.21 C; compare each *fam49* KO + FAM49(wt) cell line with its wild-type; in the case of Ax2-derived *fam49* KO + FAM49(wt) cells, only the lower half values should be considered, as the top half mostly represents cells with no obvious phenotypic rescue, as described above; in the case of Ax3-derived *fam49* KO + FAM49(wt) cells, the complete dataset of can be taken into account). We suspect that the peculiar protrusive activity of putative FAM49 overexpressor cells might render them less capable than wild-type cells – yet still more so than *fam49* KO cells – of moving efficiently, as suggested by our average speed measurements (Figure 2.21 D and E).

To better visually observe the protrusive behaviour of putative FAM49 overex-pressor cells (within the *fam49* KO + FAM49 population) and compare it with that of wild-type and plain *fam49* KO cells, we did some imaging with high magnifi-cation DIC microscopy, again in the context of under-agarose chemotaxis assays (Figure 2.22; also movies 15 to 18 for Ax2 and derived cell lines, 19 to 22 for Ax3 and derived cell lines – Appendix C). Our earlier impressions were reinforced, as we clearly observed putative FAM49 overexpressor cells making abnormally slim pseudopods and protruding in an unusually dynamic – and perhaps rather uncoor-dinated – fashion, apparently generating more new pseudopods over time than wild-type cells. Such behaviour is, without doubt, strikingly different from that of *fam49* KO cells, and indeed suggests an "excessive" phenotypic reversal. *fam49* KO cells seemed to make broader and more slowly extending pseudopods (considering those instances where pseudopods look sufficiently discrete), on average, than wild-type cells, and possibly a lower number of them over time.

As mentioned above, we could not compare FAM49 protein levels between cell lines due to the lack of availability of an antibody against it (we did not attempt to produce one ourselves due to time constraints). Nevertheless, we are strongly inclined to believe that FAM49 overexpression is indeed the reason behind the peculiar behaviour of many *fam49* KO + FAM49 cells, for a few different reasons. Firstly, as we just stated, the protrusive conduct of said cells echoes an "exces-sive" phenotypic reversal of the KO. Secondly, in the FAM49 expression vector we used, FAM49's open reading frame (ORF) is placed in an expression cassette driven by the *act15* (for actin 15 – Knecht *et al.*, 1986) promoter. According to

dictyExpress, an online database containing *D. discoideum* gene expression data from various microarray experiments (Rot *et al.*, 2009), endogenous *act15* is more highly expressed than *fam49* in vegetative Ax2 and Ax4 (an Ax3 variant – Knecht *et al.*, 1986) cells (data not shown), which suggests that our expression vector is likely to drive the production of higher-than-wild-type quantities of FAM49 mRNA, and by extension of FAM49 protein (assuming some degree of cor- relation between both). Additionally, since our expression vector was assembled from the modular vector backbone created by Veltman *et al.*, 2009a, it is highly likely to be present in multiple extrachromosomal copies in any transformant cell (Veltman *et al.*, 2009a; Hughes *et al.*, 1994), and this can be expected to further favour high FAM49 expression levels.

There is no obvious explanation for the fact that only a modest fraction (probably ≤50%) of Ax2-based *fam49* KO + FAM49 cells looked phenotypically rescued in their protrusive behaviour – many, if not most, of which actually showing a putative overexpressor phenotype – in our assays. We suspect, never- theless, that it might have been a consequence of two factors combined. First, Ax2 and derived cell lines (KO and respective transformants) multiply more slowly in axenic culture than Ax3 and derived cell lines (not shown), for which reason we had to wait longer (by a number of days) to image the former. Second, FAM49 overexpression is probably detrimental to cells in a number of ways – an excessive/unregulated protrusive behaviour may very well affect processes which are fundamental for cell survival and multiplication, such as macropinocytosis (in axenic culture) or cytokinesis –, and possibly especially so to cells with an Ax2 background; it is thus conceivable that Ax2-based *fam49* KO + FAM49 overexpressors, which probably comprised the majority of our trans- formant cells, ended up under strong negative selective pressure in culture, and non-transformants able to grow under the selection conditions in place (false positives) started to gradually take over (this would suggest that the absence of FAM49 may be less unfavourable to cells than its overexpression, at least in certain circumstances). We did, in fact, notice progressively lower proportions of Ax2-based *fam49* KO + FAM49 cells with a putative overexpression phenotype in our cultures as days passed (the rather spiky appearance of such cells made them fairly obvious, even in culture; not shown). Longer kept cultures of Ax3- based *fam49* KO + FAM49 cells, which we did not use for our assays, also looked

as if the number of putative overexpressors had decreased, yet not as strikingly as with their Ax2 counterparts.

It should be noted that although we are fairly confident of our observations and assertions on the behaviour of putative FAM49 overexpressor cells, in particular their weirdly dynamic protrusive manners and unusually thin pseudopods in comparison to wild-type cells, we did not quantify any pseudopod parameters (such as generation rate, average extension speed and average length/width) for what would be a more robust and definitive comparative analysis. Such analysis ought to be performed in the future, but in a different experimental scenario instead – one where FAM49 overexpression is either induced or not in wild-type cells (by means of an inducible expression vector – Veltman *et al.*, 2009b) and both induced and non-induced cells are imaged shortly afterwards (under-agarose chemotaxis assays would still be an optimal choice). Such approach should allow the validation of the overexpression phenotype, which will possibly manifest itself even more strongly than in our experiments herein reported. Ideally, FAM49 protein levels should also be confirmed/compared, thus efforts should be made to develop an antibody against it (which would be useful for many other experiments as well).

In general, *fam49* KO cells expressing GFP-FAM49 ("*fam49* KO + GFP-FAM49" cells) seemed less phenotypically rescued in their protrusive activity than *fam49* KO + FAM49 cells (but still noticeably so; compare movies 7 to 10 and 11 to 14), and this is well reflected in our circularity measurements (Figure 2.21 C). Furthermore, we could not identify any cases of "excessive" phenotypic reversal in the *fam49* KO + GFP-FAM49 population (i.e. we did not observe protrusive behaviours similar to that of putative FAM49 overexpressors). Overall, this conveys the idea that our GFP-FAM49 construct may be only partially functional. As we could not compare the expression levels of GFP-FAM49 in KO cells with those of endogenous FAM49 in wild-type cells and those of non-tagged FAM49 in KO cells, we can only assume they were similar to the latter (and thus probably high) since our expression vectors for GFP-FAM49 and non-tagged FAM49 share the same backbone, including promoter and terminator in the expression cassette. It is possible, however, that although our vector-encoded GFP-FAM49 and non-tagged FAM49 may share transcriptional efficiencies, their protein levels

might not be equivalent – for instance, if their mRNAs and/or proteins show very different degrees of stability.

Despite the prospect of our GFP-FAM49 lacking full functionality, we see no reason not to consider its localisation behaviour (section 2.3) as plausibly reflective of that of endogenous FAM49. There are published cases of fusion tag proteins which localise like their endogenous counterparts yet have limited functionality, e.g. GFP-actin (Aizawa *et al.*, 1997), therefore our case would not be unique.
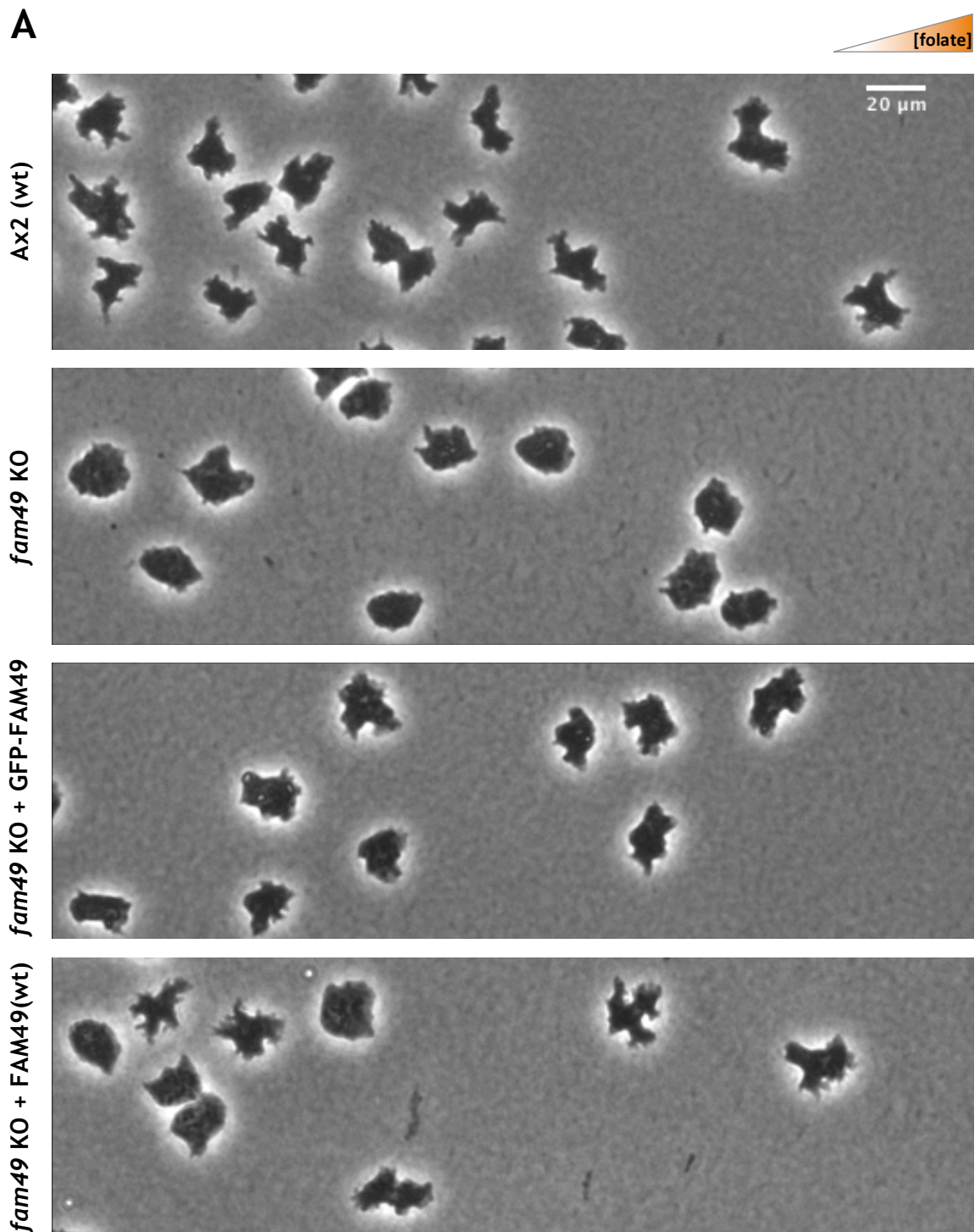
A

[folate]

20 μm

Ax2 (wt)

fam49 KO

fam49 KO + GFP-FAM49

fam49 KO + FAM49(wt)

Figure 2.21 – Motility-related defects in *fam49* KO cells are better rescued by non-tagged FAM49 than by GFP-FAM49
(continues next page)

Vegetative wild-type cells, *fam49* KO cells, *fam49* KO cells expressing GFP-FAM49 and *fam49* KO cells expressing non-tagged FAM49 ("FAM49(wt)") were imaged with phase contrast microscopy while moving up a folate gradient under an agarose gel (0.6% w/v, same concentration as in our assays for QuimP-based analysis, section 2.4.3.4). **A)** Pictures of Ax2 and Ax2-derived cell lines, taken from movies 7–10 (Appendix C). The general direction of cell movement is towards the right (towards the chemoattractant gradient, as illustrated). **B)** Pictures of Ax3 and Ax3-derived cell lines, taken from movies 11–14 (Appendix C). The general direction of cell movement is as in **A**. **C)** Cell circularity values, calculated in ImageJ/Fiji from cell outlines drawn manually on stills. A single un-cropped image, corresponding to the entire field of view captured by the microscope's camera and containing approximately 50 to 90 cells, was used in the analysis of each cell line. All images were recorded at comparable times after the start of each assay. Out-of-focus cells, as well as cells (…)

B
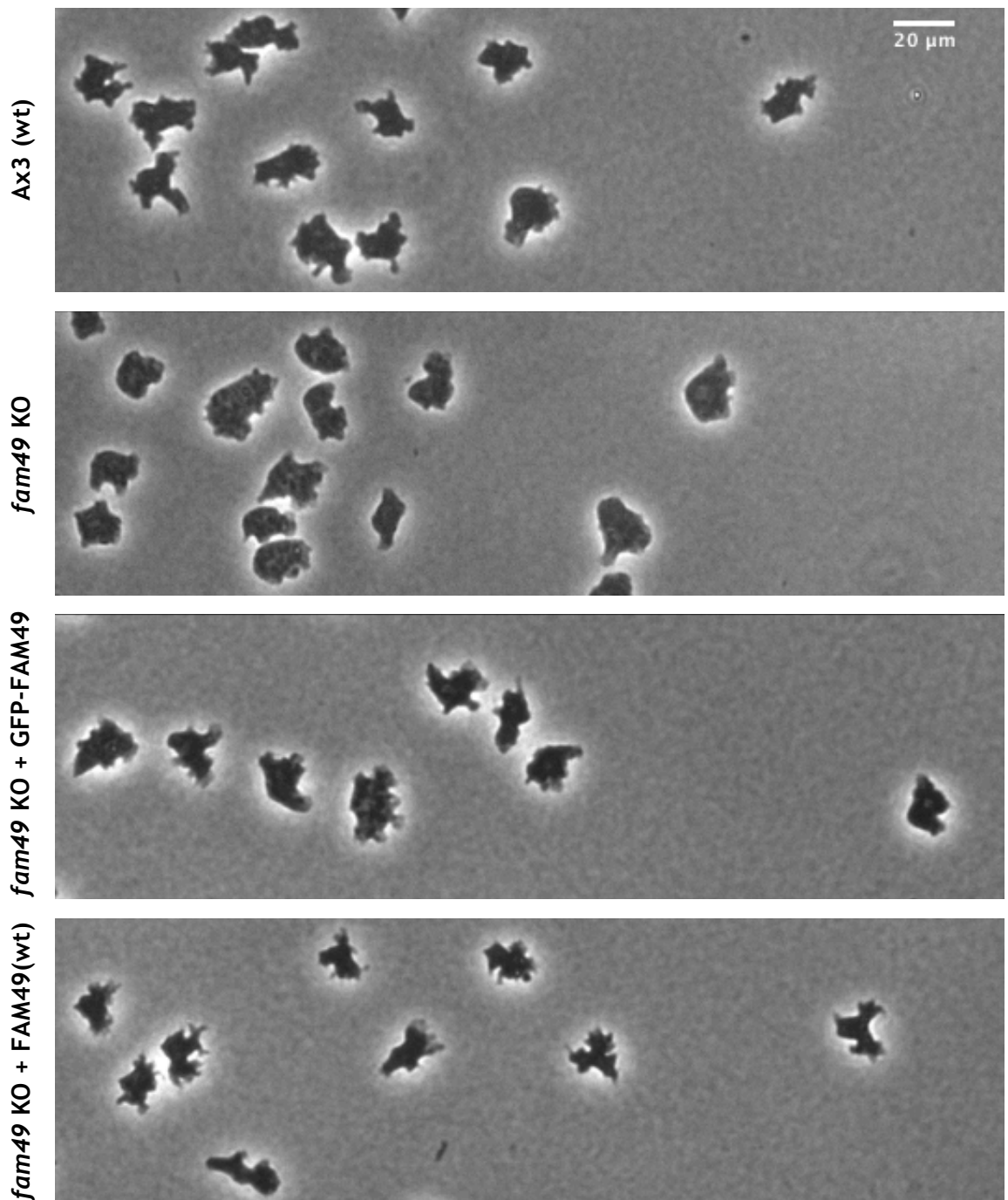
Figure 2.21 – Motility-related defects in *fam49* KO cells are better rescued by non-tagged FAM49 than by GFP-FAM49 *(continued)*
(continues next page)

(…) contacting other cells extensively or clearly attempting to divide were not considered. Plotted values represent single cells. Sample mean and 95% confidence interval for the population mean are shown for each data set. Indicated multiplicity-adjusted *p*-values (Wright, 1992) were obtained with Games-Howell multiple comparisons following a Welch's ANOVA (one-way ANOVA not assuming equal variances); "n.s." = statistically non-significant on the basis of an alpha level of 0.05. Percent changes in sample means were calculated using a formula equivalent to the one presented in the description of Table 2.6. **D)** For each represented cell line – Ax2 and Ax2-derived –, ten cells were continuously tracked over a period of 10 min, using the MTrackJ plugin for ImageJ (Meijering *et al.*, 2012); in the particular case of *fam49* KO cells expressing either GFP-FAM49 or FAM49(wt), only those looking phenotypically rescued (at least partially) in their protrusive (…)
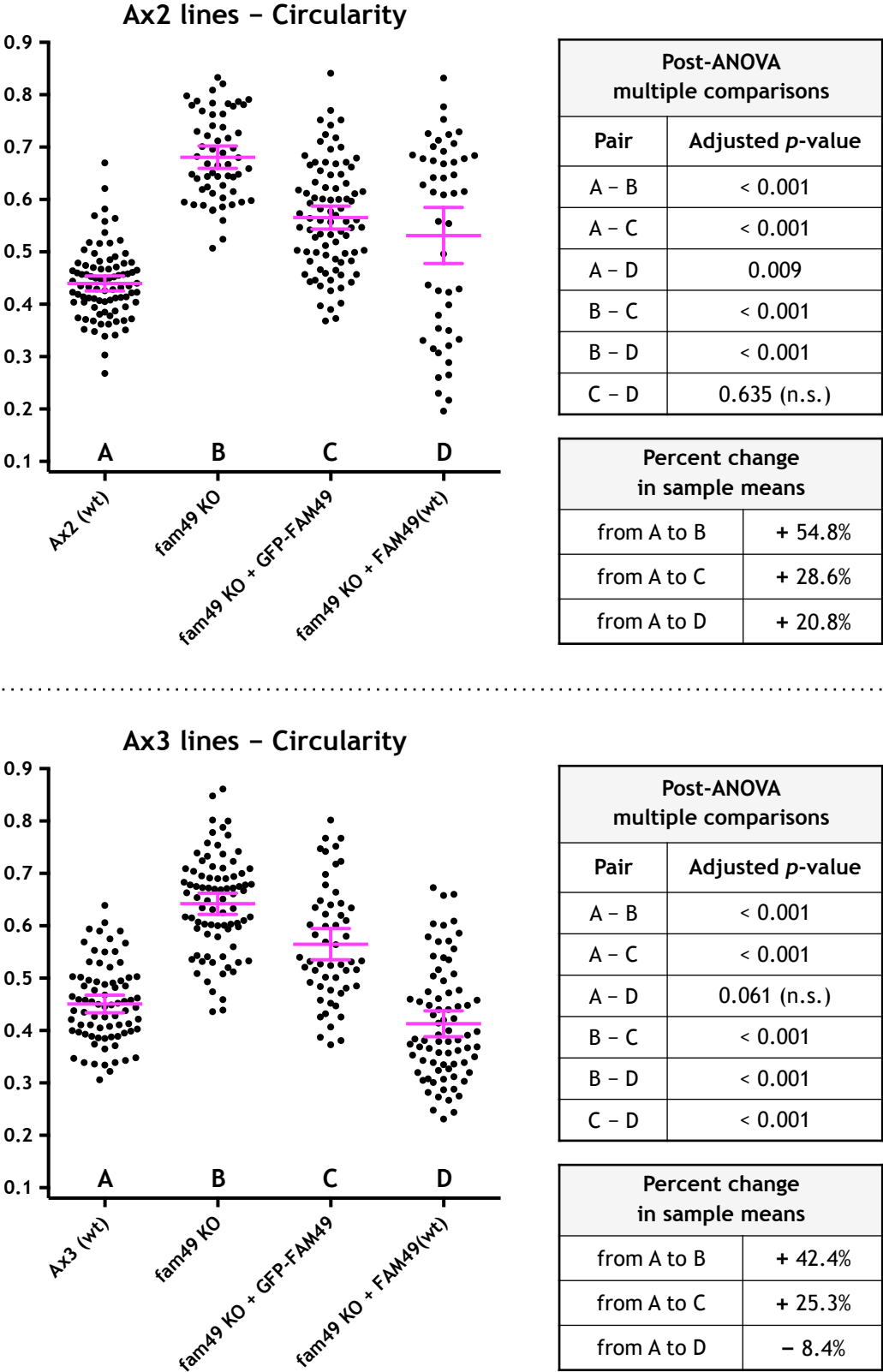
C

Ax2 lines – Circularity

Post-ANOVA multiple comparisons	
Pair	Adjusted *p*-value
A – B	< 0.001
A – C	< 0.001
A – D	0.009
B – C	< 0.001
B – D	< 0.001
C – D	0.635 (n.s.)

Percent change in sample means	
from A to B	+ 54.8%
from A to C	+ 28.6%
from A to D	+ 20.8%

Ax3 lines – Circularity

Post-ANOVA multiple comparisons	
Pair	Adjusted *p*-value
A – B	< 0.001
A – C	< 0.001
A – D	0.061 (n.s.)
B – C	< 0.001
B – D	< 0.001
C – D	< 0.001

Percent change in sample means	
from A to B	+ 42.4%
from A to C	+ 25.3%
from A to D	− 8.4%

Figure 2.21 – Motility-related defects in *fam49* KO cells are better rescued by non-tagged FAM49 than by GFP-FAM49 *(continued)*
(continues next page)

(…) behaviour were selected for tracking. The obtained trajectories were then plotted (as shown), being normalised so as to emanate from the origin ($x = 0$, $y = 0$). Axes of trajectory plots represent distance in µm. Different trajectories are shown in different colours. We also calculated the (…)

D

Ax2 lines – Tracks, speed and directionality
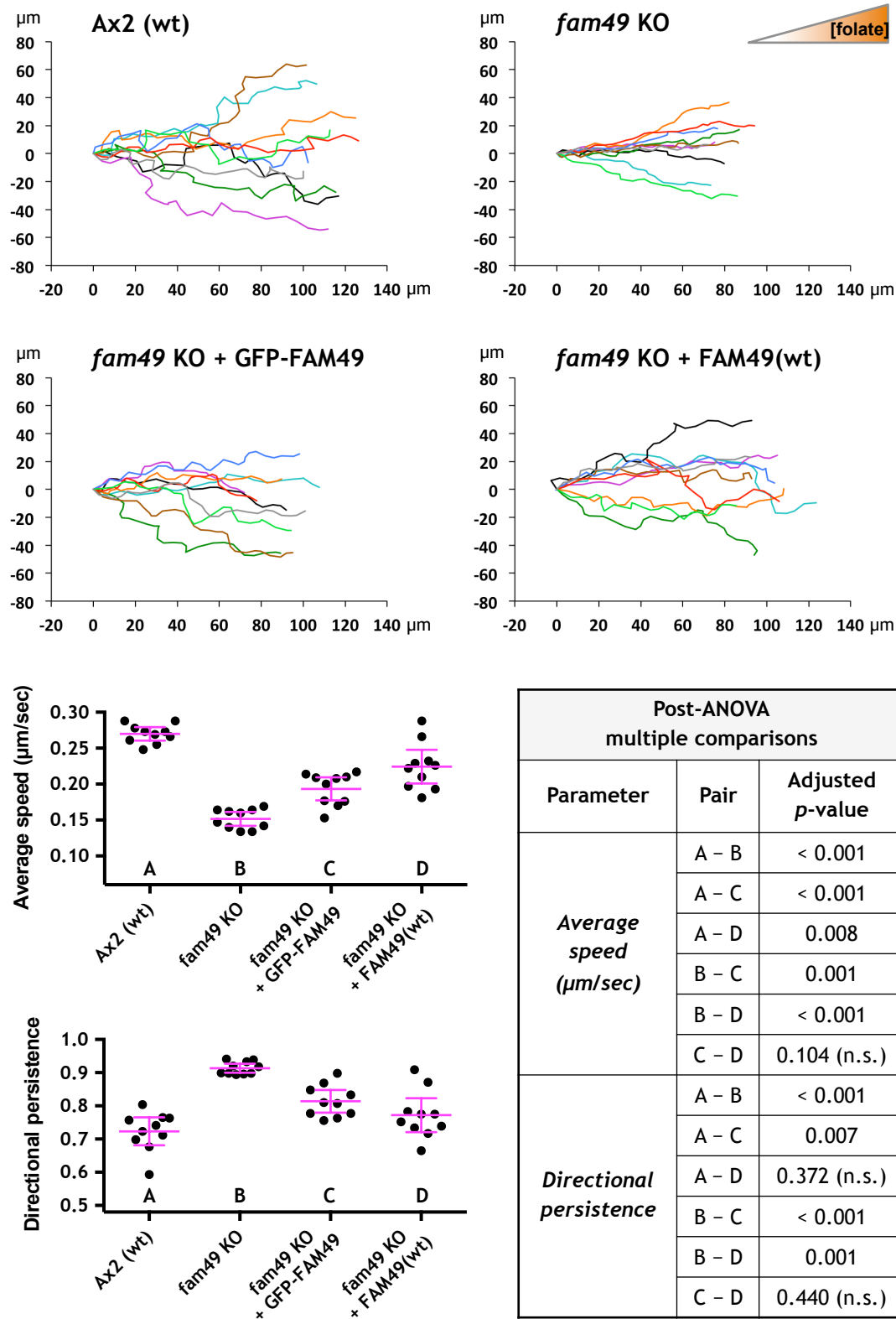
Figure 2.21 – Motility-related defects in *fam49* KO cells are better rescued by non-tagged FAM49 than by GFP-FAM49 *(continued)*
(continues next page)

(…) average speed and directional persistence of each tracked cell. For each of those two parameters, plotted values (as shown) represent single cells. Sample mean and 95% confidence interval for the population mean are shown for each data set. Statistical analysis was performed (…)

E   Ax3 lines – Tracks, speed and directionality
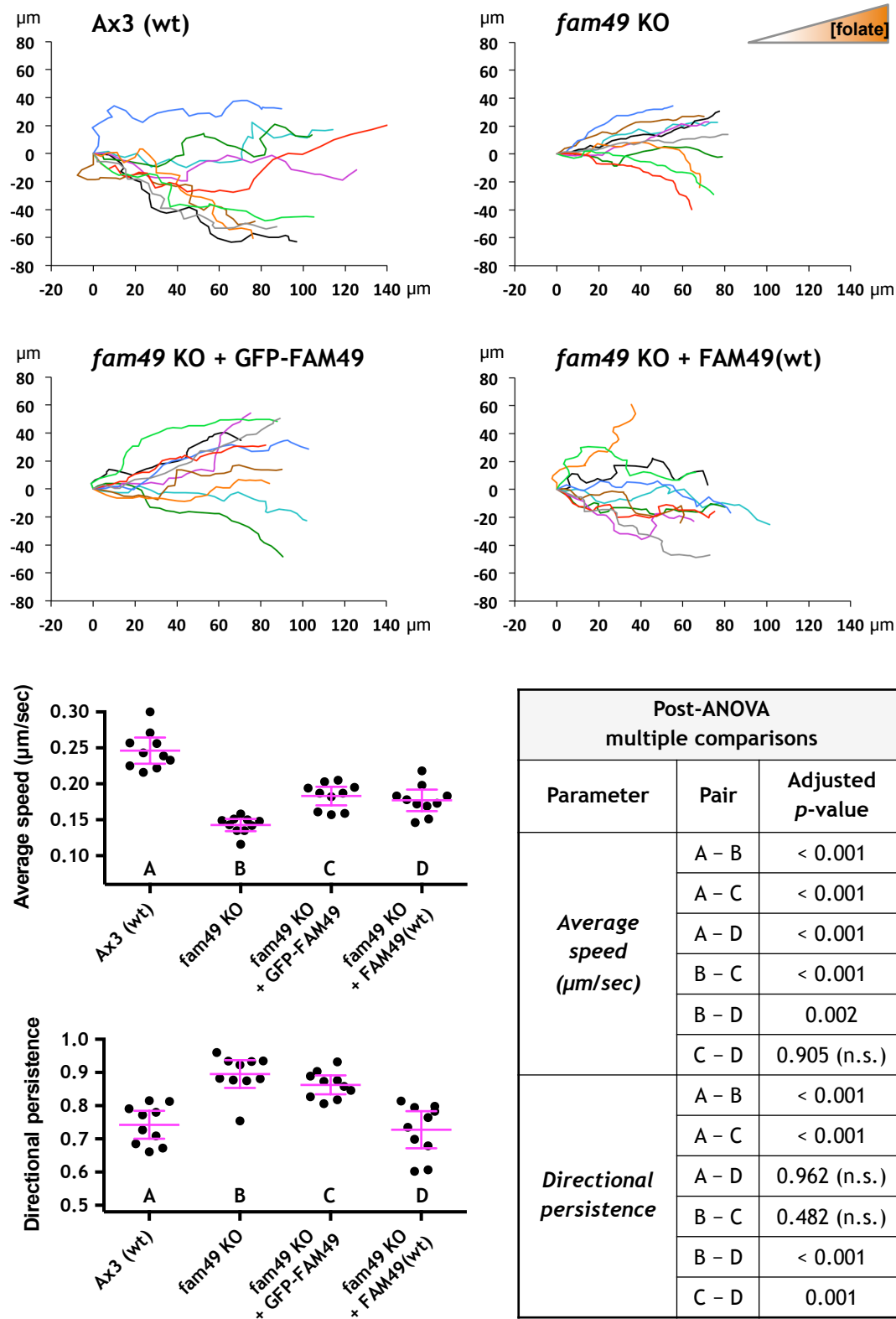
| Post-ANOVA multiple comparisons		
Parameter	Pair	Adjusted *p*-value
Average speed (µm/sec)	A – B	< 0.001
	A – C	< 0.001
	A – D	< 0.001
	B – C	< 0.001
	B – D	0.002
	C – D	0.905 (n.s.)
Directional persistence	A – B	< 0.001
	A – C	< 0.001
	A – D	0.962 (n.s.)
	B – C	0.482 (n.s.)
	B – D	< 0.001
	C – D	0.001

Figure 2.21 – Motility-related defects in *fam49* KO cells are better rescued by non-tagged FAM49 than by GFP-FAM49 *(continued)*

(…) as in **C**. **E)** Same as **D**, but for Ax3 and derived cell lines.

A (1)
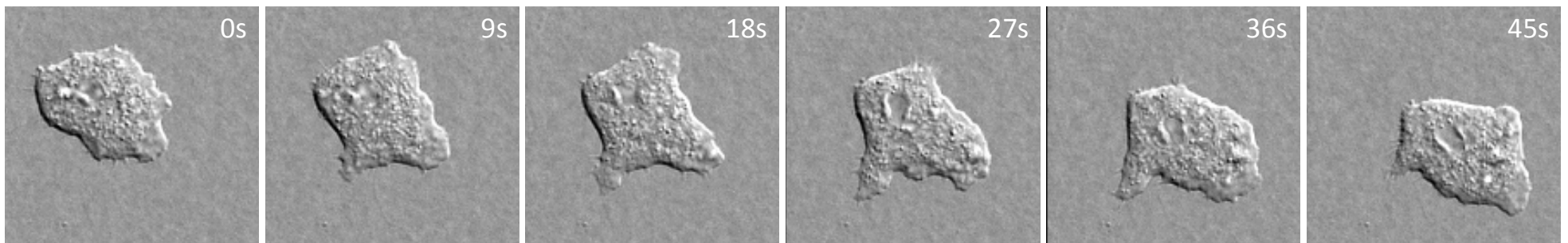
[folate]

Ax2

fam49 KO

Figure 2.22 – Both absence and overexpression of FAM49 affect the protrusive behaviour of cells
(continues next page)

Vegetative wild-type cells, *fam49* KO cells and *fam49* KO cells re-expressing FAM49 ("FAM49(wt)") – most likely at higher-than-wild-type (overexpression) levels – were imaged with DIC microscopy while moving up a folate gradient under an agarose gel (0.6% w/v). Image sequences of Ax2 and Ax2-derived cells, representative of movies 15–18 (Appendix C), are shown in **A**. Image sequences of Ax3 and Ax3-derived cells, representative of movies 19–22 (Appendix C), are shown in **B**. (…)

A (2)

fam49 KO + FAM49(wt)

[folate]

Figure 2.22 – Both absence and overexpression of FAM49 affect the protrusive behaviour of cells *(continued)*
(continues next page)

(…) Numbers indicate time in seconds. In the particular case of *fam49* KOs putatively overexpressing FAM49, the second/bottom image sequence is intended to highlight very thin (in some cases even filopod-like) pseudopods extending a substantial length beyond the bulk of the cell body (indicated by white arrows); similar pseudopods were not observed in wild-type cells.
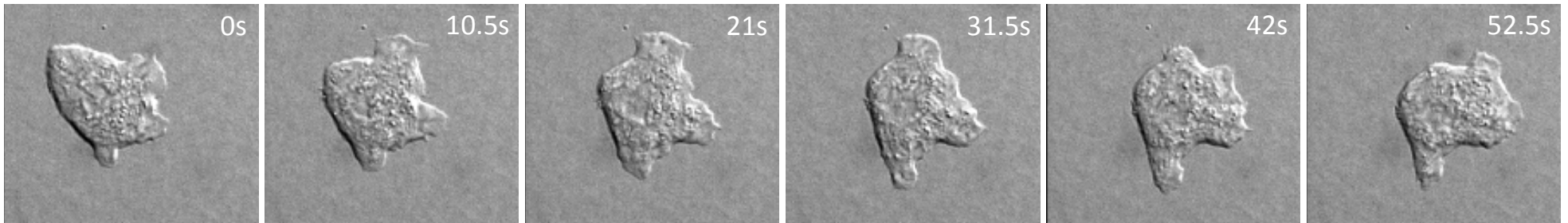
Figure 2.22 – Both absence and overexpression of FAM49 affect the protrusive behaviour of cells *(continued)*
(continues next page)

B (2)

fam49 KO + FAM49(wt)
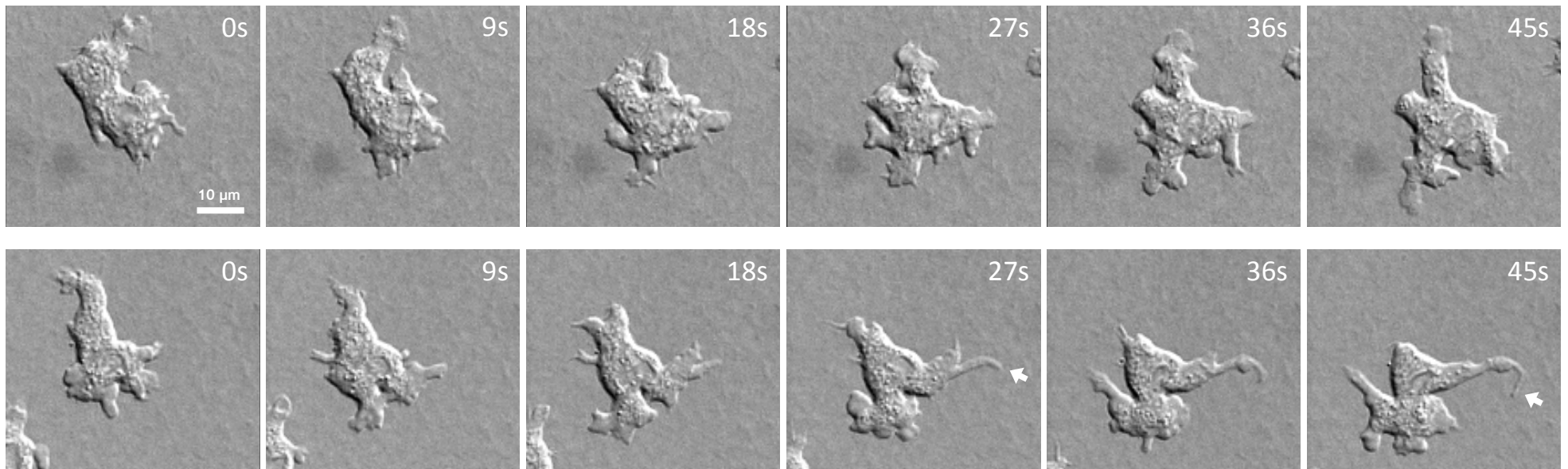
Figure 2.22 – Both absence and overexpression of FAM49 affect the protrusive behaviour of cells *(continued)*

3 Discussion

3.1 FAM49 modulates the protrusive behaviour and motility of *D. discoideum*

In the course of our research we gathered different pieces of data which collectively support a role for FAM49 in regulating the protrusive conduct, and ultimately motility, of *D. discoideum* cells.

Such role was first hinted at by our observations that GFP-FAM49 is enriched in actively extending pseudopods, showing fairly comparable spatio-temporal accumulation dynamics to active Rac. Despite the possibility of our GFP-FAM49 fusion protein not being fully functional (i.e. as functional as endogenous FAM49), we believe, in light of our other results (mentioned below), that its localization behaviour is not artefactual. We realize, nonetheless, that such behaviour might not perfectly represent that of endogenous FAM49.

We later determined that in comparison to wild-type cells, *fam49* KO cells tend to protrude less and more slowly – while exhibiting less discrete and apparently wider pseudopods –, and also move at lower speeds yet with higher directional persistence (in an under-agarose context). Although we only quantified protrusion parameters for Ax2 *fam49* KO and wild-type cells (using an approach based on QuimP), we are convinced, on the basis of careful visual inspection of moving cells and additional cell morphology and motility measurements, that Ax3 *fam49* KO and wild-type cells display differences in their protrusive behaviour which are comparable to the ones we quantified for their Ax2 counterparts.

Finally, we noticed that putative FAM49 overexpressor cells often generate pseudopods which are thinner – at times remarkably so – than those seen in wild-type cells, and also seem to protrude in an atypically highly dynamic, and perhaps less coordinated, way. Since we could not compare FAM49 expression levels between cell lines (due to the lack of availability of a FAM49 antibody), these particular observations, while strongly supportive of a role for FAM49 in modulating pseudopods, cannot be regarded as definitive and ought to be substantiated in future experiments.

According to our results, FAM49 is not essential for *D. discoideum* cells to make pseudopods and move about even in moderately restrictive environments (under low-percentage agarose gels). Nonetheless, our data point towards *fam49* KO cells being less adept at doing so than wild-type cells, which rises the possibility that FAM49 might in fact be crucial when cells face more highly restrictive contexts, perhaps common in *D. discoideum*'s natural environment (soil). Such could be the case if, for example, FAM49 somehow contributes toward pseudopods' protrusive force. The hypothesis of FAM49 being key in more restrictive environments could, in a first instance, be tested by comparing the motility of *fam49* KO and wild-type cells in under-agarose chemotaxis assays with progressively higher agarose concentrations. It has been reported that at a certain agarose concentration – about 3% w/v – wild-type cells are no longer able to force their way under it, likely because the agarose is too stiff for the cells to be able to deform it (Laevsky and Knecht, 2003); it may be, however, that such concentration/stiffness threshold is considerably lower for *fam49* KO cells (and perhaps higher for FAM49 overexpressor cells). It could also be helpful to determine whether FAM49's absence or overexpression affect pseudopod behaviour in ways that involve changes in pseudopodial F-actin's polymerization rate, density distribution and/or high order structure, as deviations in such parameters could provide hints towards FAM49's molecular function (more on this below).

3.2 A possible regulatory link between FAM49 and Rac1

The notion that *D. discoideum*'s FAM49 and its homologs contain a DUF1394 domain, which is also predicted in CYFIP/Pir121 proteins and likely involved in their binding to active Rac1 (Chen *et al.*, 2010, and this thesis), led us to speculate that FAM49 could perhaps also interact directly with Rac1. We did perform some *in vivo* imaging experiments to assess such possibility, the results of which were indeed in line with it. In particular, we determined that GFP-FAM49 and active Rac are substantially co-enriched in pseudopods and show comparable accumulation dynamics, and also that dominant-active (G12V) Rac1 triggers the recruitment and persistent accumulation of GFP-FAM49 at the plasma membrane, where both become highly co-enriched. Despite such promising results, and

mainly due to time constraints, we did not effectively test a direct interaction between *D. discoideum* FAM49 and Rac1 (or closely related Rac forms).

In our view, testing a direct FAM49-Rac1 interaction is, as it stands, the optimal starting point to try to understand the molecular workings of FAM49, and should therefore be prioritized in future research. If binding is confirmed, then functional assays may be conceived and performed, both *in vitro* and *in vivo* (e.g. testing Rac1's activity towards the SCAR/WAVE complex in the presence and absence of FAM49; more on SCAR/WAVE below). Even if a direct interaction turns out not to be validated, it could still be informative to further investigate the regulatory connection that seems to exist between FAM49 and Rac1, as suggested by our results, namely those with Rac1 G12V – by assessing, for instance, whether FAM49's absence or overexpression affect Rac1's activity levels and spatio-temporal enrichment dynamics within pseudopods.

3.3 FAM49 and SCAR/WAVE (plus some additional considerations on protein interactions and regulatory networks)

An interaction between FAM49 and the SCAR/WAVE complex was initially suggested by our screens looking for Nap1 interactors, as described at the very beginning of the *Results* chapter. As a consequence of prioritizing other experiments and ultimately due to time limitations, we did not attempt to confirm if FAM49 and the SCAR/WAVE complex may actually be binding partners. In spite of that, we now consider that testing such interaction should be a primary effort in future FAM49 research, as it could help to further uncover FAM49's activity at the molecular level.

A member of our lab, Jan Ohotski, has recently been able to purify GFP-Nap1-containing, endogenous SCAR/WAVE complex from *D. discoideum* cells (unpublished), which could potentially be used in *in vitro* assays to assess binding to FAM49. Other research groups have reported the successful purification of recombinant, as well as endogenous, human SCAR/WAVE complex (Chen *et al.*, 2010; Derivery *et al.*, 2009; Lebensohn and Kirschner, 2009), which could be

used to also test binding to human FAM49 homologs. As with active Rac1, if binding indeed occurs, then functional assays can be contemplated (e.g. assessing if FAM49's presence influences SCAR/WAVE's activity towards the Arp2/3 complex).

Although we did not attempt to confirm a FAM49-SCAR/WAVE complex interaction, we obtained data which strongly suggest that SCAR/WAVE still drives pseudopods in the absence of FAM49, and that FAM49 is still recruited to pseudopods in cells lacking a functional SCAR/WAVE complex. We also ascertained that FAM49's absence does not noticeably affect SCAR/WAVE's stability (at least in non-stimulated cells). Overall, our observations point towards FAM49 and SCAR/WAVE not requiring one another to accomplish their respective tasks; however, we cannot rule out the possibility that FAM49 might modify/fine-tune, directly or indirectly, SCAR/WAVE's activity, and/or vice-versa. An influence of FAM49 over SCAR/WAVE is, in fact, supported by our findings that pseudopodial dynamics in *fam49* KO cells and putative FAM49 overexpressor cells differ from those of wild-type cells, indicating that SCAR/WAVE's behaviour is necessarily altered – though it remains to be determined how.

It may be that FAM49 can interact with both Rac1 and the SCAR/WAVE complex (simultaneously or not), as seems to be the case with IRSp53 (Miki *et al.*, 2000) and lamellipodin (Law *et al.*, 2013). It is, of course, also conceivable that FAM49 may bind other proteins. Screening for additional FAM49 interactors would, in our view, be another good way to try to obtain more clues on what FAM49 does, and in particular how it exerts its modulatory effect on pseudopods. On this regard, GFP-FAM49 pull-downs could be attempted, ideally with a fusion construct known to be fully functional (i.e. as functional as endogenous FAM49).

It could be helpful to also determine whether FAM49 may be part of the actin cytoskeleton oscillatory network (CON) or its associated signal transduction excitable network (STEN), as defined by Huang *et al.*, 2013, in *D. discoideum* – such assessment could provide additional hints on FAM49's activity. Members of the CON group, which include the SCAR/WAVE complex, the Arp2/3 complex and F-actin, reportedly show fast oscillatory enrichments in convex, non-expanding locations around the cells' basal surface perimeter – as observed with TIRF mi-

croscopy –, and also get recruited to pseudopods in a series of bursts. Members of the STEN group, such as Ras and Rac GTPases, do not display fast oscillations and accumulate in pseudopods (for the mentioned GTPases, their active form) in a broader, smoother and more long-lasting fashion than CON members – again, as observed with TIRF microscopy (Huang *et al.*, 2013). According to the authors' STEN-CON coupling model of cell migration, the CON provides the "idling" motor force, which by itself can only drive small-amplitude plasma membrane undulations; in large protrusions, the CON is engaged by the STEN, which works as the "pacemaker" for cell movement. Although we co-imaged, using TIRF microscopy, fluorescent tagged versions of FAM49 and either SCAR/WAVE or a reporter for active Rac, we did not analyse our data in the way described by Huang *et al.*, 2013, as necessary for a clear assessment of a protein's possible inclusion into either STEN or CON, and which involves the analysis of fluorescent intensities over three-dimensional kymographs (so-called *t*-stacks). We will, nonetheless, make sure to revisit our data soon.

3.4 A role for FAM49 in cytokinesis and/or phagocytosis?

Despite the fact that we did not explore *fam49* KO's phenotypic defects other than those related to cell motility, we were left with a suspicion, on the basis of preliminary growth assays, that *fam49* KO cells might perhaps have defects in cytokinesis and/or phagocytosis.

Considering that both cytokinesis – at least its myosin II-independent, adhesion-dependent forms – and phagocytosis involve regulated actin protrusion events (King *et al.*, 2010; Cardelli, 2001), both processes might indeed be affected in the absence of FAM49 (or upon its overexpression). In myosin II-independent cytokinesis, actin protrusions at the poles drive the separation of the daughter cells (King *et al.*, 2010), whereas in phagocytosis, pseudopod-like actin protrusions allow the cell to engulf the to-be-internalized solid particles (Cardelli, 2001). When proteins such as SCAR/WAVE, ABP-120 (thought to be an F-actin cross-linker – Cox *et al.*, 1996) and DAip1 (suggested to control F-actin depolymerisation – Konzok *et al.*, 1999), which, like FAM49, regulate pseudopod acti-

vity and cell motility, are removed by gene KO in *D. discoideum*, cytokinesis and/or phagocytosis are also impaired (King *et al.*, 2010; Seastone *et al.*, 2001; Cox *et al.*, 1996; Konzok *et al.*, 1999).

Future experiments assessing cytokinesis and phagocytosis in *fam49* KO cells will allow clarifying FAM49's relevance in each of those processes.

3.5 Hypothetical model of FAM49's molecular workings

Although much needs to be clarified about FAM49, we would like to propose a model – illustrated in Figure 3.1 in a simplified, conceptual form – whereby FAM49 regulates Rac1 signalling and the SCAR/WAVE complex in *D. discoideum* cells. We think our model may, at least to some extent, explain FAM49's impact on *D. discoideum* pseudopod dynamics and motility (as well as data from our collaborators Loïc Fort and Laura Machesky, who have started investigating human FAM49B – we briefly discuss their results in section 3.6), as we clarify below.

We hypothesise, considering the data presented in this thesis, that FAM49 can indeed interact with active Rac1, doing so in a similar way to that suggested for CYFIP/Pir121 within the SCAR/WAVE complex (Chen *et al.*, 2010). We conjecture that such interaction occurs within pseudopods in a regulated fashion (more details on this below) and prevents, by means of steric blockage, the binding of Rac1 to the SCAR/WAVE complex and the concurrent activation of the latter (Figure 3.1). Furthermore, through additional steric and/or allosteric effects, FAM49's binding to active Rac1 may potentially also inhibit Rac1's signalling to other putative effectors (Figure 3.1) present in pseudopods, such as PakB, which phosphorylates and thus activates class I myosins MyoD and MyoK (Lee and Cote, 1995; Lee *et al.*, 1996; de la Roche *et al.*, 2005; Dieckmann *et al.*, 2010), both of which are thought to have roles in cell motility (Schwarz *et al.*, 2000; Chen *et al.*, 2012). Though there is a chance that FAM49 might also bind the SCAR/WAVE complex (Figure 3.1), we will not consider that possibility further.

As we just mentioned, we speculate that FAM49 is a well-regulated, competitive inhibitior of the SCAR/WAVE complex in pseudopods. We propose, in particular, that FAM49 binds active Rac1 throughout any given pseudopod except for a limited, well-defined region at its protruding edge, thus helping to confine SCAR/WAVE's activity to that region (it might be that such region harbors only a small fraction of the total number of SCAR/WAVE complex molecules that accumulate at a pseudopod's edge). Positive feedback loops acting on Rac1 and/or SCAR/WAVE will, as a result, also be circumscribed to that limited region, where for the most part actin polymerisation will also be spatially restricted to. Ultimately, this regulatory mechanism might provide control over the width of pseudopods, offering one possible explanation for the seemingly wider pseudopods of *fam49* KO cells and the thinner pseudopods of putative FAM49 overexpressing cells (in comparison to the average wild-type pseudopod). We think, however, that FAM49's potential control over SCAR/WAVE cannot explain, by itself, some other phenotypic traits we observed, particularly the slower protrusions of *fam49* KO cells and the abnormally dynamic protrusive behaviour of putative FAM49 overexpressing cells. Thus, we speculate that FAM49 might also impact Rac1 signalling to other effectors (Figure 3.1) also controlling pseudopod dynamics, leading to the particular phenotypes we saw.
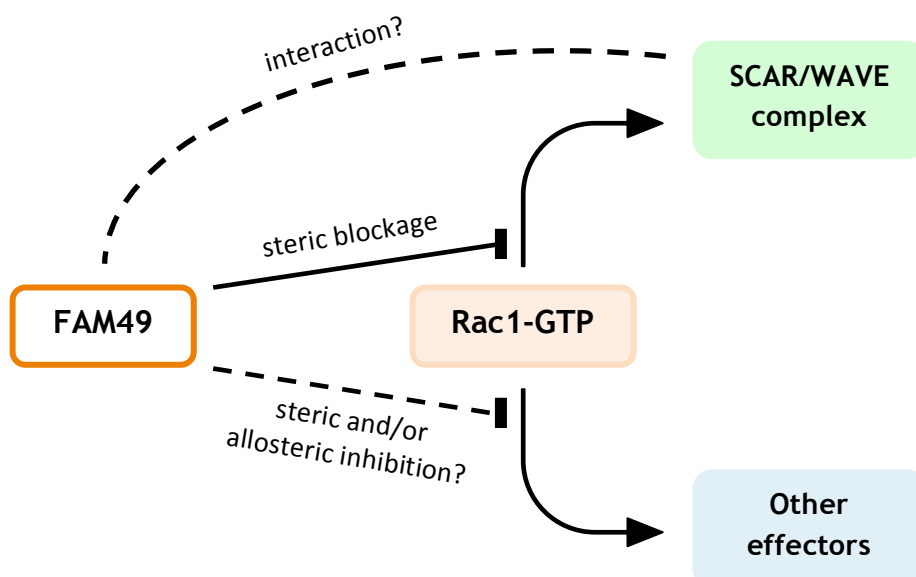
Figure 3.1 – Hypothetical model of FAM49's molecular workings
We speculate that FAM49 binds Rac1-GTP directly, blocking the latter's interaction with (and concomitant activation of) the SCAR/WAVE complex. It might be that FAM49 also inhibits Rac1 signalling to other effectors (in a steric and/or allosteric fashion). A regulatory interaction between FAM49 and the SCAR/WAVE complex is an additional possibility, which we will not speculate further about. See main text for further details and a discussion in the context of our results and those of our collaborators.

3.6 FAM49B in human cells – how it may also fit our hypothetical model

Our collaborators Loïc Fort and Laura Machesky, who have started investigating human FAM49B, recently obtained encouraging preliminary data from *in vitro* IPs which suggest that human FAM49B can bind directly to human active Rac1 but not to its inactive form or to the active forms of other Rho family GTPases, namely Cdc42 and RhoA (unpublished). Their results, together with our analyses, support the idea that a FAM49 interaction with active Rac1 might be well conserved in evolution.

L. F. and L. M. have also determined that human melanoma cells (CHL1) KO for FAM49B tend to show lamellipodial activity over wider regions of their perimeter, compared to wild-type (observations with cells plated on 2D substrates). Lamellipodial SCAR/WAVE enrichment also seems to be increased in their KO cells, suggesting higher levels of SCAR/WAVE activity (unpublished). Their results appear to be consistent with ours, since we often observed what seemed to be

wider (compared to wild-type) pseudopods in *D. discoideum fam49* KO cells. We did not, however, determine whether SCAR/WAVE complex enrichment is also typically higher and/or occupies wider regions (though we suspect that might be the case). L. F.'s and L. M.'s data are also clearly in line with our model of FAM49 limiting Rac1 signalling to the SCAR/WAVE complex, putting forward the possibility that it might be an evolutionarily well conserved role of FAM49.

Surprisingly, L. F. and L. M. also found that CHL1 cells KO for FAM49B move faster in 2D random motility assays *in vitro* (unpublished). This suggests that their protrusions might, in fact, extend faster than those of wild-type cells. These particular observations are not in accordance with ours, as we calculated lower cell speeds and lower protrusion extension speeds for *D. discoideum fam49* KO cells. It should be noted, nonetheless, that we only performed 3D-*like* under-agarose chemotaxis assays with *D. discoideum*; thus, direct comparisons should be drawn with precaution. Let us assume, for the sake of argument, that CHL1 cells KO for FAM49B protrude faster and move faster under any set of conditions, whereas the opposite is true for *D. discoideum fam49* KO cells. We are inclined to hypothesise – on the basis of our model for FAM49 – that the differences between human and *D. discoideum* cells are the outcome of dissimilarities in their Rac1 signalling networks, which FAM49 (note: here, and until the end of this paragraph, "FAM49" is used as a general term for FAM49 proteins of humans and *D. discoideum*) might modulate to different extents by means of its binding to active Rac1. We speculate, in particular, that FAM49 might provide control over not only Rac1 effectors common to human and *D. discoideum* cells – i.e. homologous proteins or protein complexes with functionally conserved roles –, namely the SCAR/WAVE complex (through a common mechanism of steric blockage), but also Rac1 effectors that may be unique to each species (through steric and/or allosteric inhibition) and which might be implicated in species-specific layers of regulation over diverse aspects of cell motility. In addition to these unique effectors, human cells and *D. discoideum* each probably express a number of species-specific proteins whose activity and/or gene expression is regulated further downstream of Rac1, and which are potentially susceptible to FAM49's actions. With this in mind, it can easily be envisioned how FAM49's removal might lead to human-specific and *D. discoideum*-specific outcomes in the finer aspects of protrusion dynamics, cell motility and overall cell behavior.

L. F. and L. M. have also observed – again, somewhat surprisingly – that CHL1 cells KO for FAM49B are more invasive in 3D invasion assays *in vitro* (unpublished). We suspect that this particular phenotype may, to a high degree, be a reflection of a higher capacity to degrade and remodel extracellular matrix (ECM) components. We base our suspicion on L. F.'s and L. M.'s additional observation that FAM49B knockdown CHL1 cells degrade more gelatin in 2D fluorescent gelatin-degradation assays in a metalloprotease (MMP)-dependent fashion (unpublished). Various reports suggest that higher levels of Rac1 activity in mammalian cells lead to enhanced expression, secretion and/or activity of different MMPs (Kheradmand *et al.*, 1998; Zhuge and Xu, 2001; Hsia *et al.*, 2003), so we are inclined to speculate that the lack of FAM49B in CHL1 cells might allow Rac1 signalling to be channeled toward ECM proteolysis (in addition to SCAR/WAVE activation and possibly other effects). It should be noted that we cannot compare these particular results with ours – in our assays, *D. discoideum* cells must force their way under the agarose and do not degrade it (Laevsky and Knecht, 2003).

L. F. and L. M. are currently attempting to determine if FAM49B is enriched in lamellipods and co-localises with active Rac1, and also what the phenotype of FAM49B-overexpressing cells might be. These additional pieces of data will allow us to make more informed guesses on the extent to which FAM49 proteins might act similarly in *D. discoideum* and human cells.

It should be noted that L. F. and L. M. have not investigated FAM49A (FAM49's second paralog in mammals) and we do not know whether it is expressed (and if so, to what degree) in CHL1 cells.

3.7 Potential relevance of FAM49 in cancer

L. F.'s and L. M.'s data suggest that human melanoma cells with reduced levels of FAM49B might become more invasive *in vivo,* thus contributing to cancer progression (Hanahan and Weinberg, 2000). As stated above, we speculate that CHL1 cells KO for FAM49B show higher invasiveness in 3D assays due to increased

Rac1 signalling not only towards SCAR/WAVE activation, but also – perhaps especially – higher expression and activity of ECM proteases. It is now well-established that the extent to which cancer cells are able to degrade and remodel the ECM is a decisive factor in their ability to invade (Hanahan and Weinberg, 2000). Conceivably, cancer cell types other than melanoma might also become more proteolytic – and thus invasive – if their levels of FAM49B (and/or FAM49A, in case it plays similar roles to FAM49B and is present in some tissues) are somehow reduced, or if FAM49B's actions towards Rac1 (according to our model) are somehow compromised by means of mutations. This rises the interesting possibility that FAM49B (and perhaps FAM49A?) might normally hinder cancer progression. Alternatively, it might be that, depending on the type of cancer, FAM49B either prevents or stimulates invasion; this is thought to be the case with SCAR/WAVE, whose activity has been suggested to support the invasion of melanoma and breast adenocarcinoma cells (Kurisu *et al.*, 2005; Sossey-Alaoui *et al.*, 2007b) but preclude that of squamous carcinoma cells (Tang *et al.*, 2013). Future experiments will tell.

We would like to add, as a final note, that Rac1 signalling has been implicated in the control of not only cancer cell invasion and metastasis but also other aspects of tumorigenesis, such as cell proliferation (Mack *et al.*, 2011). Thus, it might be that changes in FAM49B expression levels or activity lead to rather complex cancer phenotypes. Again, future experiments will be required to clarify this.

3.8 Final remarks

Overall, the work presented in this thesis strongly suggests that FAM49 has a role in modulating the protrusive behaviour of *D. discoideum* cells and ultimately the way they move, and that a regulatory connection between FAM49 and Rac1, perhaps involving a direct interaction (still to be verified), possibly exists. This thesis also lays the foundation for future research on FAM49, which will be required to clarify its activity and regulation at the molecular level. On this regard, our proposed hypothetical model of how FAM49 might affect Rac1 signalling should hopefully facilitate future studies. Data from our collaborators,

who are currently investigating human FAM49B, support the idea that a FAM49's role in controlling protrusion dynamics and cell motility has been preserved, at least to some degree, throughout evolution. This, in turn, suggests that FAM49 retained its biological relevance over time. This is hardly surprising, considering that FAM49's protein sequence is highly conserved from *D. discoideum* to humans. According to data made recently available at the International Mouse Phenotyping Consortium (IMPC) web portal (Koscielny *et al.*, 2014; database version 4.2), homozygous FAM49B KO mice have a tendency to die at preweaning age and surviving males are infertile, indicating that FAM49 is likely to be relevant at the whole-organism level in Metazoa, or at the very least in mammals. Clearly, FAM49 should get much attention in the future.

4 Materials and Methods

4.1 Bioinformatics

All protein sequences were obtained from UniProt (The-UniProt-Consortium, 2015).

BLASTP searches were run in UniProt's web-based BLASTP 2.2.29+ (The-UniProt-Consortium, 2015; Camacho *et al.*, 2009) using default settings.

Multiple sequence alignments were generated with MSAProbs 0.9.7 (Liu *et al.*, 2010), ran with default settings from within Jalview 2.8.2 (Waterhouse *et al.*, 2009). Jalview was also used for visualizing and annotating such alignments.

The phylogenetic tree in Figure 5.1 (Appendix A) was calculated with TOPALi 2.5 (Milne *et al.*, 2009) using a neighbour-joining method, default parameters and boot-strapping set at 100 runs. Final tree editing was done in FigTree 1.4.2 (Procter *et al.*, 2010).

Global pairwise sequence alignments were generated with EMBL-EBI's web-based EMBOSS Needle (Li *et al.*, 2015; Rice *et al.*, 2000) using default settings.

Data on DUF1394 was taken from its entry, PF07159, in Pfam 28.0 (Finn *et al.*, 2014).

Prediction-based 3D structure models and associated scores were obtained through the I-TASSER 4.1 web server platform (Roy *et al.*, 2010) using default parameters. Models were visualized in UCSF Chimera 1.10.2 (Pettersen *et al.*, 2004).

4.2 Cell lines and growth conditions

Axenic *D. discoideum* strains Ax2 and Ax3 were used as wild-type. *fam49* KO cells were generated in both Ax2 and Ax3 genetic backgrounds (details below). Ax3-derived *napA* KO cells are described elsewhere (Ibarra *et al.*, 2006).

Unless stated otherwise, cells were grown in HL5 medium (Formedium) with 100 U/ml penicillin and 100 µg/ml streptomycin (from Gibco's penicillin-streptomycin 10,000 U/mL formulation) in plastic Petri dishes (ø 100 mm), incubated at 21°C. The required selection markers (hygromycin and/or G418) were also added to the medium when growing cells transformed with one or more expression vectors (described below). Dish cultures were typically split every 3 to 4 days, before becoming over-confluent (i.e. with more than ~5.0-6.0 x 10^7 cells in total).

4.3 Extrachromosomal expression vectors and transformation procedure

Vectors for expression of GFP-FAM49 (pJB22) and FAM49-GFP (pJB23) were generated as follows. FAM49's open reading frame (ORF) without its stop codon was first PCR-amplified from Ax2 genomic DNA using primers 5'-GCAGATCTAAAATGG GTCAATTACTTAGTTTTATCAATGG-3' and 5'-CGACTAGTATCAAGTAATAACAATTGT TTAATGGC-3', which added BglII and SpeI restriction sites before the start codon and after the last codon, respectively. The resulting PCR product was then cloned into the commercial pCR-Blunt II-TOPO vector (Life Technologies) using the Zero Blunt TOPO PCR Cloning Kit (Life Technologies) and subsequently fully sequenced, to confirm absence of mutations (using FAM49's gene data on dictyBase as reference – Basu *et al.*, 2013). Finally, FAM49's ORF was subcloned – on the basis of BglII/SpeI site compatibility – into expression vectors pDM448 and pDM450 (Veltman *et al.*, 2009a), for N-terminal and C-terminal GFP fusion proteins, respectively.

The vector for expression of non-tagged FAM49 (pJB30), which has the same backbone as pJB22 and pJB23 above, was obtained by sub-cloning FAM49's ORF into pDM358 (Veltman *et al.*, 2009a), again on the basis of matching BglII/SpeI restriction sites.

The vector for co-expression of GFP-FAM49 and PakB(CRIB)-mCherry (pJB27) was created by excising the NgoMIV site-flanked expression cassette of PakB-(CRIB)-mCherry from "shuttle" vector pDM1023 (previously generated by Douwe Veltman in our laboratory; unpublished) and cloning it into the single NgoMIV si-

te in pJB22. The same strategy was employed to create the vector for co-expression of GFP-FAM49 and SCAR-mCherry (pJB28), with the NgoMIV site-flanked expression cassette of SCAR-mCherry being taken from "shuttle" vector pDM1061 instead (also previously generated by D. Veltman; unpublished).

The vector for doxycycline-inducible expression of dominant-active (G12V) Rac1, pDM1078, had been previously generated by D. Veltman (unpublished); it is identical to the already reported pDM987 (Veltman *et al.*, 2012), except for its resistance marker cassette, which contains a resistance gene for G418 instead of hygromycin. Rac1 G12V expression was induced by adding 10 µg/ml doxycycline to the culture medium.

Vectors pDM945 and pDM608, both previously created by D. Veltman (used, but not named, in Veltman *et al.*, 2012) allowed co-expression of HSPC300-GFP and PakB(CRIB)-mRFPmars2, and GFP-WASP A and mRFPmars2-ArpC4, respectively, each of which was imaged individually for the analysis presented in section 2.4.3.1.

Vector pAD167, previously generated by Andrew Davidson in our laboratory (unpublished), was used for co-expression of GFP-Nap1 and Lifeact-mRFPmars2.

Annotated maps of all the vectors used in this thesis are shown in Figure 4.1.

"Target" vectors
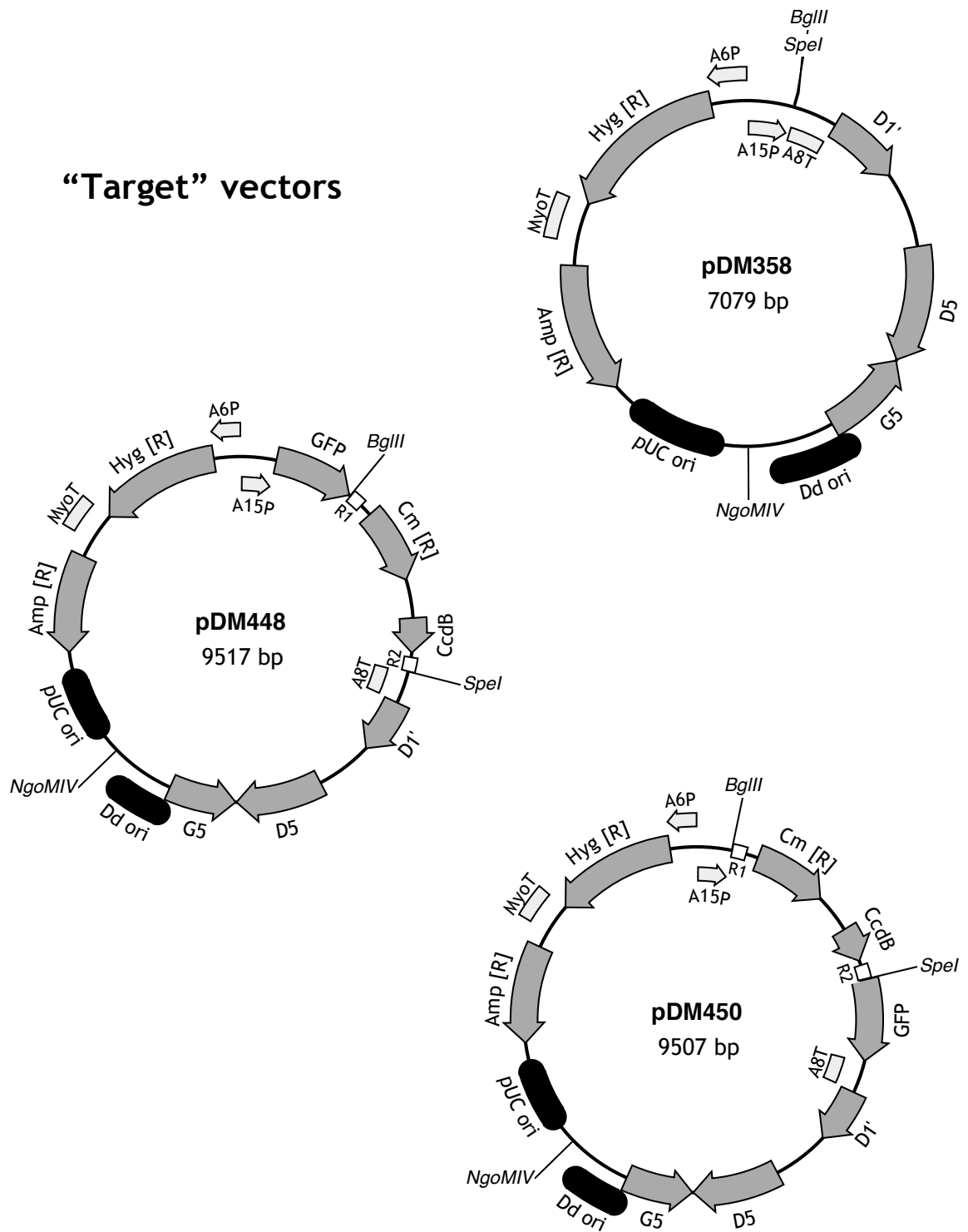
Figure 4.1 – Maps of plasmids/vectors used in this thesis
(*continues next page*)

"Target" and "shuttle" vectors were used in cloning procedures; final vectors were employed in experiments. Wide, dark grey arrows represent ORFs. Thin, light gray arrows and boxes indicate *D. discoideum* transcription promoters and terminators, respectively. Black rounded boxes denote origins of replication for *E. coli* (pUC ori) and *D. discoideum* (Dd ori). All "target" and final vectors contain a region that supports extrachromosomal replication in *D. discoideum*; said region encompasses Dd ori, G5, D5 and D1' (further details in Veltman *et al.*, 2009a). "Target" vectors pDM448 and pDM450 harbor a Gateway conversion cassette with attR recombination sequences (small white boxes R1 and R2, which stand for attR1 and attR2, respectively) within their GFP-fusion expression cassette; in both cases, the Gateway cassette is flanked by BglII and SpeI restriction sites, which allowed for its removal and subsequent cloning of FAM49's ORF, as described in (…)

"Shuttle" vectors
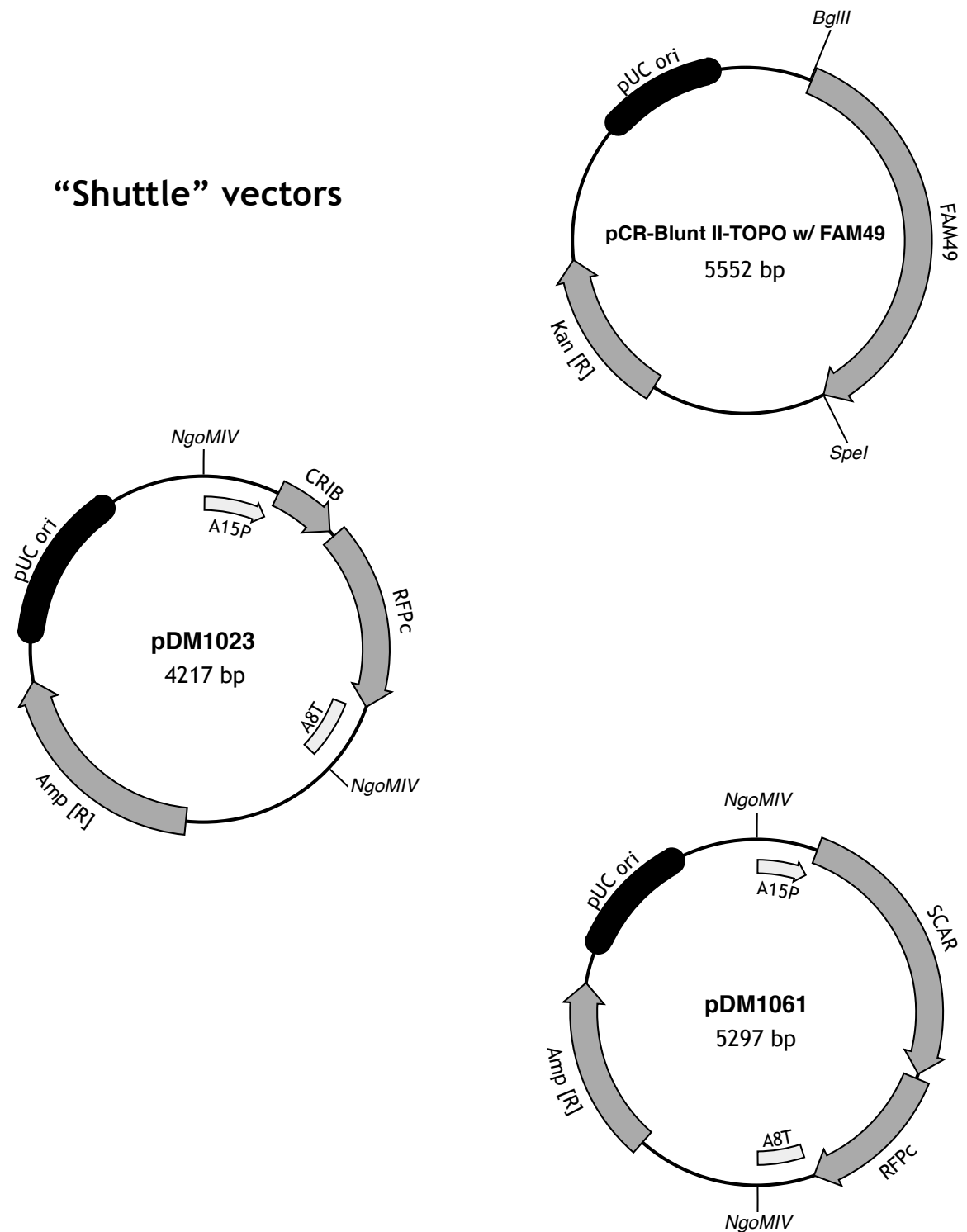
Figure 4.1 – Maps of plasmids/vectors used in this thesis *(continued)*
(*continues next page*)

(…) the main text. Hyg [R], G418 [R], Amp [R] and Kan [R] indicate resistance gene ORFs for hygromycin, G418, ampicillin and kanamycin, respectively; the first two allow the selection of *D. discoideum* transformants, whereas the last two allow the selection of *E. coli* transformants. RFP2: mRFPmars2. RFPc: mCherry. CRIB: PakB(CRIB). HSPC: HSPC300. Lf: Lifeact. Rac1A*: constitutively activated Rac1A (G12V). rtTA-M2s*: doxycycline-dependent transcriptional activator (further details in Veltman *et al.*, 2009b). A6P: *act6* promoter. A15P: *act15* promoter. cP: *coaA* promoter. TRE-Pmin: inducible promoter consisting of 7 repeats of the TetO operator fused to a minimal fragment of the *act15* promoter (further details in Veltman *et al.*, 2009b). A8T: *act8* terminator. MyoT: *mhcA* terminator.

Final vectors
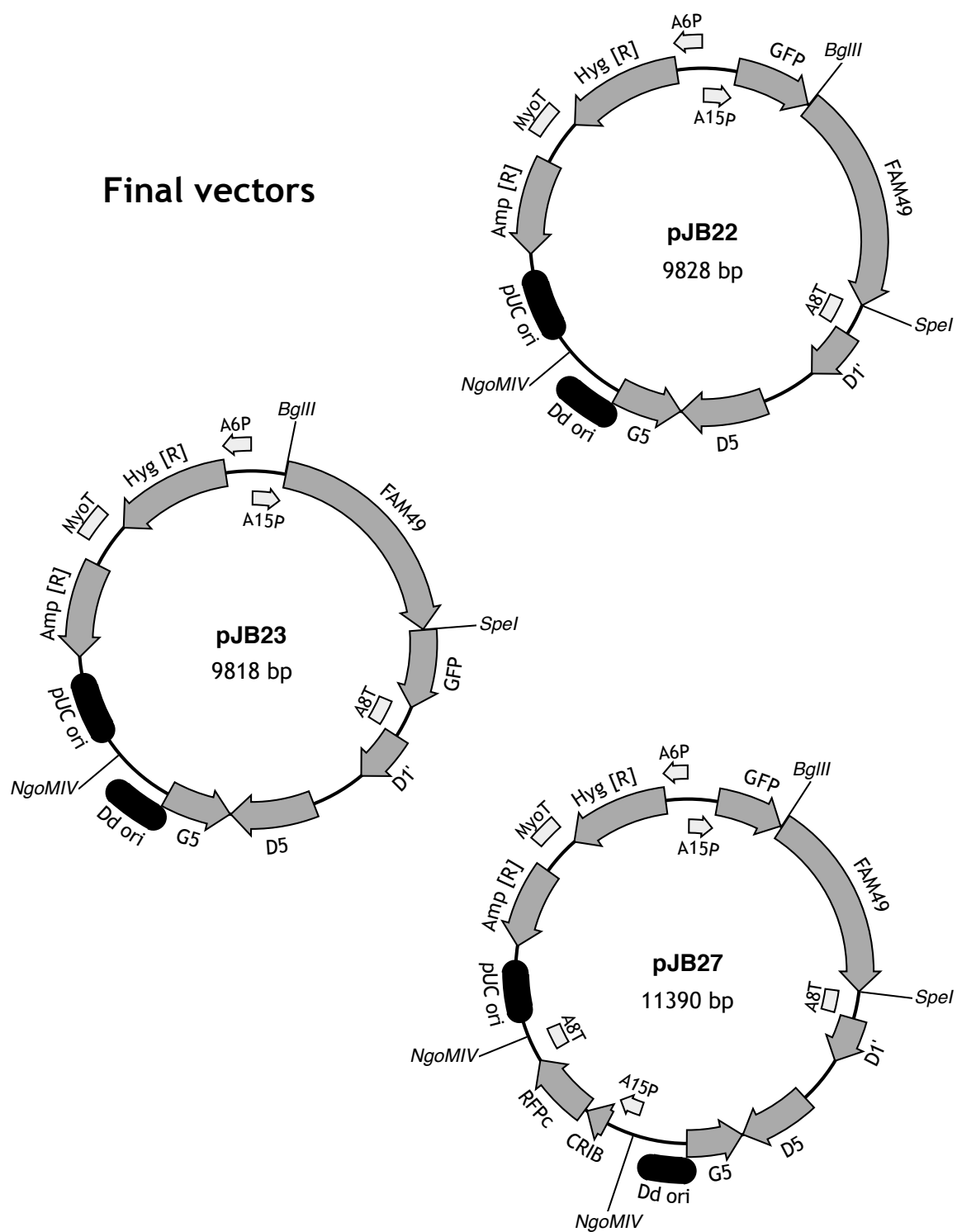
pJB22
9828 bp

pJB23
9818 bp

pJB27
11390 bp

Figure 4.1 – Maps of plasmids/vectors used in this thesis *(continued)*
(*continues next page*)
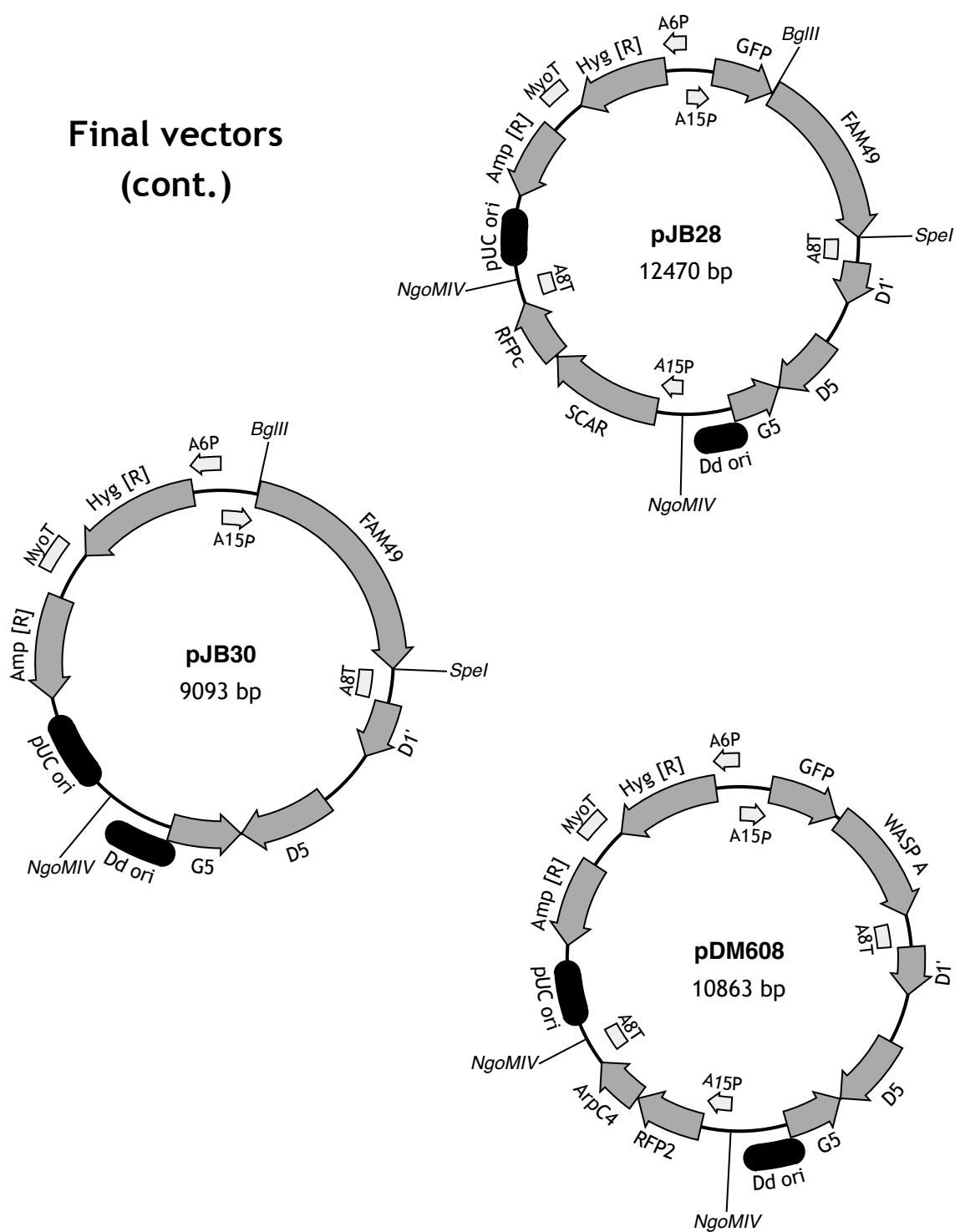
Final vectors
(cont.)

Figure 4.1 – Maps of plasmids/vectors used in this thesis *(continued)*
(*continues next page*)

Final vectors (cont.)
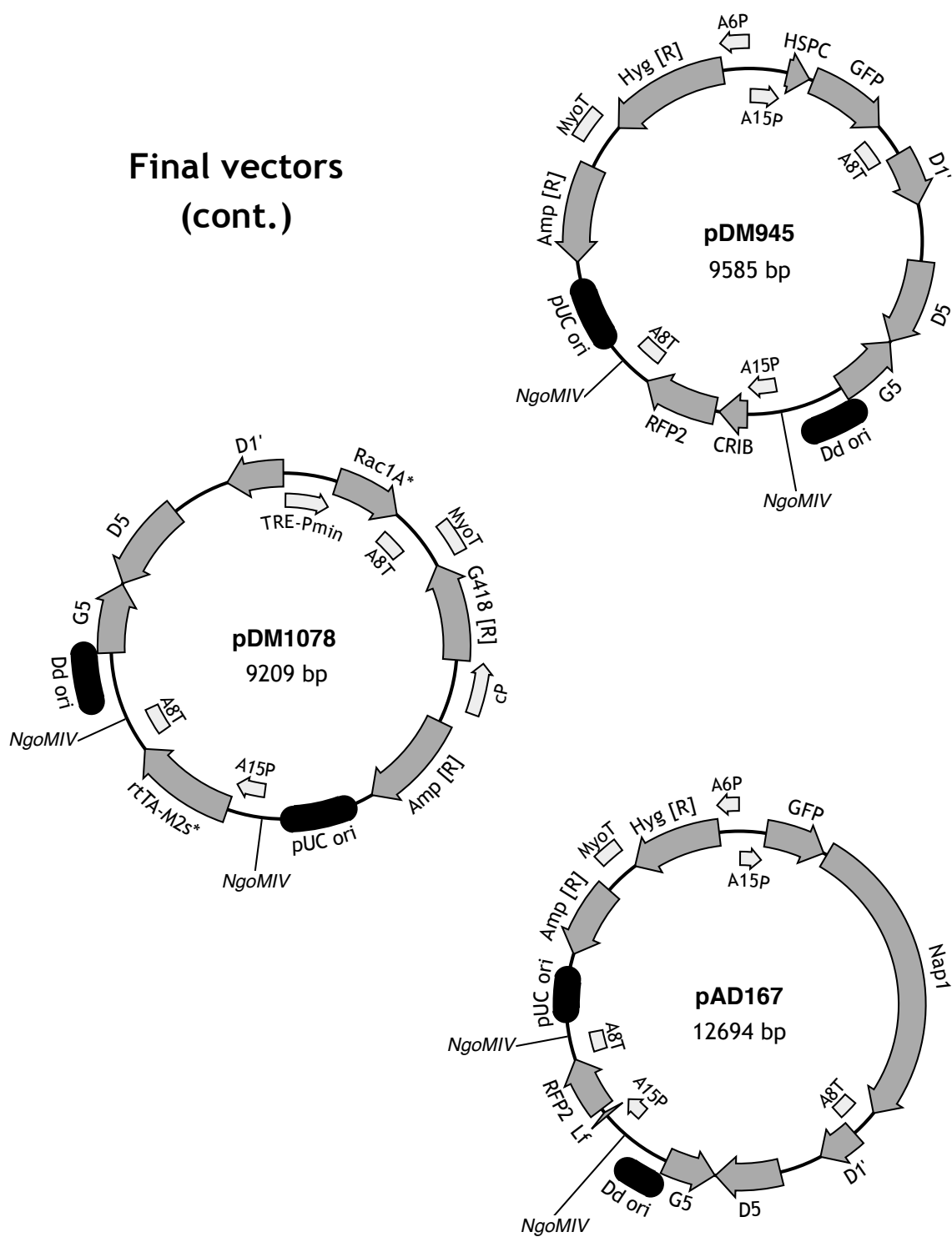
Figure 4.1 – Maps of plasmids/vectors used in this thesis *(continued)*

Transformation of cells with an expression vector (general procedure)

For each transformation, 2.5-3.0 x 10^7 cells were used, harvested from a healthy culture. Cells were first centrifuged (3 min, 330 g, 4°C), washed with 10 ml ice-cold electroporation buffer (E-buffer; 10 mM sodium phosphate buffer pH 6.1, 50 mM sucrose), centrifuged again and resuspended in 400 µl ice-cold E-buffer. The cell suspension was then transferred to an ice-cold 0.2 cm electroporation cuvette and mixed with 0.5-1.0 µg of expression vector DNA (typically 5-10 µl of a DNA miniprep). After being kept on ice for 5 min, the cuvette was exposed to a 3-4 ms ~500V pulse in a BTX-Harvard Apparatus ECM 399 electroporator and immediately returned to ice. Ten minutes later the cell suspension was transferred to a plastic Petri dish (ø 100 mm) and mixed with 4 µl of healing solution (0.1 M $MgCl_2$, 0.1 M $CaCl_2$). The cells were then incubated at 21°C for 15 min, after which 10 ml of HL5 medium were added to the dish. Following further incubation at 21°C for an additional 12-18 hours, the required selection marker was added to the medium (50 µg/ml hygromycin or 10 µg/ml G418). The culture was subsequently kept at 21°C and its medium replaced 2 days later to remove most dead cells, then again every 3 to 4 days as required (always including the appropriate selection marker). Generally, transformants reached confluence (~5.0-6.0 x 10^7 cells) within 14 days after electroporation.

Cells were never transformed with more than one expression vector except for the experiment described in section 2.3.3, which required cells transformed with two distinct vectors (pJB27 and pDM1078).

4.4 Generation and validation of *fam49* KOs

Making of, amplification and purification/concentration of the *fam49* KO construct

Our linear *fam49* KO construct (2758 bp in length), which consisted of a blasticidin resistance (Bsr) cassette flanked by sequences matching 5' and 3' regions in the *fam49* gene locus, was made as follows. First, its 5' and 3' "arms" (843 and 766 bp, respectively) were obtained/amplified by PCR using Ax2 genomic DNA and primers 5'-GTGACATTAAGGCAATAATAATAATAATAGAATTC-3' and 5'-

GTCTAGGAGCTCAGACGCCATCATAAGCAGTTCTAC-3' (5' arm), and 5'-GTGACAG TGCGTACTGGCCTCATATTATCGTCGTAC-3' and 5'-TGGTGGATGATGGTATTTGGT GATTGTGATGTTTTC-3' (3' arm); primers were designed in such a way as to add 18 bp "cross-over" sequences at the 3' end of the 5' arm and at the 5' end of the 3' arm, which matched sequences at the 5' and 3' ends, respectively, of the to-be-used Bsr cassette. Both PCR-amplified "arms" were gel-purified and subsequently used with purified Bsr cassette in another PCR reaction, this time intended to merge all three DNA segments into the final *fam49* KO construct; used primers were 5'-GTGACATTAAGGCAATAATAATAATAATAGAATTC-3' and 5'-TGGT GGATGATGGTATTTGGTGATTGTGATGTTTTC-3'. The PCR-produced *fam49* KO construct was gel-purified and then further amplified in 50 PCR reactions, each in a 50 µl volume, using the same primer pair; this was done in order to generate enough *fam49* KO construct DNA for two transformations, as described below. After pooling the volume of all PCR reactions, the KO construct DNA was purified with an equal volume of phenol:chloroform:isoamyl alcohol (25:24:1, v/v) (Thermo Fischer), collected in the aqueous fraction, precipitated by adding ~1/10 volume of sodium acetate (3 M, pH 5.2) and ~2.5 volumes of 100% ethanol, washed in 70% ethanol and finally dissolved in 30 µl of sterile TE buffer (10 mM Tris-HCl buffer pH 8.0, 0.1 mM EDTA). The obtained "KO construct prep" was then kept on ice until used for transforming cells on the same day (below).

Transformation of Ax2 and Ax3 cells with the KO construct and selection of blasticidin-resistant clones

For each transformation, 2.5-3.0 x 10^7 cells were used, harvested from a healthy culture. Cells were first centrifuged (3 min, 330 *g*, 4°C), washed with 10 ml ice-cold E-buffer without sucrose, centrifuged again, washed with 10 ml ice-cold E-buffer, centrifuged a final time and resuspended in 400 µl ice-cold E-buffer. The cell suspension was then transferred to an ice-cold 0.2 cm electroporation cuvette and mixed with 13 µl of "KO construct prep" (containing an estimated 10-15 µg of DNA). After being kept on ice for 5 min, the cuvette was exposed to a 3-4 ms ~500V pulse in a BTX-Harvard Apparatus ECM 399 electroporator and immediately returned to ice. Ten minutes later the cell suspension was transferred to a plastic Petri dish (ø 100 mm) and mixed with 4 µl of healing solution (0.1 M MgCl$_2$, 0.1 M CaCl$_2$). The cells were then incubated at 21°C for 15 min, after which 10 ml of HL5 medium were added to the dish. Following further incuba-

tion at 21°C for an additional 22-24 hours, the cells were resuspended in 90 ml of fresh HL5 with 7.5 µg/ml blasticidin and distributed in 96-well plates (150 µl per well). These plates were kept at 21°C for approximately 2 weeks, then inspected for clonal colonies. Detected clones were propagated (initially in 6-well plates) and tested for disruption of the *fam49* locus (below).

PCR-based validation of *fam49* KO clones

Clones obtained after blasticidin selection were screened/validated by PCR, as illustrated in Figure 2.12 (*Results* chapter). Primers used were 5'-GAGGTCCAGC TATCATCGA-3' and 5'-TCACATGTATCTTATGATAATG-3'. While real *fam49* KOs would yield a 2450 bp PCR product, random integrants (clones with a KO construct integration elsewhere in the genome) and wild-type cells would produce a 1983 bp PCR product instead.

4.5 Assorted assays

4.5.1 Under-agarose chemotaxis assay

With vegetative cells (standard)

This assay is based on that described by Woznica and Knecht, 2006.

One glass-bottom dish (50 mm full diameter, 30 mm central glass diameter; MatTek) was used for each individual under-agarose chemotaxis assay. First, the inner bottom surface of the dish was treated with 3 ml of 10 mg/ml BSA (in dH$_2$O) for 10 min, after which the BSA was removed and the dish left open to dry for 5 min inside a laminar flow cabinet. Next, 5 ml of molten 0.4% w/v SeaKem GTG agarose in SIH medium[*] (Formedium) were poured into the dish and left to set for 1 hour. A higher agarose concentration, 0.6%, was used in some (later) experiments, namely those intended for QuimP-based quantitative analysis of cell motility parameters (section 2.4.3.4) and subsequent phase contrast and DIC microscopy observations (section 2.4.3.5). With the agarose set, two ~17 mm long and ~5 mm wide wells were cut in it, ~5 mm apart, in the central region of the

---

[*] In our hands, SIH medium (Han *et al.*, 2004) is less fluorescent than HL5 medium, facilitating fluorescence microscopy imaging efforts with vegetative cells.

dish (glass-bottomed); this was facilitated by using a printed template. Sufficient vegetative cells (usually 500-1000 µl of a resuspended dish culture) were then harvested into a 1.5 ml tube, briefly centrifuged (~10 seconds with continuous acceleration, up to ~12000 g), washed with 1 ml of SIH, centrifuged again and resuspended in SIH at $1.0\text{-}2.0 \times 10^6$ cells/ml. One hundred microliters of cell suspension and a similar volume of SIH were then added to one agarose well, filling it to just under the brim. Ten minutes later, at which point most cells in the well were already attached to the glass surface, ~200 µl of 0.1 mM folate in SIH (prepared fresh from a 50 mM folate stock in 0.1 N NaOH) were added to the opposite well. Following this, a 20 x 20 mm glass coverslip was carefully lowered onto the agarose in such a way as to cover both wells (to minimize drying and improve optics) while leaving a small gap at their "top"/"bottom"; through such gap, the wells were then filled completely with SIH (well with cells) or 0.1 mM folate (well with folate). The dish was then kept at ~21°C for between 3h15 and 3h45 before any microscopy imaging. Generally, a good number of cells can be seen chemotaxing under the agarose by the end of such period of time, and chemotaxis will continue for at least a few hours more. Wells were replenished again whenever required.

With starved cells

For the occasion where starved cells were used (section 2.3.1), the "standard" under-agarose chemotaxis assay described above was modified slightly: SIH was replaced with Na/K phosphate buffer (PB; 10 mM Na/K phosphate buffer pH 6.6) in all instances, and cAMP (10 µM in PB, prepared fresh from a 1 mM cAMP stock in dH_2O) was used as chemoattractant. Cells were starved for 4 h in PB, as a confluent layer on dish, prior to being used in the assay.

For QuimP-based quantitative analysis of cell motility parameters (vegetative cells only)

As mentioned above, under-agarose chemotaxis assays intended for QuimP-based analysis (using vegetative cells) were prepared with 0.6% agarose. Furthermore, the agarose was mixed with 2 mg/ml of ~40 kDa TRITC-dextran (final concentration; added from a 20 mg/ml stock in dH_2O) while still molten, and left to set on the assay dish for 2 hours before cutting the wells. To minimize short-term leakage of TRITC-dextran from the agarose to the wells (and its subsequent inges-

tion by cells, which leads to undesirable intracellular fluorescence later on), they were first loaded with fresh SIH (200 µl) every ~30 min for ~2 hours, and only afterwards with cells or folate. Details on microscopy imaging, time-lapse image processing and quantitative analysis of cell motility parameters associated with these "QuimP assays" are provided below (section 4.6.1).

4.5.2 Growth in HL5 in shaking suspension

For each cell line, the cells of a nearly confluent dish culture (containing ~4.0-5.0 x 10^6 cells/ml) were resuspended and 400-500 µl seeded in 10 ml of fresh HL5 medium in a 100 ml glass flask. Flasks were then left shaking at 170 r.p.m., 21°C, for 3 days. At 30 min, 23h30, 48h and 74h after seeding, 20 µl of each shaking culture were collected so as to determine cell densities and average cell diameters using a CASY cell counter/analyzer (Innovatis). Average population doubling times were calculated with the web-based Doubling Time program (http://www.doubling-time.com) using cell density values from all time points. Final data were plotted with GraphPad Prism 6.0f.

4.5.3 Growth in live bacteria (*K. aerogenes*) lawns

For each cell line, vegetative cells were harvested into a 1.5 ml tube, briefly centrifuged (~10 seconds with continuous acceleration, up to ~12000 *g*), washed with 1 ml of PB, centrifuged again and resuspended in PB at ~1.0 x 10^3 cells/ml; next, volumes containing approximately 10, 25 and 50 cells were each mixed with a 500 µl suspension of *K. aerogenes* bacteria in PB (prepared from 200 µl of culture in LB, grown overnight at ~21°C, ~100 r.p.m.), then each final suspension seeded onto an individual SM agar plate. Plates were then incubated at 21°C for 6 days and checked every day. Pictures presented in the results were taken on the 6th day, using a Canon EOS 1000D DSLR camera coupled to a Zeiss Stemi 2000-C stereo microscope.

4.5.4 Multicellular development on buffered agar

For each cell line, the cells of a nearly confluent dish culture (containing ~4.0-5.0 x 10^7 cells in total) were collected, 2 times centrifuged (3 min, 330 g) and washed with 10 ml PB, centrifuged a final time and resuspended in 3 ml PB; the entire cell suspension was then seeded onto a PB-buffered 1.5% w/v agar plate (ø 60 mm) and the liquid PB carefully pipetted out ~1 h later, at which point the cells had already adhered to the agar. All plates were then kept inside a closed tray containing some moistened paper (to prevent the agar from drying) for 3 days, at 21°C, and checked every ~24 h. Pictures presented in the results were taken on the 3rd day, using a Canon EOS 1000D DSLR camera coupled to a Zeiss Stemi 2000-C stereo microscope.

4.5.5 Cell adhesion to plastic

For each cell line, the cells of a nearly confluent dish culture were collected, centrifuged (4 min, 330 g) and resuspended in fresh HL5 at 1.5 x 10^6 cells/ml, then 10 ml of cell suspension transferred to a new plastic Petri dish (ø 100 mm). Assay dishes were first kept stationary for 2 hours (allowing all cells to attach to the plastic bottom) at 21°C, then left shaking at ~100 r.p.m. for 30 min, after which time each medium was sampled so as to determine the density of detached cells using a CASY cell counter/analyzer (Innovatis).

4.6 Microscopy and image analysis

Laser scanning confocal microscopy (Paddock and Eliceiri, 2014) was performed with a Nikon A1R microscope system, using a 488 nm laser (for GFP excitation) and a 60×/1.40 NA apochromatic objective. Imaging was controlled through the NIS-Elements AR 4.1 software (Nikon).

Spinning-disk confocal microscopy (Oreopoulos *et al.*, 2014) was carried out with an Andor Revolution XD microscope system equipped with an Andor Neo sCMOS camera. For GFP and/or RFP (or TRITC) excitation, 488 nm and/or 561 nm lasers

were employed, respectively. Simultaneous GFP and RFP imaging was rendered possible by using an OptoSplit II dual emission image splitter (Cairn Research). A 60×/1.40 NA apochromatic objective was utilized in assays for QuimP-based analysis; a 100×/1.40 NA apochromatic objective was brought into play in all other experiments. Imaging was controlled through the Andor iQ3 software.

TIRF microscopy (Mattheyses *et al.*, 2010) was performed with a Nikon Eclipse T*i* microscope system containing a custom-built TIRF condenser and fitted with a Photometrics Evolve 512 EMCCD camera. Excitation of GFP and/or RFP were achieved through the use of 473 nm and/or 561 nm lasers, respectively. A Dual View DV2 emission splitter (Photometrics) allowed for simultaneous GFP and RFP imaging. A 100×/1.45 NA apochromatic TIRF objective was employed in all experiments. Imaging was controlled through the MetaMorph 7.7.1 software (Molecular Devices).

Phase contrast and DIC microscopies were performed with a Nikon Eclipse TE2000-E microscope system equipped with a QImaging RETIGA EXi FAST 1394 CCD camera and a pE-100 LED illumination system (CoolLED) at 525 nm. A 20×/0.45 NA Ph1 objective and a 60×/1.40 NA apochromatic DIC objective were used for phase contrast and DIC, respectively. Imaging was controlled through the µManager 1.4.9 software (Edelstein *et al.*, 2010).

All microscopy was carried out at room temperature (~21°C). All microscopy data were analysed with ImageJ/Fiji 1.49i (Schneider *et al.*, 2012).

4.6.1 Details on "QuimP assays"

The way under-agarose chemotaxis assays were prepared for QuimP-based quantitative analysis of cell motility parameters ("QuimP assays") was described in section 4.5.1. Here, details are provided on the microscopy imaging, time-lapse processing and quantitative analysis associated with those assays.

Microscopy imaging in "QuimP assays" was performed with the above-described spinning disk confocal microscope system, using a 561 nm laser for TRITC excita-

tion and a 60×/1.40 NA apochromatic objective. TRITC served the purpose of a negative stain, allowing the visualization of non-fluorescent cells against a red fluorescent agarose background. Time-lapses of chemotaxing cells were recorded with a frame rate of 1 frame / 2.5 sec, for up to 15 min. The focal plane was always set at a very short distance above the dish's bottom glass upper surface (we tried, as much as possible, to set equivalent focal planes for every time-lapse recording), where much of a cell's protrusive activity can be observed in the context of this assay. Pixel binning was set at 2x2, so as to minimize laser intensity and exposure times and thus phototoxic effects on cells over time.

Before being used for QuimP-based analysis (below), time-lapses were processed in ImageJ/Fiji 1.49i. Each time-lapse image stack was – in this order – converted to 8 bit, inverted, smoothed with a single Gaussian blur (radius = 1.00), subtracted an identically processed background image (created with cell-free regions from a few images in the original stack), applied a higher contrast, and finally 3× up-scaled (with bicubic interpolation).

Processed time-lapses were then examined with the QuimP v11b plugin package for ImageJ (Tyson *et al.*, 2014; http://www.warwick.ac.uk/QuimP). For each individual cell to be analysed, typically one or two per time-lapse, high resolution node-based outlines were generated in every frame for a continuous period of between 5 and 10 min (many cells would quickly move out of the field of view during time-lapse recording; only those continuously fully visible for at least 5 min were used in our analysis). Cell outlines were produced using the QuimP BOA plugin with the following segmentation parameters: Node spacing – 6; Max iterations – 4000; Blowup – 30; Crit velocity – 0.001; Image F – 0.2; Central F – 0.04; Contract F – 0.01; Final shrink – 2; Sample tan – 4; Sample norm – 12; "Use previous snake" – activated. All outlines were inspected by eye and corrected when required (by re-running the segmentation algorithm in individual frames).

Each sequence of cell outlines was then analysed with the QuimP BOA and ECMM plugins, with which all parameters of interest were calculated except for "Average speed of membrane extension – top 25% (μm/sec)", "Average speed of membrane extension – top 10% (μm/sec)" and "Average rate of membrane ex-

tension (μm^2/sec)", which were calculated subsequently from data generated by QuimP (average *speeds* of membrane extension) or from additional analysis of the cell outlines in ImageJ/Fiji (average *rate* of membrane extension).

Final data were plotted with GraphPad Prism 6.0f, which was also used for all statistics (descriptive statistics and two-tailed Welch's/unequal variances *t*-tests – Ruxton, 2006).

5 Appendices

5.1 Appendix A – Additional figures
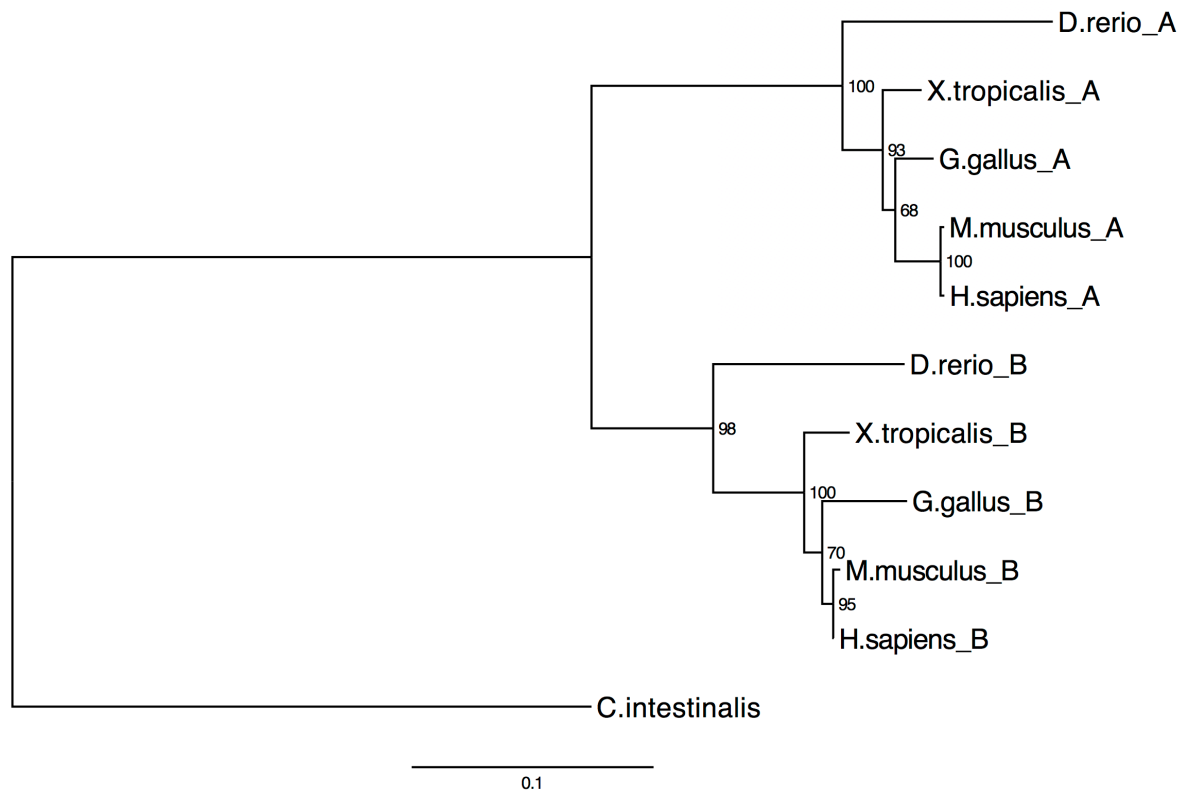
Figure 5.1 – Phylogenetic tree of a selection of vertebrate FAM49A and FAM49B proteins
Neighbour-joining(NJ)-based phylogenetic tree, calculated from a multi-alignment (not shown) of
FAM49A and FAM49B sequences from various vertebrate species (UniProt entries Q7ZW35 and
Q6NYL6 in *D. rerio* – zebrafish; Q28DJ5 and Q6GLA9 in *X. tropicalis* – western clawed frog;
Q5ZI04 and E1BWS3 in *G. gallus* – chicken; Q8BHZ0 and Q921M7 in *M. musculus* – mouse;
Q9H0Q0 and Q9NUQ9 in *H. sapiens* – human) and FAM49 from a non-vertebrate chordate
(F6PYR8 in *C. intestinalis*, on which the tree was rooted). The suffixes "_A" and "_B" in terminal
node species names represent FAM49A and FAM49B, respectively. Numbers in internal nodes
indicate bootstrap percentages. Branch lengths are proportional to the computed evolutionary
distances; the scale bar denotes 0.1 expected substitutions per site. Tree calculation was done in
Topali 2 (Milne *et al.*, 2009) using an NJ method and default parameters, with bootstrapping set at
100 runs.

Figure 5.2 – Multi-alignment of *D. discoideum* FAM49 and putative homologs from diverse eukaryotic lineages
(*continues next page*)

The putative FAM49 homologs whose sequences were used in this alignment are described in Table 2.2 (*Results* chapter). On the left side of each aligned sequence is the name of the corresponding species; "H.sapiens_A" and "H.sapiens_B" represent human FAM49A and FAM49B, respectively. Numbers above the top sequence pinpoint alignment positions. Numbers on the right side of each sequence indicate the cumulative number of amino acid residues used in the alignment. Dashes (–) represent gaps, which suggest insertion or deletion mutations in one or more sequences. Residues in the alignment are background-coloured according to the default ClustalX colour scheme, as emulated by Jalview 2 (Waterhouse *et al.*, 2009; Procter *et al.*, 2010; Chenna *et al.*, 2003). Briefly, residues are assigned a colour on the basis of both their type and their frequency at each alignment position; moreover, colours generally reflect certain physicochemical properties (Procter *et al.*, 2010). Two annotation rows, "Conservation" and "Consensus", are displayed below the alignment. "Conservation" states the overall conservation of physicochemical properties at each alignment position by means of a score (0 to 10) and a proportionally sized/coloured bar. Conservation scores were calculated by Jalview 2, in accordance with a method and a property index described by Livingstone and Barton, 1993. Essentially, shown scores indicate the number of physicochemical properties, out of 10 being considered, that are conserved at any given position. Gaps are regarded as holding all properties. Asterisks (*) mark fully identical positions, while plus signs (+) specify positions with one or more substitutions but where all properties are conserved. "Consensus" shows the most frequent residue at each position; (+) is used where two or more residues are the most frequent. Consensus bars are proportional to the frequencies of the top residues.

Figure 5.2 – Multi-alignment of *D. discoideum* FAM49 and putative homologs from diverse eukaryotic lineages (*continued*)
(*continues next page*)
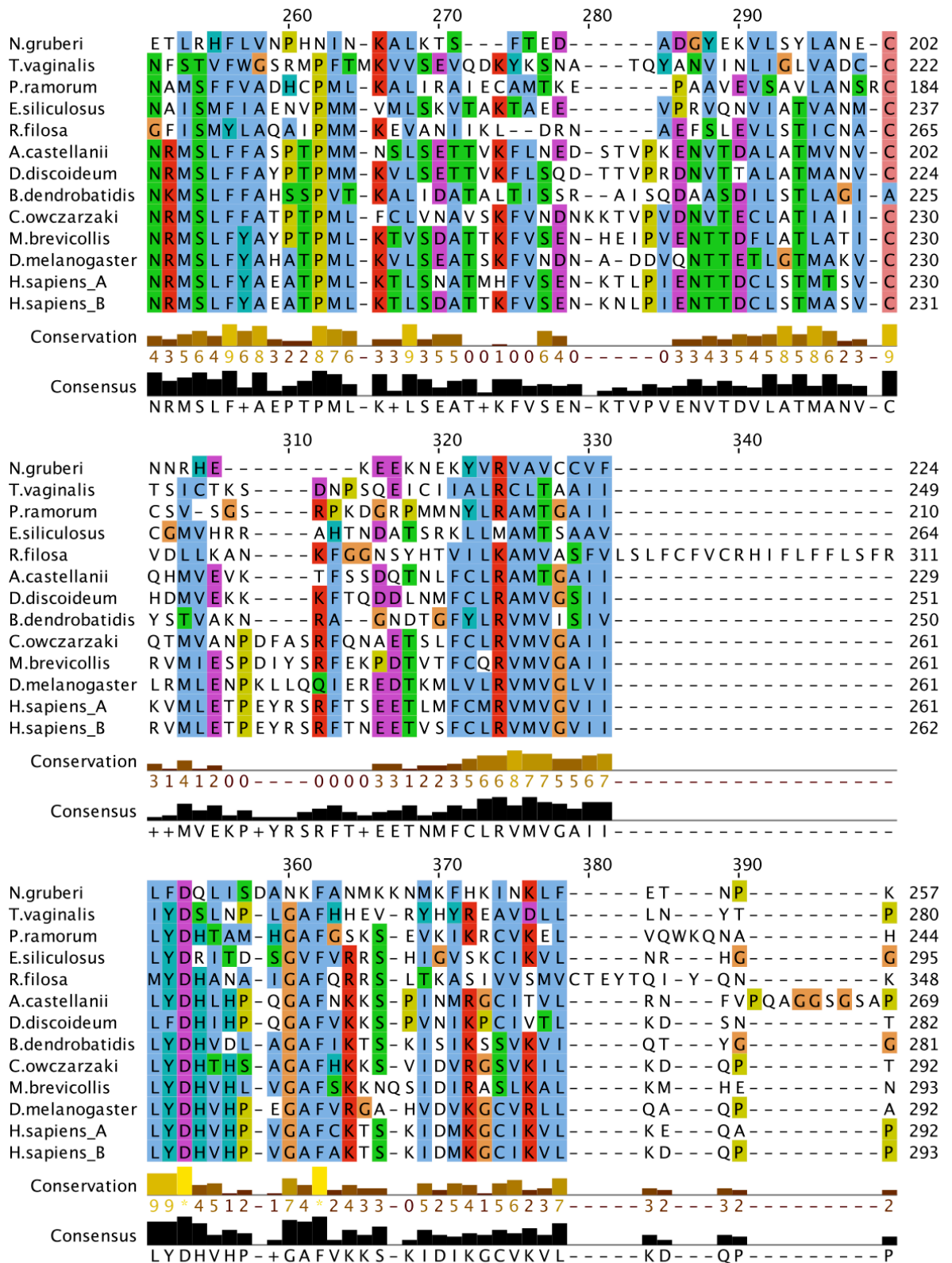
Figure 5.2 – Multi-alignment of *D. discoideum* FAM49 and putative homologs from diverse eukaryotic lineages (*continued*)
(*continues next page*)
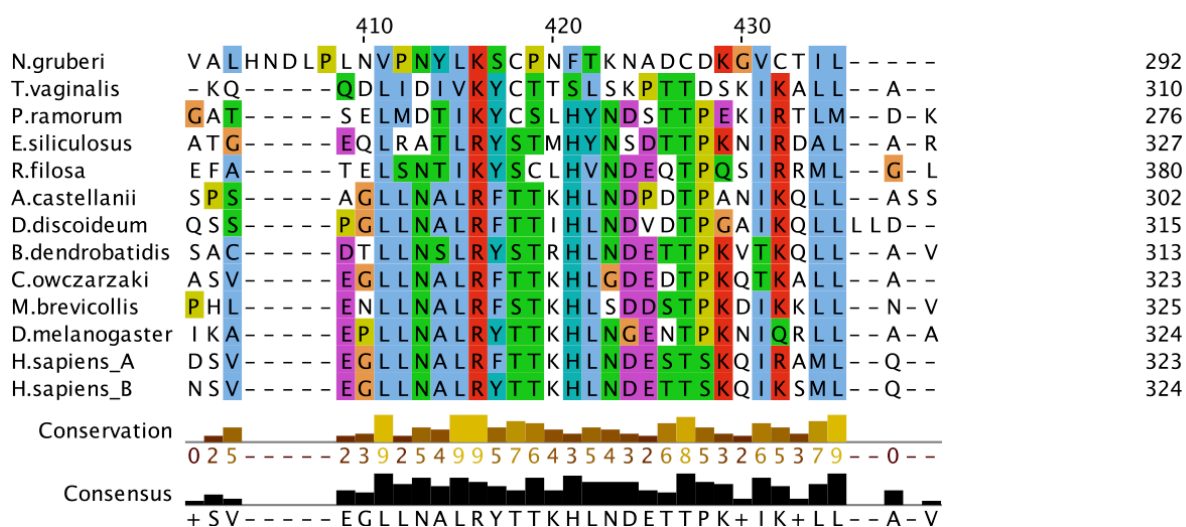
Figure 5.2 – Multi-alignment of *D. discoideum* FAM49 and putative homologs from diverse eukaryotic lineages (*continued*)

```
# Identity:      148/325 (45.5%)
# Similarity:    206/325 (63.4%)
# Gaps:           12/325 ( 3.7%)

FAM49_DICDI    1 MGQLLSFINGN-DHTEQIFIDFEHAQPSDDERELHKTVNEVLIRGPAIID   49
                 ||.||..:...  ::.....|:|||:|||::.|||:...::.||....:|:.
FA49A_HUMAN    1 MGNLLKVLTREIENYPHFFLDFENAQPTEGEREIWNQISAVLQDSESILA   50

FAM49_DICDI   50 KLLAYAGCNEFIRRAITNPGP-ETEDAAWEAVLPSVDQLQEFYDFSLELE   98
                 .|.||.|....||.||.||.. :.::.||.||.|.|.:|:.||:||:.||
FA49A_HUMAN   51 DLQAYKGAGPEIRDAIQNPNDIQLQEKAWNAVCPLVVRLKRFYEFSIRLE  100

FAM49_DICDI   99 TCFPKLLVAL-C-KNDPKASLSNQQALAKQLADIFDFVLKFDDAKMVNPA  146
                 .....||.:| |  ...|...|..:|||||:.|:|..|.|:||:.||.|||
FA49A_HUMAN  101 KALQSLLESLTCPPYTPTQHLEREQALAKEFAEILHFTLRFDELKMRNPA  150

FAM49_DICDI  147 IQNDFSYYRRTLNRMKLTKKDANI--KIRDELANRMSLFFAYPTPMMKVL  194
                 |||||||||||::|.::.....:|   ::..:|:|||||||:|..|||:|.|
FA49A_HUMAN  151 IQNDFSYYRRTISRNRINNMHLDIENEVNNEMANRMSLFYAEATPMLKTL  200

FAM49_DICDI  195 SETTVKFLSQDTTVPRDNVTTALATMANVCHDMVE----KKKFTQDDLNM  240
                 |..|:.|:|::.|:|.:|.|..|:||.:||..|:|    :.:||.:.:.|
FA49A_HUMAN  201 SNATMHFVSENKTLPIENTTDCLSTMTSVCKVMLETPEYRSRFTSEETLM  250

FAM49_DICDI  241 FCLRAMVGSIILFDHIHPQGAFVKKSPVNIKPCIVTLKDSNTQSSPGLLN  290
                 ||:|.|||.|||:||:||.|||.|.|.::|.|.||..||:....|..||||
FA49A_HUMAN  251 FCMRVMVGVIILYDHVHPVGAFCKTSKIDMKGCIKVLKEQAPDSVEGLLN  300

FAM49_DICDI  291 ALRFTTIHLNDVDTPGAIKQLLLLD  315
                 ||||||.|||||..|...|:.:|.
FA49A_HUMAN  301 ALRFTTKHLNDESTSKQIRAMLQ--  323
```
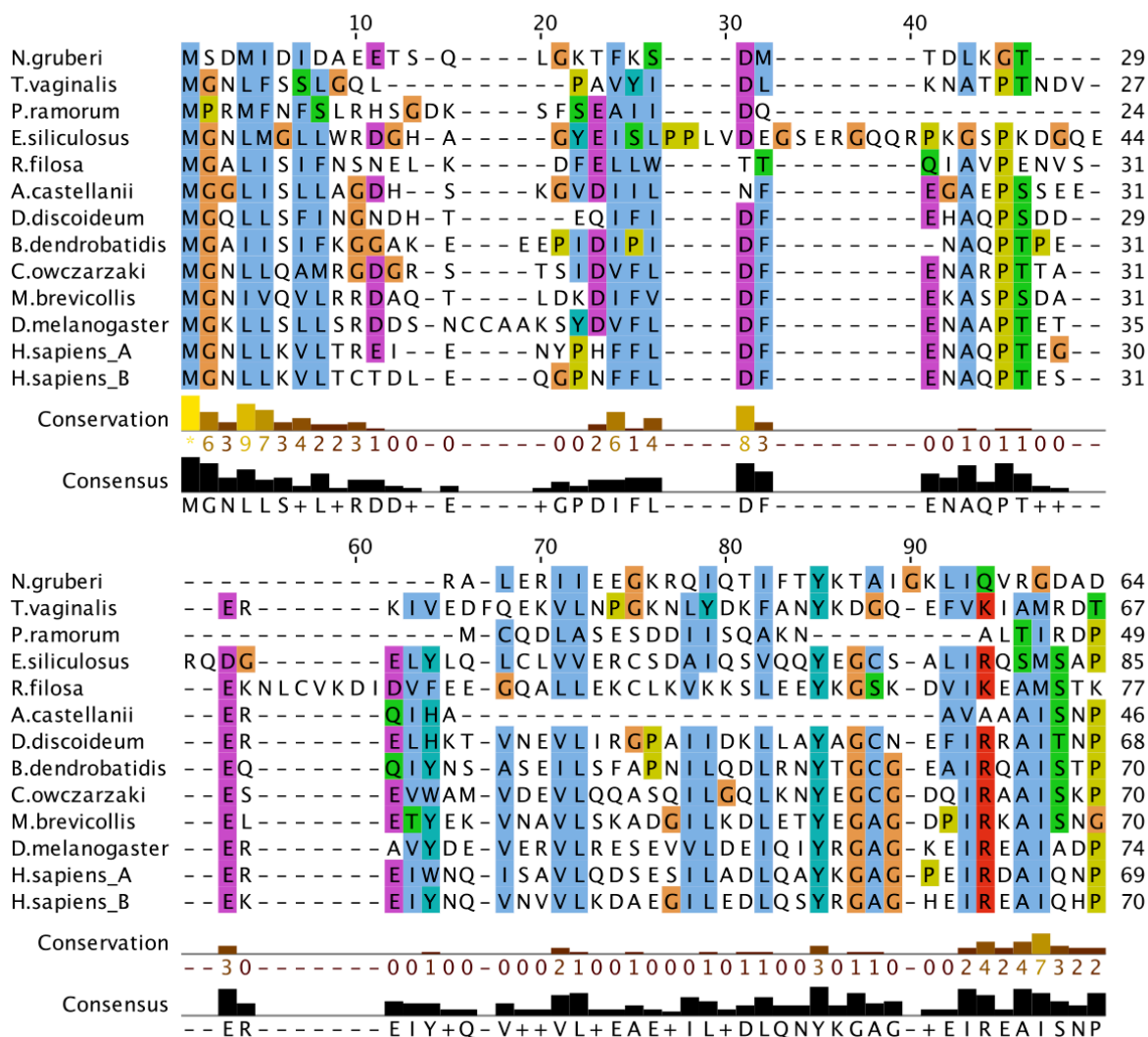
Figure 5.3 – Global pairwise alignment of *D. discoideum* FAM49 (FAM49_DICDI) and human FAM49A (FA49A_HUMAN)

Numbers on the sides of each aligned sequence indicate the cumulative number of amino acid residues used in the alignment. Dashes (–) represent gaps, which suggest insertion or deletion mutations. Vertical bars (|) pinpoint alignment positions with conserved (i.e. identical) residues; colons (:) denote positions with residue substitutions that score positively in the BLOSUM62 matrix and are frequently conservative (i.e. the different residues have rather similar physicochemical properties); periods (.) specify all remaining positions with no gaps. "Identity" shows the number and percentage of positions with conserved residues, while "Similarity" indicates the number and percentage of positions with a positive score in the BLOSUM62 matrix (includes all positions with conserved residues). Number and percentage of gaps is also displayed.

```
# Identity:      156/327 (47.7%)
# Similarity:    208/327 (63.6%)
# Gaps:           15/327 ( 4.6%)

FAM49_DICDI    1 MGQLLSFINGNDHTEQ---IFIDFEHAQPSDDERELHKTVNEVLIRGPAI   47
                 ||.||..:...| .||    .|:||||:|||::.|:|::..||.||.....|
FA49B_HUMAN    1 MGNLLKVLTCTD-LEQGPNFFLDFENAQPTESEKEIYNQVNVVLKDAEGI   49

FAM49_DICDI   48 IDKLLAYAGCNEFIRRAITNPGPE-TEDAAWEAVLPSVDQLQEFYDFSLE   96
                 ::.|.:|.|....||.||.:|..| .:::.||.||:|.|.:|::||:||..
FA49B_HUMAN   50 LEDLQSYRGAGHEIREAIQHPADEKLQEKAWGAVVPLVGKLKKFYEFSQR   99

FAM49_DICDI   97 LETCFPKLLVALCKN--DPKASLSNQQALAKQLADIFDFVLKFDDAKMVN  144
                 ||.....||.||...  .|...|..:|||||||.|:|..|.|:||:.||.|
FA49B_HUMAN  100 LEAALRGLLGALTSTPYSPTQHLEREQALAKQFAEILHFTLRFDELKMTN  149

FAM49_DICDI  145 PAIQNDFSYYRRTLNRMKLTK--KDANIKIRDELANRMSLFFAYPTPMMK  192
                 ||||||||||||||||:||::..  .:...::.:|||||||||||:|..|||:|
FA49B_HUMAN  150 PAIQNDFSYYRRTLSRMRINNVPAEGENEVNNELANRMSLFYAEATPMLK  199

FAM49_DICDI  193 VLSETTVKFLSQDTTVPRDNVTTALATMANVCHDMVE----KKKFTQDDL  238
                 .||:.|.||:|::..:|.:|.|..|:|||:||..|:|     :.:||.::.
FA49B_HUMAN  200 TLSDATTKFVSENKNLPIENTTDCLSTMASVCRVMLETPEYRSRFTNEET  249

FAM49_DICDI  239 NMFCLRAMVGSIILFDHIHPQGAFVKKSPVNIKPCIVTLKDSNTQSSPGL  288
                 ..||||.|||.|||:||:||.|||.|.|.::|.||..|||....|..||
FA49B_HUMAN  250 VSFCLRVMVGVIILYDHVHPVGAFAKTSKIDMKGCIKVLKDQPPNSVEGL  299

FAM49_DICDI  289 LNALRFTTIHLNDVDTPGAIKQLLLLD  315
                 |||||:||.||||..|...||.:|.
FA49B_HUMAN  300 LNALRYTTKHLNDETTSKQIKSMLQ--  324
```

Figure 5.4 – Global pairwise alignment of *D. discoideum* FAM49 (FAM49_DICDI) and human FAM49B (FA49B_HUMAN)

For details on how to interpret this alignment see description of Figure 5.3.

```
# Identity:       62/327 (19.0%)
# Similarity:    116/327 (35.5%)
# Gaps:           85/327 (26.0%)


DdFAM49(DUF)    1 QIFIDFEHAQPSDDERELHKTVNEVLIRGPAIIDKLLAYAGCNEFIRRAI   50
                    ..|.|::...:.| :.|||.:|.:.|:.:.:.|..|::.:
DdPirA(DUF)     1 -------ETQWSEETIGMEK-MEEVLKQGDSFINMVYTYRSCSKAL----   38

DdFAM49(DUF)   51 TNPGPETEDAA---------WEAVLPSVDQLQEFYDFSLELETCFPKLLV   91
                    |..:|.:.. :|.:.|.:.:|::|..|..:....|...:.
DdPirA(DUF)    39 --PTVKTAEQVNKTQIYEGNFEVLEPEIKKLKDFMYFQKDTIKLFCDHIK   86

DdFAM49(DUF)   92 ALCK--NDPKASLSNQQALAKQLADIFDFVLKFDDAKMVNPAIQNDFSYY  139
                    .|.. :..|.::|..:....|..|.|.:...|..|.:...:.||||::
DdPirA(DUF)    87 KLASTYDKKKETISASESFINYLVRILDLLAILDALKNMKACLNNDFSFF  136

DdFAM49(DUF)  140 RRTLNRMKLTKKDANIKIRDE------LANRMSLFFAYPTPMMKVLSETT  183
                    :|...:..::.............:.::.     |||:.|:    |..:|:.....
DdPirA(DUF)   137 KRATGFLRKQMSGTEDQTQENHTLYLFLANQNSI-----TSSLKLELHNI  181

DdFAM49(DUF)  184 VKFLSQDTTVPRDNVTTALATMANVCHDMVEKKKFTQDDLNMFCLRAMVG  233
                    .||        |::   |..:.|.|.|.:|::|:.........||.|..
DdPirA(DUF)   182 DKF---------DDI---LPMIVNQCADYLEQEKYILPSEKHCLLRVMPF  219

DdFAM49(DUF)  234 SIILFDHIHPQGAFVKKSPVNIKPCIVTLKDSNTQSSPGLLNALRFTTIH  283
                    .:.|.|.        ..|..||.      |:.|        ||..|:..|.
DdPirA(DUF)   220 VLFLIDE--------NDSKHNIN------KNKN-------LNISRYAKIF  248

DdFAM49(DUF)  284 LNDVDTP--GAIK-------------- 294
                    ..:...|  |.::
DdPirA(DUF)   249 KKNPVVPLYGDMQITLESLVKRSPHFD 275
```

Figure 5.5 – Global pairwise alignment of DUF1394 domains from *D. discoideum* FAM49 (residues 16−309) and CYFIP/Pir121 (PirA) (residues 57−331)
DUF1394 domains are as defined/predicted by Pfam 28.0 (entry PF07159). For details on how to interpret this alignment see description of Figure 5.3.

```
# Identity:      54/316 (17.1%)
# Similarity:   101/316 (32.0%)
# Gaps:          86/316 (27.2%)

HsFAM49B(DUF)     1 NFFLDFENAQPTESEKEIYNQVNVVLKDAEGILEDLQSYRGAGHEIRE--   48
                    ..:.:..::::.:|.:|::.:.....|.::|.....|.:
HsCYFIP1(DUF)     1 -----------YIEQATVHSSMNEMLEEGQEYAVMLYTWRSCSRAIPQVK   39

HsFAM49B(DUF)    49 AIQHPADEKLQEKAWGAVVPLVGKLKKFYEFSQRLEAALRGLLGALTSTP   98
                    ..:.|...:.||....:.|.|.||..|..|.:........|.:..|.
HsCYFIP1(DUF)    40 CNEQPNRVEIYEKTVEVLEPEVTKLMNFMYFQRNAIERFCGEVRRLC---   86

HsFAM49B(DUF)    99 YSPTQHLEREQALAKQ-----FAEILHFTLRFDELKMTNPAIQNDFSYYR  143
                    |.||.:....:    ..:.:::.....||||....:::||.|.|:
HsCYFIP1(DUF)    87 -----HAERRKDFVSEAYLITLGKFINMFAVLDELKNMKCSVKNDHSAYK  131

HsFAM49B(DUF)   144 RTLSRMRINNVPAEGENEVNNELANRMSLFYAEATPMLKTLSDATTKFVS  193
                    |....:|....|..:...|      :|:|.|....:.::|.. ..:.:|
HsCYFIP1(DUF)   132 RAAQFLRKMADPQSIQESQN------LSMFLANHNKITQSLQQ-QLEVIS  174

HsFAM49B(DUF)   194 ENKNLPIENTTDCLSTMASVCRVMLETPEYRSRFTNEETVSFCLRVMVGV  243
                    ..:.|            :|.:..:.::..|.|...|..|. ...|:||...
HsCYFIP1(DUF)   175 GYEEL-----------LADIVNLCVDYYENRMYLTPSEK-HMLLKVMGFG  212

HsFAM49B(DUF)   244 IILYDHVHPVGAFAKTSKIDMKGCI------KVLKDQPPNSVEGLLNALR  287
                    :.|.|       |:.:...|:|.|..|      |..|.
HsCYFIP1(DUF)   213 LYLMD-----GSVSNIYKLDAKKRINLSKIDKYFKQ--------------  243

HsFAM49B(DUF)   288 YTTKHLNDETTSKQIK  303

HsCYFIP1(DUF)   244 ----------------  243
```

Figure 5.6 – Global pairwise alignment of DUF1394 domains from human FAM49B (residues 18−320) and CYFIP1 (residues 59−301)
DUF1394 domains are as defined/predicted by Pfam 28.0 (entry PF07159). For details on how to interpret this alignment see description of Figure 5.3.

```
# Identity:       55/330 (16.7%)
# Similarity:    104/330 (31.5%)
# Gaps:          112/330 (33.9%)

HsFAM49B(DUF)      1 NFFLDFENAQPTESEKEIYNQVNVVLKDAEGILEDLQSYRGAGHEIRE--   48
                        ..:.:.::::.:|.:|::.........|.::|.....|.:
HsCYFIP2(DUF)      1 -----------YIEQATVHSSMNEMLEEGHEYAVMLYTWRSCSRAIPQVK   39

HsFAM49B(DUF)     49 AIQHPADEKLQEKAWGAVVPLVGKLKKFYEFS----QRLEAALRGLLGAL   94
                        ..:.|...::.||.....:.|.|.||.||..|.    :|..:.::.|.
HsCYFIP2(DUF)     40 CNEQPNRVEIYEKTVEVLEPEVTKLMKFMYFQRKAIERFCSEVKRLC---   86

HsFAM49B(DUF)     95 TSTPYSPTQHLER-----EQALAKQFAEILHFTLRFDELKMTNPAIQNDF  139
                        |.||       .:|......:.::.....||||...:::||.
HsCYFIP2(DUF)     87 ---------HAERRKDFVSEAYLLTLGKFINMFAVLDELKNMKCSVKNDH  127

HsFAM49B(DUF)    140 SYYRRTLSRMRINNVPAEGENEVNNELANRMSLFYAEATPMLKTLSDATT  189
                        |.|:|                              |...|:.::|..:
HsCYFIP2(DUF)    128 SAYKR----------------------------AAQFLRKMADPQS  145

HsFAM49B(DUF)    190 KFVSENKNLPI-----ENTTDCL-----------STMASVCRVMLETPEY  223
                        :.|::||.:      ...|.||         ..:|.:.::.::.|.
HsCYFIP2(DUF)    146 --IQESQNLSMFLANHNRITQCLHQQLEVIPGYEELLADIVNICVDYYEN  193

HsFAM49B(DUF)    224 RSRFTNEETVSFCLRVMVGVIILYDHVHPVGAFAKTSKIDMKGCIKVLKD  273
                        :....|..|.  ...:||.....:.|.|        |..:...:|.|...|.:.|
HsCYFIP2(DUF)    194 KMYLTPSEK-HMLLKVMGFGLYLMD-----GNVSNIYKLDAKKRINLSK-  236

HsFAM49B(DUF)    274 QPPNSVEGLLNALRYTTKHLNDETTSKQIK  303
                        ::......|:
HsCYFIP2(DUF)    237 -----IDKFFKQLQ---------------  245
```

Figure 5.7 – Global pairwise alignment of DUF1394 domains from human FAM49B (residues 18−320) and CYFIP2 (residues 59−303)

DUF1394 domains are as defined/predicted by Pfam 28.0 (entry PF07159). For details on how to interpret this alignment see description of Figure 5.3.

5.2 Appendix B – Additional table

Table 5.1 – Putative FAM49 homologs whose sequences were used to generate the profile HMM of DUF1394 in Pfam 28.0

Only sequences from putative FAM49 homologs (and not CYFIP/Pir121 homologs) – 38 in total – were selected by Pfam curators in order to create the profile HMM of DUF1394.

UniProt entry	Species	High taxonomic classification
G3TUB0	*Loxodonta africana* (african elephant)	Opisthokonta – Metazoa
F1RRT3	*Sus scrofa* (pig)	
F7EAP5	*Xenopus tropicalis* (western clawed frog)	
Q28DJ5		
H3CWG8	*Tetraodon nigroviridis* (spotted green pufferfish)	
H2LTI7	*Oryzias latipes* (medaka fish)	
Q6TLE5	*Danio rerio* (zebrafish)	
F6PYR8	*Ciona intestinalis* (transparent sea squirt)	
E4WX68	*Oikopleura dioica* (tunicate)	
C3Y224	*Branchiostoma floridae* (florida lancelet)	
W4XJS5	*Strongylocentrotus purpuratus* (purple sea urchin)	
K1RAR8	*Crassostrea gigas* (pacific oyster)	
T1EFL6	*Helobdella robusta* (californian leech)	
E9GEY7	*Daphnia pulex* (water flea)	
X1WMY8	*Acyrthosiphon pisum* (pea aphid)	
T1HVW7	*Rhodnius prolixus* (triatomid bug)	
E0W109	*Pediculus humanus subsp. corporis* (body louse)	
Q7Q613	*Anopheles gambiae* (african malaria mosquito)	
E2C4X5	*Harpegnathos saltator* (jerdon's jumping ant)	
T1KWU1	*Tetranychus urticae* (two-spotted spider mite)	
E3LRQ5	*Caenorhabditis remanei* (nematode)	
J9EBZ9	*Wuchereria bancrofti* (nematode)	
F1KXL0	*Ascaris suum* (pig roundworm)	
A0A068X498	*Hymenolepis microstoma* (rodent tapeworm)	
A7SA43	*Nematostella vectensis* (starlet sea anemone)	
I1F5T7	*Amphimedon queenslandica* (sponge)	
A9UXH2	*Monosiga brevicollis* (choanoflagellate)	Opisthokonta – Choanomonada
F2U7W7	*Salpingoeca rosetta* (choanoflagellate)	
A0A0D2U1D3	*Capsaspora owczarzaki*	Opisthokonta – Filasterea
F4P086	*Batrachochytrium dendrobatidis* (frog chytrid fungus)	Opisthokonta – Fungi
S2JLT9	*Mucor circinelloides* (mucormycosis agent)	
S2JLQ0	*Mucor circinelloides* (mucormycosis agent)	
I1BW52	*Rhizopus delemar* (mucormycosis agent)	
Q8T2H0	*Dictyostelium discoideum*	Amoebozoa – Dictyostelia
C4LXG8	*Entamoeba histolytica*	Amoebozoa – Archamoebae
C4M3D8		
C4M0W8		
A2E1F1	*Trichomonas vaginalis*	Excavata – Metamonada

5.3 Appendix C – Movies

All movies (AVI format) are included in the DVD that is annexed to this thesis. Please use QuickTime Player 7, ImageJ or similarly capable software for viewing.

Movies 1 to 6
Phase contrast microscopy time-lapse recordings of vegetative cells moving up a folate gradient under a soft agarose gel (0.4% w/v). The general direction of cell movement is towards the right. Time in MM:SS format (M = minutes; S = seconds) is indicated on the upper left corner in each case. Each movie represents 20 min of real-time imaging.

Movie 1 – Ax2 (wild-type) cells

Movie 2 – Ax2-derived *fam49* KO clone 32 cells

Movie 3 – Ax2-derived *fam49* KO clone 111 cells

Movie 4 – Ax3 (wild-type) cells

Movie 5 – Ax3-derived *fam49* KO clone 1 cells

Movie 6 – Ax3-derived *fam49* KO clone 3 cells

Note: Examples of cells attempting to divide while chemotaxing – and which, due to their distinct behaviour, may confound the untrained eye – are highlighted with green asterisks at 18:00 (two cells), 19:00 (one cell) and 20:00 (one cell) into the movie. A few such cells also appear in some other movies; please bare in mind they are not representative of a population's standard protrusive behaviour.

Movies 7 to 14
Phase contrast microscopy time-lapse recordings of vegetative cells moving up a folate gradient under an agarose gel (0.6% w/v). The general direction of cell movement is towards the right. Time in MM:SS format (M = minutes; S = seconds) is indicated on the upper left corner in each case. Each movie represents 20 min of real-time imaging.

Movie 7 – Ax2 (wild-type) cells

Movie 8 – Ax2-derived *fam49* KO cells

Movie 9 – Ax2-derived *fam49* KO cells expressing GFP-FAM49

Movie 10 – Ax2-derived *fam49* KO cells re-expressing non-tagged FAM49

Movie 11 – Ax3 (wild-type) cells

Movie 12 – Ax3-derived *fam49* KO cells

Movie 13 – Ax3-derived *fam49* KO cells expressing GFP-FAM49

Movie 14 – Ax3-derived *fam49* KO cells re-expressing non-tagged FAM49

Movies 15 to 22
DIC microscopy time-lapse recordings of vegetative cells moving up a folate gradient under an agarose gel (0.6% w/v). Time in seconds is indicated on the upper left or right corner in each case. Each movie represents 45 sec of real-time imaging, except movie 20 which runs for 52.5 sec.

Movie 15 – Ax2 (wild-type) cell

Movie 16 – Ax2-derived *fam49* KO cell

Movie 17 – Ax2-derived *fam49* KO cell re-expressing non-tagged FAM49

Movie 18 – Ax2-derived *fam49* KO cell re-expressing non-tagged FAM49
Note: Cell shows prominent thin pseudopods.

Movie 19 – Ax3 (wild-type) cell

Movie 20 – Ax3-derived *fam49* KO cell

Movie 21 – Ax3-derived *fam49* KO cell re-expressing non-tagged FAM49

Movie 22 – Ax3-derived *fam49* KO cell re-expressing non-tagged FAM49
Note: Cell shows prominent thin pseudopods.

List of References

ABOU-KHEIR, W., ISAAC, B., YAMAGUCHI, H. & COX, D. 2008. Membrane targeting of WAVE2 is not sufficient for WAVE2-dependent actin polymerization: a role for IRSp53 in mediating the interaction between Rac and WAVE2. *J Cell Sci,* 121**,** 379-90.

ABU SHAH, E. & KEREN, K. 2013. Mechanical forces and feedbacks in cell motility. *Curr Opin Cell Biol,* 25**,** 550-7.

ADL, S. M., SIMPSON, A. G., LANE, C. E., LUKES, J., BASS, D., BOWSER, S. S., BROWN, M. W., BURKI, F., DUNTHORN, M., HAMPL, V., HEISS, A., HOPPENRATH, M., LARA, E., LE GALL, L., LYNN, D. H., MCMANUS, H., MITCHELL, E. A., MOZLEY-STANRIDGE, S. E., PARFREY, L. W., PAWLOWSKI, J., RUECKERT, S., SHADWICK, R. S., SCHOCH, C. L., SMIRNOV, A. & SPIEGEL, F. W. 2012. The revised classification of eukaryotes. *J Eukaryot Microbiol,* 59**,** 429-93.

AIZAWA, H., SAMESHIMA, M. & YAHARA, I. 1997. A green fluorescent protein-actin fusion protein dominantly inhibits cytokinesis, cell spreading, and locomotion in Dictyostelium. *Cell Struct Funct,* 22**,** 335-45.

ANTHIS, N. J., HALING, J. R., OXLEY, C. L., MEMO, M., WEGENER, K. L., LIM, C. J., GINSBERG, M. H. & CAMPBELL, I. D. 2009. Beta integrin tyrosine phosphorylation is a conserved mechanism for regulating talin-induced integrin activation. *J Biol Chem,* 284**,** 36700-10.

ARDERN, H., SANDILANDS, E., MACHESKY, L. M., TIMPSON, P., FRAME, M. C. & BRUNTON, V. G. 2006. Src-dependent phosphorylation of Scar1 promotes its association with the Arp2/3 complex. *Cell Motil Cytoskeleton,* 63**,** 6-13.

ARTHUR, W. T., PETCH, L. A. & BURRIDGE, K. 2000. Integrin engagement suppresses RhoA activity via a c-Src-dependent mechanism. *Curr Biol,* 10**,** 719-22.

BAI, Y., MARKHAM, K., CHEN, F., WEERASEKERA, R., WATTS, J., HORNE, P., WAKUTANI, Y., BAGSHAW, R., MATHEWS, P. M., FRASER, P. E., WESTAWAY, D., ST GEORGE-HYSLOP, P. & SCHMITT-ULMS, G. 2008. The in vivo brain interactome of the amyloid precursor protein. *Mol Cell Proteomics,* 7**,** 15-34.

BAILLY, M., ICHETOVKIN, I., GRANT, W., ZEBDA, N., MACHESKY, L. M., SEGALL, J. E. & CONDEELIS, J. 2001. The F-actin side binding activity of the Arp2/3 complex is essential for actin nucleation and lamellipod extension. *Curr Biol,* 11**,** 620-5.

BASU, S., FEY, P., PANDIT, Y., DODSON, R., KIBBE, W. A. & CHISHOLM, R. L. 2013. dictyBase 2013: integrating multiple Dictyostelid species. *Nucleic Acids Research,* 41**,** D676-D683.

BEAR, J. E., RAWLS, J. F. & SAXE, C. L., 3RD 1998. SCAR, a WASP-related protein, isolated as a suppressor of receptor defects in late Dictyostelium development. *J Cell Biol,* 142**,** 1325-35.

BELMONT, L. D., ORLOVA, A., DRUBIN, D. G. & EGELMAN, E. H. 1999. A change in actin conformation associated with filament instability after Pi release. *Proc Natl Acad Sci U S A,* 96**,** 29-34.

BERGERT, M., CHANDRADOSS, S. D., DESAI, R. A. & PALUCH, E. 2012. Cell mechanics control rapid transitions between blebs and lamellipodia during migration. *Proc Natl Acad Sci U S A,* 109**,** 14434-9.

BEZANILLA, M., GLADFELTER, A. S., KOVAR, D. R. & LEE, W. L. 2015. Cytoskeletal dynamics: A view from the membrane. *J Cell Biol,* 209**,** 329-337.

BLAGG, S. L., STEWART, M., SAMBLES, C. & INSALL, R. H. 2003. PIR121 regulates pseudopod dynamics and SCAR activity in Dictyostelium. *Curr Biol,* 13**,** 1480-7.

BLANCHOIN, L., AMANN, K. J., HIGGS, H. N., MARCHAND, J. B., KAISER, D. A. & POLLARD, T. D. 2000. Direct observation of dendritic actin filament networks nucleated by Arp2/3 complex and WASP/Scar proteins. *Nature,* 404**,** 1007-11.

BLOOMFIELD, G., TANAKA, Y., SKELTON, J., IVENS, A. & KAY, R. R. 2008. Widespread duplications in the genomes of laboratory stocks of Dictyostelium discoideum. *Genome Biol,* 9**,** R75.

BOCZKOWSKA, M., REBOWSKI, G., KAST, D. J. & DOMINGUEZ, R. 2014. Structural analysis of the transitional state of Arp2/3 complex activation by two actin-bound WCAs. *Nat Commun,* 5**,** 3308.

BOCZKOWSKA, M., REBOWSKI, G., PETOUKHOV, M. V., HAYES, D. B., SVERGUN, D. I. & DOMINGUEZ, R. 2008. X-ray scattering study of activated Arp2/3 complex with bound actin-WCA. *Structure,* 16**,** 695-704.

BOSE, A., ROBIDA, S., FURCINITTI, P. S., CHAWLA, A., FOGARTY, K., CORVERA, S. & CZECH, M. P. 2004. Unconventional myosin Myo1c promotes membrane fusion in a regulated exocytic pathway. *Mol Cell Biol,* 24**,** 5447-58.

BOTELHO, R. J., TERUEL, M., DIERCKMAN, R., ANDERSON, R., WELLS, A., YORK, J. D., MEYER, T. & GRINSTEIN, S. 2000. Localized biphasic changes in phosphatidylinositol-4,5-bisphosphate at sites of phagocytosis. *J Cell Biol,* 151**,** 1353-68.

BREITSPRECHER, D., KIESEWETTER, A. K., LINKNER, J., URBANKE, C., RESCH, G. P., SMALL, J. V. & FAIX, J. 2008. Clustering of VASP actively drives processive, WH2 domain-mediated actin filament elongation. *EMBO J,* 27**,** 2943-54.

BUGYI, B. & CARLIER, M. F. 2010. Control of actin filament treadmilling in cell motility. *Annu Rev Biophys,* 39**,** 449-70.

BUKHAROVA, T., WEIJER, G., BOSGRAAF, L., DORMANN, D., VAN HAASTERT, P. J. & WEIJER, C. J. 2005. Paxillin is required for cell-substrate adhesion, cell sorting and slug migration during Dictyostelium development. *J Cell Sci,* 118**,** 4295-310.

CALDERWOOD, D. A. 2004. Talin controls integrin activation. *Biochem Soc Trans,* 32**,** 434-7.

CALDERWOOD, D. A., ZENT, R., GRANT, R., REES, D. J., HYNES, R. O. & GINSBERG, M. H. 1999. The Talin head domain binds to integrin beta subunit cytoplasmic tails and regulates integrin activation. *J Biol Chem,* 274**,** 28071-4.

CAMACHO, C., COULOURIS, G., AVAGYAN, V., MA, N., PAPADOPOULOS, J., BEALER, K. & MADDEN, T. L. 2009. BLAST+: architecture and applications. *BMC Bioinformatics,* 10**,** 421.

CAMPELLONE, K. G. & WELCH, M. D. 2010. A nucleator arms race: cellular control of actin assembly. *Nat Rev Mol Cell Biol,* 11**,** 237-51.

CARDELLI, J. 2001. Phagocytosis and macropinocytosis in Dictyostelium: phosphoinositide-based processes, biochemically distinct. *Traffic,* 2**,** 311-20.

CARLIER, M. F., LAURENT, V., SANTOLINI, J., MELKI, R., DIDRY, D., XIA, G. X., HONG, Y., CHUA, N. H. & PANTALONI, D. 1997. Actin depolymerizing factor (ADF/cofilin) enhances the rate of filament turnover: implication in actin-based motility. *J Cell Biol,* 136**,** 1307-22.

CARLIER, M. F. & PANTALONI, D. 1986. Direct evidence for ADP-Pi-F-actin as the major intermediate in ATP-actin polymerization. Rate of dissociation of Pi from actin filaments. *Biochemistry,* 25**,** 7789-92.

CARLSSON, A. E. 2010. Actin dynamics: from nanoscale to microscale. *Annu Rev Biophys,* 39**,** 91-110.

CASSIMERIS, L., SAFER, D., NACHMIAS, V. T. & ZIGMOND, S. H. 1992. Thymosin beta 4 sequesters the majority of G-actin in resting human polymorphonuclear leukocytes. *J Cell Biol,* 119**,** 1261-70.

CHAN, C., BELTZNER, C. C. & POLLARD, T. D. 2009. Cofilin dissociates Arp2/3 complex and branches from actin filaments. *Curr Biol,* 19**,** 537-45.

CHANG, F., LEMMON, C. A., PARK, D. & ROMER, L. H. 2007. FAK potentiates Rac1 activation and localization to matrix adhesion sites: a role for betaPIX. *Mol Biol Cell,* 18**,** 253-64.

CHEN, B., BRINKMANN, K., CHEN, Z., PAK, C. W., LIAO, Y., SHI, S., HENRY, L., GRISHIN, N. V., BOGDAN, S. & ROSEN, M. K. 2014. The WAVE regulatory complex links diverse receptors to the actin cytoskeleton. *Cell,* 156**,** 195-207.

CHEN, C. L., WANG, Y., SESAKI, H. & IIJIMA, M. 2012. Myosin I links PIP3 signaling to remodeling of the actin cytoskeleton in chemotaxis. *Sci Signal,* 5**,** ra10.

CHEN, Z., BOREK, D., PADRICK, S. B., GOMEZ, T. S., METLAGEL, Z., ISMAIL, A. M., UMETANI, J., BILLADEAU, D. D., OTWINOWSKI, Z. & ROSEN, M. K. 2010. Structure and control of the actin regulatory WAVE complex. *Nature,* 468**,** 533-8.

CHENNA, R., SUGAWARA, H., KOIKE, T., LOPEZ, R., GIBSON, T. J., HIGGINS, D. G. & THOMPSON, J. D. 2003. Multiple sequence alignment with the Clustal series of programs. *Nucleic Acids Res,* 31**,** 3497-500.

CHESARONE, M. A. & GOODE, B. L. 2009. Actin nucleation and elongation factors: mechanisms and interplay. *Curr Opin Cell Biol,* 21**,** 28-37.

CHIA, P. H., CHEN, B., LI, P., ROSEN, M. K. & SHEN, K. 2014. Local F-actin network links synapse formation and axon branching. *Cell,* 156**,** 208-20.

CHOI, C. K., VICENTE-MANZANARES, M., ZARENO, J., WHITMORE, L. A., MOGILNER, A. & HORWITZ, A. R. 2008. Actin and alpha-actinin orchestrate the assembly and maturation of nascent adhesions in a myosin II motor-independent manner. *Nat Cell Biol,* 10**,** 1039-50.

CLARK, E. A., KING, W. G., BRUGGE, J. S., SYMONS, M. & HYNES, R. O. 1998. Integrin-mediated signals regulated by members of the rho family of GTPases. *J Cell Biol,* 142**,** 573-86.

CONDEELIS, J., VAHEY, M., CARBONI, J. M., DEMEY, J. & OGIHARA, S. 1984. Properties of the 120,000- and 95,000-dalton actin-binding proteins from Dictyostelium discoideum and their possible functions in assembling the cytoplasmic matrix. *J Cell Biol,* 99**,** 119s-126s.

COPPOLINO, M. G., DIERCKMAN, R., LOIJENS, J., COLLINS, R. F., POULADI, M., JONGSTRA-BILEN, J., SCHREIBER, A. D., TRIMBLE, W. S., ANDERSON, R. & GRINSTEIN, S. 2002. Inhibition of phosphatidylinositol-4-phosphate 5-kinase Ialpha impairs localized actin remodeling and suppresses phagocytosis. *J Biol Chem,* 277**,** 43849-57.

CORNILLON, S., FROQUET, R. & COSSON, P. 2008. Involvement of Sib proteins in the regulation of cellular adhesion in Dictyostelium discoideum. *Eukaryot Cell,* 7**,** 1600-5.

CORNILLON, S., GEBBIE, L., BENGHEZAL, M., NAIR, P., KELLER, S., WEHRLE-HALLER, B., CHARETTE, S. J., BRUCKERT, F., LETOURNEUR, F. & COSSON, P. 2006. An adhesion molecule in free-living Dictyostelium amoebae with integrin beta features. *EMBO Rep,* 7**,** 617-21.

COX, D., WESSELS, D., SOLL, D. R., HARTWIG, J. & CONDEELIS, J. 1996. Re-expression of ABP-120 rescues cytoskeletal, motility, and phagocytosis defects of ABP-120- Dictyostelium mutants. *Mol Biol Cell,* 7**,** 803-23.

COZZETTO, D., KRYSHTAFOVYCH, A., FIDELIS, K., MOULT, J., ROST, B. & TRAMONTANO, A. 2009. Evaluation of template-based models in CASP8 with standard measures. *Proteins: Structure, Function, and Bioinformatics,* 77**,** 18-28.

CRAMER, L. P. 2013. Mechanism of cell rear retraction in migrating cells. *Curr Opin Cell Biol,* 25**,** 591-9.

CRITCHLEY, D. R. 2009. Biochemical and structural properties of the integrin-associated cytoskeletal protein talin. *Annu Rev Biophys,* 38**,** 235-54.

DAVIDSON, A. J. & INSALL, R. H. 2011. Actin-based motility: WAVE regulatory complex structure reopens old SCARs. *Curr Biol,* 21**,** R66-8.

DAVIDSON, A. J., KING, J. S. & INSALL, R. H. 2013a. The use of streptavidin conjugates as immunoblot loading controls and mitochondrial markers for use with Dictyostelium discoideum. *Biotechniques,* 55**,** 39-41.

DAVIDSON, A. J., URA, S., THOMASON, P. A., KALNA, G. & INSALL, R. H. 2013b. Abi is required for modulation and stability but not localization or activation of the SCAR/WAVE complex. *Eukaryot Cell,* 12**,** 1509-16.

DE LA ROCHE, M., MAHASNEH, A., LEE, S. F., RIVERO, F. & COTE, G. P. 2005. Cellular distribution and functions of wild-type and constitutively activated Dictyostelium PakB. *Mol Biol Cell,* 16**,** 238-47.

DEHAL, P. & BOORE, J. L. 2005. Two rounds of whole genome duplication in the ancestral vertebrate. *PLoS Biol,* 3**,** e314.

DERIVERY, E., LOMBARD, B., LOEW, D. & GAUTREAU, A. 2009. The Wave complex is intrinsically inactive. *Cell Motil Cytoskeleton,* 66**,** 777-90.

DIECKMANN, R., VON HEYDEN, Y., KISTLER, C., GOPALDASS, N., HAUSHERR, S., CRAWLEY, S. W., SCHWARZ, E. C., DIENSTHUBER, R. P., COTE, G. P., TSIAVALIARIS, G. & SOLDATI, T. 2010. A myosin IK-Abp1-PakB circuit acts as a switch to regulate phagocytosis efficiency. *Mol Biol Cell,* 21**,** 1505-18.

DIZ-MUNOZ, A., KRIEG, M., BERGERT, M., IBARLUCEA-BENITEZ, I., MULLER, D. J., PALUCH, E. & HEISENBERG, C. P. 2010. Control of directed cell migration in vivo by membrane-to-cortex attachment. *PLoS Biol,* 8**,** e1000544.

DUMONTIER, M., HOCHT, P., MINTERT, U. & FAIX, J. 2000. Rac1 GTPases control filopodia formation, cell motility, endocytosis, cytokinesis and development in Dictyostelium. *J Cell Sci,* 113 (Pt 12)**,** 2253-65.

DURRWANG, U., FUJITA-BECKER, S., ERENT, M., KULL, F. J., TSIAVALIARIS, G., GEEVES, M. A. & MANSTEIN, D. J. 2006. Dictyostelium myosin-IE is a fast molecular motor involved in phagocytosis. *J Cell Sci,* 119**,** 550-8.

EDDY, S. R. 1998. Profile hidden Markov models. *Bioinformatics,* 14**,** 755-63.

EDDY, S. R. 2004. Where did the BLOSUM62 alignment score matrix come from? *Nat Biotech,* 22**,** 1035-1036.

EDELSTEIN, A., AMODAJ, N., HOOVER, K., VALE, R. & STUURMAN, N. 2010. Computer control of microscopes using microManager. *Curr Protoc Mol Biol,* Chapter 14**,** Unit14 20.

EDEN, S., ROHATGI, R., PODTELEJNIKOV, A. V., MANN, M. & KIRSCHNER, M. W. 2002. Mechanism of regulation of WAVE1-induced actin nucleation by Rac1 and Nck. *Nature,* 418**,** 790-3.

EDWARDS, M., ZWOLAK, A., SCHAFER, D. A., SEPT, D., DOMINGUEZ, R. & COOPER, J. A. 2014. Capping protein regulators fine-tune actin assembly dynamics. *Nat Rev Mol Cell Biol,* 15**,** 677-89.

EICHINGER, L., LEE, S. S. & SCHLEICHER, M. 1999. Dictyostelium as model system for studies of the actin cytoskeleton by molecular genetics. *Microsc Res Tech,* 47**,** 124-34.

EICHINGER, L., PACHEBAT, J. A., GLOCKNER, G., RAJANDREAM, M. A., SUCGANG, R., BERRIMAN, M., SONG, J., OLSEN, R., SZAFRANSKI, K., XU, Q., TUNGGAL, B., KUMMERFELD, S., MADERA, M., KONFORTOV, B. A., RIVERO, F., BANKIER, A. T., LEHMANN, R., HAMLIN, N., DAVIES, R., GAUDET, P., FEY, P., PILCHER, K., CHEN, G., SAUNDERS, D., SODERGREN, E., DAVIS, P., KERHORNOU, A., NIE, X., HALL, N., ANJARD, C., HEMPHILL, L., BASON, N., FARBROTHER, P., DESANY, B., JUST, E., MORIO, T., ROST, R., CHURCHER, C., COOPER, J., HAYDOCK, S., VAN DRIESSCHE, N., CRONIN, A., GOODHEAD, I., MUZNY, D., MOURIER, T., PAIN, A., LU, M., HARPER, D., LINDSAY, R., HAUSER, H., JAMES, K., QUILES, M., MADAN BABU, M., SAITO, T., BUCHRIESER, C., WARDROPER, A., FELDER, M., THANGAVELU, M., JOHNSON, D., KNIGHTS, A., LOULSEGED, H., MUNGALL, K., OLIVER, K., PRICE, C., QUAIL, M. A., URUSHIHARA, H., HERNANDEZ, J., RABBINOWITSCH, E., STEFFEN, D., SANDERS, M., MA, J., KOHARA, Y., SHARP, S., SIMMONDS, M., SPIEGLER, S., TIVEY, A., SUGANO, S., WHITE, B., WALKER, D., WOODWARD, J., WINCKLER, T., TANAKA, Y., SHAULSKY, G., SCHLEICHER, M., WEINSTOCK, G., ROSENTHAL, A., COX, E. C., CHISHOLM, R. L., GIBBS, R., LOOMIS, W. F., PLATZER, M., KAY, R. R., WILLIAMS, J., DEAR, P. H., NOEGEL, A. A., BARRELL, B. & KUSPA, A. 2005. The genome of the social amoeba Dictyostelium discoideum. *Nature,* 435**,** 43-57.

ELIAS, B. C., BHATTACHARYA, S., RAY, R. M. & JOHNSON, L. R. 2010. Polyamine-dependent activation of Rac1 is stimulated by focal adhesion-mediated Tiam1 activation. *Cell Adh Migr,* 4**,** 419-30.

ESTES, J. E., SELDEN, L. A., KINOSIAN, H. J. & GERSHMAN, L. C. 1992. Tightly-bound divalent cation of actin. *J Muscle Res Cell Motil,* 13**,** 272-84.

ESUE, O., TSENG, Y. & WIRTZ, D. 2009. Alpha-actinin and filamin cooperatively enhance the stiffness of actin filament networks. *PLoS One,* 4**,** e4411.

FAGARASANU, A., FAGARASANU, M., EITZEN, G. A., AITCHISON, J. D. & RACHUBINSKI, R. A. 2006. The peroxisomal membrane protein Inp2p is the peroxisome-specific receptor for the myosin V motor Myo2p of Saccharomyces cerevisiae. *Dev Cell,* 10**,** 587-600.

FALK, D. L., WESSELS, D., JENKINS, L., PHAM, T., KUHL, S., TITUS, M. A. & SOLL, D. R. 2003. Shared, unique and redundant functions of three members of the class I myosins (MyoA, MyoB and MyoF) in motility and chemotaxis in Dictyostelium. *J Cell Sci,* 116**,** 3985-99.

FERRON, F., REBOWSKI, G., LEE, S. H. & DOMINGUEZ, R. 2007. Structural basis for the recruitment of profilin-actin complexes during filament elongation by Ena/VASP. *EMBO J,* 26**,** 4597-606.

FEY, P., KOWAL, A. S., GAUDET, P., PILCHER, K. E. & CHISHOLM, R. L. 2007. Protocols for growth and development of Dictyostelium discoideum. *Nat Protoc,* 2**,** 1307-16.

FINN, R. D., BATEMAN, A., CLEMENTS, J., COGGILL, P., EBERHARDT, R. Y., EDDY, S. R., HEGER, A., HETHERINGTON, K., HOLM, L., MISTRY, J., SONNHAMMER, E. L., TATE, J. & PUNTA, M. 2014. Pfam: the protein families database. *Nucleic Acids Res*, 42, D222-30.

FOURNIER, M. F., SAUSER, R., AMBROSI, D., MEISTER, J. J. & VERKHOVSKY, A. B. 2010. Force transmission in migrating cells. *J Cell Biol*, 188, 287-97.

FRALEY, S. I., FENG, Y., KRISHNAMURTHY, R., KIM, D. H., CELEDON, A., LONGMORE, G. D. & WIRTZ, D. 2010. A distinctive role for focal adhesion proteins in three-dimensional cell motility. *Nat Cell Biol*, 12, 598-604.

FRANCO, S. J., RODGERS, M. A., PERRIN, B. J., HAN, J., BENNIN, D. A., CRITCHLEY, D. R. & HUTTENLOCHER, A. 2004. Calpain-mediated proteolysis of talin regulates adhesion dynamics. *Nat Cell Biol*, 6, 977-83.

FROQUET, R., LE COADIC, M., PERRIN, J., CHERIX, N., CORNILLON, S. & COSSON, P. 2012. TM9/Phg1 and SadA proteins control surface expression and stability of SibA adhesion molecules in Dictyostelium. *Mol Biol Cell*, 23, 679-86.

FROST, A., UNGER, V. M. & DE CAMILLI, P. 2009. The BAR domain superfamily: membrane-molding macromolecules. *Cell*, 137, 191-6.

FUKUI, Y., LYNCH, T. J., BRZESKA, H. & KORN, E. D. 1989. Myosin I is located at the leading edges of locomoting Dictyostelium amoebae. *Nature*, 341, 328-31.

GALLOP, J. L., WALRANT, A., CANTLEY, L. C. & KIRSCHNER, M. W. 2013. Phosphoinositides and membrane curvature switch the mode of actin polymerization via selective recruitment of toca-1 and Snx9. *Proc Natl Acad Sci U S A*, 110, 7193-8.

GANDHI, M., ACHARD, V., BLANCHOIN, L. & GOODE, B. L. 2009. Coronin switches roles in actin disassembly depending on the nucleotide state of actin. *Mol Cell*, 34, 364-74.

GANDHI, M., SMITH, B. A., BOVELLAN, M., PAAVILAINEN, V., DAUGHERTY-CLARKE, K., GELLES, J., LAPPALAINEN, P. & GOODE, B. L. 2010. GMF is a cofilin homolog that binds Arp2/3 complex to stimulate filament debranching and inhibit actin nucleation. *Curr Biol*, 20, 861-7.

GARCIA-MATA, R., BOULTER, E. & BURRIDGE, K. 2011. The 'invisible hand': regulation of RHO GTPases by RHOGDIs. *Nat Rev Mol Cell Biol*, 12, 493-504.

GEIGER, T. & ZAIDEL-BAR, R. 2012. Opening the floodgates: proteomics and the integrin adhesome. *Curr Opin Cell Biol*, 24, 562-8.

GLOTZER, M. 2001. Animal cell cytokinesis. *Annu Rev Cell Dev Biol*, 17, 351-86.

GOLDSCHMIDT-CLERMONT, P. J., MACHESKY, L. M., DOBERSTEIN, S. K. & POLLARD, T. D. 1991. Mechanism of the interaction of human platelet profilin with actin. *J Cell Biol*, 113, 1081-9.

GOLEY, E. D., RODENBUSCH, S. E., MARTIN, A. C. & WELCH, M. D. 2004. Critical conformational changes in the Arp2/3 complex are induced by nucleotide and nucleation promoting factor. *Mol Cell*, 16, 269-79.

GOTTSCHALK, K. E., ADAMS, P. D., BRUNGER, A. T. & KESSLER, H. 2002. Transmembrane signal transduction of the alpha(IIb)beta(3) integrin. *Protein Sci*, 11, 1800-12.

GUERRERO, C., MILENKOVIC, T., PRZULJ, N., KAISER, P. & HUANG, L. 2008. Characterization of the proteasome interaction network using a QTAX-based tag-team strategy and protein interaction network analysis. *Proc Natl Acad Sci U S A*, 105, 13333-8.

GUILLUY, C., GARCIA-MATA, R. & BURRIDGE, K. 2011. Rho protein crosstalk: another social network? *Trends Cell Biol,* 21**,** 718-26.

GUPTA, P., GAUTHIER, N. C., CHENG-HAN, Y., ZUANNING, Y., PONTES, B., OHMSTEDE, M., MARTIN, R., KNOLKER, H. J., DOBEREINER, H. G., KRENDEL, M. & SHEETZ, M. 2013. Myosin 1E localizes to actin polymerization sites in lamellipodia, affecting actin dynamics and adhesion formation. *Biol Open,* 2, 1288-99.

GUPTON, S. L. & GERTLER, F. B. 2007. Filopodia: the fingers that do the walking. *Sci STKE,* 2007**,** re5.

HACKER, U., ALBRECHT, R. & MANIAK, M. 1997. Fluid-phase uptake by macropinocytosis in Dictyostelium. *J Cell Sci,* 110 (Pt 2)**,** 105-12.

HALL, A. 2012. Rho family GTPases. *Biochem Soc Trans,* 40**,** 1378-82.

HAN, S.-I., FRIEHS, K. & FLASCHEL, E. 2004. Improvement of a synthetic medium for Dictyostelium discoideum. *Process Biochemistry,* 39**,** 925-930.

HANAHAN, D. & WEINBERG, R. A. 2000. The hallmarks of cancer. *Cell,* 100**,** 57-70.

HANSEN, S. D. & MULLINS, R. D. 2010. VASP is a processive actin polymerase that requires monomeric actin for barbed end association. *J Cell Biol,* 191**,** 571-84.

HARTMAN, M. A., FINAN, D., SIVARAMAKRISHNAN, S. & SPUDICH, J. A. 2011. Principles of unconventional myosin function and targeting. *Annu Rev Cell Dev Biol,* 27**,** 133-55.

HARTMAN, M. A. & SPUDICH, J. A. 2012. The myosin superfamily at a glance. *J Cell Sci,* 125**,** 1627-32.

HEASMAN, S. J. & RIDLEY, A. J. 2008. Mammalian Rho GTPases: new insights into their functions from in vivo studies. *Nat Rev Mol Cell Biol,* 9**,** 690-701.

HEISSLER, S. M. & SELLERS, J. R. 2014. Myosin light chains: Teaching old dogs new tricks. *Bioarchitecture,* 4**,** 169-88.

HELGESON, L. A. & NOLEN, B. J. 2013. Mechanism of synergistic activation of Arp2/3 complex by cortactin and N-WASP. *Elife,* 2**,** e00884.

HELGESON, L. A., PRENDERGAST, J. G., WAGNER, A. R., RODNICK-SMITH, M. & NOLEN, B. J. 2014. Interactions with actin monomers, actin filaments, and Arp2/3 complex define the roles of WASP family proteins and cortactin in coordinately regulating branched actin networks. *J Biol Chem,* 289, 28856-69.

HERMAN, I. M. 1993. Actin isoforms. *Curr Opin Cell Biol,* 5**,** 48-55.

HIGGS, H. N., BLANCHOIN, L. & POLLARD, T. D. 1999. Influence of the C terminus of Wiskott-Aldrich syndrome protein (WASp) and the Arp2/3 complex on actin polymerization. *Biochemistry,* 38**,** 15212-22.

HIGGS, H. N. & POLLARD, T. D. 2000. Activation by Cdc42 and PIP(2) of Wiskott-Aldrich syndrome protein (WASp) stimulates actin nucleation by Arp2/3 complex. *J Cell Biol,* 150**,** 1311-20.

HILD, G., BUGYI, B. & NYITRAI, M. 2010. Conformational dynamics of actin: effectors and implications for biological function. *Cytoskeleton (Hoboken),* 67**,** 609-29.

HILL, K. L., CATLETT, N. L. & WEISMAN, L. S. 1996. Actin and myosin function in directed vacuole movement during cell division in Saccharomyces cerevisiae. *J Cell Biol,* 135**,** 1535-49.

HORTON, E. R., BYRON, A., ASKARI, J. A., NG, D. H., MILLON-FREMILLON, A., ROBERTSON, J., KOPER, E. J., PAUL, N. R., WARWOOD, S., KNIGHT, D., HUMPHRIES, J. D. & HUMPHRIES, M. J. 2015. Definition of a consensus

integrin adhesome and its dynamics during adhesion complex assembly and disassembly. *Nat Cell Biol,* 17, 1577-87.

HSIA, D. A., MITRA, S. K., HAUCK, C. R., STREBLOW, D. N., NELSON, J. A., ILIC, D., HUANG, S., LI, E., NEMEROW, G. R., LENG, J., SPENCER, K. S., CHERESH, D. A. & SCHLAEPFER, D. D. 2003. Differential regulation of cell motility and invasion by FAK. *J Cell Biol,* 160, 753-67.

HUANG, C. H., TANG, M., SHI, C., IGLESIAS, P. A. & DEVREOTES, P. N. 2013. An excitable signal integrator couples to an idling cytoskeletal oscillator to drive cell migration. *Nat Cell Biol,* 15, 1307-16.

HUANG, Y. J., MAO, B., ARAMINI, J. M. & MONTELIONE, G. T. 2014. Assessment of template-based protein structure predictions in CASP10. *Proteins: Structure, Function, and Bioinformatics,* 82, 43-56.

HUBER, F., BOIRE, A., LOPEZ, M. P. & KOENDERINK, G. H. 2015. Cytoskeletal crosstalk: when three different personalities team up. *Curr Opin Cell Biol,* 32, 39-47.

HUBER, R. J. & O'DAY, D. H. 2012. EGF-like peptide-enhanced cell movement in Dictyostelium is mediated by protein kinases and the activity of several cytoskeletal proteins. *Cell Signal,* 24, 1770-80.

HUGHES, J. E., KIYOSAWA, H. & WELKER, D. L. 1994. Plasmid maintenance functions encoded on Dictyostelium discoideum nuclear plasmid Ddp1. *Mol Cell Biol,* 14, 6117-24.

HUMPHREYS, D., LIU, T., DAVIDSON, A. C., HUME, P. J. & KORONAKIS, V. 2012. The Drosophila Arf1 homologue Arf79F is essential for lamellipodium formation. *J Cell Sci,* 125, 5630-5.

IBARRA, N., BLAGG, S. L., VAZQUEZ, F. & INSALL, R. H. 2006. Nap1 regulates Dictyostelium cell motility and adhesion through SCAR-dependent and -independent pathways. *Curr Biol,* 16, 717-22.

INGERMAN, E., HSIAO, J. Y. & MULLINS, R. D. 2013. Arp2/3 complex ATP hydrolysis promotes lamellipodial actin network disassembly but is dispensable for assembly. *J Cell Biol,* 200, 619-33.

INSALL, R. 2013. The interaction between pseudopods and extracellular signalling during chemotaxis and directed migration. *Curr Opin Cell Biol,* 25, 526-31.

INSALL, R. H. & MACHESKY, L. M. 2009. Actin dynamics at the leading edge: from simple machinery to complex networks. *Dev Cell,* 17, 310-22.

ISMAIL, A. M., PADRICK, S. B., CHEN, B., UMETANI, J. & ROSEN, M. K. 2009. The WAVE regulatory complex is inhibited. *Nat Struct Mol Biol,* 16, 561-3.

IWANICKI, M. P., VOMASTEK, T., TILGHMAN, R. W., MARTIN, K. H., BANERJEE, J., WEDEGAERTNER, P. B. & PARSONS, J. T. 2008. FAK, PDZ-RhoGEF and ROCKII cooperate to regulate adhesion movement and trailing-edge retraction in fibroblasts. *J Cell Sci,* 121, 895-905.

JOHNSON, H. E., KING, S. J., ASOKAN, S. B., ROTTY, J. D., BEAR, J. E. & HAUGH, J. M. 2015. F-actin bundles direct the initiation and orientation of lamellipodia through adhesion-based signaling. *J Cell Biol,* 208, 443-55.

JUNG, G., TITUS, M. A. & HAMMER, J. A., 3RD 2009. The Dictyostelium type V myosin MyoJ is responsible for the cortical association and motility of contractile vacuole membranes. *J Cell Biol,* 186, 555-70.

JUNG, G., WU, X. & HAMMER, J. A., 3RD 1996. Dictyostelium mutants lacking multiple classic myosin I isoforms reveal combinations of shared and distinct functions. *J Cell Biol,* 133, 305-23.

KABSCH, W., MANNHERZ, H. G., SUCK, D., PAI, E. F. & HOLMES, K. C. 1990. Atomic structure of the actin:DNase I complex. *Nature,* 347, 37-44.

KANCHANAWONG, P., SHTENGEL, G., PASAPERA, A. M., RAMKO, E. B., DAVIDSON, M. W., HESS, H. F. & WATERMAN, C. M. 2010. Nanoscale architecture of integrin-based cell adhesions. *Nature,* 468**,** 580-4.

KAST, D. J., YANG, C., DISANZA, A., BOCZKOWSKA, M., MADASU, Y., SCITA, G., SVITKINA, T. & DOMINGUEZ, R. 2014. Mechanism of IRSp53 inhibition and combinatorial activation by Cdc42 and downstream effectors. *Nat Struct Mol Biol,* 21, 413-22.

KHERADMAND, F., WERNER, E., TREMBLE, P., SYMONS, M. & WERB, Z. 1998. Role of Rac1 and oxygen radicals in collagenase-1 expression induced by cell shape change. *Science,* 280, 898-902.

KIM, S. V., MEHAL, W. Z., DONG, X., HEINRICH, V., PYPAERT, M., MELLMAN, I., DEMBO, M., MOOSEKER, M. S., WU, D. & FLAVELL, R. A. 2006. Modulation of cell adhesion and motility in the immune system by Myo1f. *Science,* 314**,** 136-9.

KING, J. S., VELTMAN, D. M., GEORGIOU, M., BAUM, B. & INSALL, R. H. 2010. SCAR/WAVE is activated at mitosis and drives myosin-independent cytokinesis. *J Cell Sci,* 123**,** 2246-55.

KNECHT, D. A., COHEN, S. M., LOOMIS, W. F. & LODISH, H. F. 1986. Developmental regulation of Dictyostelium discoideum actin gene fusions carried on low-copy and high-copy transformation vectors. *Mol Cell Biol,* 6**,** 3973-83.

KOBAYASHI, K., KURODA, S., FUKATA, M., NAKAMURA, T., NAGASE, T., NOMURA, N., MATSUURA, Y., YOSHIDA-KUBOMURA, N., IWAMATSU, A. & KAIBUCHI, K. 1998. p140Sra-1 (specifically Rac1-associated protein) is a novel specific target for Rac1 small GTPase. *J Biol Chem,* 273**,** 291-5.

KOLLMAR, M. 2006. Thirteen is enough: the myosins of Dictyostelium discoideum and their light chains. *BMC Genomics,* 7**,** 183.

KONZOK, A., WEBER, I., SIMMETH, E., HACKER, U., MANIAK, M. & MULLER-TAUBENBERGER, A. 1999. DAip1, a Dictyostelium homologue of the yeast actin-interacting protein 1, is involved in endocytosis, cytokinesis, and motility. *J Cell Biol,* 146**,** 453-64.

KOROBOVA, F. & SVITKINA, T. 2008. Arp2/3 complex is important for filopodia formation, growth cone motility, and neuritogenesis in neuronal cells. *Mol Biol Cell,* 19**,** 1561-74.

KORONAKIS, V., HUME, P. J., HUMPHREYS, D., LIU, T., HORNING, O., JENSEN, O. N. & MCGHIE, E. J. 2011. WAVE regulatory complex activation by cooperating GTPases Arf and Rac1. *Proc Natl Acad Sci U S A,* 108**,** 14449-54.

KORTHOLT, A., KATARIA, R., KEIZER-GUNNINK, I., VAN EGMOND, W. N., KHANNA, A. & VAN HAASTERT, P. J. 2011. Dictyostelium chemotaxis: essential Ras activation and accessory signalling pathways for amplification. *EMBO Rep,* 12**,** 1273-9.

KOSCIELNY, G., YAIKHOM, G., IYER, V., MEEHAN, T. F., MORGAN, H., ATIENZA-HERRERO, J., BLAKE, A., CHEN, C. K., EASTY, R., DI FENZA, A., FIEGEL, T., GRIFITHS, M., HORNE, A., KARP, N. A., KURBATOVA, N., MASON, J. C., MATTHEWS, P., OAKLEY, D. J., QAZI, A., REGNART, J., RETHA, A., SANTOS, L. A., SNEDDON, D. J., WARREN, J., WESTERBERG, H., WILSON, R. J., MELVIN, D. G., SMEDLEY, D., BROWN, S. D., FLICEK, P., SKARNES, W. C., MALLON, A. M. & PARKINSON, H. 2014. The International Mouse Phenotyping Consortium Web Portal, a unified point of access for knockout mice and related phenotyping data. *Nucleic Acids Res,* 42**,** D802-9.

KOVAR, D. R., HARRIS, E. S., MAHAFFY, R., HIGGS, H. N. & POLLARD, T. D. 2006. Control of the assembly of ATP- and ADP-actin by formins and profilin. *Cell,* 124**,** 423-35.

KOVAR, D. R. & POLLARD, T. D. 2004. Insertional assembly of actin filament barbed ends in association with formins produces piconewton forces. *Proc Natl Acad Sci U S A,* 101**,** 14725-30.

KRAUSE, M. & GAUTREAU, A. 2014. Steering cell migration: lamellipodium dynamics and the regulation of directional persistence. *Nat Rev Mol Cell Biol,* 15**,** 577-90.

KRAUSE, M., LESLIE, J. D., STEWART, M., LAFUENTE, E. M., VALDERRAMA, F., JAGANNATHAN, R., STRASSER, G. A., RUBINSON, D. A., LIU, H., WAY, M., YAFFE, M. B., BOUSSIOTIS, V. A. & GERTLER, F. B. 2004. Lamellipodin, an Ena/VASP ligand, is implicated in the regulation of lamellipodial dynamics. *Dev Cell,* 7**,** 571-83.

KREITMEIER, M., GERISCH, G., HEIZER, C. & MULLER-TAUBENBERGER, A. 1995. A talin homologue of Dictyostelium rapidly assembles at the leading edge of cells in response to chemoattractant. *J Cell Biol,* 129**,** 179-88.

KRENDEL, M., OSTERWEIL, E. K. & MOOSEKER, M. S. 2007. Myosin 1E interacts with synaptojanin-1 and dynamin and is involved in endocytosis. *FEBS Lett,* 581**,** 644-50.

KRUGMANN, S., JORDENS, I., GEVAERT, K., DRIESSENS, M., VANDEKERCKHOVE, J. & HALL, A. 2001. Cdc42 induces filopodia by promoting the formation of an IRSp53:Mena complex. *Curr Biol,* 11**,** 1645-55.

KUBOW, K. E. & HORWITZ, A. R. 2011. Reducing background fluorescence reveals adhesions in 3D matrices. *Nat Cell Biol,* 13**,** 3-5; author reply 5-7.

KUDRYASHOV, D. S., GRINTSEVICH, E. E., RUBENSTEIN, P. A. & REISLER, E. 2010. A nucleotide state-sensing region on actin. *J Biol Chem,* 285**,** 25591-601.

KUMAGAI, A., HADWIGER, J. A., PUPILLO, M. & FIRTEL, R. A. 1991. Molecular genetic analysis of two G alpha protein subunits in Dictyostelium. *J Biol Chem,* 266**,** 1220-8.

KUMAGAI, A., PUPILLO, M., GUNDERSEN, R., MIAKE-LYE, R., DEVREOTES, P. N. & FIRTEL, R. A. 1989. Regulation and function of G alpha protein subunits in Dictyostelium. *Cell,* 57**,** 265-75.

KUNDA, P., CRAIG, G., DOMINGUEZ, V. & BAUM, B. 2003. Abi, Sra1, and Kette control the stability and localization of SCAR/WAVE to regulate the formation of actin-based protrusions. *Curr Biol,* 13**,** 1867-75.

KUO, J. C., HAN, X., HSIAO, C. T., YATES, J. R., 3RD & WATERMAN, C. M. 2011. Analysis of the myosin-II-responsive focal adhesion proteome reveals a role for beta-Pix in negative regulation of focal adhesion maturation. *Nat Cell Biol,* 13**,** 383-93.

KURISU, S., SUETSUGU, S., YAMAZAKI, D., YAMAGUCHI, H. & TAKENAWA, T. 2005. Rac-WAVE2 signaling is involved in the invasive and metastatic phenotypes of murine melanoma cells. *Oncogene,* 24**,** 1309-19.

KUROKAWA, K. & MATSUDA, M. 2005. Localized RhoA activation as a requirement for the induction of membrane ruffling. *Mol Biol Cell,* 16**,** 4294-303.

LAEVSKY, G. & KNECHT, D. A. 2003. Cross-linking of actin filaments by myosin II is a major contributor to cortical integrity and cell motility in restrictive environments. *J Cell Sci,* 116**,** 3761-70.

LAI, F. P., SZCZODRAK, M., BLOCK, J., FAIX, J., BREITSPRECHER, D., MANNHERZ, H. G., STRADAL, T. E., DUNN, G. A., SMALL, J. V. & ROTTNER, K. 2008. Arp2/3 complex interactions and actin network turnover in lamellipodia. *EMBO J,* 27**,** 982-92.

LAMMERMANN, T., BADER, B. L., MONKLEY, S. J., WORBS, T., WEDLICH-SOLDNER, R., HIRSCH, K., KELLER, M., FORSTER, R., CRITCHLEY, D. R., FASSLER, R. & SIXT, M. 2008. Rapid leukocyte migration by integrin-independent flowing and squeezing. *Nature,* 453**,** 51-5.

LAMMERMANN, T. & SIXT, M. 2009. Mechanical modes of 'amoeboid' cell migration. *Curr Opin Cell Biol,* 21**,** 636-44.

LAMMERS, M., MEYER, S., KUHLMANN, D. & WITTINGHOFER, A. 2008. Specificity of interactions between mDia isoforms and Rho proteins. *J Biol Chem,* 283**,** 35236-46.

LAW, A. L., VEHLOW, A., KOTINI, M., DODGSON, L., SOONG, D., THEVENEAU, E., BODO, C., TAYLOR, E., NAVARRO, C., PERERA, U., MICHAEL, M., DUNN, G. A., BENNETT, D., MAYOR, R. & KRAUSE, M. 2013. Lamellipodin and the Scar/WAVE complex cooperate to promote cell migration in vivo. *J Cell Biol,* 203**,** 673-89.

LEBENSOHN, A. M. & KIRSCHNER, M. W. 2009. Activation of the WAVE complex by coincident signals controls actin assembly. *Mol Cell,* 36**,** 512-24.

LECLAIRE, L. L., 3RD, BAUMGARTNER, M., IWASA, J. H., MULLINS, R. D. & BARBER, D. L. 2008. Phosphorylation of the Arp2/3 complex is necessary to nucleate actin filaments. *J Cell Biol,* 182**,** 647-54.

LEE, S. F. & COTE, G. P. 1995. Purification and characterization of a Dictyostelium protein kinase required for actin activation of the Mg2+ ATPase activity of Dictyostelium myosin ID. *J Biol Chem,* 270**,** 11776-82.

LEE, S. F., EGELHOFF, T. T., MAHASNEH, A. & COTE, G. P. 1996. Cloning and characterization of a Dictyostelium myosin I heavy chain kinase activated by Cdc42 and Rac. *J Biol Chem,* 271**,** 27044-8.

LEGATE, K. R. & FASSLER, R. 2009. Mechanisms that regulate adaptor binding to beta-integrin cytoplasmic tails. *J Cell Sci,* 122**,** 187-98.

LENG, Y., ZHANG, J., BADOUR, K., ARPAIA, E., FREEMAN, S., CHEUNG, P., SIU, M. & SIMINOVITCH, K. 2005. Abelson-interactor-1 promotes WAVE2 membrane translocation and Abelson-mediated tyrosine phosphorylation required for WAVE2 activation. *Proc Natl Acad Sci U S A,* 102**,** 1098-103.

LI, F. & HIGGS, H. N. 2003. The mouse Formin mDia1 is a potent actin nucleation factor regulated by autoinhibition. *Curr Biol,* 13**,** 1335-40.

LI, F. & HIGGS, H. N. 2005. Dissecting requirements for auto-inhibition of actin nucleation by the formin, mDia1. *J Biol Chem,* 280**,** 6986-92.

LI, W., COWLEY, A., ULUDAG, M., GUR, T., MCWILLIAM, H., SQUIZZATO, S., PARK, Y. M., BUSO, N. & LOPEZ, R. 2015. The EMBL-EBI bioinformatics web and programmatic tools framework. *Nucleic Acids Res,* 43**,** W580-4.

LINARDOPOULOU, E. V., PARGHI, S. S., FRIEDMAN, C., OSBORN, G. E., PARKHURST, S. M. & TRASK, B. J. 2007. Human subtelomeric WASH genes encode a new subclass of the WASP family. *PLoS Genet,* 3**,** e237.

LING, K., SCHILL, N. J., WAGONER, M. P., SUN, Y. & ANDERSON, R. A. 2006. Movin' on up: the role of PtdIns(4,5)P(2) in cell migration. *Trends Cell Biol,* 16**,** 276-84.

LIU, J., DAS, M., YANG, J., ITHYCHANDA, S. S., YAKUBENKO, V. P., PLOW, E. F. & QIN, J. 2015. Structural mechanism of integrin inactivation by filamin. *Nat Struct Mol Biol,* 22**,** 383-9.

LIU, Y., SCHMIDT, B. & MASKELL, D. L. 2010. MSAProbs: multiple sequence alignment based on pair hidden Markov models and partition function posterior probabilities. *Bioinformatics,* 26**,** 1958-64.

LIVINGSTONE, C. D. & BARTON, G. J. 1993. Protein sequence alignments: a strategy for the hierarchical analysis of residue conservation. *Comput Appl Biosci,* 9**,** 745-56.

LOMBARDI, M. L., KNECHT, D. A., DEMBO, M. & LEE, J. 2007. Traction force microscopy in Dictyostelium reveals distinct roles for myosin II motor and actin-crosslinking activity in polarized cell movement. *J Cell Sci,* 120**,** 1624-34.

LOOMIS, W. F., JR. 1971. Sensitivity of Dictyostelium discoideum to nucleic acid analogues. *Exp Cell Res,* 64**,** 484-6.

MACHACEK, M., HODGSON, L., WELCH, C., ELLIOTT, H., PERTZ, O., NALBANT, P., ABELL, A., JOHNSON, G. L., HAHN, K. M. & DANUSER, G. 2009. Coordination of Rho GTPase activities during cell protrusion. *Nature,* 461**,** 99-103.

MACHESKY, L. M., ATKINSON, S. J., AMPE, C., VANDEKERCKHOVE, J. & POLLARD, T. D. 1994. Purification of a cortical complex containing two unconventional actins from Acanthamoeba by affinity chromatography on profilin-agarose. *J Cell Biol,* 127**,** 107-15.

MACHESKY, L. M. & INSALL, R. H. 1998. Scar1 and the related Wiskott-Aldrich syndrome protein, WASP, regulate the actin cytoskeleton through the Arp2/3 complex. *Curr Biol,* 8**,** 1347-56.

MACHESKY, L. M., MULLINS, R. D., HIGGS, H. N., KAISER, D. A., BLANCHOIN, L., MAY, R. C., HALL, M. E. & POLLARD, T. D. 1999. Scar, a WASp-related protein, activates nucleation of actin filaments by the Arp2/3 complex. *Proc Natl Acad Sci U S A,* 96**,** 3739-44.

MACK, N. A., WHALLEY, H. J., CASTILLO-LLUVA, S. & MALLIRI, A. 2011. The diverse roles of Rac signaling in tumorigenesis. *Cell Cycle,* 10, 1571-81.

MANSTEIN, D. J., TITUS, M. A., DE LOZANNE, A. & SPUDICH, J. A. 1989. Gene replacement in Dictyostelium: generation of myosin null mutants. *EMBO J,* 8**,** 923-32.

MARGADANT, C., MONSUUR, H. N., NORMAN, J. C. & SONNENBERG, A. 2011. Mechanisms of integrin activation and trafficking. *Curr Opin Cell Biol,* 23**,** 607-14.

MARIANI, V., KIEFER, F., SCHMIDT, T., HAAS, J. & SCHWEDE, T. 2011. Assessment of template based protein structure predictions in CASP9. *Proteins: Structure, Function, and Bioinformatics,* 79, 37-58.

MARTIN, A. C., WELCH, M. D. & DRUBIN, D. G. 2006. Arp2/3 ATP hydrolysis-catalysed branch dissociation is critical for endocytic force generation. *Nat Cell Biol,* 8**,** 826-33.

MARTIN, A. C., XU, X. P., ROUILLER, I., KAKSONEN, M., SUN, Y., BELMONT, L., VOLKMANN, N., HANEIN, D., WELCH, M. & DRUBIN, D. G. 2005. Effects of Arp2 and Arp3 nucleotide-binding pocket mutations on Arp2/3 complex function. *J Cell Biol,* 168**,** 315-28.

MATTHEYSES, A. L., SIMON, S. M. & RAPPOPORT, J. Z. 2010. Imaging with total internal reflection fluorescence microscopy for the cell biologist. *J Cell Sci,* 123, 3621-8.

MAXEINER, S., SHI, N., SCHALLA, C., AYDIN, G., HOSS, M., VOGEL, S., ZENKE, M. & SECHI, A. S. 2015. Crucial role for the LSP1-myosin1e bimolecular complex in the regulation of Fcgamma receptor-driven phagocytosis. *Mol Biol Cell,* 26, 1652-64.

MEIJERING, E., DZYUBACHYK, O. & SMAL, I. 2012. Methods for cell and particle tracking. *Methods Enzymol,* 504**,** 183-200.

MELLER, J., VIDALI, L. & SCHWARTZ, M. A. 2008. Endogenous RhoG is dispensable for integrin-mediated cell spreading but contributes to Rac-independent migration. *J Cell Sci,* 121**,** 1981-9.

MELLOR, H. 2010. The role of formins in filopodia formation. *Biochim Biophys Acta,* 1803**,** 191-200.

MENDOZA, M. C. 2013. Phosphoregulation of the WAVE regulatory complex and signal integration. *Semin Cell Dev Biol,* 24**,** 272-9.

MICHELOT, A. & DRUBIN, D. G. 2011. Building distinct actin filament networks in a common cytoplasm. *Curr Biol,* 21**,** R560-9.

MIKI, H., SUETSUGU, S. & TAKENAWA, T. 1998. WAVE, a novel WASP-family protein involved in actin reorganization induced by Rac. *EMBO J,* 17**,** 6932-41.

MIKI, H., YAMAGUCHI, H., SUETSUGU, S. & TAKENAWA, T. 2000. IRSp53 is an essential intermediate between Rac and WAVE in the regulation of membrane ruffling. *Nature,* 408**,** 732-5.

MILNE, I., LINDNER, D., BAYER, M., HUSMEIER, D., MCGUIRE, G., MARSHALL, D. F. & WRIGHT, F. 2009. TOPALi v2: a rich graphical interface for evolutionary analyses of multiple alignments on HPC clusters and multi-core desktops. *Bioinformatics,* 25**,** 126-7.

MOORES, S. L., SABRY, J. H. & SPUDICH, J. A. 1996. Myosin dynamics in live Dictyostelium cells. *Proc Natl Acad Sci U S A,* 93**,** 443-6.

MOSER, M., LEGATE, K. R., ZENT, R. & FASSLER, R. 2009. The tail of integrins, talin, and kindlins. *Science,* 324**,** 895-9.

MSEKA, T. & CRAMER, L. P. 2011. Actin depolymerization-based force retracts the cell rear in polarizing and migrating cells. *Curr Biol,* 21**,** 2085-91.

MULLER, V. S., JUNGBLUT, P. R., MEYER, T. F. & HUNKE, S. 2011. Membrane-SPINE: an improved method to identify protein-protein interaction partners of membrane proteins in vivo. *Proteomics,* 11**,** 2124-8.

MULLINS, R. D. & HANSEN, S. D. 2013. In vitro studies of actin filament and network dynamics. *Curr Opin Cell Biol,* 25**,** 6-13.

MULLINS, R. D., HEUSER, J. A. & POLLARD, T. D. 1998. The interaction of Arp2/3 complex with actin: nucleation, high affinity pointed end capping, and formation of branching networks of filaments. *Proc Natl Acad Sci U S A,* 95**,** 6181-6.

MURAKAMI, K., YASUNAGA, T., NOGUCHI, T. Q., GOMIBUCHI, Y., NGO, K. X., UYEDA, T. Q. & WAKABAYASHI, T. 2010. Structural basis for actin assembly, activation of ATP hydrolysis, and delayed phosphate release. *Cell,* 143**,** 275-87.

MURALI, A. & RAJALINGAM, K. 2014. Small Rho GTPases in the control of cell shape and mobility. *Cell Mol Life Sci,* 71**,** 1703-21.

NAGARAJAN, N. A., GONZALEZ, F. & SHASTRI, N. 2012. Nonclassical MHC class Ib-restricted cytotoxic T cells monitor antigen processing in the endoplasmic reticulum. *Nat Immunol,* 13**,** 579-86.

NAKAO, S., PLATEK, A., HIRANO, S. & TAKEICHI, M. 2008. Contact-dependent promotion of cell migration by the OL-protocadherin-Nap1 interaction. *J Cell Biol,* 182**,** 395-410.

NEIDL, C. & ENGEL, J. 1979. Exchange of ADP, ATP and 1: N6-ethenoadenosine 5'-triphosphate at G-actin. Equilibrium and kinetics. *Eur J Biochem,* 101**,** 163-9.

NGO, K. X., KODERA, N., KATAYAMA, E., ANDO, T. & UYEDA, T. Q. 2015. Cofilin-induced unidirectional cooperative conformational changes in actin filaments revealed by high-speed atomic force microscopy. *Elife,* 4.

NIEWOHNER, J., WEBER, I., MANIAK, M., MULLER-TAUBENBERGER, A. & GERISCH, G. 1997. Talin-null cells of Dictyostelium are strongly defective in adhesion to particle and substrate surfaces and slightly impaired in cytokinesis. *J Cell Biol*, 138, 349-61.

ODA, T., IWASA, M., AIHARA, T., MAEDA, Y. & NARITA, A. 2009. The nature of the globular- to fibrous-actin transition. *Nature*, 457, 441-5.

OREOPOULOS, J., BERMAN, R. & BROWNE, M. 2014. Spinning-disk confocal microscopy: present technology and future trends. *Methods Cell Biol*, 123, 153-75.

OTOMO, T., TOMCHICK, D. R., OTOMO, C., PANCHAL, S. C., MACHIUS, M. & ROSEN, M. K. 2005. Structural basis of actin filament nucleation and processive capping by a formin homology 2 domain. *Nature*, 433, 488-94.

PADDOCK, S. W. & ELICEIRI, K. W. 2014. Laser scanning confocal microscopy: history, applications, and related optical sectioning techniques. *Methods Mol Biol*, 1075, 9-47.

PADRICK, S. B., CHENG, H. C., ISMAIL, A. M., PANCHAL, S. C., DOOLITTLE, L. K., KIM, S., SKEHAN, B. M., UMETANI, J., BRAUTIGAM, C. A., LEONG, J. M. & ROSEN, M. K. 2008. Hierarchical regulation of WASP/WAVE proteins. *Mol Cell*, 32, 426-38.

PADRICK, S. B., DOOLITTLE, L. K., BRAUTIGAM, C. A., KING, D. S. & ROSEN, M. K. 2011. Arp2/3 complex is bound and activated by two WASP proteins. *Proc Natl Acad Sci U S A*, 108, E472-9.

PALUCH, E. K. & RAZ, E. 2013. The role and regulation of blebs in cell migration. *Curr Opin Cell Biol*, 25, 582-90.

PANOPOULOS, A., HOWELL, M., FOTEDAR, R. & MARGOLIS, R. L. 2011. Glioblastoma motility occurs in the absence of actin polymer. *Mol Biol Cell*, 22, 2212-20.

PARENT, C. A. & WEINER, O. D. 2013. The symphony of cell movement: how cells orchestrate diverse signals and forces to control migration. *Curr Opin Cell Biol*, 25, 523-5.

PARSONS, J. T., HORWITZ, A. R. & SCHWARTZ, M. A. 2010. Cell adhesion: integrating cytoskeletal dynamics and cellular tension. *Nat Rev Mol Cell Biol*, 11, 633-43.

PATEL, H., KONIG, I., TSUJIOKA, M., FRAME, M. C., ANDERSON, K. I. & BRUNTON, V. G. 2008. The multi-FERM-domain-containing protein FrmA is required for turnover of paxillin-adhesion sites during cell migration of Dictyostelium. *J Cell Sci*, 121, 1159-64.

PEARSON, W. R. 2013. An introduction to sequence similarity ("homology") searching. *Curr Protoc Bioinformatics*, Chapter 3, Unit3 1.

PECKHAM, M. 2011. Coiled coils and SAH domains in cytoskeletal molecular motors. *Biochem Soc Trans*, 39, 1142-8.

PELLEGRIN, S. & MELLOR, H. 2005. The Rho family GTPase Rif induces filopodia through mDia2. *Curr Biol*, 15, 129-33.

PENG, J., WALLAR, B. J., FLANDERS, A., SWIATEK, P. J. & ALBERTS, A. S. 2003. Disruption of the Diaphanous-related formin Drf1 gene encoding mDia1 reveals a role for Drf3 as an effector for Cdc42. *Curr Biol*, 13, 534-45.

PETTERSEN, E. F., GODDARD, T. D., HUANG, C. C., COUCH, G. S., GREENBLATT, D. M., MENG, E. C. & FERRIN, T. E. 2004. UCSF Chimera--a visualization system for exploratory research and analysis. *J Comput Chem*, 25, 1605-12.

POLLARD, T. D. 1986. Rate constants for the reactions of ATP- and ADP-actin with the ends of actin filaments. *J Cell Biol*, 103, 2747-54.

POLLARD, T. D., BLANCHOIN, L. & MULLINS, R. D. 2000. Molecular mechanisms controlling actin filament dynamics in nonmuscle cells. *Annu Rev Biophys Biomol Struct,* 29, 545-76.

POLLARD, T. D. & COOPER, J. A. 1984. Quantitative analysis of the effect of Acanthamoeba profilin on actin filament nucleation and elongation. *Biochemistry,* 23, 6631-41.

POLLARD, T. D. & COOPER, J. A. 2009. Actin, a central player in cell shape and movement. *Science,* 326, 1208-12.

POLLITT, A. Y. & INSALL, R. H. 2008. Abi mutants in Dictyostelium reveal specific roles for the SCAR/WAVE complex in cytokinesis. *Curr Biol,* 18, 203-10.

POLLITT, A. Y. & INSALL, R. H. 2009. Loss of Dictyostelium HSPC300 causes a scar-like phenotype and loss of SCAR protein. *BMC Cell Biol,* 10, 13.

PONTE, E., RIVERO, F., FECHHEIMER, M., NOEGEL, A. & BOZZARO, S. 2000. Severe developmental defects in Dictyostelium null mutants for actin-binding proteins. *Mech Dev,* 91, 153-61.

PRING, M., WEBER, A. & BUBB, M. R. 1992. Profilin-actin complexes directly elongate actin filaments at the barbed end. *Biochemistry,* 31, 1827-36.

PROCTER, J. B., THOMPSON, J., LETUNIC, I., CREEVEY, C., JOSSINET, F. & BARTON, G. J. 2010. Visualization of multiple alignments, phylogenies and gene family evolution. *Nat Methods,* 7, S16-25.

RAUCHER, D., STAUFFER, T., CHEN, W., SHEN, K., GUO, S., YORK, J. D., SHEETZ, M. P. & MEYER, T. 2000. Phosphatidylinositol 4,5-bisphosphate functions as a second messenger that regulates cytoskeleton-plasma membrane adhesion. *Cell,* 100, 221-8.

RICE, P., LONGDEN, I. & BLEASBY, A. 2000. EMBOSS: the European Molecular Biology Open Software Suite. *Trends Genet,* 16, 276-7.

RIDLEY, A. J. 2011. Life at the leading edge. *Cell,* 145, 1012-22.

RIEDL, J., CREVENNA, A. H., KESSENBROCK, K., YU, J. H., NEUKIRCHEN, D., BISTA, M., BRADKE, F., JENNE, D., HOLAK, T. A., WERB, Z., SIXT, M. & WEDLICH-SOLDNER, R. 2008. Lifeact: a versatile marker to visualize F-actin. *Nat Methods,* 5, 605-7.

RIVERO, F., DISLICH, H., GLOCKNER, G. & NOEGEL, A. A. 2001. The Dictyostelium discoideum family of Rho-related proteins. *Nucleic Acids Res,* 29, 1068-79.

ROCA-CUSACHS, P., SUNYER, R. & TREPAT, X. 2013. Mechanical guidance of cell migration: lessons from chemotaxis. *Curr Opin Cell Biol,* 25, 543-9.

RODAL, A. A., SOKOLOVA, O., ROBINS, D. B., DAUGHERTY, K. M., HIPPENMEYER, S., RIEZMAN, H., GRIGORIEFF, N. & GOODE, B. L. 2005. Conformational changes in the Arp2/3 complex leading to actin nucleation. *Nat Struct Mol Biol,* 12, 26-31.

ROGERS, S. L. & GELFAND, V. I. 1998. Myosin cooperates with microtubule motors during organelle transport in melanophores. *Curr Biol,* 8, 161-4.

ROGERS, S. L., WIEDEMANN, U., STUURMAN, N. & VALE, R. D. 2003. Molecular requirements for actin-based lamella formation in Drosophila S2 cells. *J Cell Biol,* 162, 1079-88.

ROHATGI, R., HO, H. Y. & KIRSCHNER, M. W. 2000. Mechanism of N-WASP activation by CDC42 and phosphatidylinositol 4, 5-bisphosphate. *J Cell Biol,* 150, 1299-310.

ROJAS, A. M., FUENTES, G., RAUSELL, A. & VALENCIA, A. 2012. The Ras protein superfamily: evolutionary tree and role of conserved amino acids. *J Cell Biol,* 196, 189-201.

ROSE, P. W., PRLIC, A., BI, C., BLUHM, W. F., CHRISTIE, C. H., DUTTA, S., GREEN, R. K., GOODSELL, D. S., WESTBROOK, J. D., WOO, J., YOUNG, J., ZARDECKI, C., BERMAN, H. M., BOURNE, P. E. & BURLEY, S. K. 2015. The RCSB Protein Data Bank: views of structural biology for basic and applied research and education. *Nucleic Acids Res,* 43**,** D345-56.

ROT, G., PARIKH, A., CURK, T., KUSPA, A., SHAULSKY, G. & ZUPAN, B. 2009. dictyExpress: a Dictyostelium discoideum gene expression database with an explorative data analysis web-based interface. *BMC Bioinformatics,* 10**,** 265.

ROTHBAUER, U., ZOLGHADR, K., MUYLDERMANS, S., SCHEPERS, A., CARDOSO, M. C. & LEONHARDT, H. 2008. A versatile nanotrap for biochemical and functional studies with fluorescent fusion proteins. *Mol Cell Proteomics,* 7**,** 282-9.

ROUILLER, I., XU, X. P., AMANN, K. J., EGILE, C., NICKELL, S., NICASTRO, D., LI, R., POLLARD, T. D., VOLKMANN, N. & HANEIN, D. 2008. The structural basis of actin filament branching by the Arp2/3 complex. *J Cell Biol,* 180**,** 887-95.

ROY, A., KUCUKURAL, A. & ZHANG, Y. 2010. I-TASSER: a unified platform for automated protein structure and function prediction. *Nat Protoc,* 5**,** 725-38.

ROZELLE, A. L., MACHESKY, L. M., YAMAMOTO, M., DRIESSENS, M. H., INSALL, R. H., ROTH, M. G., LUBY-PHELPS, K., MARRIOTT, G., HALL, A. & YIN, H. L. 2000. Phosphatidylinositol 4,5-bisphosphate induces actin-based movement of raft-enriched vesicles through WASP-Arp2/3. *Curr Biol,* 10**,** 311-20.

RUBENSTEIN, P. A. 1990. The functional importance of multiple actin isoforms. *Bioessays,* 12**,** 309-15.

RUXTON, G. D. 2006. The unequal variance t-test is an underused alternative to Student's t-test and the Mann–Whitney U test. *Behavioral Ecology,* 17**,** 688-690.

SAARIKANGAS, J., ZHAO, H. & LAPPALAINEN, P. 2010. Regulation of the actin cytoskeleton-plasma membrane interplay by phosphoinositides. *Physiol Rev,* 90**,** 259-89.

SAFER, D., ELZINGA, M. & NACHMIAS, V. T. 1991. Thymosin beta 4 and Fx, an actin-sequestering peptide, are indistinguishable. *J Biol Chem,* 266**,** 4029-32.

SANZ-MORENO, V., GADEA, G., AHN, J., PATERSON, H., MARRA, P., PINNER, S., SAHAI, E. & MARSHALL, C. J. 2008. Rac activation and inactivation control plasticity of tumor cell movement. *Cell,* 135**,** 510-23.

SCALES, T. M. & PARSONS, M. 2011. Spatial and temporal regulation of integrin signalling during cell migration. *Curr Opin Cell Biol,* 23**,** 562-8.

SCHILLER, H. B., FRIEDEL, C. C., BOULEGUE, C. & FASSLER, R. 2011. Quantitative proteomics of the integrin adhesome show a myosin II-dependent recruitment of LIM domain proteins. *EMBO Rep,* 12**,** 259-66.

SCHMITT-ULMS, G., HANSEN, K., LIU, J., COWDREY, C., YANG, J., DEARMOND, S. J., COHEN, F. E., PRUSINER, S. B. & BALDWIN, M. A. 2004. Time-controlled transcardiac perfusion cross-linking for the study of protein interactions in complex tissues. *Nat Biotechnol,* 22**,** 724-31.

SCHNEIDER, C. A., RASBAND, W. S. & ELICEIRI, K. W. 2012. NIH Image to ImageJ: 25 years of image analysis. *Nat Methods,* 9**,** 671-5.

SCHNEIDER, D. & ENGELMAN, D. M. 2004. Involvement of transmembrane domain interactions in signal transduction by alpha/beta integrins. *J Biol Chem,* 279**,** 9840-6.

SCHOTT, D. H., COLLINS, R. N. & BRETSCHER, A. 2002. Secretory vesicle transport velocity in living cells depends on the myosin-V lever arm length. *J Cell Biol,* 156**,** 35-9.

SCHWAB, A., FABIAN, A., HANLEY, P. J. & STOCK, C. 2012. Role of ion channels and transporters in cell migration. *Physiol Rev,* 92**,** 1865-913.

SCHWARZ, E. C., NEUHAUS, E. M., KISTLER, C., HENKEL, A. W. & SOLDATI, T. 2000. Dictyostelium myosin IK is involved in the maintenance of cortical tension and affects motility and phagocytosis. *J Cell Sci,* 113 (Pt 4)**,** 621-33.

SEASTONE, D. J., HARRIS, E., TEMESVARI, L. A., BEAR, J. E., SAXE, C. L. & CARDELLI, J. 2001. The WASp-like protein scar regulates macropinocytosis, phagocytosis and endosomal membrane flow in Dictyostelium. *J Cell Sci,* 114, 2673-83.

SEBE-PEDROS, A., GRAU-BOVE, X., RICHARDS, T. A. & RUIZ-TRILLO, I. 2014. Evolution and classification of myosins, a paneukaryotic whole-genome approach. *Genome Biol Evol,* 6**,** 290-305.

SEBE-PEDROS, A., ROGER, A. J., LANG, F. B., KING, N. & RUIZ-TRILLO, I. 2010. Ancient origin of the integrin-mediated adhesion and signaling machinery. *Proc Natl Acad Sci U S A,* 107**,** 10142-7.

SERRELS, B., SERRELS, A., BRUNTON, V. G., HOLT, M., MCLEAN, G. W., GRAY, C. H., JONES, G. E. & FRAME, M. C. 2007. Focal adhesion kinase controls actin assembly via a FERM-mediated interaction with the Arp2/3 complex. *Nat Cell Biol,* 9**,** 1046-56.

SETH, A., OTOMO, C. & ROSEN, M. K. 2006. Autoinhibition regulates cellular localization and actin assembly activity of the diaphanous-related formins FRLalpha and mDia1. *J Cell Biol,* 174**,** 701-13.

SIMSON, R., WALLRAFF, E., FAIX, J., NIEWOHNER, J., GERISCH, G. & SACKMANN, E. 1998. Membrane bending modulus and adhesion energy of wild-type and mutant cells of Dictyostelium lacking talin or cortexillins. *Biophys J,* 74**,** 514-22.

SOBCZYK, G. J., WANG, J. & WEIJER, C. J. 2014. SILAC-based proteomic quantification of chemoattractant-induced cytoskeleton dynamics on a second to minute timescale. *Nat Commun,* 5**,** 3319.

SOKAC, A. M., SCHIETROMA, C., GUNDERSEN, C. B. & BEMENT, W. M. 2006. Myosin-1c couples assembling actin to membranes to drive compensatory endocytosis. *Dev Cell,* 11**,** 629-40.

SOSSEY-ALAOUI, K., LI, X. & COWELL, J. K. 2007a. c-Abl-mediated phosphorylation of WAVE3 is required for lamellipodia formation and cell migration. *J Biol Chem,* 282**,** 26257-65.

SOSSEY-ALAOUI, K., SAFINA, A., LI, X., VAUGHAN, M. M., HICKS, D. G., BAKIN, A. V. & COWELL, J. K. 2007b. Down-regulation of WAVE3, a metastasis promoter gene, inhibits invasion and metastasis of breast cancer cells. *Am J Pathol,* 170**,** 2112-21.

STEFFEN, A., LADWEIN, M., DIMCHEV, G. A., HEIN, A., SCHWENKMEZGER, L., ARENS, S., LADWEIN, K. I., MARGIT HOLLEBOOM, J., SCHUR, F., VICTOR SMALL, J., SCHWARZ, J., GERHARD, R., FAIX, J., STRADAL, T. E., BRAKEBUSCH, C. & ROTTNER, K. 2013. Rac function is crucial for cell migration but is not required for spreading and focal adhesion formation. *J Cell Sci,* 126**,** 4572-88.

STEFFEN, A., ROTTNER, K., EHINGER, J., INNOCENTI, M., SCITA, G., WEHLAND, J. & STRADAL, T. E. 2004. Sra-1 and Nap1 link Rac to actin assembly driving lamellipodia formation. *EMBO J*, 23**,** 749-59.

STOVOLD, C. F., MILLARD, T. H. & MACHESKY, L. M. 2005. Inclusion of Scar/WAVE3 in a similar complex to Scar/WAVE1 and 2. *BMC Cell Biol,* 6**,** 11.

STRAUB, F. 1942. Actin. *Stud. Inst. Med. Chem. Univ. Szeged,* 2**,** 3-15.

STUART, J. R., GONZALEZ, F. H., KAWAI, H. & YUAN, Z. M. 2006. c-Abl interacts with the WAVE2 signaling complex to induce membrane ruffling and cell spreading. *J Biol Chem,* 281**,** 31290-7.

SUAREZ, C., ROLAND, J., BOUJEMAA-PATERSKI, R., KANG, H., MCCULLOUGH, B. R., REYMANN, A. C., GUERIN, C., MARTIEL, J. L., DE LA CRUZ, E. M. & BLANCHOIN, L. 2011. Cofilin tunes the nucleotide state of actin filaments and severs at bare and decorated segment boundaries. *Curr Biol,* 21**,** 862-8.

SUETSUGU, S. & GAUTREAU, A. 2012. Synergistic BAR-NPF interactions in actin-driven membrane remodeling. *Trends Cell Biol,* 22**,** 141-50.

SUETSUGU, S., KURISU, S., OIKAWA, T., YAMAZAKI, D., ODA, A. & TAKENAWA, T. 2006. Optimization of WAVE2 complex-induced actin polymerization by membrane-bound IRSp53, PIP(3), and Rac. *J Cell Biol,* 173**,** 571-85.

SUETSUGU, S., YAMAZAKI, D., KURISU, S. & TAKENAWA, T. 2003. Differential roles of WAVE1 and WAVE2 in dorsal and peripheral ruffle formation for fibroblast cell migration. *Dev Cell,* 5**,** 595-609.

SURANENI, P., RUBINSTEIN, B., UNRUH, J. R., DURNIN, M., HANEIN, D. & LI, R. 2012. The Arp2/3 complex is required for lamellipodia extension and directional fibroblast cell migration. *J Cell Biol,* 197**,** 239-51.

SUTHERLAND, B. W., TOEWS, J. & KAST, J. 2008. Utility of formaldehyde cross-linking and mass spectrometry in the study of protein-protein interactions. *J Mass Spectrom,* 43**,** 699-715.

SVITKINA, T. M. 2013. Ultrastructure of protrusive actin filament arrays. *Curr Opin Cell Biol,* 25**,** 574-81.

SVITKINA, T. M., BULANOVA, E. A., CHAGA, O. Y., VIGNJEVIC, D. M., KOJIMA, S., VASILIEV, J. M. & BORISY, G. G. 2003. Mechanism of filopodia initiation by reorganization of a dendritic network. *J Cell Biol,* 160**,** 409-21.

TAKANO, K., TOYOOKA, K. & SUETSUGU, S. 2008. EFC/F-BAR proteins and the N-WASP-WIP complex induce membrane curvature-dependent actin polymerization. *EMBO J,* 27**,** 2817-28.

TANG, H., LI, A., BI, J., VELTMAN, D. M., ZECH, T., SPENCE, H. J., YU, X., TIMPSON, P., INSALL, R. H., FRAME, M. C. & MACHESKY, L. M. 2013. Loss of Scar/WAVE complex promotes N-WASP- and FAK-dependent invasion. *Curr Biol,* 23**,** 107-17.

THE-UNIPROT-CONSORTIUM 2015. UniProt: a hub for protein information. *Nucleic Acids Research,* 43**,** D204-D212.

TOJKANDER, S., GATEVA, G. & LAPPALAINEN, P. 2012. Actin stress fibers--assembly, dynamics and biological roles. *J Cell Sci,* 125**,** 1855-64.

TOMAR, A. & SCHLAEPFER, D. D. 2009. Focal adhesion kinase: switching between GAPs and GEFs in the regulation of cell motility. *Curr Opin Cell Biol,* 21**,** 676-83.

TONDELEIR, D., LAMBRECHTS, A., MULLER, M., JONCKHEERE, V., DOLL, T., VANDAMME, D., BAKKALI, K., WATERSCHOOT, D., LEMAISTRE, M., DEBEIR, O., DECAESTECKER, C., HINZ, B., STAES, A., TIMMERMAN, E., COLAERT, N., GEVAERT, K., VANDEKERCKHOVE, J. & AMPE, C. 2012. Cells lacking

beta-actin are genetically reprogrammed and maintain conditional migratory capacity. *Mol Cell Proteomics,* 11**,** 255-71.

TSENG, Y., KOLE, T. P., LEE, J. S., FEDOROV, E., ALMO, S. C., SCHAFER, B. W. & WIRTZ, D. 2005. How actin crosslinking and bundling proteins cooperate to generate an enhanced cell mechanical response. *Biochem Biophys Res Commun,* 334**,** 183-92.

TSENG, Y., SCHAFER, B. W., ALMO, S. C. & WIRTZ, D. 2002. Functional synergy of actin filament cross-linking proteins. *J Biol Chem,* 277**,** 25609-16.

TSUJIOKA, M., MACHESKY, L. M., COLE, S. L., YAHATA, K. & INOUYE, K. 1999. A unique talin homologue with a villin headpiece-like domain is required for multicellular morphogenesis in Dictyostelium. *Curr Biol,* 9**,** 389-92.

TSUJIOKA, M., YOSHIDA, K., NAGASAKI, A., YONEMURA, S., MULLER-TAUBENBERGER, A. & UYEDA, T. Q. 2008. Overlapping functions of the two talin homologues in Dictyostelium. *Eukaryot Cell,* 7**,** 906-16.

TUXWORTH, R. I., WEBER, I., WESSELS, D., ADDICKS, G. C., SOLL, D. R., GERISCH, G. & TITUS, M. A. 2001. A role for myosin VII in dynamic cell adhesion. *Curr Biol,* 11**,** 318-29.

TYSON, R. A., ZATULOVSKIY, E., KAY, R. R. & BRETSCHNEIDER, T. 2014. How blebs and pseudopods cooperate during chemotaxis. *Proc Natl Acad Sci U S A,* 111**,** 11703-8.

URA, S., POLLITT, A. Y., VELTMAN, D. M., MORRICE, N. A., MACHESKY, L. M. & INSALL, R. H. 2012. Pseudopod growth and evolution during cell movement is controlled through SCAR/WAVE dephosphorylation. *Curr Biol,* 22**,** 553-61.

UYEDA, T. Q., KITAYAMA, C. & YUMURA, S. 2000. Myosin II-independent cytokinesis in Dictyostelium: its mechanism and implications. *Cell Struct Funct,* 25**,** 1-10.

VASILESCU, J., GUO, X. & KAST, J. 2004. Identification of protein-protein interactions using in vivo cross-linking and mass spectrometry. *Proteomics,* 4**,** 3845-54.

VELTMAN, D. M., AKAR, G., BOSGRAAF, L. & VAN HAASTERT, P. J. 2009a. A new set of small, extrachromosomal expression vectors for Dictyostelium discoideum. *Plasmid,* 61, 110-8.

VELTMAN, D. M. & INSALL, R. H. 2010. WASP family proteins: their evolution and its physiological implications. *Mol Biol Cell,* 21**,** 2880-93.

VELTMAN, D. M., KEIZER-GUNNINK, I. & HAASTERT, P. J. 2009b. An extrachromosomal, inducible expression system for Dictyostelium discoideum. *Plasmid,* 61**,** 119-25.

VELTMAN, D. M., KING, J. S., MACHESKY, L. M. & INSALL, R. H. 2012. SCAR knockouts in Dictyostelium: WASP assumes SCAR's position and upstream regulators in pseudopods. *J Cell Biol,* 198**,** 501-8.

VICENTE-MANZANARES, M., MA, X., ADELSTEIN, R. S. & HORWITZ, A. R. 2009. Non-muscle myosin II takes centre stage in cell adhesion and migration. *Nat Rev Mol Cell Biol,* 10**,** 778-90.

VINSON, V. K., DE LA CRUZ, E. M., HIGGS, H. N. & POLLARD, T. D. 1998. Interactions of Acanthamoeba profilin with actin and nucleotides bound to actin. *Biochemistry,* 37**,** 10871-80.

VON DER ECKEN, J., MULLER, M., LEHMAN, W., MANSTEIN, D. J., PENCZEK, P. A. & RAUNSER, S. 2015. Structure of the F-actin-tropomyosin complex. *Nature,* 519**,** 114-7.

WAGNER, W., BRENOWITZ, S. D. & HAMMER, J. A., 3RD 2011. Myosin-Va transports the endoplasmic reticulum into the dendritic spines of Purkinje neurons. *Nat Cell Biol,* 13**,** 40-8.

WANG, Z., EDWARDS, J. G., RILEY, N., PROVANCE, D. W., JR., KARCHER, R., LI, X. D., DAVISON, I. G., IKEBE, M., MERCER, J. A., KAUER, J. A. & EHLERS, M. D. 2008. Myosin Vb mobilizes recycling endosomes and AMPA receptors for postsynaptic plasticity. *Cell,* 135**,** 535-48.

WATERHOUSE, A. M., PROCTER, J. B., MARTIN, D. M., CLAMP, M. & BARTON, G. J. 2009. Jalview Version 2--a multiple sequence alignment editor and analysis workbench. *Bioinformatics,* 25**,** 1189-91.

WATTS, D. J. & ASHWORTH, J. M. 1970. Growth of myxameobae of the cellular slime mould Dictyostelium discoideum in axenic culture. *Biochem J,* 119**,** 171-4.

WEAVER, A. M., KARGINOV, A. V., KINLEY, A. W., WEED, S. A., LI, Y., PARSONS, J. T. & COOPER, J. A. 2001. Cortactin promotes and stabilizes Arp2/3-induced actin filament network formation. *Curr Biol,* 11**,** 370-4.

WEBB, D. J., DONAIS, K., WHITMORE, L. A., THOMAS, S. M., TURNER, C. E., PARSONS, J. T. & HORWITZ, A. F. 2004. FAK-Src signalling through paxillin, ERK and MLCK regulates adhesion disassembly. *Nat Cell Biol,* 6**,** 154-61.

WEBER, I. 1999. Computer-assisted morphometry of cell-substratum contacts. *Croat Med J,* 40**,** 334-9.

WEIJER, C. J. 2004. Dictyostelium morphogenesis. *Curr Opin Genet Dev,* 14**,** 392-8.

WELLS, A. L., LIN, A. W., CHEN, L. Q., SAFER, D., CAIN, S. M., HASSON, T., CARRAGHER, B. O., MILLIGAN, R. A. & SWEENEY, H. L. 1999. Myosin VI is an actin-based motor that moves backwards. *Nature,* 401**,** 505-8.

WESSELS, D., SOLL, D. R., KNECHT, D., LOOMIS, W. F., DE LOZANNE, A. & SPUDICH, J. 1988. Cell motility and chemotaxis in Dictyostelium amebae lacking myosin heavy chain. *Dev Biol,* 128**,** 164-77.

WESSELS, D., TITUS, M. & SOLL, D. R. 1996. A Dictyostelium myosin I plays a crucial role in regulating the frequency of pseudopods formed on the substratum. *Cell Motil Cytoskeleton,* 33, 64-79.

WHITTAKER, C. A. & HYNES, R. O. 2002. Distribution and evolution of von Willebrand/integrin A domains: widely dispersed domains with roles in cell adhesion and elsewhere. *Mol Biol Cell,* 13**,** 3369-87.

WOZNICA, D. & KNECHT, D. A. 2006. Under-agarose chemotaxis of Dictyostelium discoideum. *Methods Mol Biol,* 346**,** 311-25.

WRIGHT, S. P. 1992. Adjusted P-Values for Simultaneous Inference. *Biometrics,* 48**,** 1005-1013.

WU, C., ASOKAN, S. B., BERGINSKI, M. E., HAYNES, E. M., SHARPLESS, N. E., GRIFFITH, J. D., GOMEZ, S. M. & BEAR, J. E. 2012. Arp2/3 is critical for lamellipodia and response to extracellular matrix cues but is dispensable for chemotaxis. *Cell,* 148**,** 973-87.

XU, J. & ZHANG, Y. 2010. How significant is a protein structure similarity with TM-score = 0.5? *Bioinformatics,* 26**,** 889-95.

YAMAMOTO, M., HILGEMANN, D. H., FENG, S., BITO, H., ISHIHARA, H., SHIBASAKI, Y. & YIN, H. L. 2001. Phosphatidylinositol 4,5-bisphosphate induces actin stress-fiber formation and inhibits membrane ruffling in CV1 cells. *J Cell Biol,* 152**,** 867-76.

YAMAZAKI, D., FUJIWARA, T., SUETSUGU, S. & TAKENAWA, T. 2005. A novel function of WAVE in lamellipodia: WAVE1 is required for stabilization of lamellipodial protrusions during cell spreading. *Genes Cells,* 10**,** 381-92.

YAN, C., MARTINEZ-QUILES, N., EDEN, S., SHIBATA, T., TAKESHIMA, F., SHINKURA, R., FUJIWARA, Y., BRONSON, R., SNAPPER, S. B., KIRSCHNER, M. W., GEHA, R., ROSEN, F. S. & ALT, F. W. 2003. WAVE2 deficiency reveals distinct roles in embryogenesis and Rac-mediated actin-based motility. *EMBO J,* 22**,** 3602-12.

YANG, C., CZECH, L., GERBOTH, S., KOJIMA, S., SCITA, G. & SVITKINA, T. 2007. Novel roles of formin mDia2 in lamellipodia and filopodia formation in motile cells. *PLoS Biol,* 5**,** e317.

YDENBERG, C. A., PADRICK, S. B., SWEENEY, M. O., GANDHI, M., SOKOLOVA, O. & GOODE, B. L. 2013. GMF severs actin-Arp2/3 complex branch junctions by a cofilin-like mechanism. *Curr Biol,* 23**,** 1037-45.

YOSHIDA, K. & SOLDATI, T. 2006. Dissection of amoeboid movement into two mechanically distinct modes. *J Cell Sci,* 119**,** 3833-44.

ZANG, J. H., CAVET, G., SABRY, J. H., WAGNER, P., MOORES, S. L. & SPUDICH, J. A. 1997. On the role of myosin-II in cytokinesis: division of Dictyostelium cells under adhesive and nonadhesive conditions. *Mol Biol Cell,* 8**,** 2617-29.

ZATULOVSKIY, E., TYSON, R., BRETSCHNEIDER, T. & KAY, R. R. 2014. Bleb-driven chemotaxis of Dictyostelium cells. *J Cell Biol,* 204**,** 1027-44.

ZHUGE, Y. & XU, J. 2001. Rac1 mediates type I collagen-dependent MMP-2 activation. role in cell invasion across collagen barrier. *J Biol Chem,* 276**,** 16248-56.

ZUCHERO, J. B., COUTTS, A. S., QUINLAN, M. E., THANGUE, N. B. & MULLINS, R. D. 2009. p53-cofactor JMY is a multifunctional actin nucleation factor. *Nat Cell Biol,* 11**,** 451-9.